



**UNIVERSIDADE DE LISBOA
INSTITUTO SUPERIOR TÉCNICO**

Development of new methodologies for upscaling local models into regional models

João Luís Lopes da Cruz de Barros Sobrinho

Supervisor: Doctor Ramiro Joaquim de Jesus Neves

Co-Supervisor: Doctor Lúgia Laximi Machado de Amorim Pinto

Thesis approved in public session to obtain the PhD Degree in

Environmental Engineering

Jury final classification : Pass with Distinction

2021

UNIVERSIDADE DE LISBOA
INSTITUTO SUPERIOR TÉCNICO

**Development of new methodologies for upscaling local
models into regional models**

João Luís Lopes da Cruz de Barros Sobrinho

Supervisor: Doctor Ramiro Joaquim de Jesus Neves

Co-Supervisor: Doctor Lúgia Laximi Machado de Amorim Pinto

Thesis approved in public session to obtain the PhD Degree in
Environmental Engineering

Jury final classification : Pass with Distinction

Jury

Chairperson: Doctor Paulo Manuel Cadete Ferrão, Instituto Superior Técnico, Universidade de Lisboa

Members of the Committee:

Doctor Ramiro Joaquim de Jesus Neves, Instituto Superior Técnico, Universidade de Lisboa;

Doutor Rui Miguel Lage Ferreira, Instituto Superior Técnico, Universidade de Lisboa;

Doutor Flávio Augusto Bastos da Cruz Martins, Instituto Superior de Engenharia, Universidade do Algarve;

Doutor Luiz Paulo de Freitas Assad, Instituto de Geociências, Universidade Federal do Rio de Janeiro, Brasil.

To my wife Marta,
who made this thesis all the more fun.

Resumo

Recentemente, a Europa tem aumentado os seus esforços na transferência de conhecimento das universidades para a indústria, com foco nos oceanos e os seus recursos, como demonstrado pelos fundos dirigidos para os digital twin oceans, que contribuirão para o Green Deal da Comissão Europeia. Para estes objetivos, a modelação oceânica servirá como ferramenta para melhor entender as dinâmicas do oceano e para prever estado do mar - útil não só para o sector industrial, como para entidades públicas. Para fornecer informação útil (e em modo de previsão) aos decisores destes sectores, são precisas maiores resoluções de malha para representar os processos hidrodinâmicos locais, e incluir as principais características de uma zona costeira, como rios e estuários. No entanto, o custo computacional de aumentar a resolução de malha é alto, e o padrão atual para descargas de água doce em modelos regionais de previsão consiste na descarga direta com base em dados climatológicos. Este tipo de implementação é mais simples, mas tem falhas na representação de plumas de água doce, devido à maior difusão numérica, e por ignorar o efeito de mistura exercido pela maré. Esta tese fornece três metodologias diferentes para estes problemas através do upscaling de domínios locais para regionais. As duas primeiras consistem no upscaling através da relaxação do domínio regional para o modelo local, mas enquanto a primeira se aplica a acoplamentos online, a segunda foca-se no modo de simulação offline, onde os domínios correm em separado, sendo uma ótima abordagem para modelação operacional por não afetar os tempos de simulação. Também aproveita a vantagem do serviço CMEMS, ao permitir o upscaling de domínios locais produzidos por diferentes instituições num mesmo domínio regional. A terceira foi implementada diretamente no MOHID, calcula os fluxos de maré a partir dos resultados de representações esquemáticas (e rápidas) de rios e estuários, e impõe-nos no domínio regional como descarga de quantidade de movimento. Desta forma, é conseguida a mistura de águas doces e salgadas a uma escala global sem os grandes custos computacionais e de infraestrutura normalmente associados. Todas as metodologias de upscaling por relaxação foram testadas e validadas com domínios esquemáticos e num sistema de modelação composto pelo modelo para a costa portuguesa (PCOMS) e um domínio para o estuário do Tejo. O upscaling offline de fluxos de mare por descarga de quantidade de movimento foi testado e validado usando o PCOMS e os maiores rios portugueses e o Guadalquivir.

Palavras-chave: Online Upscaling; Offline upscaling; hidrodinâmica em zonas costeiras; modelo bidirecional, plumas estuarinas

Abstract

Recently, Europe has been increasing its efforts in the transfer of knowledge from universities to the industry, with a focus on the ocean and its resources, as demonstrated by the funds for digital twin oceans, which will contribute to the European Commission's Green Deal. Ocean modelling will play its part in these efforts, as a tool for understanding the ocean dynamics and sea state forecasts – useful not only to several industries, such as aquaculture or offshore energy, but also states and municipalities. To provide reliable model-driven information to decision makers, higher model grid resolutions have been required to properly represent local hydrodynamic processes. Also, all main features of a given area must be included in the models (such as rivers and estuaries), and all ocean variables must be forecasted. However, the cost of increasing a regional structured grid domain resolution is too high, and the current standard in regional forecasts is a direct discharge of freshwater obtained from river runoff climatology, which will not properly reproduce a freshwater plume due to the higher diffusion of a regional domains lower grid resolution, and because tide-driven mixing of saltwater with freshwater is neglected. This thesis addresses these issues through the upscaling local domains into regional domains. Three different upscaling approaches were developed. The first two consist on the upscaling through nudging of the regional domain towards the local domain, but while the first applies to online coupling, the second is made for offline couplings, where both domains are run separately, which is an optimal solution for forecast modelling as it comes at zero expense in time consumption. It also takes advantage of the CMEMS capabilities, allowing the upscaling of local models produced in local institution into a regional model developed by another. The third one consists on the computation (integrated in MOHID) of tidal fluxes from fast running schematic local rivers and estuary domains, which are imposed in the regional domain via a momentum discharge. This way, salt and freshwater mixing on a global scale can now be performed at a low cost of simulation time, power and infrastructure. All upscaling by nudging methodologies were tested and validated using schematic domains and a nested system comprised of the Portuguese Coast Operational Modelling System (PCOMS) and a Tagus estuary model domain. The offline upscaling via momentum discharges was tested and validated using PCOMS and all major Portuguese rivers plus Guadalquivir.

Keywords: Upscaling; Hydrodynamics; two-way, estuarine plumes; coastal areas

Acknowledgments

There are too many people for me to thank for their patience, guidance, support and conversations. First of all, I would like to thank my Supervisor Prof. Ramiro Neves for his guidance and teachings during the last 8 years in Maretec, starting with my master's degree and now my PhD degree. Our conversations over the years have undoubtedly changed my views regarding not only the ocean and its many physical and biogeochemical processes but also in many aspects of life in general (for the positive). Secondly, I would like to thank Dr. Lgia Pinto, my co-supervisor for her guidance and support during this thesis, especially for the many early conversations regarding the model implementations and the direction of the thesis, but also for her help in the implementation and maintenance of operational modelling systems such as the ones developed in the MARPOCS project, presented in Annex.

I would also thank all my former colleagues of Maretec for their constant support and teachings during my first years in the modelling life, especially David Brito, Eduardo Jauch, Guillaume Riflet, Isabella Ascione and Marcos Mateus. Without them I do not think this thesis would ever even have started.

Other colleagues were just as important during the course of this thesis for their support and patience during the more stressful times, and off course in celebrations (including the ending of this thesis). Of these I have to thank in particular to Carina Almeida, which did a good part of her thesis at the same time as me, Jorge Palma, Ana Oliveira and Lucian Simionesei. I would also like to thank Jorge Palma for all his help in understanding the basics of linux as well as his support in maintaining the IST meteorological MM5 setup, the Maretec network, and in the development of the thredds service now available at Maretec.

Furthermore, I would like to thank Hilda de Pablo, my eternal PhD colleague who is trying to finish her own PhD while helping me with mine, and who has always been there to help (literally at the desk next to me) during the entire thesis development and writing. Her company during the last 6 years have made my stay in Maretec an even better experience, both professionally and personally, and I have her to thank for finishing this thesis in time. Without her insistence, support and motivation, I would probably still be writing the introduction.

I would also like to thank Francisco Campuzano for his help not only in maintaining the operational systems at Maretec but also for all his support and discussions over the years. Chapter 5 of this

thesis is based on a methodology he developed and the conversations with him lead to the decision of writing said chapter with the addition of the offline upscaling algorithm I had just created in Chapter 4 (with some modifications). He has also been the best (or worse depending on the point of view) beta tester for all my developments, and for that I thank him.

Outside Maretec (but formerly a student of the same house), I would like to thank Paulo Chambel of HIDROMOD for the discussions regarding the upscaling and two-way systems, as well as for all his help in the migration of all my chaotic code from my github to the official MOHID branch. Without it I think I would have introduced a good number of very difficult to track bugs in MOHID. Furthermore, I would like to thank Prof. Aires dos Santos for pushing me to perform more tests to the online couplings, which at the end were very helpful to improve the upscaling methodologies, and to Manuela Juliano for her help with post processing tools, extremely useful in the creation of many of the figures of these thesis.

I would like to thank to the institutions that contributed to this research by uploading their observations to data sharing initiatives such as EMODnet, CMEMS, and SNIRH.

Near the end of the thesis I joined the +Atlantic team, which was a bit chaotic for me but at the same a welcome change in scenery. I would like to thank for their support and understanding during the last year of this thesis when all the pieces of the puzzled had to be put together to create this document.

I would like to thank my family and friends for their support and patience during the entire thesis and for enduring my absence during the last few years while I was absorbed by the thesis. In particular, I would like to thank my parents who thought me to be resilient no matter how hard the times were, and my mother for proofreading the entire thesis and associated articles.

Finally, I would like to thank my wife Marta for her support and patience, for pretending to be very interested in my conversations on hydrodynamics of any kind and most importantly, for keeping me fed during the last year and a half of the thesis. Without her I would take twice as long to finish the work, and I estimate I now owe her one or two years' worth of vacations and cooking.

Index

Chapter 1	Introduction	3
1.1	Context and objectives	3
1.2	Numerical modelling as a tool for ocean and coastal processes.....	5
1.2.1	Before numerical models.....	5
1.2.2	The introduction of meteorological and ocean numerical models.....	7
1.2.3	MOHID modelling system	8
1.2.4	Numerical methods and approximations	11
1.3	Communication between model grid domains	14
1.4	Thesis structure and rationale.....	15
Chapter 2	Downscaling from regional to local domains – a proven solution.....	21
2.1	Introduction	21
2.1.1	Downscaling from Regional to Local domains	22
2.1.2	Open boundary conditions for downscaling	24
2.1.3	The offline downscaling methodology	29
2.2	The PCOMS – Tagus ROFI modelling system	31
2.2.1	The study area	32
2.2.1.1	General circulation of the west coast of the Iberian Peninsula.....	32
2.2.1.2	The Tagus estuary	34
2.2.2	The MOHID Tagus ROFI modelling system as a tool for research studies, coastal management, and decision making.....	35
2.2.3	Application performance during an extreme precipitation event	37
2.2.3.1	Methodology	38
2.2.3.2	Results and discussion.....	42
2.3	Partial conclusions.....	62
Chapter 3	Upscaling local domains into regional domains – online coupling.....	67
3.1	Rationale for an upscaling algorithm	68
3.2	Upscaling Algorithm	71
3.2.1	Code implementation	74
3.2.2	Schematic case: wave through a 1D channel.....	77
3.2.3	Schematic case: stratified 3D domain under constant north wind.....	81
3.2.3.1	Surface temperature fields.....	83
3.2.3.2	Vertical stratification	84

3.2.4	Schematic case: 3D Coastal domain with lateral discharge	87
3.2.4.1	Discharge in all domains	89
3.2.4.2	Discharge only in the higher resolution domains	92
3.2.4.3	Model setup	95
3.2.4.4	Results	97
3.2.5	TwoWay nesting in Tagus ROFI.....	101
3.2.5.1	Setup.....	101
3.2.5.2	One-way vs two-way.....	103
3.3	Partial conclusions.....	113
Chapter 4	Offline upscaling – Tagus ROFI	119
4.1	Rationale.....	119
4.2	Code implementation	121
4.2.1	Modules and implementation files	121
4.2.2	Handling of multiple upscaling domains.....	125
4.2.3	Time interpolation and grid communication	126
4.2.4	Parallelization.....	128
4.3	Real case test – PCOMS - Tagus ROFI modelling system	128
4.3.1	Setup.....	129
4.3.1.1	Grid communication management	129
4.3.1.2	Implementation setup	131
4.3.2	Results	133
4.3.2.1	Water level validation	134
4.3.2.2	Surface salinity validation	137
4.3.2.3	Salinity transition at the open boundary	139
4.3.2.4	Vertical profiles	141
4.4	Partial conclusions.....	144
Chapter 5	Coupling rivers and estuaries with an ocean model: an improved methodology	149
5.1	Rationale.....	149
5.2	Offline upscaling by discharge.....	153
5.3	Code implementation	155
5.3.1	Implementation files.....	156
5.4	Application to the Iberian Peninsula	158
5.4.1	Automatic running tool	160

5.4.2	Model setup	160
5.4.3	Results	164
5.4.3.1	Estuaries tidal prism	164
5.4.3.2	Comparison with in-situ data.....	166
5.4.3.3	Surface salinity maps.....	170
5.4.3.4	Satellite SST analysis	172
5.5	Partial conclusions.....	175
Chapter 6	Conclusions and future work	179
6.1	Conclusions	179
6.1.1	Downscaling overview	179
6.2	Upscaling local into regional ocean model domains	181
6.2.1	Online upscaling coupling.....	182
6.2.2	Offline upscaling	184
6.2.3	Upscaling via momentum discharge	185
6.3	Future work	186
References	189
Annex	195

List of Figures

Figure 1: Main model structure of the hydrodynamic processes. Other processes such as water quality, benthic ecology, seagrass, vertical movement of particulate properties, and sediment are included as dependencies of the Waterproperties, InterfaceSedimentWater, and Hydrodynamic modules.	9
Figure 2: Structured grid with variable grid step, implemented in the Tagus ROFI modelling system running at Maretec. This grid has a higher grid resolution at the mouth of the estuary at the expense of higher resolution in open waters.....	23
Figure 3: Schematic representation of an open boundary a PD and its nested CD on an Arakawa C grid.	25
Figure 4: Bathymetry and model domains of the offline downscaling systems running at Maretec for the Portuguese coast. The Tagus application provides outputs for other nested domains, also using the offline methodology.....	31
Figure 5: The Azores high pressure system and the Icelandic low pressure system, and their impact in wind patterns of the North Atlantic. Adapted from (Campuzano, 2018).	33
Figure 6: Main geomorphological features off the West Iberian Coast	33
Figure 7. Model domains a) PCOMS (Level 2) and b) TagusROFI (Level3). The colour scale represents bathymetry and scale of Level3 (b) is logarithmic. Level 1 bathymetry is the same as Level 2, although with 2 more numerical cells in each direction (needed for open-boundary conditions in downscaling), and for that reason is not presented here.....	38
Figure 8: Map of the Tagus ROFI area showing the location of the in-situ stations used in the validation process as well as the vertical profiles used for comparison between modelling grids. CTG–Cascais Tide Gauge; CTD–Conductivity, Temperature, and Depth probe; ADCP–Acoustic Doppler Current Profiler; P1-4 – vertical profiles.....	42
Figure 9: Comparison of water levels obtained with the Cascais tide gauge and Level2 modelling domain for the period between 11 January and 13 March 2013.	43
Figure 10: Comparison of water levels obtained with the Cascais tide gauge and Level3 modelling domain for the period between 11 January and 13 March 2013.	44
Figure 11: Correlation and performance results for the period between 11 January and 13 March 2013, between the Cascais tide gauge and the different model implementations: a) Level2 in one-way, b) Level3 in one-way.....	45
Figure 12: Salinity profile from Level3 model domain at the mouth of the estuary during ebb and flood of 1 April 2013, when the flow value reached its maximum.....	46
Figure 13: Performance of model results (Level3 domain) against field data (obtained with a CTD). At the top) Comparison between salinity field data for the period between 15 January and 10 April 10; At the bottom) correlation between model (Level3) and CTD data for the period between 1 March and 10 April.	46
Figure 14: Comparison between velocity profiles obtained by the Level3 model domain (Tagus ROFI) and the ADCP for the period between 2and 17 July 2009. From: (de Pablo et al., 2019).	49
Figure 15: Interannual comparison of surface seawater temperature between MOHID and Satellite L4 gridded products (OSTIA-5 km, ODYSSEA-2 km; and MUR 1 km) for the period 2014–2016.....	50
Figure 16: Average surface velocity field obtained with Level2 and Level3, for each selected period. The velocity fields shown are the result of an interpolation of both model domains to a 200 x 200 m grid. Bathymetry is in logarithmic scale.	52
Figure 17: Salinity maps obtained by Level2 and Level3 and respective comparison.	53
Figure 18: Salinity profiles obtained by Level2 and Level3 over the simulated period. Profiles every 12h are represented in grey, while the average over each analysed period is represented in black.	55

Figure 19: Comparison between vertical profiles of salinity obtained by Level2 and Level3 domains at the five defined locations for the three analysed periods. 57

Figure 20: Temperature profiles obtained by Level2 and Level3 over the simulated period. Profiles every 12h are represented in grey, while the average over each analysed period is represented in black. 59

Figure 21: Comparison between vertical profiles of temperature obtained by Level2 and Level3 domains at the five defined locations for the three analysed periods. 60

Figure 22: Time series of surface salinity obtained by Level2 and Level3 at a point near the northeastern open boundary of Level3 (see Figure 8)..... 61

Figure 23: Two-way time scale for one parent domain iteration, with a time refinement factor of 2..... 72

Figure 24: Water level produced by the parent (level1 in one-way and two-way) and the reference domains along the extent of the CD domain after a period of 6 h of simulation. Difference between domains is presented in green..... 79

Figure 25: Kinetic energy variation obtained by the parent (level1 in one-way and two-way) and reference domains over 12 hours of simulation. Difference between domains is presented in green..... 80

Figure 26: Bathymetries of the three domains simulated and locations of the vertical profiles used for the analysis of the stratification of the water column..... 81

Figure 27: Surface temperature and velocity fields obtained by the Reference domain, Level1 in one-way and Level1 in two-way with three different parametrizations..... 83

Figure 28: Surface temperature fields obtained by the Level1 in two-way, with three most impactful parametrizations. 84

Figure 29: Vertical profiles of temperature at three different locations: in the deep area, at the slope and at the shallow area. Please note that the difference axis changes from P1 to P2 and P3, by a factor of 10. ... 85

Figure 30: Total mass variation of the Reference and Level1 domains over the 6 days of simulation period. 86

Figure 31: Reference, Level1 and Level2 domains with the locations of the time series PN (north point) and PS (south Point) used in the analyses of the fresh water plume discharge (DP). 87

Figure 32: Surface salinity field overlapped by the velocity vectors, obtained by the Reference, Level1 and Level2 domains under the several upscaling parametrizations. Level1 alone is represented on the left, while an overlapping of Level2 on Level1 is represented on the right with a frame (in black) over the open boundary of Level2). 90

Figure 33: Salinity time series obtained at the north boundary (PN) of Level 2 by the Reference domain and Level1 domain under one-way and two-way modes (with three different parametrizations of upscaling). 91

Figure 34: Salinity time series obtained at the south boundary (PS) of Level 2 by the Reference domain and Level1 domain under one-way and two-way modes (with three different parametrizations of upscaling). 92

Figure 35: Surface salinity field overlapped by the velocity vectors, obtained by the Reference, Level1 and Level2 domains under three upscaling parametrizations. The Reference domain is represented on the left, while the remaining maps show the overlapping of Level2 on Level1 with a frame (in black) over the open boundary of Level2. 93

Figure 36: Salinity time series obtained at the north boundary (PN) of Level 2 by the Reference domain and Level1 domain under two-way mode (with three different parametrizations of upscaling).Schematic case: Geostrophic equilibrium..... 94

Figure 37: Surface elevation maps overlapped by the velocity fields, obtained for the geostrophic equilibrium by the Reference domain, Level1 domain in one-way mode and in two-way mode for three different upscaling parametrizations: Upscale of horizontal velocities with a Td of 120 s, upscale of horizontal velocities plus water level with a Td of 120 s, and upscale of horizontal velocities with a Td of 3600 s. 98

Figure 38: Water level (left) and normal velocity (right), perpendicular to the density front, obtained by the Reference, Level1 in one-way and two-way modes with different parametrizations, and by the analytical solution.	99
Figure 39: Average temperature over the simulation period obtained by the Reference, Level1 in one-way and Level1 in two-way with the three different parametrizations.	100
Figure 40: Total water volume variation (represented in both graphs) over the simulation period obtained by the Reference, Level1 in one-way and Level1 in two-way with the three different parametrizations. Volume loss referenced to the initial volume is represented on the right.	101
Figure 41: Map of the Tagus ROFI area showing the location of the in-situ stations used in the validation process, as well as the vertical profiles used for comparing modelling grids. CTG–Cascais Tide Gauge; CTD–Conductivity, Temperature, and Depth probe; P1-5 – vertical profiles.	104
Figure 42: Correlation and performance results for the period of 11 th of January to the 10 th of April 2013, between the Cascais tide gauge and the different model implementations: a) Level2 in one-way, b) Level2 in two-way, c) Level3 in one-way and d) Level3 in two-way.	105
Figure 43: Performance of model results (Level3 domain) against field data (obtained with a CTD). a) Comparison between salinity field data for the period between 25 March and 10 April, b) one-way (blue) and two-way (orange) correlations between model and CTD data for the period between 1 March and 10 April.	106
Figure 44. Impact of the feedback operation on the salinity field transition between Level2 and Level3 model grids during the Tagus plume evolution at its peak flow, from 0h to 10h of 5 April, under a) one-way and b) two-way methodologies.	107
Figure 45. Time series of Salinity at Pp (computed by Level2) and Pc (computed by Level3) locations obtained through one-way and two-way methodologies.	107
Figure 46: Comparison between vertical profiles of temperature obtained by Level2 and Level3 domains at the five defined locations for the three analysed periods, under one-way and two-way modes.	110
Figure 47: Comparison between vertical profiles of temperature obtained by Level2 and Level3 domains at the five defined locations for the three analysed periods, under one-way and two-way modes.	111
Figure 48: Illustration of an example where the LD has numerical cells in an area where the RD cell is land. Grid ratio is 1:3. Green squares represent the LD scalar cells, u_{LD} is the LD u velocities which would be volume-averaged to be upscaled by u_{RD} (but are not because u_{RD} is set to 0). $u_{LD} *$ are the LD velocities which are volume-averaged to be upscaled by $u_{RD} *$. $\eta_{RD} *$ represents the surface elevation of the discharge cell in contact with a land cell. In light blue: a RD cell adjacent to land (velocity is computed at the faces, as these are Arakawa-C type grids). In grey: RD land cell.	123
Figure 49: Implementation files and respective parametrizations required for offline upscaling. Discharges are only required when the CD covers an inland area not represented by the PD and which produces and tidal prism.	124
Figure 50: Time integration schemes for a simulation with a PD and a CD. On top: a representation of downscaling plus upscaling operations (in this scheme it is considered offline two-way). On the bottom: a representation of the online two-way simulation.	127
Figure 51: Model domains of PCOMS (left) and TagusROFI (right). The WestIberia bathymetry is the same as PCOMS, although with 2 more numerical cells in each direction. The location of the in-situ stations (CTG–Cascais Tide Gauge - 38.69°N, 9.42°W; CTD–Conductivity, Temperature, and Depth probe - 38.69°N, 9.23°W) used in the validation process, the vertical profiles (P1 – Lisbon Canyon (38.37°N, 9.51°W), P2 – western boundary of Tagus ROFI (38.61°N, 9.99°W) and P3- northeast boundary of Tagus ROFI (39.14°N, 9.45°W) used for comparing modelling grids and the time series extracted from near the open boundary of Tagus ROFI (39.19N, 9.44W) are presented on the right.	133

Figure 52: Comparison between water level obtained by the different PCOMS model implementations. From the top: water level over the simulation period obtained by the tide gauge and the one-way offline downscaling implementation; Overlapped bias of the different implementations towards the tide gauge; Bias of the different model implementations and their average bias towards the tide gauge; correlation between each implementation and the tide gauge. 135

Figure 53: Comparison between water level obtained by the different Tagus model implementations. From the top: water level over the simulation period obtained by the tide gauge and the one-way offline downscaling implementation; Overlapped bias of the different implementations towards the tide gauge; Bias of the different model implementations and their average bias towards the tide gauge; correlation between each implementation and the tide gauge 136

Figure 54: Comparison between surface salinity obtained by the different model implementations of Tagus ROFI. From the top: surface salinity time series over the simulation period obtained by the CTD, the one-way offline downscaling implementation, and the offline two-way implementation with one 1 day of upscaling; Overlapped bias of the different implementations towards the CTD; Bias of the different model implementations and their average bias towards the CTD; correlation between each implementation and the CTD..... 138

Figure 55: Time series of surface salinity at the northeastern open boundary of Tagus ROFI, obtained by PCOMS and Tagus ROFI, showing the impact of upscaling in the transition between model grids and the feedback it generates into Tagus ROFI when the upscaling procedure is executed 2 times per day. 140

Figure 56. Salinity fields obtained by the three implementations. At the top: offline downscaling (left), 1 day of offline upscaling (middle) and two days of offline upscaling (right); at the bottom: difference between the downscaling simulation and the 1 day upscaling simulation (left), and the difference between the downscaling simulation and the 2 days upscaling simulation (right), for the period between 25 Mar and 10 April 2013. 141

Figure 57: Comparison between vertical profiles of temperature obtained by PCOMS and Tagus ROFI domains at the five defined locations for the two analysed periods, under one-way and two-way modes. 143

Figure 58: Surface temperature and velocity fields produced by the offline one-way (only downscaling) and offline two-way (with one and two incremental offline upscaling days) implementations. 143

Figure 59: Illustration of an example where the CD has numerical cells in an area where the PD cell is land. Grid ration is 1:3. In red: the CD cells that will be used to compute the volume-weighted average for the upscaling into the PD u velocity. In green the grid of the CD. In light blue: a PD cell adjacent to land (velocity is computed at the faces -as these are Arakawa-C type grids). In Gray: PD land cell 156

Figure 60: Implementation files and respective parametrizations required for a discharge via offline upscaling of a local domain. 157

Figure 61: Time integration schemes for a simulation with a regional and a local domain. On top: a representation of downscaling plus upscaling operations (in this scheme it is considered offline two-way). On the bottom: a representation of the online two-way simulation. 158

Figure 62: Representation of the study area as well as the most important bathymetric features and location of the time series used in the validation of the results. The area corresponds to the PCOMS grid domain and its bathymetry (on the map) and that of each schematic river and estuary (on the right) is also shown (in this case the dimensions are shortened in order to fit in the image. The real dimensions of these domains are presented in Table 15). 159

Figure 63: Tidal prism flow rate obtained by the schematic and real representations of the Douro, Minho, Mondego, Tagus and Guadiana rivers and estuaries. A positive flow rate is observed in the flood tide and a negative one in the ebb tide. Guadalquivir was not included because a real representation of this estuary was not being simulated in Maretec. 166

Figure 64: Salinity and temperature time series produced by the three PCOMS implementations and the Silleiro in-situ moored buoy during the period between Jan 1 and May 1 of 2018.	168
Figure 65: Salinity and temperature time series produced by the three PCOMS implementations and the Estaca de Bares in-situ moored buoy during the period between Jan 1 and May 1 of 2018.	169
Figure 66: Average surface salinity maps for the entire domain (top) and a zoom over the area of interest in the west coast of the IP (bottom) produced by the three implementations: No Rivers (Left), De-tached (middle) and Integrated (right) methodologies over the peak flow period (Mar 18 to Apr 1 of 2018).	171
Figure 67: Difference between average surface salinity maps for the entire domain (top) and a zoom over the area of interest in the west coast of the IP (bottom) produced by: Integrated minus Detached (Left) and Integrated minus No Rivers (right) over the peak flow period (Mar 18 to Apr 1 of 2018).	172
Figure 68: Average surface temperature maps for the entire domain (top) and a zoom over the area of interest in the west coast of the IP (bottom) produced by the two implementations: Satellite SST (left), No Rivers (middle) and Integrated (right) methodologies and at the peak flow (Mar 20 of 2018).	173
Figure 69: Difference between surface temperature maps for the entire domain (top) and a zoom over the area of interest in the west coast of the IP (bottom) produced by: No Rivers minus Satellite (Left) and Integrated minus Satellite (right) at the peak flow period (Mar 20 of 2018).	173
Figure 70: Model domains implemented for the MARPOCS project.	197
Figure 71: Water level obtained by LP1 and LP2 domains and by the tide gauge.	201
Figure 72: Vertical profiles from the PLOCAN field campaign and MARPOCS model domain for the three samplings made by PLOCAN.	202
Figure 73: Comparison between profiles obtained with ARGO buoys and MARPOCS modelling domain.	204
Figure 74: Comparison between profiles obtained with ARGO buoys and the CI modelling domain for 15 May 2017.	204
Figure 75: Seasonal, permanent and weak permanent upwelling zones in the west coast of Africa, where a good part of the MARPOCS domain is located. From: (<i>Gómez-Letona et al., 2017</i>).	205
Figure 76: Comparison between surface temperature obtained by the MARPOCS model domain and Fusion satellite product over (from top to bottom): spring, summer, autumn and winter.	209
Figure 77: Residual circulation from Jun 2017 to March 2020. Velocities arrows overlay the bathymetry colour.	210

List of Tables

Table 1: Some of the main modules and the properties and processes under their responsibility.	10
Table 2: Boundary conditions implemented in the MOHD Modelling system.....	29
Table 3. Model setup configuration for the Tagus ROFI area.....	41
Table 4. Statistical parameters obtained for salinity comparison with CTD data with Level3 domain for the period between 1 March and 10 April.....	47
Table 5: Current velocity and direction. Data summary and results of statistics used to assess the level of agreement between measured data and modelling results. <i>n</i> —number of observations; <i>r</i> —correlation coefficient; <i>BIAS</i> —Average bias; <i>RMSE</i> —Root mean square error. From (de Pablo et al., 2019)	49
Table 6: Results of statistics used to assess the level of agreement between SST obtained via remote sensing data and modelling results. <i>n</i> —number of observations; <i>r</i> —correlation coefficient; <i>BIAS</i> —Average bias; <i>RMSE</i> —Root mean square error. Adapted from: (de Pablo et al., 2019).....	51
Table 9: Upscaling keywords needed in the hydrodynamic.dat implementation file of the nested Domains. Default values are included in parenthesis. These keywords are added outside any existing property block (which look like <begin...> <end...>).	75
Table 10: Upscaling keywords needed in the WaterProperties.dat implementation file of the nested Domains. Default values are included in parenthesis. These keywords are added inside existing property block which the user wants to upscale (which look like <begin...> <end...>).	75
Table 11: Description of the model domain implementations for the geostrophic equilibrium schematic case.	96
Table 12. Model setup configuration for the Tagus ROFI area in two-way mode.....	102
Table 13. Model setup configuration for the Tagus ROFI area in two-way mode.....	131
Table 14: Statistical parameters of the three implementations: offline downscaling, offline downscaling plus upscaling with one and two runs of the same day with upscaling enabled, for the water level at the Cascais tide gauge.	137
Table 15: Statistical parameters obtained for the comparison against surface salinity at Algés, of the three implementations: offline downscaling, offline downscaling plus upscaling with one and two runs of the same day with upscaling enabled.	139
Table 16: Model setup configuration for the TagusROFI area.	162
Table 17: Dimensions of the schematic river and estuary domains.	162
Table 18: River flow and respective source of data used to feed the schematic channels.	163
Table 19: Statistical parameters obtained for the validation of the three methodologies against field data (Silleiro moored buoy).	168
Table 20: Statistical parameters obtained for the validation of the three methodologies against field data (Estaca de Bares moored buoy).....	169
Table 7: Implemented domain grids.....	197
Table 8: Model setup configuration for the various implemented domains.	200

CHAPTER I

Chapter 1 Introduction

1.1 Context and objectives

Europe has been focusing its efforts on the transfer of knowledge from universities to the industry for at least the past two decades, with the clear objective of providing the industry with innovative and more efficient processes. Nowadays, this effort is increasingly being oriented to the ocean and its resources, as demonstrated by the emergence of funds for digital twin oceans, which will contribute to the European Commission's Green Deal. One of the components necessary for this effort is ocean hydrodynamic and biogeochemical modelling as a tool for understanding the ocean dynamics and for forecasting the sea state. This knowledge is to be (and has been) used by the several industry sectors, such as aquaculture, deep sea mining, offshore wind and wave energy, oil and gas platforms, and shipping. Additionally, states and municipalities are urged to develop strategic plans for the effect of sea and meteorological conditions in coastal structures, erosion, ecological state and water quality – particularly near bathing areas. As these needs grow, so do the modelling efforts necessary to represent the relevant ocean and coastal processes. These efforts are driven by the need for higher resolution grids used in model applications, but also for incorporating local processes – at the scale of estuaries and coastal areas – in regional or global model applications such as those provided by the Copernicus program CMEMS. In the case of rivers and estuaries, the current standard is to use climatological values for each river runoff and add its correspondent volume into the first numerical cell adjacent to land of the regional domain. Although much easier to implement, this solution will not properly create a river plume due to numerical diffusion associated with a lower grid resolution of the regional domain. It will also disrupt the vertical stratification, as these discharges are implemented at the surface layer only without the vertical mixing caused by the density gradients and tidal effects at the inlets. One possible solution to this problem is to incorporate these local processes via a *two-way* coupling, in which a regional domain provides open boundary conditions to a local, higher grid resolution domain, which then updates the regional domain. However, this implies that both model applications must be run in the same institution and with the same model, as the simulation must be online (information is transferred in run-time at a specific time-step). This work aims to provide a new offline (transfer of information is made on a daily simulation basis, allowing for both

applications to run separately) upscaling methodology based on the relaxation of a local domain into a regional domain, which will enable the upscaling of different local model applications produced by different entities using different models, into regional model applications. This methodology will also act as a stepping stone to the creation of a coupling tool between ocean and watershed models.

The main objectives of this theses are:

1. Apply and describe the advantages and disadvantages of a downscaling approach from a regional ocean model domain to a coastal area.
2. Develop and test an online coupling, nudge-based upscaling algorithm, to transfer information from a local domain into a regional domain.
3. Develop an offline coupling, nudge-based upscaling algorithm, to transfer information from a local domain into a regional domain, and compare it with an online coupling.
4. Develop and compare, with current methodologies, an upscaling algorithm for online and offline coupling, applicable to a single regional domain grid cell, which intakes a momentum discharge at the land boundary provided by a local domain.

This work and all its developments were done in the MOHID3D modelling system (MOHID) developed at the Maretec marine technology centre, based at the University of Lisbon. For the first objective, a downscaling approach was applied to two model domains extensively studied at Maretec: the regional Portuguese Coastal Modelling System (PCOMS) and the nested local model domain Tagus3D, setting a baseline for comparison with the online (*two-way*) and offline upscaling methods developed under the second and third objectives. The online coupling implemented in objective two is but a testing ground for the ultimate objective of this thesis, which is the creation of an offline, model independent, upscaling algorithm. This algorithm aims to solve the problem of incorporating local information into a regional model domain, and seeks to reduce the computational time of ever higher resolution forecasting systems. The developments made for objective four were made for an easier integration of rivers and estuaries into regional ocean domains – specifically on the mixing processes not currently represented in these domains – such as in the CMEMS solutions. However, they also intend to provide a stepping stone for the future integration of ocean models with watershed models.

1.2 Numerical modelling as a tool for ocean and coastal processes

Oceans play an essential role in the environment of the planet. They are vital to the planet's thermal regulation due to their extensive ability to store heat and carbon, and to transport heat and moisture across the globe. At a global scale, currents transport warm water and precipitation from the equator toward the poles, and cold water from the poles back to the tropics. By doing this, they contribute to a more even distribution of the solar radiation that reaches the planet's surface. Without this transport, temperatures at the equator would be much higher whilst at the poles they would be much lower, impacting many of today's inhabited areas. In coastal areas subject to upwelling, they return nutrients stored at the bottom to the surface, sustaining marine wild life and all species dependent on them in the food chain, including us.

1.2.1 Before numerical models

From a mankind perspective, knowledge of ocean currents and wind patterns such as the trade winds were decisive in the establishment of trade routes between continents by sea, especially from the late 1400s when the Europeans began their voyages to discover new continents. However, it was not until the 19th century that modern oceanography was born, with the scientific expeditions launched by Americans, British and Europeans. The innovative part of these expeditions was their focus on other variables such as the chemical composition of ocean waters, depth, specific gravity, light penetration, and discovery and mapping of the distribution of marine species. Later, during WW2, underwater acoustics was extensively studied due to submarine warfare, leading to the creation of the SONAR. Data collection of depth, temperature, salinity and some marine species was vital not only for detecting ships, other submarines and mines, but also for avoiding detection by hiding, for example, below large agglomerations of jelly fish or thermal layers. The SONAR and the knowledge created at the time was then used by fishing vessels to detect fish schools, as well as to map the seafloor. In short, as knowledge of the ocean and its variables increased, so did its uses and the retrieval of resources, which, in turn, increased the demand for more knowledge. This same process of knowledge gathering occurred in coastal areas, but with different objectives and at different stages of development. With regard to human use in coastal areas, tide and bathymetric data would be at the top of the list of ocean variables due to their importance for naval

operations, whether civilian or military. Tidal currents near the entrance of ports, bays, estuaries or rivers determined the approach a vessel should follow, and bathymetric data was essential for navigation during low tides due to the risk of grounding. During the discoveries, ocean navigation charts were created to assist pilots in their voyages – especially for merchant navy at the beginning – but before that pilots relied upon local knowledge and charts to enter or exit ports. Nowadays, ports must follow strict protocols for entry and exit, and port authorities assist any ship entering that requests assistance. Other ocean and sea variables such as temperature, salinity, water quality and nutrients began to be studied on a wider scale in the 19th century with scientific expeditions (Deacon, 2018). However, the use of this data near coastal areas only became relevant during the 19th century, related to rapidly increasing water pollution of inland water bodies. With the increase of population in coastal areas, water quality issues related to sewage become more relevant, and led to many outbreaks of water borne diseases in the late 19th century. Fishing in rivers and lakes also began to decrease due to oxygenation problems arising from increased organic matter in the water. The following century was marked by water treatment facilities in these highly populated areas of the most advanced countries, and with it came the need for more monitoring of rivers and lakes. At the same time, many countries started measuring river flows, necessary for deciding on the installation of dams and forecast their available power. By the end of the 20th century, available in-situ data on water variables was focused (and still is to this day) on inland waters, explained not only by higher costs related to the acquisition of this type of data in the oceans and seas, but also due to the higher socio-economical relevance of fresh water. However, in-situ sampling has two drawbacks: data is often sparse in time and space, making it more difficult to understand spatial and temporal processes, and to achieve a good distribution of data is too expensive; and monitoring solutions are neither suitable for studying real case scenarios nor for forecasting the state of the weather or the ocean. Though WFD requires the monitoring of several biological and chemical elements for establishing reference conditions in terms of water quality, long-term continuous monitoring with high temporal resolution are rarely deployed in estuaries (Garel et al., 2009) and, when they are, some sensors show lower adaptation for longstanding observation (Garel and Ferreira, 2015). For these reasons, numerical models are able to support in situ monitoring by completing the datasets spatially and temporally, and by contrasting the ambiguous observed values. Also numerical models can help describe the transitional waters, including the extension and influence of the estuarine plumes in the near ocean.

1.2.2 The introduction of meteorological and ocean numerical models

The first numerical weather forecast models were designed by Lewis F. Richardson (Richardson, 1922) using some of the work of Bjerknes's primitive equations (Bjerknes, 1999). However, at a time when computers were not yet available, his version of a weather forecast model would require thousands of people solving the equations for a model domain. There were not many developments until after the WWII, when the computer power rose to a level which allowed the first weather prediction models. The first modern (as in routine) weather forecasts appeared in Sweden, provided by the Swedish meteorological institute in 1954, followed by global climate models in the late 50s, early 60s. As for global ocean circulation models, the first ones include the works of Cox (1975) and Takano (1975), roughly a decade after global atmospheric circulation models, taking advantage of the meteorological modelling knowledge acquired in that last decade. Numerical ocean models as forecasting started in the early 80s with a first experimental forecast of the California ocean current system made at Harvard University by (Robinson et al., 1984) later improved in (Spall and Robinson, 1989) as a service to the US Navy. The use of these tools grew significantly during the 80s and 90s, with uses in the fields of ocean circulation patterns, climate change and weather patterns such as the El Niño (by coupling between ocean and atmospheric models), pollution, fisheries management, and iceberg drifting and melting – sea-ice interactions. The evolution of both meteorological and ocean models from then on relied mostly on the constant increase in computation power, which allowed for higher grid resolutions and the consequent study of smaller scale physical processes. The socioeconomic aspect of environmental data can also explain why the meteorological models were always in the vanguard of atmospheric and oceanic numerical modelling. For the majority of the public and private entities as much as single individuals, knowing tomorrow's weather conditions – such as wind or precipitation levels – is more important than knowing the sea surface temperature, or its currents, waves or concentration of nutrients. Since then, the bigger part of the schemes applied in this field were imported from meteorological modelling advances.

Nowadays, models have improved their versatility, included more complex processes such as the biogeochemical cycle, algae growth, sediment dynamics, acidification, population dynamics, and have adapted to new computer technologies, such as parallel processing, to reduce their computational time. These developments allowed numerical models to increase their usability, not

only as a forecasting tool for sea conditions, but also in scenario simulations, in the fields of recreation, water quality in bathing areas, coastal engineering (including infrastructure design, erosion processes and WWTPs effluent discharge through submarine outfalls), search and rescue operations, navigation, oil and HNS spills, plastics and pharmaceutical drugs, offshore renewable energies, and aquaculture. With the growing awareness of coastal populations and governments giving more weight to the human impact on the health of oceans (and vice-versa), these tools are increasing their foothold and gaining the acceptance of society, due mainly to climate change modelling scenarios on sea level rise and frequency of extreme events, which will greatly affect the socio-economics of any coastal area. In this regard, modelling tools play a vital role in coastal planning and adaptation to climate change, but also in providing answers and solutions for any new existing phenomena, such as the impact of plastics or pharmaceutical drugs on the environment, on human activities, and on humans themselves. More historical reviews on this subject are available in works by (McWilliams, 1996; Pinardi et al., 2017; Vallis, 2016; Wunsch and Ferrari, 2018).

1.2.3 MOHID modelling system

The MOHID Water model is a 3D finite volume model developed at MARETEC (IST - University of Lisbon) for Arakawa-C staggered grids, which solves the 3D incompressible primitive equations (Leitão, 2002; Leitão et al., 2005; Martins et al., 2001, 1998), built and developed using an object-oriented philosophy (Braunschweig et al., 2004). In the early 2000s, the MOHID system was substantially reformulated with a view to incorporating all the knowledge acquired over the previous 15 years. At that time, three hydrodynamic models (Neves, 1985; Santos, 1995; Martins, 2000), the lagrangian tracers model (Leitao, 1996), the water quality model (Miranda, 1999) and the vertical turbulence model (Coelho, 1996) were maintained. It was from these various components that an effort was made to create a single modelling tool capable of merging all this knowledge and with the ability to incorporate new developments. At the time of these developments, Fortran did not yet have the capabilities for modern object-oriented philosophy. As such, code structure follows an object-oriented philosophy, but the code uses very few of the modern object-oriented capabilities such as encapsulation and abstraction. The approach followed at the time, which has remained mostly untouched since then, is a process-oriented, modular structure in which a module is considered a single object responsible for the computation of single

or multiple processes, depending on the module. From a broader perspective, these modules could be considered classes, but there is no encapsulation or abstraction of all the methods. From a current point of view of a programmer, this could be considered blasphemy, but, back then, compilers were still in their early days of object-oriented philosophy, the tools were developed by non-programmers, and a very large number of people were making contributions to the software. A simplification of the programming language was essential for many contributors with no experience in programming, to include their inputs and to help the software's versatility grow. Nowadays, the modular structure of the MOHID software includes more than 40 modules, representing not only the physical, biogeochemical, wave and sediment processes, but also a number of auxiliary modules for input and output, common functions, and object management. An overview of the main structure for hydrodynamics is presented in Figure 1, but a more detailed overview of the programming and modular structure can be found in (Leitão, 2002) and (Braunschweig et al., 2004).

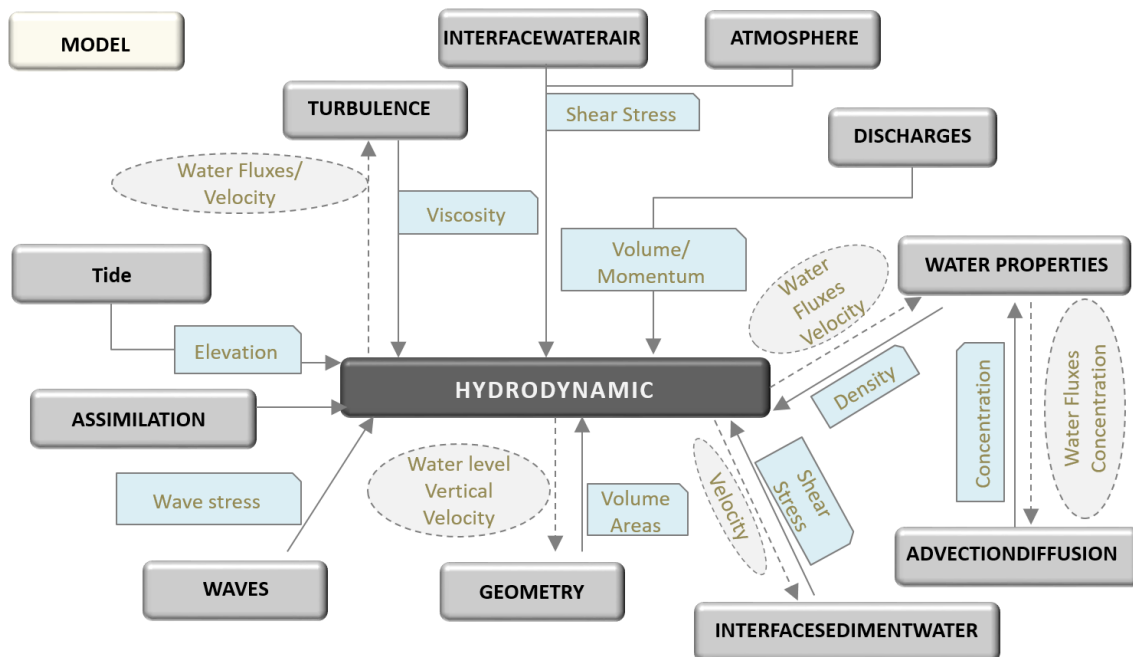


Figure 1: Main model structure of the hydrodynamic processes. Other processes such as water quality, benthic ecology, seagrass, vertical movement of particulate properties, and sediment are included as dependencies of the Waterproperties, InterfaceSedimentWater, and Hydrodynamic modules.

Each of these modules is responsible for one or a set of processes or properties. A description of the main modules is presented in Table 1.

Table 1: Some of the main modules and the properties and processes under their responsibility.

Hydrodynamic	Non-turbulent properties such as velocity and water level fields	Balance of forces and continuity
Turbulence	Turbulent properties such as viscosity	Turbulent processes
Assimilation	Data assimilation and nudging of non-turbulent properties	*
InterfaceSedimentWater	Rugosity, shear stress and fluxes between sediment and the water column.	Erosion, deposition, consolidation Organic matter degradation, benthic and seagrass processes
Geometry	Volumes, areas, distances	Vertical discretization grid processes
WaterProperties	Water properties such as temperature, salinity cohesive sediments and nutrients	*
AdvectionDiffusion	**	Advection diffusion processes of water properties
Atmosphere	Atmospheric variables such as incoming radiation, wind and air temperature	*
InterfaceWaterAir	Shear stress, heat and gas fluxes	Shear stress processes Heat and gas transfer Precipitation and evaporation
Waves	Wave stress, stokes drift	Wind fetch processes

*Module is not responsible for processes, only properties and/or input/output

**Module is not responsible for properties management, only processes.

Processes added since then include and are described, as in this present case, in PhD theses. Some of these developments and their correspondent thesis can be found in:

- Biogeochemical model (Mateus, 2006)
- Wave integration with currents (Delpy, 2013)
- Bivalve modelling (Saraiva, 2014)
- Benthic marine systems modelling (Ascione, 2014)
- Sediment dynamics (Franz, 2017)
- Oil spill modelling (Fernandes, 2018)

Each of these modelling components of the MOHID modelling system was designed in a specific module, independent from the hydrodynamic equations, making the system, as a whole, more robust. This process integration philosophy – which includes many methods for a given process –

is responsible for the designation of MOHID as a numerical laboratory in (Leitão, 2002). Over the years, the software grew in versatility much due to the multidisciplinary team working at Maretec, allowing the model to serve as tool for research and problem solving of real life cases. On the downside, efficient computation was, in most cases, set aside, leading to an accumulation over time of inefficient functions and routines. This issue is briefly addressed in this thesis and many routines of the main routines of modules *hydrodynamic*, *waterproperties* and *advectiondiffusion* have been updated to reduce computational time required for simulations. These updates tackled the routines responsible for 50% of computational time and accomplished a global simulation time consumption reduction of 11-30% depending on the size of the domain, with increasing gains with domain size.

1.2.4 Numerical methods and approximations

The MOHID Water model is a finite-differences family model that evolved to a finite-volume model. Variables are placed in space using the Arakawa-C staggered grid. Velocity components are computed over the faces of the scalars control volume and so are the advective and diffusive fluxes. Water-volume fluxes across the faces of the control volume are computed using the last known velocities and the concentration at the face is obtained by interpolation of the values known inside the finite-volumes using different alternative methods, including upwind, central differences, QUICK and TVD. New values can be computed using explicit or semi-implicit algorithms. This approach ensures that the flux leaving a cell across a face is the flux entering in the cell sharing that face, guaranteeing that advection is conservative. Diffusivities are also computed over the finite-volume faces assuring that diffusion is also conservative. Momentum fluxes are computed using the same rationale. The model solves the 3D incompressible primitive equations (Leitão, 2002; Leitão et al., 2005; Martins et al., 2001, 1998), built and developed using an object-oriented philosophy (Braunschweig et al., 2004). Its modular structure includes more than 40 modules, representing hydrodynamic, biogeochemical, wave and sediment processes. Some of these processes and their correspondent descriptions include: Biogeochemical model (Mateus, 2006); Wave integration with currents (Delpey, 2013); Bivalve modelling (Saraiva, 2014); Benthic marine systems modelling (Ascione, 2014); Sediment dynamics (Franz, 2017); Oil spill modelling (Fernandes, 2018).

The model assumes Hydrostatic equilibrium and partially assumes the Boussinesq approximation. The density value used in the horizontal momentum equation is time and space dependent, but momentum fluxes are computed per unit of mass. Null velocity divergence is also assumed,

$$\frac{\partial u_i}{\partial x_i} = 0 \quad (1)$$

Where u_i are the three velocity components. Density is computed as a function of temperature, salinity, or suspended matter. Integrating the along the water column between the bottom ($-h$) and a depth z , one gets the vertical velocity at that level.

$$(u_3)_{x_3=z} = -\frac{\partial}{\partial x_1} \left(\int_{-h}^z u_1 dx_3 \right) - \frac{\partial}{\partial x_2} \left(\int_{-h}^z u_2 dx_3 \right) + \int_{-h}^z q dx_3 \quad (2)$$

Where q are natural or anthropogenic local water sources. Integrating up to the free surface one gets the free surface level η rate of change,

$$\frac{\partial \eta}{\partial t} + \frac{\partial}{\partial x_1} \left(\int_{-h}^{\eta} u_1 dx_3 \right) + \frac{\partial}{\partial x_2} \left(\int_{-h}^{\eta} u_2 dx_3 \right) = \int_{-h}^{\eta} q dx_3 \quad (3)$$

In this equation, q includes rain and evaporation. Using the hydrostatic approximation the vertical momentum equation becomes,

$$\frac{\partial p}{\partial x_3} = -\rho g \quad (4)$$

That integrated over the water column between the free surface and a depth z gives,

$$(p)_{x_3=z} = p_{atm} + \int_z^{\eta} \rho g dx_3 \quad (5)$$

If one performs the derivative along the horizontal axis, one gets the pressure gradient,

$$\left(\frac{\partial p}{\partial x_i} \right)_{x_3=z} = \frac{\partial p_{atm}}{\partial x_i} + g(\rho)_{x_3=\eta} \frac{\partial \eta}{\partial x_i} + g \int_z^{\eta} \frac{\partial \rho}{\partial x_i} dx_3 \quad (6)$$

And the horizontal momentum equations can be written as:

$$\rho \left(\frac{\partial u_1}{\partial t} + \frac{\partial(u_1 u_j)}{\partial x_j} - f u_2 \right) = - \frac{\partial p_{atm}}{\partial x_1} - g(\rho)_{x_3=\eta} \frac{\partial \eta}{\partial x_1} - g \int_z^\eta \frac{\partial \rho}{\partial x_1} dz + \frac{\partial}{\partial x_j} \left(\mu \frac{\partial u_1}{\partial x_j} \right) \quad (7)$$

$$\rho \left(\frac{\partial u_2}{\partial t} + \frac{\partial(u_2 u_j)}{\partial x_j} + f u_1 \right) = - \frac{\partial p_{atm}}{\partial x_2} - g(\rho)_{x_3=\eta} \frac{\partial \eta}{\partial x_2} - g \int_z^\eta \frac{\partial \rho}{\partial x_2} dz + \frac{\partial}{\partial x_j} \left(\mu \frac{\partial u_2}{\partial x_j} \right) \quad (8)$$

Where f and μ represent the Coriolis parameter, a parallel line to the surface elevation and the turbulent viscosity respectively. These are the equations solved by the model version used in this work. The non-hydrostatic pressure component permitted by MOHID would require extra computing power and is not relevant for the purpose of this work. Temporal discretization is done using a semi-implicit scheme – alternating direction implicit (ADI) with two time levels per iteration. The numerical schemes implemented include the Abbot's 4 equations system (Abbott et al., 1973), where the water level is computed at $\Delta t/2$ and the velocities at Δt , and the Leendertse's 6 equations system (Leendertse, 1967), where both the water level and the velocities are computed at $\Delta t/2$. Currently, and unless specifically indicated by a user, the model uses the latter.

Tracer properties such as temperature and salinity are calculated with the computed flow using:

$$\frac{\partial P}{\partial t} + \frac{\partial(P u_i)}{\partial x_i} = \frac{\partial}{\partial x_i} \left(v \frac{\partial P}{\partial x_i} \right) + S_P \quad ; i=1,2,3 \quad (9)$$

Where SP stands for sink-sources of the property (P) in question.

Six methods for horizontal and vertical advection schemes are implemented, and include the 1st, 2nd and 3rd order upwind schemes, a Total Varying Diminishing TVD scheme, the central differences and the leapfrog scheme. All the model applications present in this thesis were simulated using the TVD advection scheme – a combination of a high order scheme (in the case of MOHID, a hybrid between 1st and 3rd order upwind schemes) with a flux limiter – which is found to reduce spurious oscillations generated from shocks, discontinuities or sharp changes in bathymetry, by imposing monotonicity of the solution. The following flux limiter algorithms are implemented in MOHID: Superbee (Roe, 2003), MinMod (Roe, 2003), Van Leer (van Leer, 1974) and Muscl (van Leer, 1979). In this thesis, the limitation method considered was the Superbee – default method in MOHID – and the comparison of methods falls outside the scope of the thesis.

However, the existence of a number of different methods still in use is a sign that there is no method superior to all others for any given model application. As such, users are encouraged to perform a sensibility analysis of the different methods in order to choose the one that best suits their specific model application.

1.3 Communication between model grid domains

Hydrodynamics in the open ocean is commonly stable, with depths up to 1000 times greater than the surface elevation and density gradients which do not justify high resolution grid domains. However, near continental platforms, islands or any coastal areas characterized by highly variable depths, whose order of magnitude is 10 to 100 times the surface elevation, the pressure gradients become much more important than in the open ocean. Additionally, coastal areas are often subject to freshwater inputs, which greatly increase the density gradients. This increase in pressure and density gradients requires higher resolution grids in order to correctly compute these forces, which, in turn, increases the computational time of simulation. In structured semi-implicit finite volume modelling systems such as the MOHID, the transition between ocean and coastal areas is not feasible through the use of a single modelling grid, as the need for high resolution grid spacing near coastal areas implies a high resolution grid in the entire domain. Although structured grids allow for a high resolution near specific areas by reducing the spatial step, they still need to be applied to the entire length or width of the model grid (in order to be a structured grid). The computational effort required by this methodology would increase not only due to the number of grid cells, but also to stability demands, which would require the use of a time step suited to the lowest spatial step of the grid. One initial solution to this problem was proposed by Hill in (Hill, 1968), whereby a telescoping methodology would be used to overcome the computational effort required to simulate large areas with a high resolution model grid. The use of larger, courser model grid domains to provide initial conditions and open boundary conditions was (and still is to this day) the only feasible way to study lower scale processes at higher resolution. In the 70s, many developments were done in the coupling methods between grids and included, for example, the works of (Williamson and Browning, 1974) and (Davies, 1976) in the fields of atmospheric modelling. In the field of climate studies, (Dickinson, 1989) applied this downscaling approach to create a regional climate model for the Western United States, at a time when climate change was already a worrying issue for the scientific community, and was driven by the need to study potential

sites for nuclear waste repositories. On the ocean modelling side, downscaling by means of grid nesting can be traced back to 1989 in the works of (Spall and Robinson, 1989). Over the next decade, parallel developments were conducted by other authors (a review can be found in (Debreu and Blayo, 2008), with the study of a two-way coupling between model grids, especially for structured grids, in order to improve the courser grid domains. In this approach, an upscaling stage (or feedback operation) from the finer grid to the courser grid would follow a typical downscaling stage from the courser to the nested finer grid. Transferring results from smaller to larger scale reduces numerical diffusion in high gradient regions, but also allows the modification of the large-scale flow by local features, as is the case of tidal jets at the mouth of large estuaries, especially in tidal estuaries. This provides stronger mixing of the water column, changes the local Coriolis effect on the PD improving its horizontal and vertical solution, and changes the coastal transport. The downscaling and upscaling approaches will be addressed in detail in Chapters 2 and 3.

1.4 Thesis structure and rationale

The rationale of this thesis is based on the need to incorporate local features into regional model applications. To address this, the thesis provides an offline upscaling methodology – currently implemented in MOHID – which can be exported to other modelling systems, be it for hindcast or forecast purposes, with a clear mindset to improve existing modelling solutions and pave the road for new coupling techniques with watershed models. In its early days, this thesis included only an upscaling scheme designed for ocean models by means of relaxation over the overlapped area of a nested grid system. In its final form, it now includes a pilot implementation for an upscaling technique based solely on momentum discharges – which could be set as first coupling method between ocean and watershed models specifically applicable for underground fluxes along the shoreline.

This thesis is structured as follows, in addition to a short description:

Chapter 2: Describes the current downscaling philosophy implemented in the MOHID modelling system and in other existing models, and demonstrates its advantages and disadvantages as a modelling tool. Examples of this solution are presented, including the Tagus model application – nested in the Portuguese Coast Operational modelling system (PCOMS) – implemented at Maretec,

and a multi-nested grid modelling system for the Canary and Moroccan coast implemented during the MARPOCS research project.

Chapter 3: Describes the upscaling algorithm implemented in MOHID for online coupling, which nudges a regional model domain into a local domain. Online upscaling added to the traditional downscaling (two-way nesting) is compared to the standard downscaling approach using the implementation and domains defined in Chapter 2 – PCOMS and a Tagus estuary model application.

Chapter 4: Describes the upscaling algorithm implemented in MOHID for offline coupling, which nudges a regional model domain into a local domain. This algorithm is then applied to the nested system comprised of PCOMS and a Tagus estuary model application. Three PCOMS implementations are tested and include a version with one run per day of simulation with upscaling enabled, a version with two runs per day (increased grid communication between domains) and a version without upscaling the Tagus model application solution. Results provided by PCOMS and the Tagus estuary model application are then validated and the methodology is compared to the current offline downscaling approach.

Chapter 5: A new approach is described, in which upscaling via a momentum discharge is applied to a modelling system comprised of the PCOMS and several nested domains of approximations of Portuguese and one Spanish estuary, and its results are compared to the methodology developed by Campuzano (2018).

Chapter 6: Presents the conclusions of the thesis and describes the forthcoming work.

1.5 Related publications

Every chapter in this thesis has a correspondent publication, which include part or the majority of the methodology and results presented herein. Other publications, although not directly related to the thesis scope, they were relevant for the author's gain in knowledge and skill in implementation and analysis of models and their results.

The following are publications directly related to this thesis:

Chapter 2: Hilda de Pablo; João Sobrinho; Mariangel Garcia; Francisco Campuzano; Manuela Juliano; Ramiro Neves. 2019. "Validation of the 3D-MOHID Hydrodynamic Model for the Tagus Coastal Area". *Water* 11 (8): 1713-1713. <https://doi.org/10.3390/w11081713>.

Includes part of the results presented in this thesis, and contributions from the author in the implementation and simulation of the model.

Chapter 3: Sobrinho, J., de Pablo, H., Pinto, L., and Neves, R. (2021). Improving 3D-MOHID water model with an upscaling algorithm. *Environ. Model. Softw.* 135. doi:10.1016/j.envsoft.2020.104920.

Includes the methodology and results presented in the thesis. Contributions of the author include software development and validation, implementation and simulation of the model domains as well as the analysis of the results.

Chapter 4: Sobrinho, J., de Pablo, H., Pinto, L., and Neves, R. (2021). Upscaling local domains in regional domains: an offline approach. *Environ. Model. Softw.* (Submitted).

Includes the methodology and results presented in the thesis. Contributions of the author include software development and validation, implementation and simulation of the model domains as well as the analysis of the results.

Chapter 5: Sobrinho, J., de Pablo, H., Campuzano, F., Neves, R., 2021. Coupling Rivers and Estuaries with an Ocean Model: An Improved Methodology. *Water* 13, 2284. <https://doi.org/10.3390/w13162284>

Includes the methodology and results presented in the thesis. Contributions of the author include software development and validation, part of the implementation and simulations of the model domains as well as the analysis of the results.

The following were published during the course of this thesis and were important for the author's gain in knowledge and skill in implementation and analysis of models and their results:

- Rhomad, H., Khalil, K., Neves, R., Sobrinho, J., Dias, J.M., Elkalay, A., Hbid, M.L., Ettahiri, O., Bougadir, B. (2021). Three-dimensional hydrodynamic modelling of the Moroccan Atlantic coast: A case study of Agadir bay. *Estuarine, Coastal and Shelf Science*. (Submitted)

This work includes the model implementations designed and implemented by the author, whose brief description and validation (although not for the Agadir bay) are presented in Annex.

- Desmit X, Thieu V, Billen G, Campuzano F, Dulière V, Garnier J, Lassaletta L, Ménesguen A, Neves R, Pinto L, Silvestre M, Sobrinho JL, Lacroix G. Reducing marine eutrophication may require a paradigmatic change. *Science of The Total Environment*. 2018; 635: 1444-1466

In this publication and in the work related to it, the author contributed with the collection of all the river flow and its water parameters for all Portuguese rivers included in the study, as well as with the implementation and simulation of all reduction scenarios using the eularian approach in the PCOMS model domain and many of the lagrangian simulations for the tracking of nutrient trajectories from the Portuguese rivers.

- Brito D, Campuzano FJ, Sobrinho J, Fernandes R, Neves R.,2015. Integrating operational watershed and coastal models for the Iberian Coast: Watershed model implementation – A first approach. *Estuarine, Coastal and Shelf Science*, 167(2015), pp. 138-146. <https://doi.org/10.1016/j.ecss.2015.10.022>

In this publication the author contributed with the production and analysis of some of the results such as the impact of the dams in the flow rate of the Tagus river.

CHAPTER II

Part of the results provided in this chapter originated the article:

de Pablo, H., Sobrinho, J., Garcia, M., Campuzano, F., Juliano, M., and Neves, R. (2019b). Validation of the 3D-MOHID Hydrodynamic Model for the Tagus Coastal Area. *Water* 11, 1713. doi:10.3390/w11081713.

Chapter 2 Downscaling from regional to local domains – a proven solution

2.1 Introduction

When regional ocean model applications first emerged, the main issues involved the initial and open boundary conditions, which are essential for any model to reproduce physical processes represented by their equations as a reasonable approximation of reality. As these model applications did not cover the entire globe, an open boundary condition with the ocean was created, where velocities, surface elevation, and every water property simulated had to be known at the exterior of the model grid, so fluxes could be computed.

A clear example is tide propagation. Global tide models have similar issues with global circulation models related to their grid resolution and the processes they are able to represent. As such, they lose accuracy near some coastal areas where small depths and bathymetric variability produce flow regimes strongly influenced by non-linear processes (Lefevre, 2000). This issue is solved by nesting higher resolution regional domains that imposed the global tide models at the open boundary, and propagate it near the coast.

Since the first regional ocean models in the 70ss, a number of formulations for the definition of these exterior values and the computation of fluxes across the open boundary were developed and set the bases of modern approaches. In the late 90s early 2000s, exterior values could be obtained from 3 sources: from measured data (in-situ, remote or a combination of both), from simplified equations, or from a reference solution obtained by a larger model application domain. However, the growth in data assimilation schemes and amount of available data from satellite (altimetry, SST) and in-situ (including depth profiles from the ARGO floats) improved the first approach, but the methodology shifted towards model initialization and upkeep of the interior domain, driven by improving global modelling solutions. As such, the main options for computation of the external values now include the use of simplified equations and reference solutions.

The downscaling approach is defined in this thesis, as the use of a larger, courser grid model application as the reference solution for the finer resolution grid (one-way nesting). This section

briefly describes the existing open boundary conditions and the current algorithms implemented in the MOHID modelling system for one-way implementations.

2.1.1 Downscaling from Regional to Local domains

As mentioned in the introduction chapter, modelling systems such as the MOHID, which solve the continuity and momentum equations for structure grids using finite volumes, cannot make a computationally viable transition from ocean to coastal areas and to estuaries. This lack of viability comes from the fact that pressure and density driven forces near coastal areas – influenced by higher bathymetric gradients and lower depths – generate local scale processes that can only be accurately resolved with lower grid steps. It was also mentioned that these grids are allowed to reduce their grid step in both directions. However, in order for these grids to be structured a grid cells needs to know before-hand its neighbouring cells – as the numerical code computes all forces by computing differences between adjacent cells. If these grids were not structured, then link matrixes indicating the IDs of all adjacent cells for each grid cell would be required, making the programming more difficult and much slower computations. Even the numerical schemes would need to change as the same cell face would now be able to receive fluxes from more than one adjacent cells, also complicating the overall computations. The use of such unstructured grids is more commonly found in explicit schemes, whose numerical properties do not require matrix inversions (which is responsible for the majority of the computational time in implicit methods). These methods do require much lower time steps, whose numerical stability is restricted to the Courant–Friedrichs–Lewy (CFL) condition, but as the computational power along with parallel methodologies such as MPI, openMP and the use of GPUs increases, so does the efficiency of these explicit methods. In any case, the existence and application of both methodologies only proves that neither solution provides the best solution for every application.

Back to the structured grids, there are only two ways to increase grid resolution in a specific area of a model domain: reducing the grid step along an entire strip of the domain; or using curvilinear grids. The first solution implies a smaller grid step in an area much larger than required (Figure 2), while the second is better suited for smaller estuaries and for the simulation of meandering rivers where these grids can follow the river flow with less need for interpolations and less numerical cells.

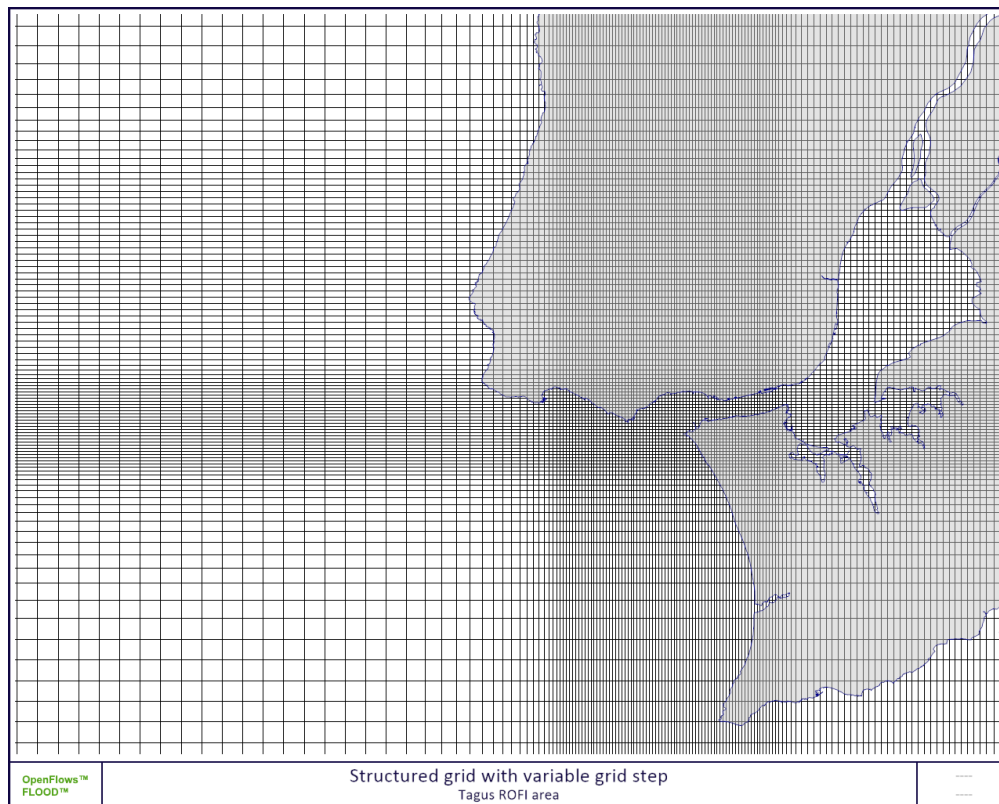


Figure 2: Structured grid with variable grid step, implemented in the Tagus ROFI modelling system running at Maretec. This grid has a higher grid resolution at the mouth of the estuary at the expense of higher resolution in open waters.

With the increase in demand for local scale modelling solutions by government agencies, aquaculture, energy companies, ports and navies (both merchant and military), private and public entities are pressured to develop updated grid domains for coastal areas. Higher resolution nested grids lead to better numerical skills of the model and allow the use of more refined bathymetric and atmospheric data, improving the overall hydrodynamic solution and reducing the errors of the downstream transport models. This higher level of detail allows a direct comparison between very local field data (e.g. currents) and model results, increasing the modelling system's confidence.

Downscaling from a parent domain (PD) to a child domain (CD) is still the most common option to simulate the effect of large-scale on local processes in the MOHID Water model (Campuzano, 2018; Fossati and Piedra-Cueva, 2013; G. Franz et al., 2014; Franz et al., 2016; Gutiérrez JM et al., 2015; Huhn et al., 2012; Janeiro et al., 2017) and in many other structured grid models such as ECO-MARS3D (Desmit et al., 2018), MIKE3 (Gallego et al., 2017), POM (Nagy et al., 2017), NEMO (Katavouta and Thompson, 2016), ROMS (Dabrowski et al., 2014), and Delft3D (Yin et al., 2019). When using this methodology, care must be taken to avoid drifting of the (CD) over time or instabilities will be produced at the border. Drifting can occur

due to local features not reproduced by the parent domain, noise created inside the child domain which is not kept under control, and loss of properties mass conservation at the open boundary. These issues are addressed in (Debreu and Blayo, 2008; Flather, 1976; Palma and Matano, 1998), where a number of solutions are provided to preserve mass conservation, control noise at the open boundary and to smooth the transition between parent and child solutions. The most common solutions for downscaling systems include the use of a Flather (Flather, 1976) boundary condition for the barotropic flow, allied with a radiation scheme such as that described in Marchesiello et al. (Marchesiello et al., 2001) and a flow relaxation scheme described by Martinsen and Engedahl (Martinsen and Engedahl, 1987). Another option commonly considered is the use of a biharmonic filter described by Kantha and Clayson (Kantha and Clayson, 2000). This filter (included in MOHID via eq. (10) works by adding a term to the horizontal turbulent viscous flux, filtering high frequency oscillations with wave-length equal to one or two widths of the horizontal grid step.

$$J = -K \cdot \nabla C + \nabla_h (\kappa_4 \nabla_h^2 C) \quad (10)$$

where J represents the horizontal turbulent viscous flux, K is the Laplacian diffusion tensor, C is the concentration of a given property, κ_4 is the horizontal coefficient for biharmonic mixing, and ∇_h is the horizontal isopycnic part of the ∇ differential operator (Delhez and Deleersnijder, 2007). To facilitate the performance of these techniques, the boundary between nested domains should be far enough from local hydrodynamic features. This way, nested domains will produce comparable results in the interface, allowing for easier radiation of outgoing waves and the elimination of noise produced in the child domain.

2.1.2 Open boundary conditions for downscaling

Downscaling from a regional model domain (PD) requires an open boundary condition (OBC) in the nested, high resolution grid domain (CD) for surface elevation, velocities, and other water properties (e.g. temperature) included in the model application. This communication flow is commonly called one-way nesting.

Figure 3 shows an example of a downscaling implementation where a higher grid resolution CD is nested in a lower grid resolution PD. In this case, in order to compute u_{CD} , the CD will need the PD's water level η_{PD} – used in the barotropic force term of the momentum equation. Velocities u_{PD} and v_{PD} will also be required for the computation of the boundary advective and diffusive fluxes in the u direction, and v_{PD} is used in the Coriolis effect.

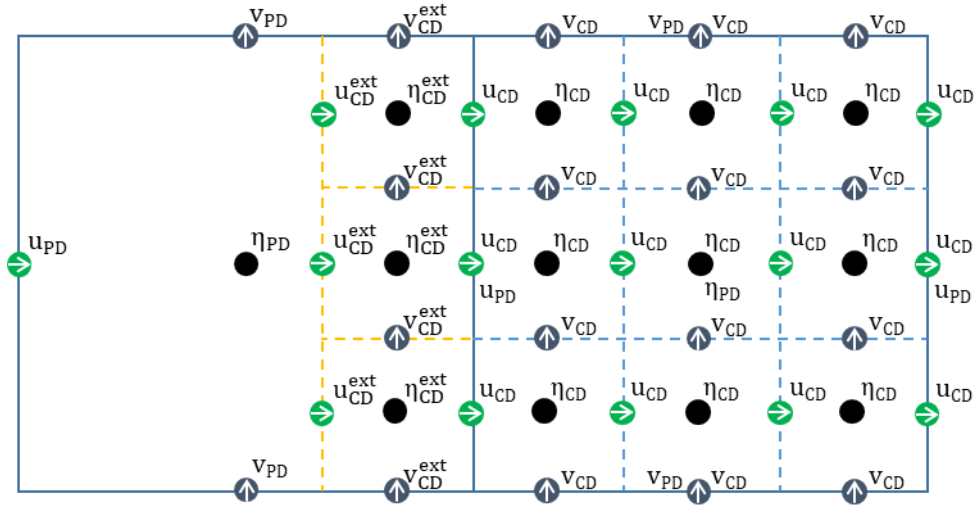


Figure 3: Schematic representation of an open boundary a PD and its nested CD on an Arakawa C grid.

Each of these CD variables can have its own boundary condition to determine the exterior value from the PD reference solution. Two main methodologies have been implemented to obtain the exterior value. The first obtains it directly from the interpolation of the PD's variables at the open boundary, while the second computes it using radiative equations (Palma and Matano, 1998; Perkins, 1997) – where the reference solution is the PD. Imposing water levels and velocities at the boundary, using a Dirichlet condition, is easier to program and computations are made faster due to its simplicity. However, these conditions only impose the variables used at the boundary – active condition – and because the CD solves scales smaller than those solved by the PD, reflections will occur at the open boundary of the CD and propagate to its interior, destroying flow patterns of the solution (Koch and McQueen, 1987; Marchesiello et al., 2001; Palma and Matano, 2000). During the late 90s and early 2000s new solutions were developed and validated, considering the two other methodologies for OBCs in nested one-way systems, which are still in use nowadays and are also implemented in MOHID.

Radiative schemes can act both as active and passive conditions. The most straightforward use of a radiative scheme is the null gradient OBC in which u_{CD}^{ext} is set equal to u_{CD} therefore removing any gradient at the open boundary between PD and CD. However, this option is less used in downscaling from larger domains, as it does not make use of the PD's solution. When the CD simulates additional properties such as nutrients or sediments which the PD does not simulate, then the null gradient condition can become a good option for short simulation periods. For longer periods if there are sources of a property inside the domain – such as a river – then these properties will accumulate over time, producing unrealistic solutions. They

accumulate because an increase in the interior of the domain inherently leads to the increase in the exterior value – to keep a null gradient. Therefore, an outgoing flow will increase the properties' concentrations near the open boundary, and the following incoming flow will bring higher concentration values – increasing the total mass and creating unrealistic solutions.

Hybrid schemes that take the PD domain as an external solution to which the CD is radiated consist on an active condition for when the flow is entering the CD from the PD, and a passive condition otherwise. While the active condition forces the CD, the passive conditions allow perturbations generated in the CD to exit through the open boundary without being reflected back into the CD. The use of only active or only passive conditions inherently lead to the drifting of the two nested model domains over time. As such, hybrid schemes – with an active and a passive condition – are the most commonly used. Two main hybrid radiative schemes are implemented in MOHID for exterior value of the water level: the Blumberg and Kantha (Blumberg and Kantha, 1985):

$$\frac{\partial \eta}{\partial t} + \left(\vec{c}_E \cdot \vec{n} \right) \nabla \eta = \frac{1}{T_d} (\eta_{ext} - \eta) \quad (11)$$

and the Flather (Flather, 1976):

$$\mathbf{q} - \mathbf{q}_{ext} = (\eta - \eta_{ext}) \left(\vec{c}_E \cdot \vec{n} \right) \quad (12)$$

where η and η_{ext} stand for interior and exterior water level, \vec{n} the direction perpendicular to the open boundary, c_E the celerity of the perturbation to be radiated, T_d the decay time for nudging to η_{ext} , \mathbf{q} and \mathbf{q}_{ext} the interior and exterior specific flows. Both of these solutions have their advantages and disadvantages. Many of these are evaluated in (Leitão, 2002) whose experiments with MOHID and the accumulated experience at Maretec proved that when a reference solution is available – such as the case of a CD in a nested system – the Flather boundary conditions produces a better solution. This radiative condition is constantly correcting the water level to the reference level, ensuring that the nested model does not drift from the reference solution while keeping conservation errors at a minimum. On the other hand, the Blumberg and Kantha provides a better solution when only the water level is present in the reference solution. Nowadays the majority of nested applications for coastal areas using MOHID use the Flather condition, as the number and area covered by regional domains increase. In both OBC radiative schemes, the passive component is determined by the celerity

(c_E) – which is basically a propagation velocity – of the perturbation coming from the interior of the domain. Typically, it is assumed that perturbations in water level propagate as external waves with a celerity of \sqrt{gh} .

The barotropic velocity at the exterior of the CD is computed from the water level obtained with (eq 5 e 6), using:

$$\begin{aligned} q_{\text{barotropic}} &= -\frac{\partial \eta}{\partial t} H_b + q \\ v_{\text{barotropic}} &= q_{\text{Barotropic}} / H_b \end{aligned} \quad (13)$$

where H_b represents the depth at the boundary.

As for baroclinic velocities, the use of a radiative scheme is important in highly stratified flows, which can more easily produce internal waves. If these internal waves are not radiated outwards, the stratification will slowly be destroyed. In these conditions it is important to accurately compute the baroclinic velocity due to its impact in the vertical fluxes at the open boundary. Radiation of baroclinic velocity is achieved the same way as for the water level, with a radiative scheme similar to that of Blumberg and Kantha plus a nudging term (Marchesiello et al., 2001):

$$\frac{\partial v_{\text{baroclinic}}}{\partial t} + c_{Ix} \frac{\partial v_{\text{baroclinic}}}{\partial x} + c_{Iy} \frac{\partial v_{\text{baroclinic}}}{\partial y} = \frac{(v_{\text{baroclinic}}^{\text{ext}} - v_{\text{baroclinic}})}{T_d} \quad (14)$$

where c_{Ix} and c_{Iy} stand for internal wave celerity in the x and y direction, and T_d the time decay for relaxation towards the exterior (reference) baroclinic velocity. The use of a nudging term ensures that the CD does not drift from the PD, while the radiative terms allow the dissipation of internal perturbations in the density vertical structure.

The celerity of a perturbation in the density field is harder to calculate as it depends highly on the vertical and horizontal gradients of density. There are three possible ways to compute this celerity. While the first considers it proportional to the water depth:

$$c_I = \sqrt{10^{-3} \cdot gh} \quad (15)$$

as proposed by (Oey and Chen, 1992), the second uses simplified equations such as the two layer equations for reduced gravity, resulting in:

$$c_I = \sqrt{g' h_s}; g' = g \cdot \Delta \rho / \rho_0 \quad (16)$$

where h_s is the depth of the surface layer, $\Delta \rho$ stands for the density gradient between the two layers and ρ_0 the density of the surface layer. As it stands, this celerity considers only the first

baroclinic mode – because it considers a constant vertical celerity. Assuming that the majority of internal oscillations are linked to the first baroclinic mode, this option provides a simple and effective computation of the celerity. However, these two options do have limitations when forces such as Coriolis, wind or bottom stress or are present. In fact, these options consider that the pressure force is mainly responsible for the oscillations in the baroclinic field at the open boundary. When effects such as the wind, the bottom stress or the Coriolis – separate or combined – produce forces of the same order of magnitude as the barotropic pressure force, then the internal celerity will fail to reproduce the internal oscillations, generating new perturbations to the baroclinic field. A solution to this problem is to compute the internal celerity using the internal variability of the CD's baroclinic velocity field, as proposed by Orlanski in (Orlanski, 1976), added to a nudging term suggested by (Marchesiello et al., 2001):

$$\frac{\partial P}{\partial t} + c_x \frac{\partial P}{\partial x} + c_y \frac{\partial P}{\partial y} = \frac{P_{ext} - P}{T_d} \quad (17)$$

where T_d stands for the time decay, which has 2 two values, one T_{dout} for when the direction of the propagation is outwards ($c_x < 0$) and another T_{din} for an inward propagation. The objective of this nudging term is to reduce the impact of strong shifts in the propagation direction and intensity which could create instabilities, while still allowing outward propagation of internal waves. This is accomplished by setting T_{dout} much higher than T_{din} . With this in mind, the two directional celerities are computed using:

$$c_x = \frac{\Delta P_t \times \Delta P_x}{\Delta P_x^2 + \Delta P_y^2} \quad (18)$$

$$c_y = \frac{\Delta P_t \times \Delta P_y}{\Delta P_x^2 + \Delta P_y^2} \quad (19)$$

To trace properties such as temperature and salinity an open boundary condition similar to that of the baroclinic velocity is applied:

$$\frac{\partial P}{\partial t} + (v_x + c_{lx}) \frac{\partial P}{\partial x} + (v_y + c_{ly}) \frac{\partial P}{\partial y} = \frac{1}{T_d} (P_{ext} - P) \quad (20)$$

The boundary conditions discussed so far consider the radiation of perturbations produced inside the CD and the computation of the external boundary values for water level, velocities and water properties such as temperature and salinity. However, in order to produce a smooth transition of information from PD to CD as well as prevent long-term drifting of the CD, a flux

relaxation scheme proposed in (Martinsen and Engedahl, 1987) was also added. This scheme is applied to the entire overlapped area of the nested domains, and nudges the CD's variables to the PD over a strip (of n CD cells) parallel to the open boundary, using a space varying decay time – higher at the open boundary, decaying linearly or exponentially until the N th cell from the boundary, and lower thereafter inwards. This equation is applied to every variable, although with some differences in water level and velocities. A summary of all the open boundary conditions and nudging equations applied to the interior of the CD, implemented for nested domains in MOHID is presented in Table 2.

Table 2: Boundary conditions implemented in the MOHD Modelling system.

Open Boundary	Open Boundary condition	Nudging condition interior of the domain
Water level	$\frac{\partial \eta}{\partial t} + \left(\vec{c}_E \cdot \vec{n} \right) \nabla \eta = \frac{1}{T_d} (\eta_{ext} - \eta)$ $\mathbf{q} - \mathbf{q}_{ext} = (\eta - \eta_{ext}) \left(\vec{c}_E \cdot \vec{n} \right)$	$\eta^{t+\Delta t} = \eta^* + (\eta^{ext} - \eta^*) \frac{\Delta t}{T_d}$
Barotropic velocity	$\mathbf{q}_{barotropic} = -\frac{\partial \eta}{\partial t} H_b + \mathbf{q}$ $\mathbf{v}_{barotropic} = \mathbf{q}_{Barotropic} / H_b$	$\frac{\partial \mathbf{v}}{\partial t} = \sum F + \frac{\mathbf{v} - \mathbf{v}_{ext}}{T_d}$
Baroclinic velocity	$\frac{\partial \mathbf{v}_{baroclinic}}{\partial t} + c_{lx} \frac{\partial \mathbf{v}_{baroclinic}}{\partial x} + c_{ly} \frac{\partial \mathbf{v}_{baroclinic}}{\partial y} =$ $\frac{(\mathbf{v}_{baroclinic}^{ext} - \mathbf{v}_{baroclinic})}{T_d}$	
Water properties	$\frac{\partial P}{\partial t} + (\mathbf{v}_x + c_{lx}) \frac{\partial P}{\partial x} + (\mathbf{v}_y + c_{ly}) \frac{\partial P}{\partial y} = \frac{1}{T_d} (P_{ext} - P)$	$P^{t+\Delta t} = P^* + (P^{ext} - P^*) \frac{\Delta t}{T_d}$

2.1.3 The offline downscaling methodology

The downscaling methodology described in the previous sections consisted of an online coupling mode, meaning that PD and CD are run simultaneously, with transfer of information from PD to CD at the frequency of the CD time step (via time interpolation of the PD solution). From a coupling point of view, this methodology is more accurate as information is transferred at high frequency. Yet, from every other angle, this option is costlier. Take for instance an

implementation of a modelling domain in a coastal area, whose exterior values for open boundary conditions are provided by a regional domain. In this case, when the modeller needs to test different parametrizations of the CD or when a new process needs to be added (e.g. a different turbulent parametrization, or a fresh water discharge), they will need to run both models again when the only change occurs in the CD. This would also render impossible the use of CMEMS solutions as the modeller would need to run those models as well. Now, consider a modeller or organisation that needs to implement several CDs nested in the same PD, applied to different local areas with different processes and parametrizations. In this case, the same institution would be running several instances of the same PD, which would be inefficient both in computational time, hardware allocation, and storage of information. Finally, the most critical aspect is related to operational modelling used in forecasting systems. These systems must be as efficient as possible in order to provide a forecast at a frequency useful for the general public with as little maintenance costs as possible. As such, if local domains need to run in a coupled manner, they will require much more hardware, as each implementation includes the processor power, disk storage, and memory available of both PD and CD. Similar to other entities, Maretec is running many operational modelling systems (some 28, including currents, biogeochemical cycle, and waves) providing forecasts for the majority of the Portuguese estuaries, the Portuguese coast, and the Portuguese Exclusive Economic Zone, all using the downscaling methodology (Figure 4). With an online downscaling methodology, these solutions would require an immense amount of computational power. The solution to the duplication of work was to run these local CDs in an offline manner, taking information from a single PD implementation (Campuzano et al., 2012; Mateus et al., 2012b). Transfer of information is done via HDF files produced by the PD with fields of water level, velocities, temperature, salinity, nutrients and primary producers with a typical frequency of 15 min. This offline methodology allows for multiple nested grids each running in the same computer (or using more computational power per application), leaving more room for optimization of the operational systems. During this thesis, a practical implementation of the offline downscaling approach was implemented during the [MARPOCS](#) project and included several nested domains which covered a good part of the Moroccan coast, the Canary Islands and the Madeira Islands, with the objective of providing reliable currents for use in a platform for oil and HNS spill tracking, backtracking and coastal risk assessment. An overview of the implementation and its results is presented in Annex. The main objective of this thesis is to provide a similar

independence for upscaling local domains into regional domains, as a two-way coupling system would inherit all the issues discussed until now.

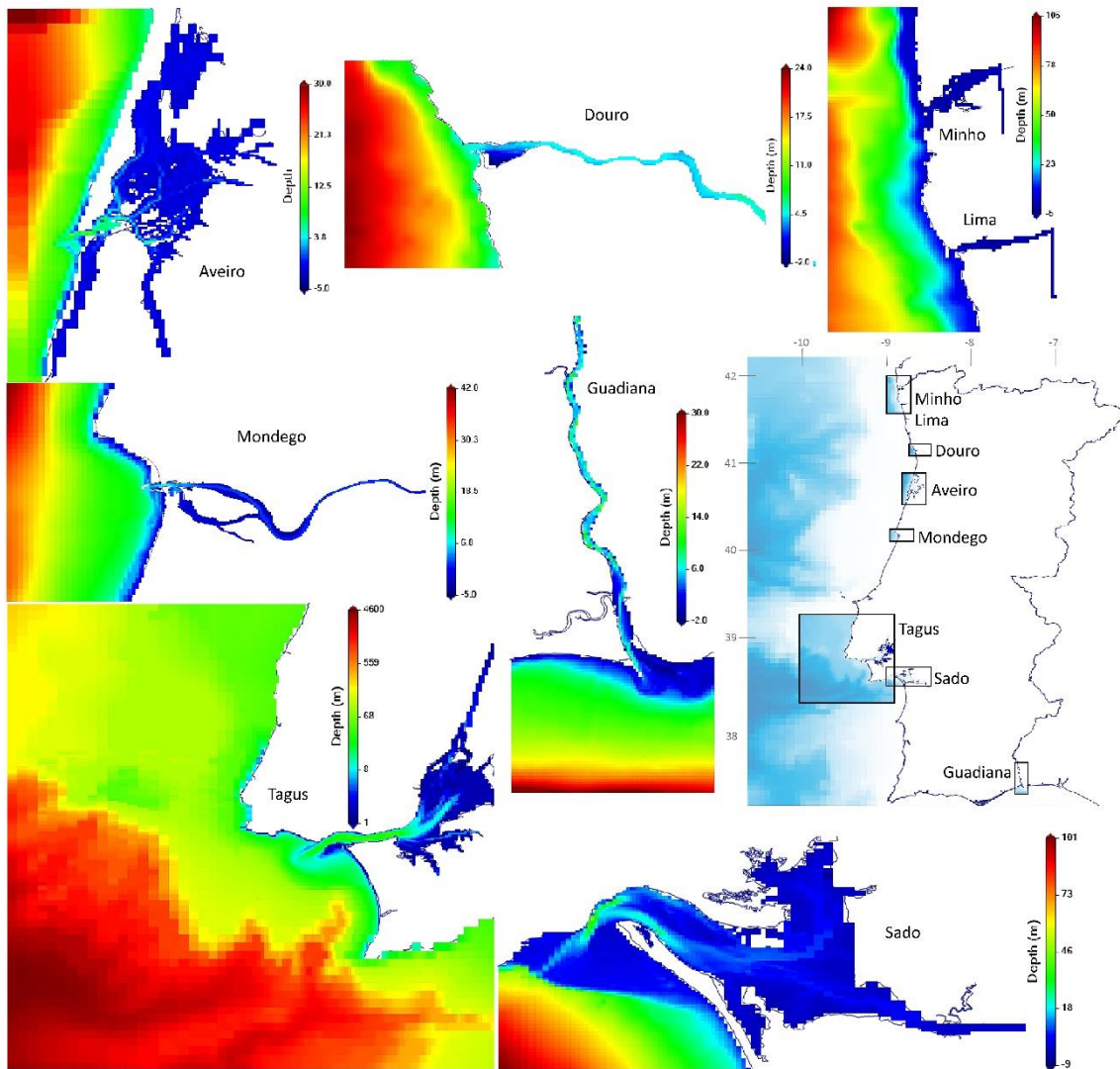


Figure 4: Bathymetry and model domains of the offline downscaling systems running at Maretec for the Portuguese coast. The Tagus application provides outputs for other nested domains, also using the offline methodology.

2.2 The PCOMS – Tagus ROFI modelling system

This section starts with an overview of the major processes occurring in the coastal area where the Tagus estuary is located, and a description of Maretec’s offline downscaling system implemented for this area. Then, an overview of the validation of the system is made, followed by a description of the modelling system’s contribution to coastal management and decision

making over the years. The section concludes with a more thorough analysis of the grid coupling and the downscaling drawbacks of the system.

2.2.1 The study area

2.2.1.1 General circulation of the west coast of the Iberian Peninsula

Extending from Cape São Vicente (37°N) to Cape Finisterre (43°N) (Figure 6) at a longitude of 9°W, the Western Iberian coastal circulation is linked to the North Atlantic atmospheric circulation, whose major driving force is the North Atlantic Oscillation (NAO). This oscillation is created by an atmospheric pressure gradient between a low pressure system in Iceland and a high pressure system in the Azores (Ottersen et al., 2001; Hurrell and Dickson, 2005). The seasonality and intensity of this oscillation is due to the relative position of the two pressure systems. As winds rotate clockwise in a high pressure system and counter clock-wise in low pressure systems, westerly winds are dominant in the intersection area between the two centres (Figure 5). The atmospheric patterns in the Western Iberian Peninsula are highly dependent on the location of these two pressure systems. During winter, the Azores High moves southeast, and the Western Iberia Peninsula becomes dominated by westerly winds. In the summer, the Azores High moves North up to 45°N and the Peninsula is dominated by northerly winds (due to the clockwise rotation associated to a high pressure system). The ocean circulation is determined by these pressure systems. The dominant winds during summer are responsible for an equatorward flow (Fiúza et al., 1982) and combined with the effect of the Coriolis force drives surface waters offshore upwelling deep, cold waters to the surface near the coast (Fiúza, 1983; Ruiz-Villarreal, 2002). During autumn and winter, when the Azores High moves southeast, the northerly winds lose strength and the weak southeast winds predominant winds are associated with a generally poleward current (Portugal Coastal Counter Current; Ambar and Fiúza, 1994) as well as the Iberian Poleward Current (IPC; Peliz et al., 2005). During this winter period, fresh water discharges from the major north-western Iberian rivers (Mondego, Aveiro, Douro, Lima, Minho and the Galician Rias), producing a strong surface freshwater plume with an upper salinity limit below 35.7–35.8, called West Iberia Buoyant Plume(WIBP), causing stratification of the surface waters near the coast along with strong haline fronts (Peliz et al., 2005, 2002).

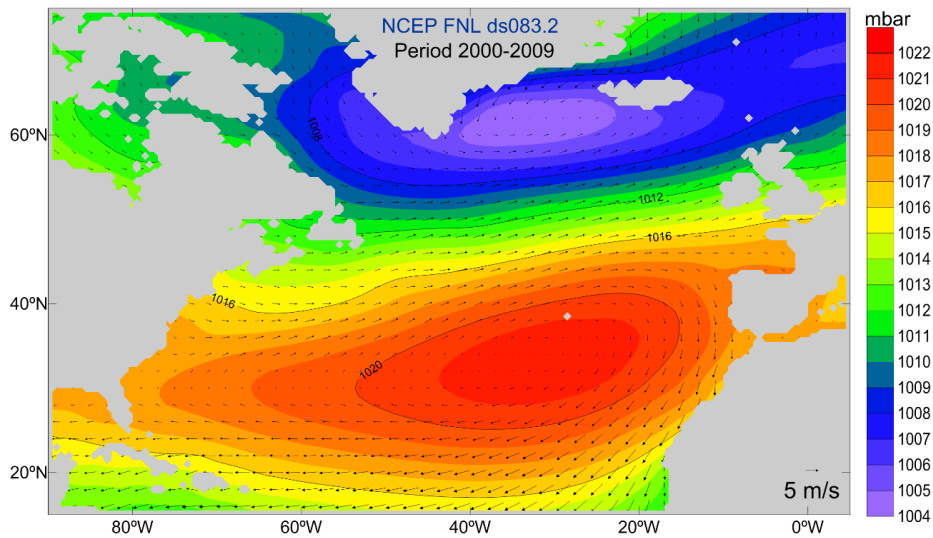


Figure 5: The Azores high pressure system and the Icelandic low pressure system, and their impact in wind patterns of the North Atlantic. Adapted from (Campuzano, 2018).

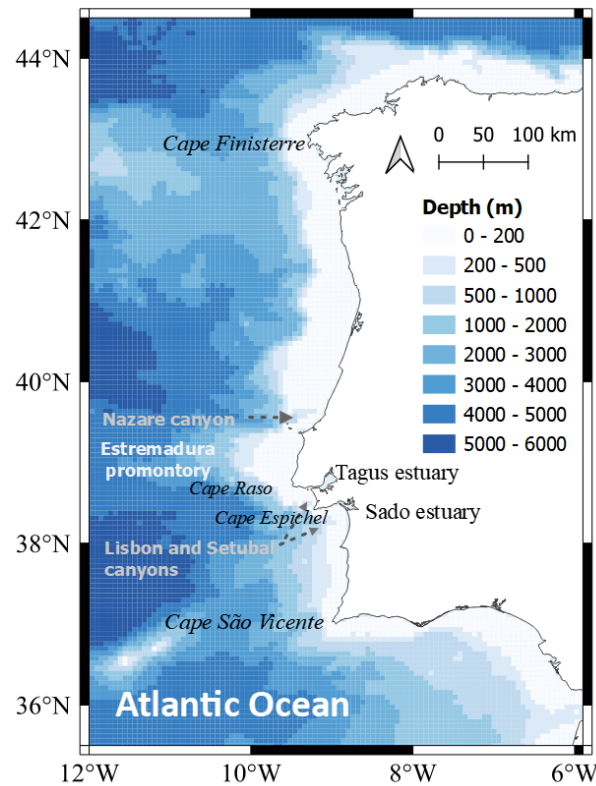


Figure 6: Main geomorphological features off the West Iberian Coast

In the vicinity of the Tagus estuary, the surface circulation is determined by the general circulation patterns previously described, as well as by bathymetric features such as the continental platform (Jouanneau et al., 1998) and the estuary itself. The coastal zone includes 70 km of continental shelf, limited to the north by the Cape Raso and south by Cape Espichel, and is influenced by the Lisbon, Cascais and Sado submarine canyons, as well as the Estremadura promontory and the Tagus plateau (Figure 6).

One example of the impact of these features is the Estremadura promontory link to a diurnal continental shelf wave (CSW) trapped in the Tagus plateau, whose formation and intensity are highly dependent on the bathymetry of the region (Fortunato et al., 2002; Quaresma and Pichon, 2013).

Furthermore, internal waves can be found in this area, due to both the Lisbon canyon and the Tagus plateau. They create extensive areas with strong bathymetry gradients (100 m to 2000 m over a short distance), which are responsible for the vertical advection of deeper water to the surface during ebb tide and to the bottom during the flood tide (Leitão, 2002). The area is also known for upwelling events associated to northerly winds, as well as due to jet-like flows whose extent can sometimes reach 20 km from land (Moita et al., 2003). The joint effect of these features is responsible for the extremely dynamical circulation in this adjacent coastal area, which is only possible to understand through the use of numerical models.

2.2.1.2 The Tagus estuary

Located in southwest Portugal (30.6° N–9.5° W), crossing Lisbon and with a surface area of 320 km², of which 40% is intertidal (Fortunato et al., 2017), an average depth of 5.1 m (Fortunato et al., 1999) and a volume of 1.9×10^9 m³ (Guerreiro et al., 2015), the Tagus estuary is one of the largest estuaries in Europe. Tides with an average amplitude of 2.4 m in the river mouth with the tidal range varying from 0.9 m to around 4.1 m during neap tides and spring tides, respectively (Gameiro et al., 2007), set it as mesotidal estuary. Its large tidal flats are also responsible for its definition of an ebb dominated estuary – longer periods for ebb than for flood – (Fortunato et al., 1999). Tidal fluxes are more intense near the estuary mouth, a 12 km long and 2 km wide channel that has been found to form a NE-SW oriented talweg (Fernández-Nóvoa et al., 2017). The Tagus river, which is its main source of fresh water, has a mean flow of 258 m³s⁻¹ measured by a hydrometric station upstream (<http://snirh.apambiente.pt>) from 2006 to 2018, representing about 2% of the tidal prism. Although average flow values are not enough to cause stratification of the water column, extreme flow values during storms can produce flow values that have reached 15000 m³s⁻¹. This thesis is focused in the 2013 extreme event which generated a flow of almost 9000 m³s⁻¹ and submerged the hydrometric monitoring buoy used to estimate the flow.

The Tagus region of fresh water influence (ROFI) is a typical coastal area where the transfer and accumulation of particulate and dissolved matter from land to ocean (Henrichs et al., 2000)

– both sediments and nutrients – is of extreme importance to the biogeochemical cycle and geomorphologic evolution of the surrounding areas. More studies on the hydrodynamic features of the estuary can be found in (Canas et al., 2009; Dias et al., 2013; Fortunato et al., 1999; G. Franz et al., 2014; Leitão, 2002; Vaz et al., 2015).

2.2.2 The MOHID Tagus ROFI modelling system as a tool for research studies, coastal management, and decision making

The Tagus ROFI was chosen in this thesis because it is the most studied marine system by means of modelling, not only by the Maretec group but also by many other research centres, universities, companies, and state laboratories. This was extremely important to understand possible issues related to an upscaling algorithm by analysing the results it provided with knowledge acquired over the years.

Even if in the beginning of these studies the focal point was the hydrodynamics and sediment transport, it later became clear that a multidisciplinary effort was necessary, and that was reflected, as pointed out in (Leitão, 2002) in the scientific projects tackling this ROFI, such as that of Maretec, which soon began to build a multidisciplinary team composed of biologists, physicists, engineers specialized in several different areas including sediment transport, hydrodynamics, biogeochemical cycle, benthonic systems, meteorology, programming languages and data visualization/processes. Early studies were mainly focused on the hydrodynamic features of the ROFI, but due to the Tagus estuary pollution levels many studies began to analyse the water quality processes, of which the work of (Rodrigues et al., 1982), who used a 2D model for currents and water quality evaluation, is pioneer. In Maretec, the first version of the modelling software was developed in 1985 by Neves (1985) and applied to the Tagus estuary by the Maretec spinoff Hidromod to provide engineering answers for fluvial terminals (Hidromod, 1997, 1996) and a submarine outfall (Hidromod, 1998a). In Maretec's history, this submarine outfall (Guia) located off the coast of Cascais has, in part, been the driver of the development of new features of MOHID as well as many downstream applications using its results for decision making processes, constantly in collaboration with the SANEST water utilities company (responsible for the outfall). Of these studies and applications, the most relevant ones include: (Neves, 1998) whose modelling approach integrated in a monitoring program allowed for a derogation (EEC, 2001) regarding urban waste water treatment for the agglomeration of the Estoril coast; (Neves et al., 2002), who presented a broader view of the

entire system – sewage transport, dispersion through the emissary, dilution in the receiving waters and methodology for monitoring the impacts over time. Benefiting from the work of (Leitão, 2002) who continued the works of (Martins, 1999; Neves, 1985; Santos, 1995), the objective of these studies was to support the monitoring campaigns on the Estoril Coast and near the submarine outfall's diffuser, as well as to improve the knowledge of the hydrodynamic processes dominant in the area, whose importance is critical for explaining the spatial and temporal variability of the measured parameters (such as nutrients, heavy metals and bacteria). Later these modelling implementations were made operational, providing forecasts which allowed for the creation of a basis for an alert system for the Estoril coast (Viegas and Nunes, 2009) and an operational implementation was implemented in 2012 during the LENVIS project (LENVIS: Localised Environmental & Health Information Services lenvis.eu). This time offline downscaling was already being used, allowing for faster implementations, with grid domains running in different computers. Another important use case of MOHID as a tool for management and decision making processes focused on the Tagus estuary itself, including the interdisciplinary work of Maretec (IMAR, 2007) for the characterization of the nutrient loads from several WWTPs and the estuary river inputs. These studies were part of services provided to the water utility companies SIMTEJO, SIMARSUL between the mid-2000s and 2013 all related to the characterisation of the WWTPs impact in the estuary as well as the study of reduction scenarios. The management plan of the Tagus estuary (POE) also benefited from the use of this modelling system whose contribution was focused in the water quality processes in the estuary (REF??). On the side of research projects, these were fundamental for the future services and use cases of modelling as a tool for decision making, due to their inheriting model developments. One of the earliest and most important for future implementations for water quality was the work of (Portela, 1996), whose many formulations are still in use in the MOHID's biogeochemical module. Since the early 2000s many other parametrizations and features were included in the context of international projects. The most relevant applications for the Tagus estuary and its ROFI include the works of (Braunschweig et al., 2004, 2003; Canas, 2009; Canas et al., 2009; Coelho et al., 1999; Leitão, 2002; Martins et al., 1998; Santos et al., 2002) for the hydrodynamics of the estuary and its coastal area (with new modelling features or code updates), and (Ascione, 2014; Mateus, 2006; Mateus et al., 2012a; Mateus and Neves, 2008; Vaz et al., 2015) for the biogeochemical cycle. As regards sediment dynamics, some of the most recent works include the validation, operationalization/automation and forecast services (Franz, 2017; G. Franz et al., 2014). This author developed a

geomorphological model capable of combining several types of sediments, applicable to coastal protection modelling studies. Finally, broader studies, validation, automation and forecast capabilities were developed in the works of (Campuzano et al., 2012; de Pablo et al., 2019; G Franz et al., 2014; Mateus et al., 2012b; Riflet, 2010). More review cases not exclusive to the Tagus ROFI are available in the works by (Mateus and Neves, 2013; Vaz et al., 2020).

The Tagus ROFI area has been studied extensively since the 1990s, where modelling took a big part in the understanding of its physical and biogeochemical processes that contributed to services provided for companies and decision makers present in the area. The majority of these models used the downscaling methodology, especially from the mid-2000s, and the offline downscaling significantly improved the versatility of the model which is currently applied to the majority of the Portuguese estuaries through this methodology. During the next sections, the coupling between the Tagus ROFI modelling domain and its PD – the PCOMS domain – will be analysed and its advantages and drawbacks will be discussed. Validations for this period were done only for the Tagus ROFI modelling domain, due to its importance for upscaling purposes – any errors produced in the CD would be transferred to its PD resulting in loss of performance of the entire modelling system.

2.2.3 Application performance during an extreme precipitation event

In this section, the PCOMS – Tagus ROFI modelling system is applied to study the extreme precipitation event which took place between the end of March and mid-April 2013. Validation is also performed with regard to water level and salinity for the current period and a brief mention of velocity and temperature validation for other periods but with the same implementation is also made. During this event the flow rate of the Tagus river, whose average is $258 \text{ m}^3\text{s}^{-1}$, exceeded $7500 \text{ m}^3\text{s}^{-1}$ for over 72h, leading to extremely low salinity values in the adjacent area (de Pablo et al., 2019; Sobrinho et al., 2021b). Simulations made by (Campuzano, 2018) for this period showed that during this event the Tagus and Sado buoyant plume become large enough to reach the WIBP and create a continuous buoyant plume along the Portuguese Coast. This extreme event will be studied in the next sections using a one-way methodology, and in Chapter 3 using two-way and upscaling methodologies, as it represents one of the particular cases where comparison between these methodologies is made easier and where two-way and upscaling methodologies will have the most impact.

2.2.3.1 Methodology

The PCOMS-Tagus ROFI modelling system uses the 3D-MOHID Water model in a nested grid configuration, transferring information only from the PCOMS to the Tagus ROFI in a typical one-way nesting. This downscaling approach is based on the outcomes of projects such as the “European coastal-shelf sea operational observing and forecasting system” (ECOOP) and “Development and pre-operational validation of upgraded GMES Marine Core Services and capabilities” (MyOcean) and is fully integrated in the downscaling rationale of the CMEMS service. The nested system is comprised of three domains (Figure 7) : 1) 2D barotropic regional domain with 5.7 km constant grid resolution for the Portuguese Coast (Level1) (33.5° N - 49.9° N, 1.0° W - 13.5° W), running only with tidal forcing from FES2004 (Lefèvre et al., 2002; Lyard et al., 2006); 2) 3D full baroclinic regional domain for the Portuguese Coast (Level2) (34.4° N – 45.0° N and 12.6° W – 5.5° W) with a grid resolution of 5.7 km and 50 vertical layers (7 sigma at the surface and 43 Cartesian below); 3) 3D full baroclinic domain for the Tagus ROFI (Level3) and adjacent coastal area with a variable grid from 2 km to 200 m (38.15° N – 39.2° N, 10° W – 8.9° W), and 50 vertical layers (7 sigma at the surface and 43 Cartesian below). A full description of the first two domains is available in Mateus et al. (2012), and a description of the Tagus ROFI domain (one-way) is described in Campuzano et al. (2012).

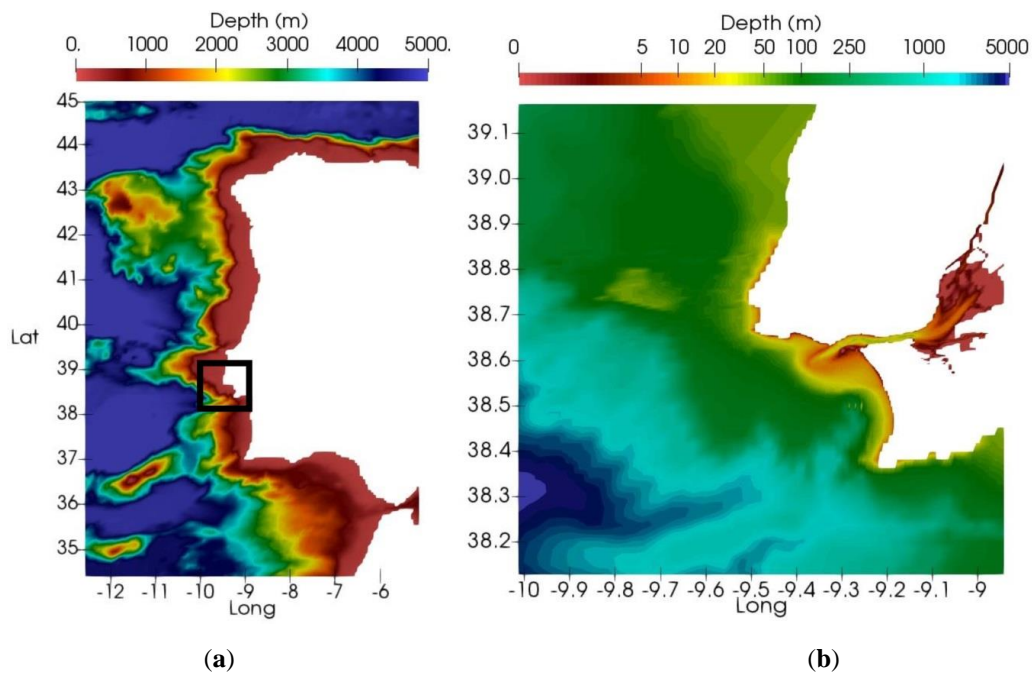


Figure 7. Model domains a) PCOMS (Level 2) and b) TagusROFI (Level3). The colour scale represents bathymetry and scale of Level3 (b) is logarithmic. Level 1 bathymetry is the same as Level 2, although with 2 more numerical cells in each direction (needed for open-boundary conditions in downscaling), and for that reason is not presented here.

Bathymetric data for Levels 1 and 2 was obtained from the EMODnet Bathymetry portal (<https://www.emodnet-bathymetry.eu/>). Level3 bathymetric data was collected from the Hydrographic Institute (IH) between 1964 and 2009 for the Tagus estuary, and from the General Bathymetric Chart of the Oceans (GEBCO) for adjacent coastal area. Initial conditions were not necessary as the system started from the results of the operational systems. The period from January to April 2013 was simulated, corresponding to a period of high precipitation in Portugal, which lead to an extreme event (de Pablo et al., 2019) in the flow rate of the Tagus River.

The entire system was run online so a comparison with a two-way methodology could be made in Chapter 3, integrating the currently in-place downscaling and the newly developed upscaling algorithm. Time steps for the 3 levels were 60 s, 60 s and 6 s respectively, representing a time refinement factor of 10 for the last level.

Level1 domain is forced on its open boundary only by astronomic tides and a Blumberg-Kantha radiation condition (Blumberg and Kantha, 1985) is applied to the water level on the open boundary. A biharmonic filter (Kantha and Clayson, 2000) of $10^{10} \text{ m}^4\text{s}^{-1}$ is also added to filter high frequency oscillations. Its order of magnitude was based on the following equation:

$$B = \frac{U}{16} \cdot \delta_x^3 \quad (21)$$

where U is a typical maximum velocity (0.1 ms^{-1}) and δ_x is the horizontal cell resolution in meters. Level2 domain receives its lateral open boundary conditions from the 2D barotropic domain and the [Mercator Ocean Psy2V4](#). To cope with the absence of barotropic velocities in the Mercator solution, the 2D solution (Level1) is linearly superimposed on the Mercator solution as proposed in Leitão et al. (2005). To this integrated solution, a Flather (1976) radiation scheme was applied at the open boundary as well as a Flow Relaxation Scheme proposed by Martinsen and Engedahl (1987) to the Mercator solution as described in Leitão et al. (2005). The water level from Level1 is also corrected with the inverted barometer approximation using the mean sea level pressure provided by the MM5 meteorological model (described below). The flow relaxation scheme in this setup considers an exponential decreasing relaxation coefficient for the first 10 numerical cells of Level2, starting with a value 10^5 s in the first boundary cell and ending at the 10th cell with 10^9 s. The rest of the domain is relaxed to the Mercator solution with a coefficient of 10^9 s. The Coriolis term is computed as well as the tide potential for 12 harmonic components (M2, S2, K2, N2, K1, O1, P1, Q1, Ssa,

Mm, Mf, M3) as described by (Lefevre, 2000). Additionally, a biharmonic filter of $5.5 \times 10^9 \text{ m}^4 \text{ s}^{-1}$ is applied to reduce high frequency noise, and a variable horizontal viscosity is used, with constant value of $55 \text{ m}^2 \text{ s}^{-1}$ in the interior of the domain and exponentially increasing from the 10th cell from the lateral open boundary to a value of $60000 \text{ m}^2 \text{ s}^{-1}$.

Level3 domain is forced solely by Level2 at the lateral open boundary, using a Flather radiation scheme and nudging the solution with a flow relaxation scheme using the same 10 cells and a nudging coefficient varying from 900 s in the first cell to 10^9 s in the 10th cell.

A constant viscosity of $20 \text{ m}^2 \text{ s}^{-1}$ is used with an increased value of $45 \text{ m}^2 \text{ s}^{-1}$ in the deeper areas near the lateral open boundary where the submarine canyons are located. Both Level2 and Level3 use the global ocean turbulence model (Burchard et al., 1999) coupled to MOHID by (Ruiz Villarreal et al., 2005). The application used in this thesis uses a k- ϵ model as the Mellor-Yamada second order turbulent closure model (Mellor and Yamada, 1982).

At the atmospheric boundary, Level2 was forced by the combination of two Mesoscale Model (MM5) (Grell et al., 1994) domains running in MARETEC, one with 12 km resolution covering the West Iberian region and a nested one with 9 km resolution for the Portuguese coast. Level3 was forced with a Weather Research and Forecasting (WRF) domain with a 3 km grid resolution (Trancoso, 2012).

Regarding freshwater inputs, three main freshwater sources contributions were added: Tagus, Sorraia and Trancão rivers. The minor rivers (Trancão and Sorraia) were imposed using climatological values, with river flow ranging between 3 and $60 \text{ m}^3 \text{ s}^{-1}$ for Sorraia River and between 1 and $9 \text{ m}^3 \text{ s}^{-1}$ for Trancão River. For the Tagus River, water level was retrieved from the Almourol hydrometrical station (<https://snirh.apambiente.pt/>) and then a flow curve was used to extract the flow rate. The simulated period included an extreme precipitation event which resulted in a flow rate for the Tagus River of over $7.500 \text{ m}^3 \text{ s}^{-1}$ for over 72 h, compared to an average flow rate of $258 \text{ m}^3 \text{ s}^{-1}$. No discharge is implemented in Level2 in order to accurately represent the current operational implementation in Maretec – which does not consider river discharges.

A description of the implementation is summarized in Table 3.

Table 3. Model setup configuration for the Tagus ROFI area.

Settings	Level1 – West Iberia	Level2 – PCOMS	Level3 – Tagus ROFI
Model characteristics	2D - Barotropic	3D – Baroclinic	3D - Baroclinic
Grid corners	33.50° N - 49.90° N 1.00° W - 13.50° W	34.38° N – 45.00° N 12.60° W – 5.50° W	38.16° N – 39.21° N 10.02° W – 8.90° W
Cells dimension	208 x 156	177 x 125	121 x 146
Bathymetry	EMODnet Bathymetry portal	EMODnet Bathymetry portal	IH Data and GEBCO
Horizontal Grid	Regular: (\approx 5.7 km)	Regular: (\approx 5.7 km)	Irregular: 200 m to 2 km
Vertical Grid	1 layer	7 Sigma Layer (0 - 8.68 m) 43 Cartesian layers	7 Sigma Layer (0 - 8.68 m) 43 Cartesian layers
Δt	60 seconds	60 seconds	6 seconds
Tides	FES2004	From Level1	From Level2
OBC Water	...	From MercatorOcéan PSY2V4 (Releases 1- 4)	From Level2
Nudging	...	Flow relaxation scheme of 10 cells with a time decay of 1 week at the open boundary and 0 inside the domain	Flow relaxation scheme of 10 cells with a time decay of 1 week at the open boundary and 0 inside the domain
OBC Atmosphere	-	MM5 (12 km and 9 km)	WRF (3 km)
Discharges	No	No	Tagus (hourly), Sorraia, Trancão (monthly)
Turbulence	...	GOTM*	GOTM*
Bottom	Rugosity of 0.0025 m ² s ⁻¹	Rugosity of 0. 0025 m ² s ⁻¹	Rugosity of 0. 0025 m ² s ⁻¹

*General Ocean Turbulence Model (Burchard et al., 1999) coupled to MOHID (Ruiz Villarreal et al., 2005).

In regards to the forecast system, this implementation has been running uninterruptedly since 2011 and provides a 3-day forecast once per day, for water velocity, water level, surface seawater temperature, salinity, and biogeochemical properties. The system runs a 5-day simulation period every day, consisting of 1 hindcast day, the present day and 3 forecast days and the entire operational modelling system takes around 3.8 h per day. In this thesis the system only runs hydrodynamics, and in the one-way nesting approach it takes between 2.5 h and 4 h (depending on the computer being used) to run one day of simulation.

As for validation, the focus will be on the Tagus ROFI domain, which has more available data and because the aim is to perform an analysis at the vicinity of the open boundary between the two domains.

2.2.3.2 Results and discussion

The Tagus ROFI modelling system was chosen due to the amount of studies performed with this system as well as the accumulated experience of Maretec in this estuary, and the amount of validations conducted. Validation of the MOHID Tagus ROFI modelling system has been done over the years through the publication of several articles, of which the most recent include the works of (de Pablo et al., 2019; Franz et al., 2017; G Franz et al., 2014). (Franz, 2017), performing a validation of the sediment dynamics in the Tagus estuary and its adjacent area including the effect of waves through fetch created inside the estuary, as well as the effects of an extreme event in the beaches located south of the estuary mouth, while (de Pablo et al., 2019) and making a comprehensive validation of the Tagus ROFI analysing hydrodynamics as well as the biogeochemical properties such as nutrients and chlorophyll. Said work uses in situ measurements from several types of sensors (tidal gauges, CTD, and ADCP, Figure 8) as well as satellite L4 products (OSTIA, ODYSSEA, and MUR) to validate model results, something that had not been done yet for the MOHID model in the Tagus ROFI area.

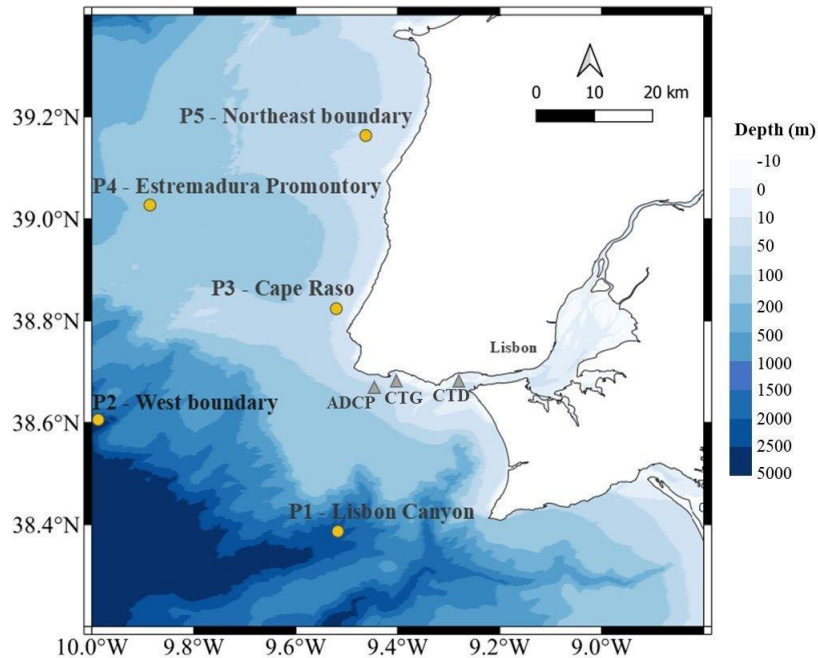


Figure 8: Map of the Tagus ROFI area showing the location of the in-situ stations used in the validation process as well as the vertical profiles used for comparison between modelling grids. CTG–Cascais Tide Gauge; CTD–Conductivity, Temperature, and Depth probe; ADCP–Acoustic Doppler Current Profiler; P1-4 – vertical profiles.

Regarding the validation of the Level2 model domain, as the Level3 area of study is very small when compared to Level2, validation was not made. However, the implementation has been extensively studied and validated in works such as (Campuzano, 2018; Mateus et al., 2012b;

Verelst, 2008). On the tide propagation from the Level2 open boundary to the coast line, (Campuzano, 2018) concluded that the model correctly reproduces the tide propagation as the total error is of the same scale as that of the original solution – FES2012.

All of the results presented in this next section were published in (de Pablo et al., 2019; Sobrinho et al., 2021b).

2.2.3.2.1 Water level validation

Water level obtained by the two model implementations (Level2 and Level3) was validated against the Cascais tide gauge during the period between 11 January and 13 March 2013 (Figure 9 and Figure 10).

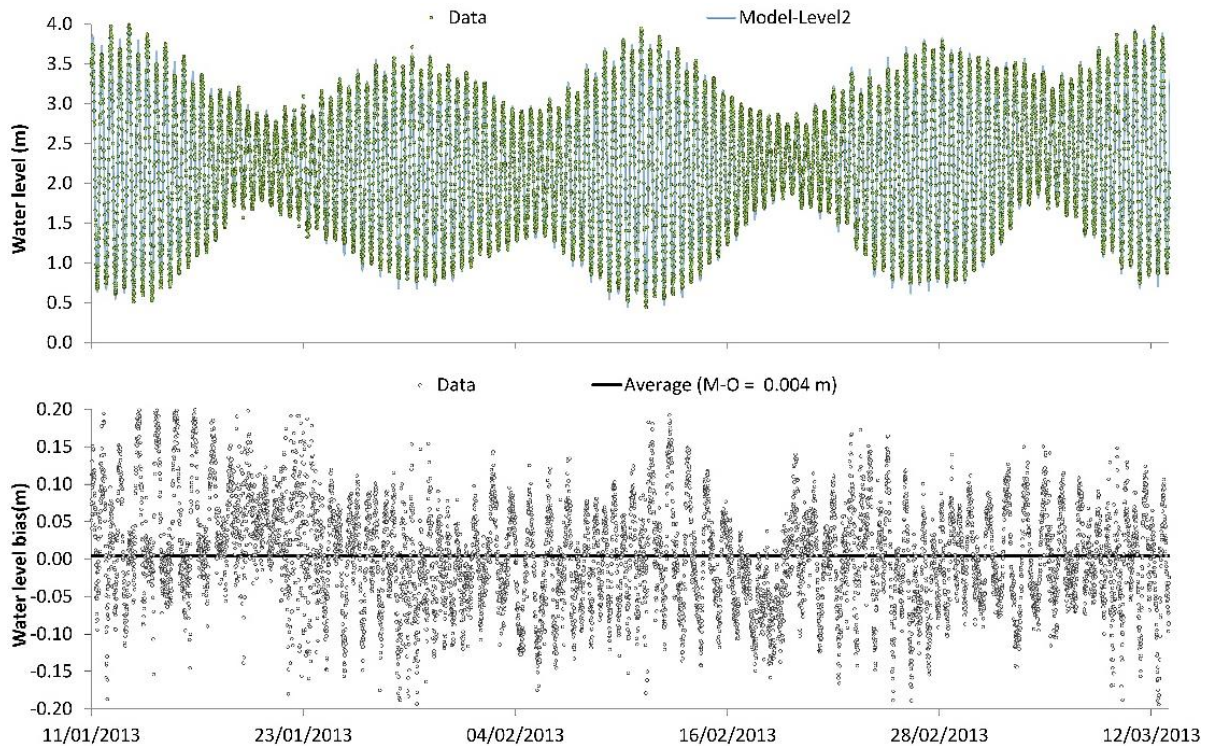


Figure 9: Comparison of water levels obtained with the Cascais tide gauge and Level2 modelling domain for the period between 11 January and 13 March 2013.

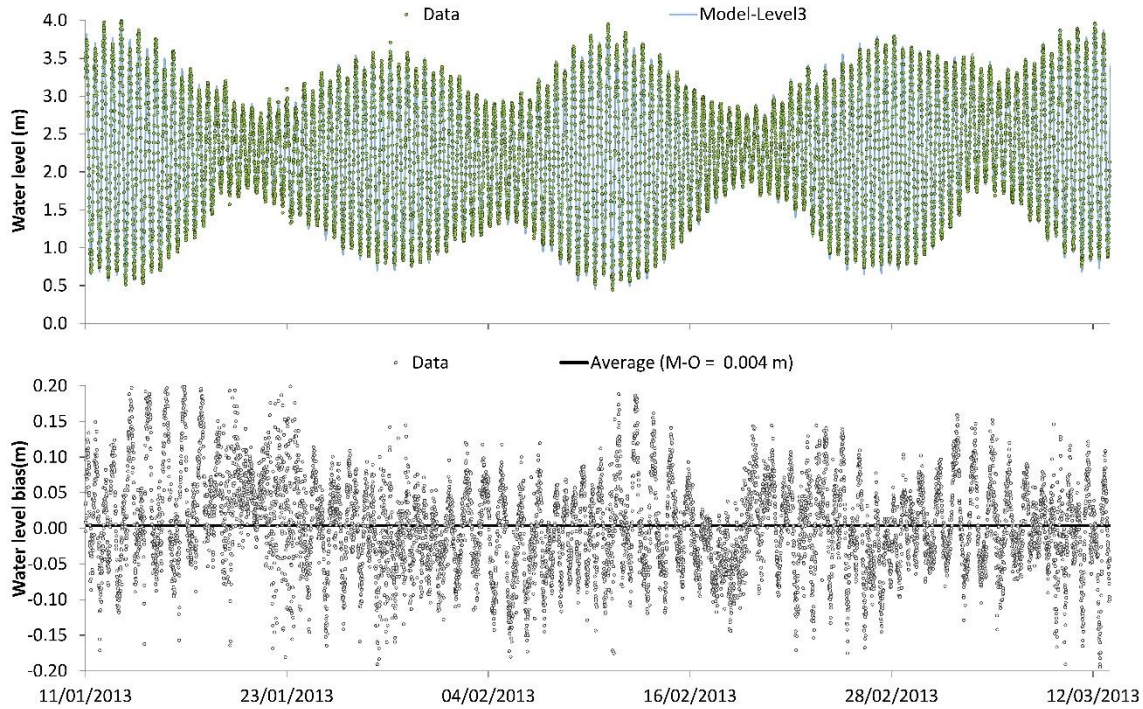
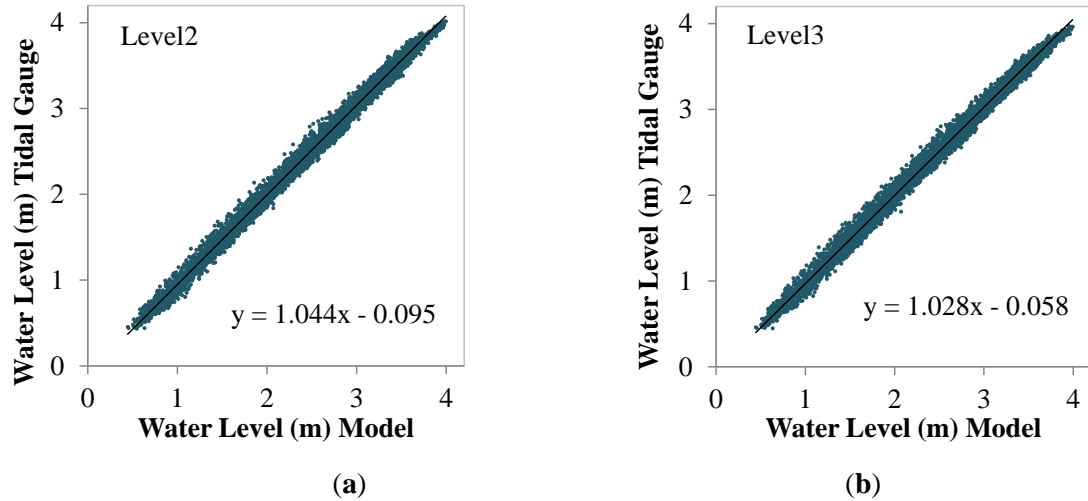


Figure 10: Comparison of water levels obtained with the Cascais tide gauge and Level3 modelling domain for the period between 11 January and 13 March 2013.

Results obtained by either domain have correlations above 0.99 (Figure 11), demonstrating the model's capacity to represent water level variability. Mean bias values vary between 4.12 mm on Level2 and 4.02 mm on Level3. Median values are more representative when extreme values occur, and in this case, for Level2 (2.20 mm) it is more than the double the height of Level3 (1.03 mm), indicating more extreme (overestimation) bias values in Level2 and the contrary for Level3. With regard to correlation between model data and tide gauge data, all implementations provided results with a Pearson value superior to 0.99 indicating a good agreement with the tide gauge. RMSE values showed a better performance for Level3 (0.0684) than for Level2 (0.074), indicating an improvement of the results when downscaling is applied. These results are in agreement with those obtained by de Pablo et al. (2019), who covered a different time period – October 2012 – and demonstrate both the ability of the MOHID model to reproduce water level in a highly dynamic region, and the advantage of the downscaling approach for the transition between the deep ocean and coastal areas.



Bias(Mean):	0.00412	0.00402
Bias(Median):	0.00220	0.00103
Pearson:	0.997	0.997
RMSE:	0.074	0.0684
n	8819	

Figure 11: Correlation and performance results for the period between 11 January and 13 March 2013, between the Cascais tide gauge and the different model implementations: a) Level2 in one-way, b) Level3 in one-way.

2.2.3.2.2 *Salinity validation*

In the Tagus ROFI modelling system – whose PD does not consider land discharges – salinity is the most useful water property to analyse the estuarine plume and study the stratification process in the Level3 domain as well as the coupling with its PD (Level2). As mentioned before, stratification in the Tagus estuary and its adjacent coastal area is mainly present during the winter and particularly during high precipitation events. In this chapter, the simulation period is focused in the March-April of 2013 event, which produced extreme values of flow rate – more than $7500 \text{ m}^3\text{s}^{-1}$ over a period of 72h.

During this event, salinity values dropped from their typical values of around 30, to less than 6. As mentioned in (de Pablo et al., 2019), during this time the Tagus river alone was responsible for more than 10% of the tidal prism of the estuary, accompanied by a strong stratification of the water column (Figure 12).

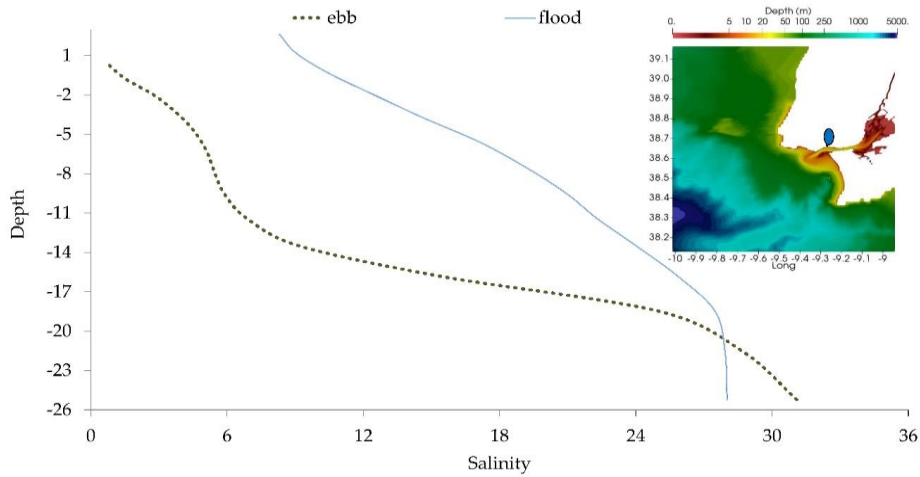


Figure 12: Salinity profile from Level3 model domain at the mouth of the estuary during ebb and flood of 1 April 2013, when the flow value reached its maximum.

Modelled surface salinity was validated against CTD data obtained between March and April 2013 (Figure 13) in a moored station located near the mouth of the estuary, and shows the impact of this high flow rate in the salinity values near the mouth of the estuary (Algés buoy, see Figure 8).

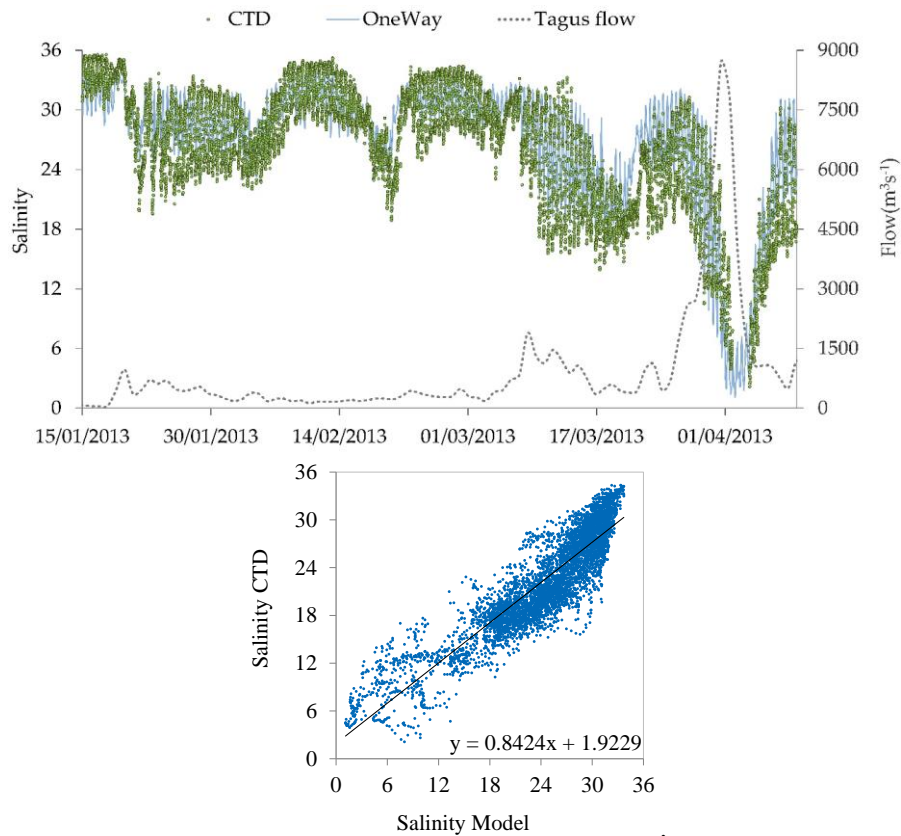


Figure 13: Performance of model results (Level3 domain) against field data (obtained with a CTD). At the top) Comparison between salinity field data for the period between 15 January and 10 April 2013; At the bottom) correlation between model (Level3) and CTD data for the period between 1 March and 10 April.

Comparisons between data and Level3 results show that the model was able to properly reproduce salinity variation during this period of extreme flow rate. Additionally, the model has the ability to fill the missing data gap in the first days of April – caused by a submergence of the buoy during the peak flow – which in this case points to a very low salinity of 1 at the mouth of the estuary. Modelled mean and median bias for Level3 (1.92 and 1.82 respectively) (Table 4) implementation confirm a small overestimation of the surface salinity throughout the extreme event (1 March to 10 April). As regards correlation and model performance, Pearson (0.90) and the NASH (0.69) values (Table 4) indicate a good agreement with field data.

These results demonstrate the importance of extreme flow rates from the Tagus River flow at the mouth of the estuary, which can mask potential errors from the open boundary of the model domain. However, model results obtained by (de Pablo et al., 2019) demonstrate the ability of the implementation to reproduce the major hydrodynamic processes of the Tagus ROFI area.

Table 4. Statistical parameters obtained for salinity comparison with CTD data with Level3 domain for the period between 1 March and 10 April.

Statistical parameter	Level3 – Tagus ROFI
Bias(Mean):	1.92
Bias(Median):	1.82
Pearson:	0.90
RMSE:	3.55
NASH:	0.69
n	5468

2.2.3.2.3 *Validations performed outside the simulation period*

As many of the in-situ data for this region is scarce in time and space, many of the validations must consider different time periods. Remote sensing has a similar problem, especially during precipitation events where cloud cover associated with storm makes its use impossible. As such, velocity and temperature fields were validated for other time periods. A more detailed analysis of this validation effort is made in (de Pablo et al., 2019).

Current velocity was measured between 2 and 17 July 2009 with an ADCP placed at surface, off Cascais (Figure 8), which recorded eastward and northward current with a 15 min sampling rate for the entire water column at every 1 m. After analysing the profile of the current velocity, the water column was split into two layers from 2.5 and 15 m and from 15 to 30 m. This

separation was made in accordance with the hydrodynamics of the study area, where surface currents, in contrast with bottom currents, are more intense and dependent on wind stress.

Spatial-temporal validation of temperature was done by comparing results obtained from MOHID and satellite images. For a more exhaustive analysis, three level 4 gridded RS data products were used, namely, OSTIA (Stark et al., 2007) with a 5 km grid resolution, ODYSSEA (<http://marine.copernicus.eu/>; (Autret et al., 2017)) with a 2 km grid resolution, and MUR (<http://doi.org/10.5067/GHGMR-4FJ01>) with a 1 km grid resolution. Level4 products were chosen due their higher accuracy, as they are an aggregated product that takes into consideration several satellite sensors and in situ instruments. As they are subject to statistical interpolation and temporal average, these products provide gap-free gridded outputs, making the comparison with modelling results easier. Daily SST satellite images were compared with the daily average of hourly SST model results for the period 2014–2016 and annual temperature averages were obtained from the daily averages of SST.

Velocity

The ADCP is located in a very turbulent area, highly influenced by tide, bathymetric features of the coastal area and wind, which is why it was chosen as the location of the diffuser of a WWTP submarine outfall. Profile results obtained by the ADCP show more intense velocities at the surface, especially in the North-South direction, and a clear southward flow over the analysed period Figure 14. In the East-West direction the velocity average indicates a residual flow towards the East and the mouth of the estuary, across the entire water column.

Figure 14 shows all the profiles made during the analysed period of 15 days, and besides the already mentioned higher intensities at the surface, tide influence can also be observed in the variability between positive and negative velocities of the U and V directions, both in the ADCP and model results. Level3 model results have accurately captured these tendencies as well as intensity, with average values at the surface (0.1 ms⁻¹ in the U direction and 0.15 ms⁻¹ in the V direction) demonstrating a stronger North-South flow than East-West. This higher intensity is associated with the predominant northerly wind with an average intensity of 3.4 ms⁻¹ during the simulated period combined with the lower influence of the estuarine plume at the ADCP location (de Pablo et al., 2019).

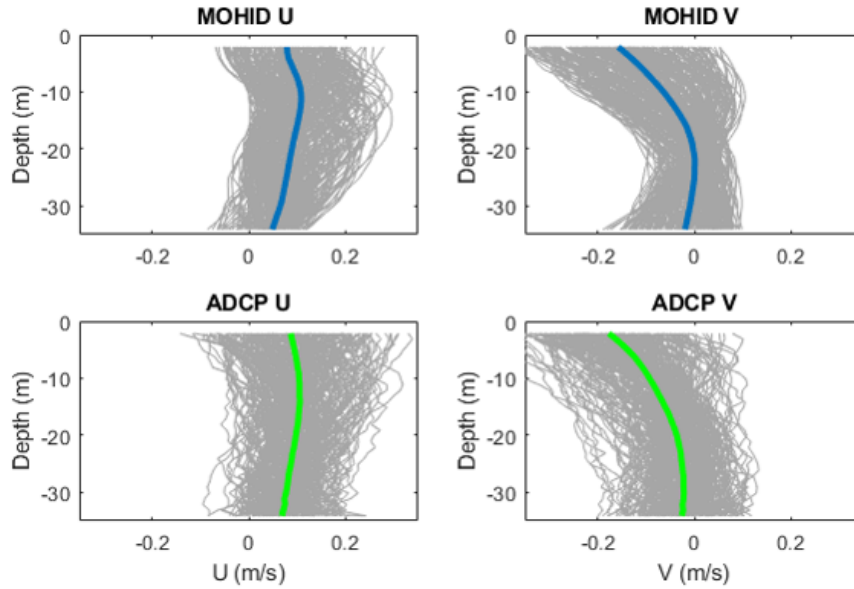


Figure 14: Comparison between velocity profiles obtained by the Level3 model domain (Tagus ROFI) and the ADCP for the period between 2 and 17 July 2009. From: (de Pablo et al., 2019).

Model results are well correlated with the ADCP data, with correlation coefficients for u and v velocity components of 0.63, 0.73, 0.62 and 0.71 for surface and bottom waters respectively, and 0.62 and 0.71. RMSE and BIAS values obtained for velocity modulus and its u and v components did not drop below 0.2, and the model also correctly estimated the global velocity direction, showing RMSE values between 45 and 50 and BIAS values varying from -9.8 rad in the surface layer and -14 rad in the bottom layer. These values are in accordance with the minimum-level BIAS values for model performance suggested by Williams and Esteves (Williams and Esteves, 2017).

Table 5: Current velocity and direction. Data summary and results of statistics used to assess the level of agreement between measured data and modelling results. n —number of observations; r —correlation coefficient; BIAS—Average bias; RMSE—Root mean square error. From (de Pablo et al., 2019)

	Average (min-max) MOHID	Average (min-max) ADCP	n	Pearson (r)	BIAS	RMSE
Depth (2.5 m–15 m)						
Vel. Modulus ($m s^{-1}$)	0.16 (0.0087–0.41)	0.17 (0.0054–0.43)	1440	0.68	0.014	0.10
Direction (rad)	151 (0.2–360)	134 (2.4–359)		0.63	-9.8	45
Velocity u ($m s^{-1}$)	0.097 (-0.069–0.30)	0.099 (-0.14–0.34)		0.63	0.0019	0.092
Velocity v ($m s^{-1}$)	-0.089 (-0.38–0.11)	-0.11 (-0.43–0.11)		0.73	-0.025	0.11
Depth (15 m–30 m)						
Vel. Modulus ($m s^{-1}$)	0.10 (0.0039–0.30)	0.12 (0.0025–0.34)	1440	0.62	0.018	0.065
Direction (rad)	151 (0.2–360)	164 (2–358)		0.66	-14	50
Velocity u ($m s^{-1}$)	0.084 (-0.046–0.30)	0.092 (-0.086–0.29)		0.63	0.0082	0.066
Velocity v ($m s^{-1}$)	-0.052 (-0.15–0.098)	-0.035 (-0.26–0.13)		0.71	-0.029	0.071

Temperature

Temperature spatial-temporal validation was made by comparison with three different satellite sources and was focused on daily averages for the adjacent area of the Tagus estuary at the first meter of depth (Figure 15). The advantage of using satellite information is the amount of temporal data available as well as its coverage which largely exceeds that of in-situ measurements. Of these sources, the ODYSSEA product gave the most similar results to Level3 modelling domain and is the only one where a clear upwelling area can be identified north of Cape Raso.

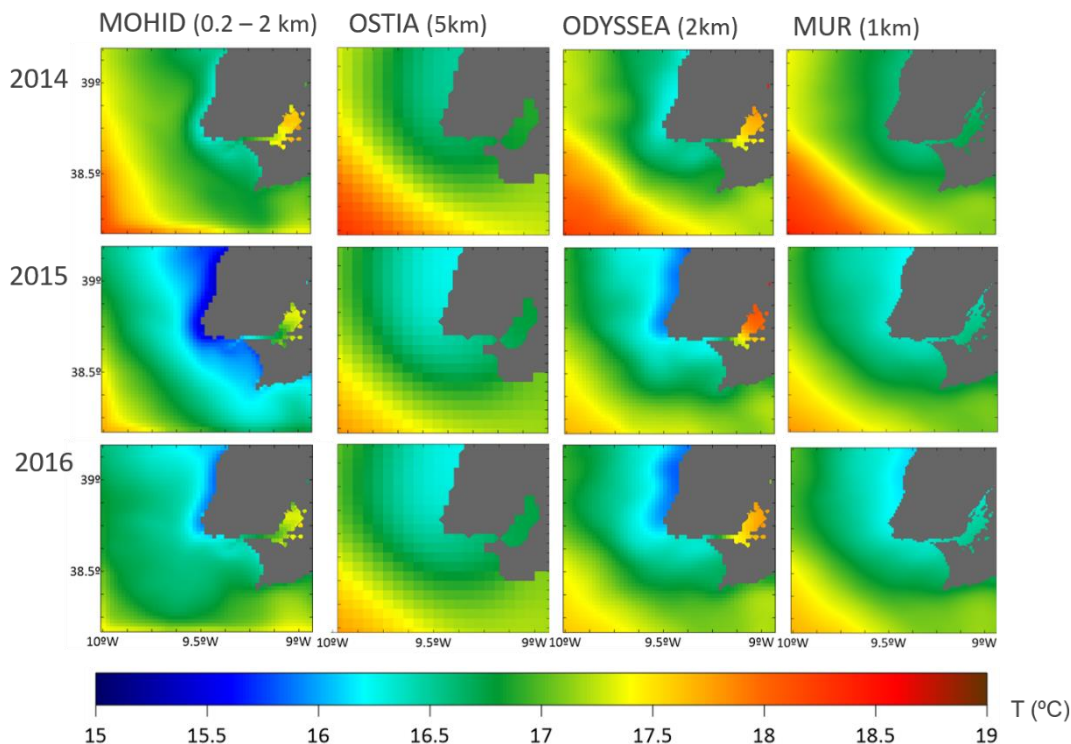


Figure 15: Interannual comparison of surface seawater temperature between MOHID and Satellite L4 gridded products (OSTIA-5 km, ODYSSEA-2 km; and MUR 1 km) for the period 2014–2016.

Table 6 shows the various statistical parameters analysed for the 3-year validation. From a global perspective, the Pearson correlation coefficients (r) (minimum of 0.864), the BIAS (maximum of -0.4) and the RMSE (maximum of 0.992) parameters obtained for all satellites demonstrate the ability of the modelling domain to represent the spatial and temporal processes of the region.

Table 6: Results of statistics used to assess the level of agreement between SST obtained via remote sensing data and modelling results. n –number of observations; r –correlation coefficient; $BIAS$ –Average bias; $RMSE$ –Root mean square error. Adapted from: (de Pablo et al., 2019).

Year	Satellite	Average MOHID	Average L4 products	n (per day)	Pearson (r)	BIAS	RMSE
2014	OSTIA	17.11	17.18	355	0.937	-0.064	0.846
	ODYSSEA	17.11	17.17	2095	0.948	-0.059	0.773
	MUR	17.12	17.20	8356	0.934	-0.078	0.894
2015	OSTIA	16.50	16.91	255	0.919	-0.407	0.946
	ODYSSEA	16.51	16.83	2095	0.924	-0.320	0.889
	MUR	16.56	16.87	8356	0.912	-0.359	0.992
2016	OSTIA	16.74	16.19	355	0.930	-0.176	0.866
	ODYSSEA	16.71	16.83	2095	0.864	-0.127	0.978
	MUR	16.73	16.83	8356	0.916	-0.102	0.914

2.2.3.2.4 Comparison between domains

In order to analyse the one-way solution, a comparison is made between results obtained by Level2 and Level3. This comparison is focused on the residual circulation and salinity at the surface, and on the vertical structure of the model domain results by means of vertical profiles (location in Figure 8). As the domains have different grid resolutions, and Level3 runs on a variable grid size – which makes it more difficult to view velocity arrows in a grid map – results from both domains were interpolated into a new grid with 200 x 200 m. The selected periods were based in the flow of the Tagus River, which starts increasing in the beginning of March and flow values surpass $2000 \text{ m}^3\text{s}^{-1}$ from then until 4 April. As such, three simulation periods were considered: from 11 January to 10 April; from 1 March to 10 April; and from 25 March to 10 April. As for surface salinity, the comparison considered the entire period to better represent the statistical parameters of the difference between model domains.

Residual circulation

Figure 16 shows the residual circulation for the aforementioned periods, where the impact of the Tagus River flow in the circulation patterns increase as the comparison periods focus more in the peak flow period (between 25 March and 10 April). This impact is mostly felt along the lower depths near the coast, particularly on the northeast coast, past the Cape Raso, where directions differ substantially in intensity and direction. As the river flow increases, the flow produced by Level3 – originated by the estuarine plume – rotates right due to the Coriolis force and intensifies the near-shore currents (from 0.2 ms^{-1} in the total period, to 0.4 ms^{-1} during the peak flow, whereas Level2 residual velocities remain near 0.1 ms^{-1} in all the considered periods.

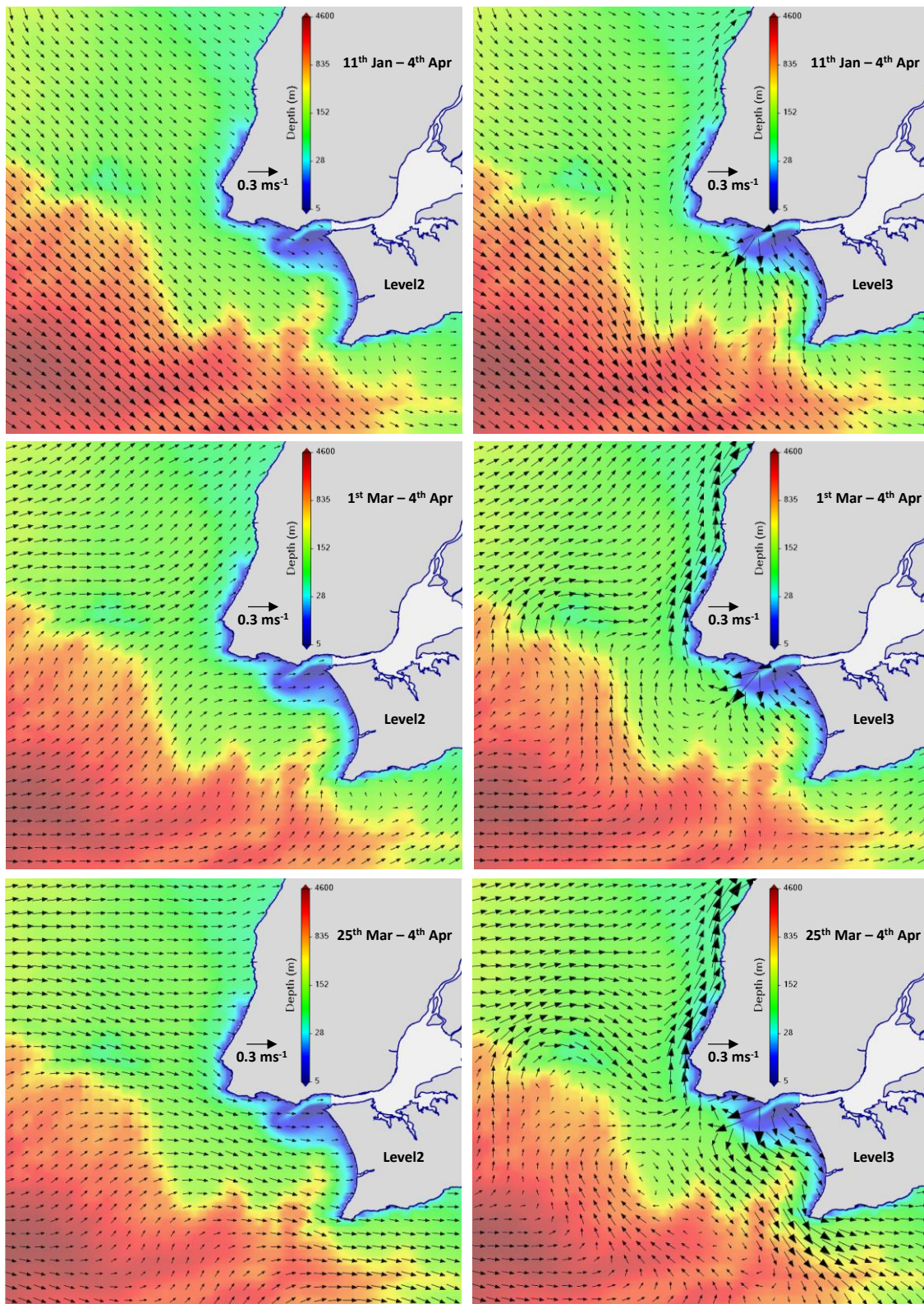


Figure 16: Average surface velocity field obtained with Level2 and Level3, for each selected period. The velocity fields shown are the result of an interpolation of both model domains to a 200 x 200 m grid. Bathymetry is in logarithmic scale.

These results were expected as Level2 domain does not include the river discharge, but compromises the idea behind downscaling where a CD domain size should take into consideration that the CD features near the borders should differ as little as possible to avoid inconsistencies. Nevertheless, this impact only produces significant differences during high flow rates of the Tagus – average above $3500 \text{ m}^3\text{s}^{-1}$. At the open boundary, Level3 produced a circulation much like Level2 did for the first two analysed periods. During the peak river flow, however, the residual velocity obtained by level3 is higher (around 20%) near the southeast boundary and the flow pattern is rotated 20° clockwise. At higher depths, differences between domains are negligible.

Surface salinity

A comparison between modelled surface salinity results obtained by Level2 and Level3 is important to detect the full extent of the Tagus plume over the entire domain and particularly near the open boundaries. Once again the main cause for differences between model results is the lack of river discharges in the Level2 implementation. The analysis of the residual circulation suggested a strong influence near the open boundaries, especially in the northeast and southeast boundaries of Level3. However, smaller gradients are generally observed in surface velocities, while salinity gradients are quite large due to the effect of the estuarine plume. As such, surface salinity is used to easily detect the impact of the downscaling approach in Level3, particularly during extreme events. Figure 17 demonstrates the impact of not including an estuary discharge in regional coastal domains such as the Level2 domain. In these figures, the influence of the Tagus estuary can be detected even for the average of the entire simulation period (11 January to 10 April).

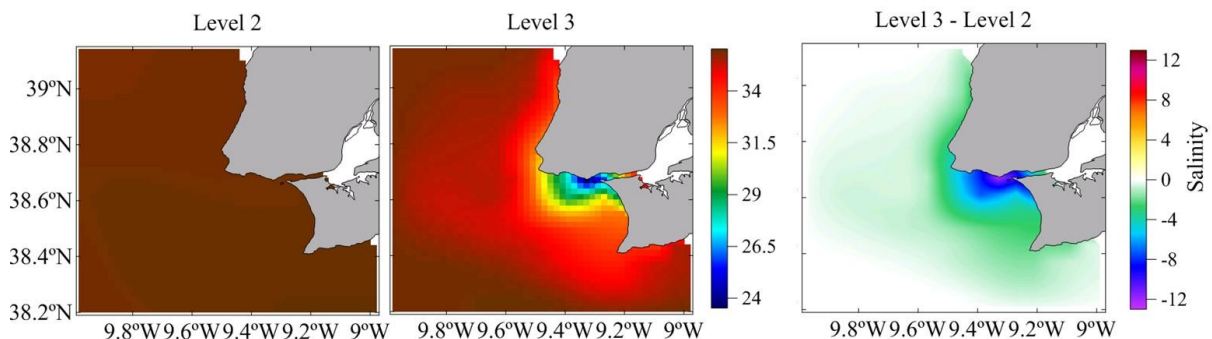


Figure 17: Salinity maps obtained by Level2 and Level3 and respective comparison.

Vertical profiles

Vertical profiles are helpful to analyse the vertical structure of the circulation. In this case they are used to estimate the impact of Level2 on Level3 during an extreme precipitation event. While salinity is more important to analyse the impact of the plume – due to the higher gradient between fresh and salt water masses – temperature is more suited for studying the impact of the bathymetry in the vertical transport, as the vertical gradient is higher. The locations of the profiles (Figure 8) were chosen according to these guidelines, and included two points near the west coast beyond Cape Raso, one at the Extremadura promontory, one at the Lisbon canyon, and one near the west open boundary of Level3.

Starting with salinity, the results (Figure 18) clearly show the estuarine plume signal in all locations, although with different intensities. The most impacted locations are the ones near the west coast past Cape Raso with a range in the order of 13 salinity units for the southernmost point, and 10 salinity units for the point closest to the Level3 open boundary. At the end of the Lisbon canyon salinity shows a range of 3 salinity units and at the remaining locations this range drops to around 0.8 salinity units. The variability observed at the different points, although with a small number of events where a salinity drop is seen, produces different average profiles for Level2 and Level3. Results obtained by Level3 show a strong stratification during the times when the plume passes by the profile locations and the intensity and number of events is enough to produce stratification in all locations, particularly for the period when the Tagus flow is highest. In depth, the impact of the plume is visible up to 50 m in the Lisbon canyon and around 20 m in the remaining locations, when compared to results obtained by Level2. At the Extremadura promontory, which in this location is 100 m deep, and at the westernmost profile (near the Level3 open boundary), profiles show the estuarine water signal, demonstrating the far reach of the estuarine plume. In regards to time variability of the salinity profiles, results show a consistently smaller range of salinity values even for higher depth locations such as the Lisbon Canyon and the westernmost open boundary of Level3. This is consistent with a change in costal currents from winter to spring, such as the weakening of the poleward current. At higher depths (from 800 to 1300 m) a belly-like shape can be seen, which corresponds to the Mediterranean water mass.

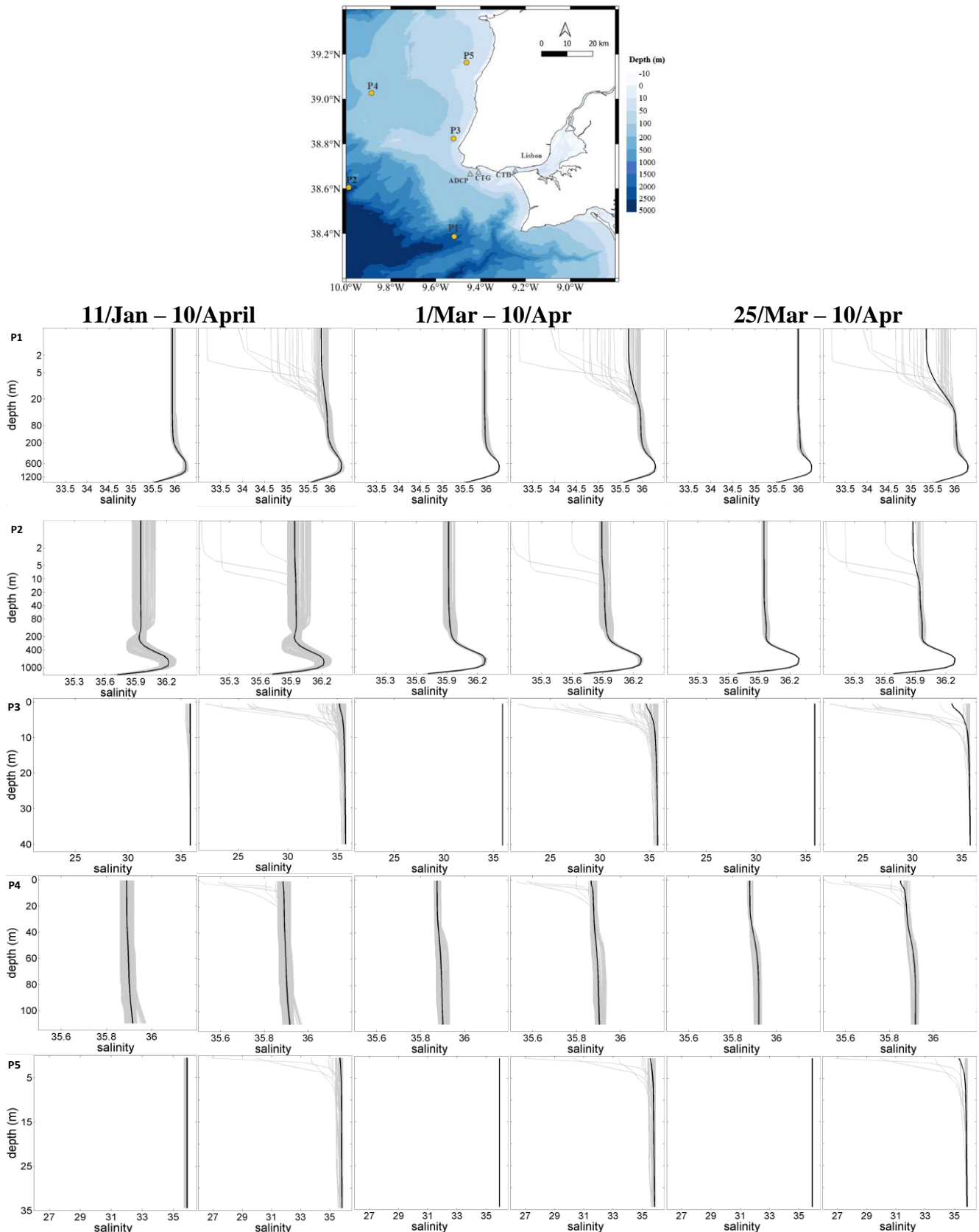


Figure 18: Salinity profiles obtained by Level2 and Level3 over the simulated period. Profiles every 12h are represented in grey, while the average over each analysed period is represented in black.

In order to facilitate the comparison between salinity profiles obtained by the two model domains, average profiles along the analysed periods were extracted (Figure 19). It shows the differences of salinity obtained by parent and child domain for the different locations analysed.

As in the previous figure, salinity profiles obtained by Level3 are considerably different from the ones obtained by Level2, in particular, at the west coast past Cape Raso and over the Lisbon Canyon where the plumes influence reaches 50 m in depth. In the shallower areas near the coast the difference is close to 1.7 salinity units, which is quite large considering the distance to the mouth of the estuary.

As the river flow increase towards the end of March and until 4 April, an increase in differences between domains can be seen in all locations, which also shows that the plume's trajectory is not constant over time, shifting due to wind conditions and offshore circulation patterns, such as the shift in currents and the poleward slope current.

This analysis only considers the impact on salinity along the water column of having an estuary implemented in a nested domain, which is not implemented in its PD. However, another important aspect of the two different domains is the bathymetric resolution which can have an impact in vertical velocities especially for long term iterations and in areas with highly variable bathymetries and subject to upwelling and downwelling conditions such as the one under study.

In the next pages, temperature is also analysed, but this time specifically targeting the vertical structure of the water column.

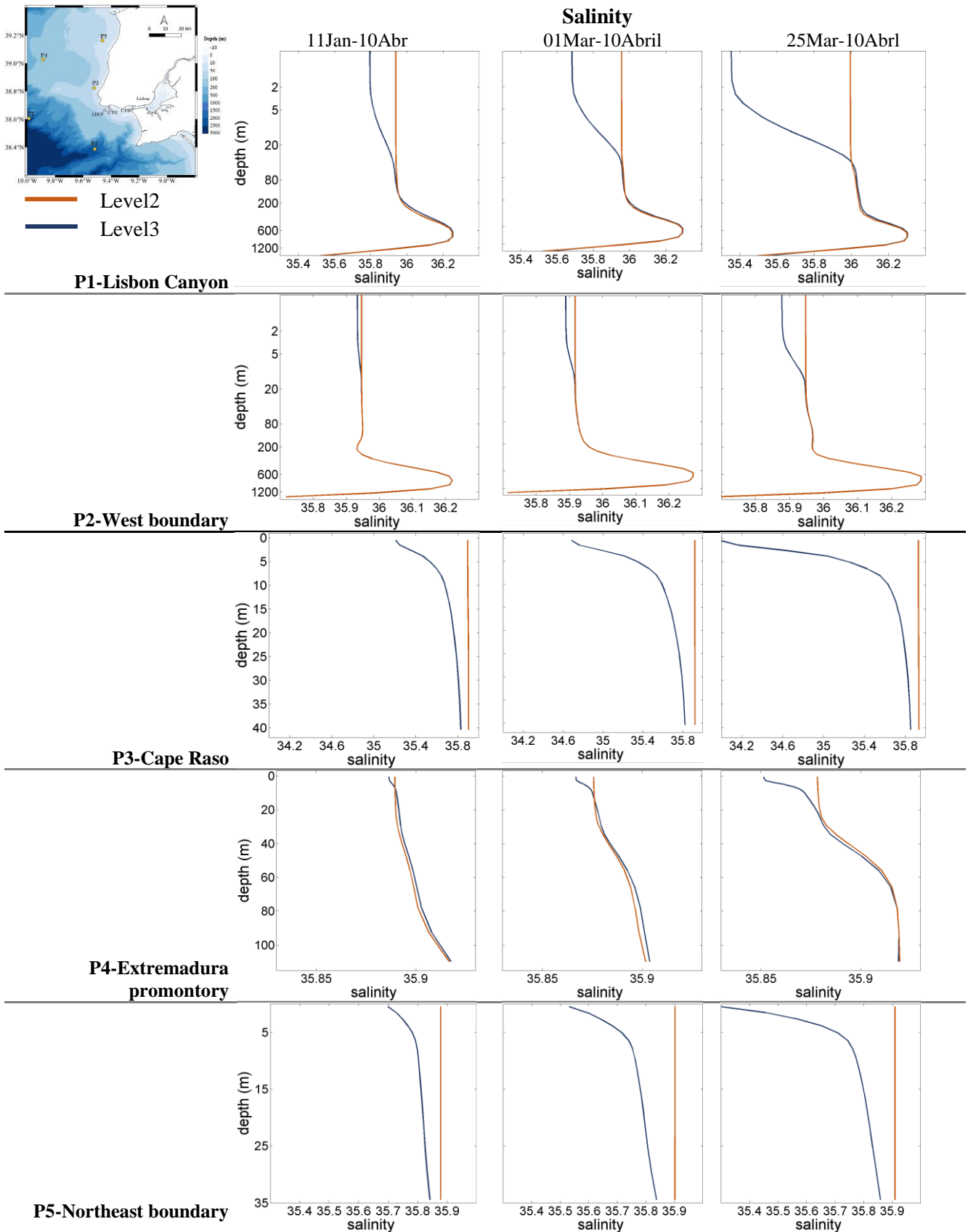


Figure 19: Comparison between vertical profiles of salinity obtained by Level2 and Level3 domains at the five defined locations for the three analysed periods.

Temperature is parameter that is more complicated to use in a comparison between model domains specifically in regards to the surface. In this particular case, the most differentiating aspect is the estuarine plume. However, temperature differences between estuary and ocean are much smaller (in the order of 1 or 2 °C) than salinity variations (which can reach almost 36 - Figure 13).

Profile results obtained for temperature by Level2 and Level3 (Figure 20) demonstrate the more complicated analysis. Noticeable differences can only be observed in the shallower locations such as the west coast (P3 and P5) and at the Extremadura promontory (P4). Over time, the profiles' variability, much like for salinity, diminishes and the temperature tends to increase due to the shift from winter to spring, bringing with it more radiation and changes in the coastal currents. In regards to depth variations, Figure 20 shows some differences, as is the case of the most shallow areas.

The comparison between temperature results obtained by the two domains is easier to observe in Figure 21, showing maximum differences of around 0.1°C for shallow waters. Another important aspect is the colder water verified in the Extremadura promontory (P4) by Level3 in comparison with Level2, suggesting a stronger upwelling of colder waters from below affecting the entire water column and decreasing the depth of the thermocline. At the surface of this location there is a small impact of the fresh water plume, which at this time of the year is higher than that of the ocean. At the west coast, P3 and P5 show a different trend. Although the differences between model domains remain similar, the temperature of the entire water column decreases only in the period between 1 March and 25 March. This aspect was not pursued further as it was not the focus of the thesis, but is likely to be a result of a colder water mass moving towards the coast during that time.

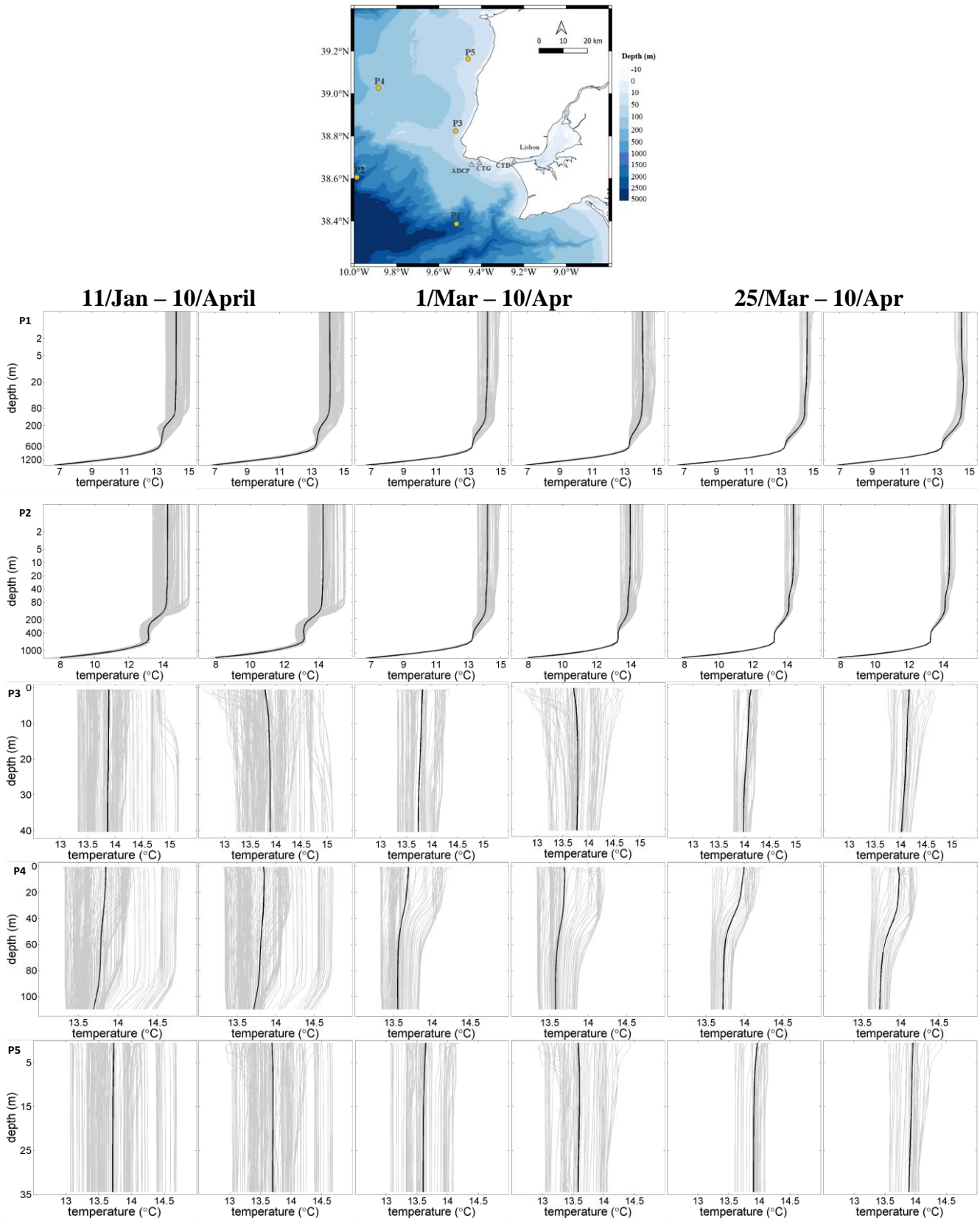


Figure 20: Temperature profiles obtained by Level2 and Level3 over the simulated period. Profiles every 12h are represented in grey, while the average over each analysed period is represented in black.

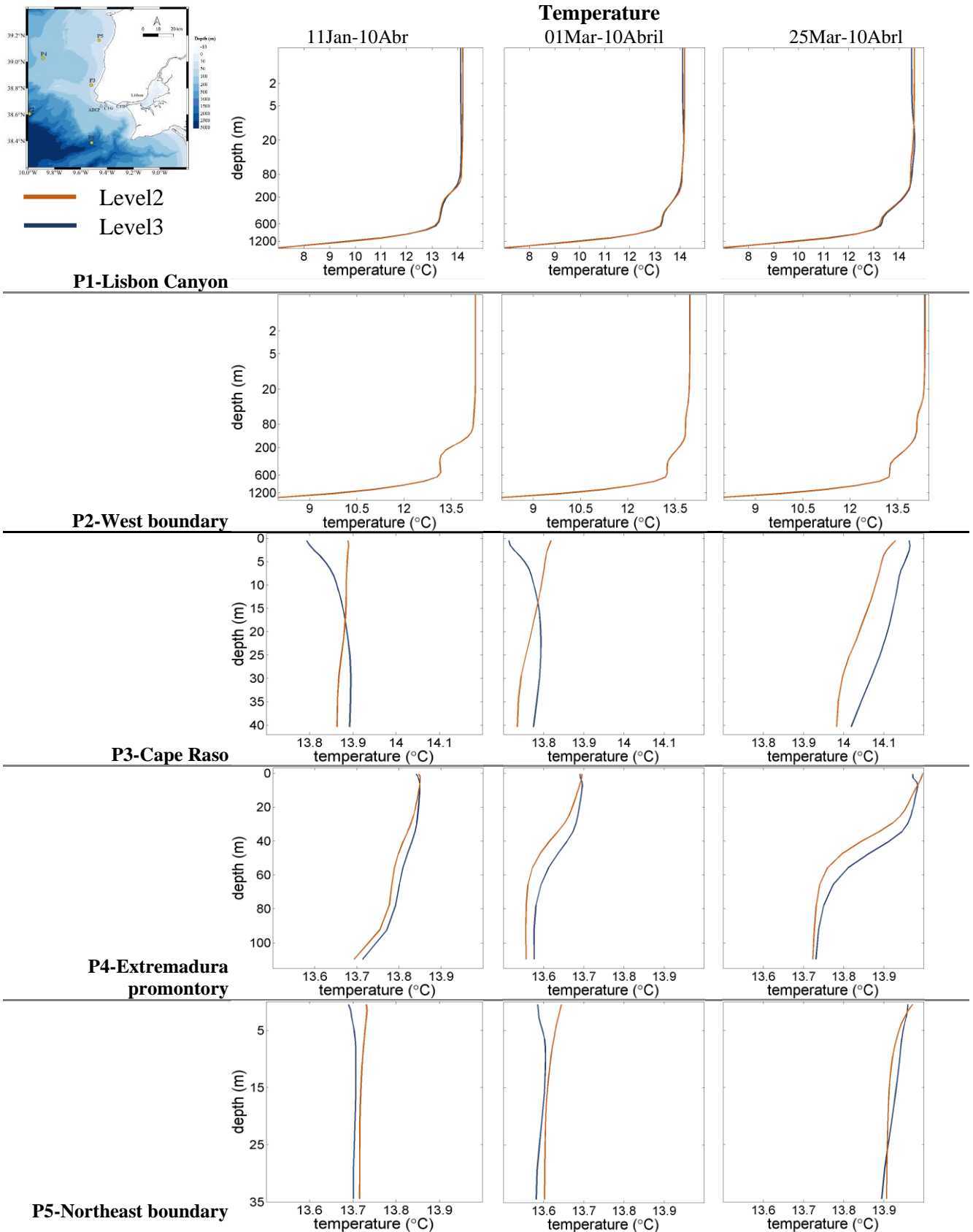


Figure 21: Comparison between vertical profiles of temperature obtained by Level2 and Level3 domains at the five defined locations for the three analysed periods.

Salinity variation at the open boundary

Until now, the impact of the downscaling considered the surface residual circulation and the surface variability over the overlapped area between PD (Level2) and CD (Level3), and the vertical stratification of temperature and salinity. This last section is focused on the surface salinity transition between model grids at the northeast open boundary near the shore line (Figure 8), which has been identified as the area where the Tagus flow impact is highest.

Figure 22 shows the surface salinity comparison between Level2 and Level3. In it, 4 events of low salinity produced by Level3 can be identified during the period of extreme flow rates of the Tagus River. There is no signal in Level2 due to the absence of a river discharge, and the impact of this solution is easy to identify by the rapidly increasing salinity values of Level3 just after the event, due to the flux relaxation scheme from PD to CD. Even though the selected point is the northernmost grid cell of the Level3 domain, the salinity values decreased almost 5 units, bringing into perspective the amount of freshwater discharged by the estuary's rivers. As regards the communication between grid domains, this event brings out the issue of the CD size and the need for river discharges in regional domains. Without it, Level3 will never lose salinity over time, and it is the reason why many times a “frame” can be seen in the open boundaries of Level3 – which is also identified in Figure 22. The reason for the model's good performance over long integration periods is the nudging component implemented in Level2, which maintains the salinity and temperature fields offshore from global solutions.

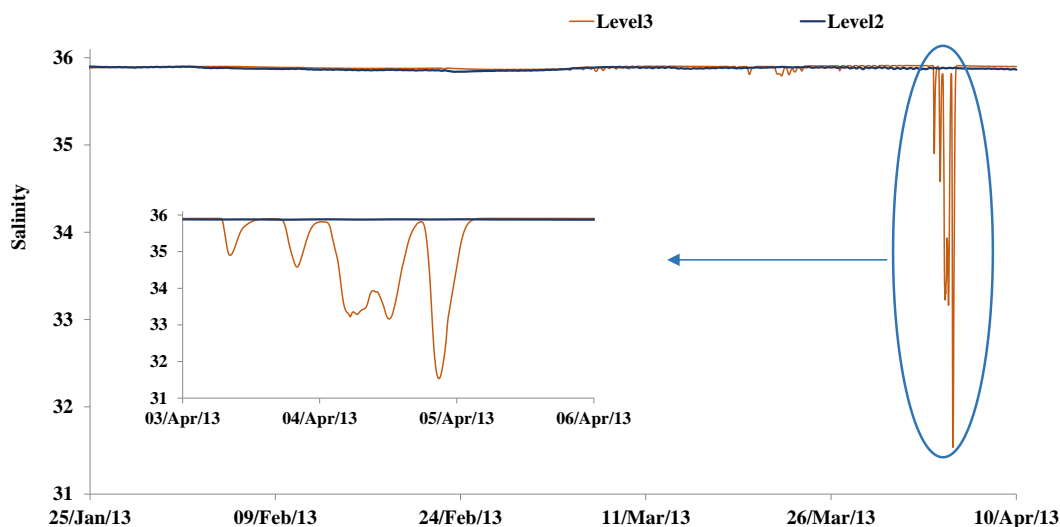


Figure 22: Time series of surface salinity obtained by Level2 and Level3 at a point near the northeastern open boundary of Level3 (see Figure 8).

2.3 Partial conclusions

This chapter covered the downscaling approach and focused in the Tagus ROFI modelling system, which was the elected region for the real case testing of the upscaling methods developed in the next chapters.

The Tagus ROFI area is one of the most studied estuary in Portugal, by Maretec and many other research groups, which contributed to a well established consensus of the circulation patterns as well as the main features determining the circulation inside the estuary and in its adjacent coastal area. This was perhaps the major reason behind the decision to study this particular modelling system, the other being the extreme precipitation event of 2013 which led to flow rates of the Tagus river higher than $7500 \text{ m}^3\text{s}^{-1}$ for over 72 h, when average flow rate is $258 \text{ m}^3\text{s}^{-1}$. As this domain and this specific period – January until April – will be used for comparison between one-way and two-way methodologies as well as offline downscaling and offline upscaling, there was a need for an extensive validation of the operational modelling system currently implemented at Maretec. Validation of the modelling system was accomplished by comparing model results of the Tagus ROFI domain (Level3) with in-situ data from an ADCP and CTD, as well as remote sensing images of surface temperature, which was published in (Hilda de Pablo et al., 2019) and (Sobrinho et al., 2021). It proved the model application's ability to represent the major features of this coastal area and set the baseline for future comparisons. After validating the application, a closer look into the grid coupling was taken, as well as the vertical structure of the water column at the overlapped area of the domains. This was done through the comparison between Level2 and Level3 surface residual circulation, time series and vertical profiles. The residual circulation showed a strong difference in the interior of the Level3 domain – particularly near the coast past Cape Raso – with the Tagus estuary plume being the most important factor. Time series were extracted from the Portuguese Coast Operational Modelling system (PCOMS – Level2) and compared to time series produced by the Tagus ROFI domain, and proved that the estuaries' plume reaches all four open boundary domains, but with a stronger salinity gradient (4.5 salinity units during the peak flow) verified at the Northern boundary (due to the Coriolis effect in the plume's trajectory). Several vertical profiles complemented this information and demonstrated the far reach of the estuarine plume – up to 50 m in depth – as well as the growing impact of the plume over three averaging periods (11th of January until the 10th of April, 1st of March until the 10th of April and from the 25th of March until the 10th of April). Temperature profiles were similar for the deeper areas

(although the wider scales associated with the 7 °C below 1500 m difficult the analysis). However, they do suggest an increase in upwelled waters, whose influence can be from the simple effect of having the discharge, which can increase upwelling at a local level, but also due to higher bathymetric detail, specially near the continental slope and submarine canyons. As Level2 domain does not consider river discharges, its nested domain (Level3) is not able to simulate the complete salinity variability over its domain and its open boundaries, for example during a transition between a southerly wind to a northerly wind. In this case higher salinities from its parent domain – Level2 – will override the lower salinities leaving Level3. Possible solutions to improve these modelling systems are described in more detail in the next chapters.

CHAPTER III

This chapter originated the article:

Sobrinho, J., de Pablo, H., Pinto, L., and Neves, R. (2021). Improving 3D-MOHID water model with an upscaling algorithm. *Environ. Model. Softw.* 135. doi:10.1016/j.envsoft.2020.104920.

Chapter 3 Upscaling local domains into regional domains – online coupling

This chapter describes the upscaling algorithm implemented in the MOHID model and the philosophy behind it. Throughout the thesis, a distinction is made between online and offline approaches. In downscaling, while an online approach demands that both parent domain (PD) and child domain (CD) run at the same time in one stand-alone application, an offline approach allows the PD domain to run separately from its CD, with advantages in computational effort. In this approach, open boundary conditions (OBCs) of the CD are added through higher temporal resolution of the PD results (typically 900 s), allowing for different CD implementations running with OBCs from a single PD simulation. Considering this philosophy, when an upscaling algorithm – transfer of information from CD to PD – is added to an online downscaling approach, the result is a Two-way simulation. Finally, offline upscaling is defined for simulations where a local (higher resolution grid) domain produces results which are then used to improve any regional (lower resolution grid) domain. If the regional domain forcing the CD is the same as the regional domain which is updated by the CD, then the simulation is considered an offline Two-way simulation. However, if the regional domain is different, then the simulation falls into the offline upscaling approach category. This means that a local model can be used to update different regional model domains each with their own characteristics (or even model software).

This chapter is focused on the upscaling algorithm implemented in the MOHID model and includes a comparison analysis between online one-way and two-way approaches. These include three schematic domains: a 2D open channel forced by 10 cm amplitude waves; a 3D schematic coastal area with a steep slope forced by a north wind; a 3D domain with a lateral discharge. In the end, a real case simulation with the Portuguese coast and the Tagus estuary (same application as the one presented in Chapter 2) is analysed. However, the main goal of this thesis is to develop the offline upscaling algorithm which will allow the introduction of local processes into regional domains (such as estuaries) and provide a stepping-stone for ocean-watershed model couplings. As such, the purpose of the comparison between online one-way and Two-way simulations was to identify the major sources of error produced by the upscaling algorithm, as well as to identify and correct all the programming errors which naturally occurred during this thesis. All the schematic cases are now a good baseline for future changes in the code, allowing for early detection of code bugs.

3.1 Rationale for an upscaling algorithm

Increasing demand for high resolution model applications by government agencies, aquaculture and energy companies is driving private and public entities to develop updated grid domains for coastal areas. Higher resolution nested grids lead to better numerical skills of the model and allow the use of more refined bathymetric and atmospheric data, improving the overall hydrodynamic solution and reducing the errors of the downstream transport models. This higher level of detail allows a direct comparison between very local field data (e.g. currents) and model results, increasing the modelling system's confidence.

Downscaling from a parent domain (PD) to a child domain (CD) is still the most common option to simulate the effect of large-scale on local processes in MOHID Water model (Campuzano, 2018; de Pablo et al., 2019; Fossati and Piedra-Cueva, 2013; G. Franz et al., 2014; Franz et al., 2016; Gutiérrez JM et al., 2015; Huhn et al., 2012; Janeiro et al., 2017) and in many other structured grid models such as ECO-MARS3D (Desmit et al., 2018), MIKE3 (Gallego et al., 2017), POM (Nagy et al., 2017), NEMO (Katavouta and Thompson, 2016), ROMS (Dabrowski et al., 2014), and Delft3D (Yin et al., 2019). When using this methodology, care must be taken to avoid drifting of the (CD) over time or instabilities will be produced at the border. Drifting can occur due to local features not reproduced by the parent domain, noise created inside the child domain which is not kept under control, and loss of properties mass conservation at the open boundary. These issues are addressed in (Debreu and Blayo, 2008; Flather, 1976; Palma and Matano, 1998), where a number of solutions are provided to preserve mass conservation, control noise at the open boundary and to smooth the transition between parent and child solutions. The most common solution for downscaling systems – particularly in the MOHID system – is the use of a Flather (Flather, 1976) boundary condition for the barotropic flow, allied with a radiation scheme such as described in Marchesiello et al. (2001) and a flow relaxation scheme described by Martinsen and Engedahl (Martinsen and Engedahl, 1987). Another option commonly considered is the use of a biharmonic filter described by Kantha and Clayson (Kantha and Clayson, 2000) that removes small wave length oscillations inside the child domain, although it is more relevant in low dissipative environments. To facilitate the performance of these techniques, the boundary between nested domains should be far enough from local hydrodynamic features. This way, nested domains will produce comparable results in the interface, allowing for easier radiation of outgoing waves and elimination of noise produced in the child domain.

one-way nested models assume that large scale processes affect local scale processes, and enable the building of local solutions using global services (e.g. [Copernicus](#) or [EMODnet](#)), but not the other way around. These web services provide solutions at the ocean scale that are downscaled offline by regional and local models to provide services to coastal areas end users.

A way to fill this local information gap is to allow the CD – which typically has local knowledge embedded – to update the parent domain (PD), also known as the upscaling stage of a Two-way nesting. Transferring results from smaller to larger scale reduces numerical diffusion in high gradient regions, but also allows the modification of the large-scale flow by local features, as is the case of tidal jets at the mouth of large estuaries, especially in tidal estuaries. This provides stronger mixing of the water column, changes the local Coriolis effect on the PD improving its horizontal and vertical solution, and changes the coastal transport.

Different methodologies to implement Two-way nesting have been proposed in the literature. Studies by Urrego-Blanco et al. (2016, 2014) used the semi-prognostic method proposed by Greatbatch et al. (Greatbatch et al., 2004), which introduces a pressure correction term in the horizontal momentum equations. Marchesiello et al. (2011) applied the ROMS-AGRIF Two-way capability (Debreu et al., 2012) – created for split-explicit models –, which considers the feedback of surface elevation, velocities and tracer properties, and introduce a flux correction scheme (Berger and Colella, 1989) to enforce mass conservation at the interface between grid domains. Kelly et al. (2016) studied tide dynamics using the fully implicit in time and space scheme developed by Haley and Lermusiaux (2010). In all of these methodologies the common approach is to relax (although in the semi-prognostic method it is not considered a typical relaxation) the parent domain to its CD, which has been considered a successful option in transferring information from the local scale to the regional scale. This option also has the advantage of using local measured data to improve the entire nesting system, via feedback from the child domain. Another approach which has gained traction in the modelling community is the use of assimilation techniques to transfer information from CD to PD. In this methodology, as in any other two-way methodologies, the CD solution is considered to be more accurate than that of its PD. Due to the amount of “data” available, the assimilation techniques become easier to use. (Barth et al., 2007) applied this methodology successfully to the Ligurian Sea by assimilating temperature, salinity and surface elevation fields. More recently, and driven by the need for faster computations in operational forecasting, (Vandenbulcke and Barth, 2019) used assimilation techniques to transfer information from CD to PD. In their work, they separate downscaling from upscaling because CD and PD are run offline, which coincides with the

definition applied in this thesis. Much like in this thesis, the overall process can be considered an offline two-way simulation because information does travel in both directions. However, the implementation and calibration of the assimilation techniques are typically more difficult and subject to higher errors as mentioned in these studies. These techniques which are commonly based on the use of Kalman filters, tend to require ensemble simulations to obtain a larger spectrum of possible solutions. Furthermore, statistical methods will degrade solutions faster, as the balance between fluxes entering and exiting a numerical cell is not the priority and will require flux corrections as well as the occasional restart of the model system to avoid divergences. For these reasons, this thesis will be focused on upscaling through relaxation using a volume-average algorithm, which will transfer information from a LD to a RD with lower chances of compromising the physical processes. Another advantage of this methodology over the data assimilation is the variables upscaled from the LD. While the work of (Vandenbulcke and Barth, 2019) focusses on solely temperature and salinity, this thesis will focus also on velocities and water level, promoting a better physical representation of the processes. The novel part their work is that it follows the same trend of this thesis, which is the separation between downscaling and upscaling – with the ultimate goal of performing upscaling operations between different model implementations run in different countries, by different institutions. Offline upscaling is also the main goal of this thesis for that same reason and because model solutions such as those provided by CMEMS can be improved by these methodologies.

In un-structured grids a Two-way system is easier to implement because the grids can be optimally nested, as demonstrated by Qi et al. (2018). In their study, the feedback was done only at the open boundary level, which is possible due to the smooth transition between grid resolutions. However, the time step in explicit schemes in unstructured grids is bound by the Courant–Friedrichs–Lewy, resulting in very low time steps which require bigger computational systems, especially for larger domains. A review on the main methodologies for a Two-way nesting system can be found in Debreu et al. (Debreu and Blayo, 2008) and (Holt et al., 2017), which provides a comprehensive description of the available modelling techniques, a comparative analysis between one-way and two-way grid coupling in structured grids and unstructured grids, and hints at the direction of ocean and coastal modeling.

Conceptually, transferring information from a CD to a PD in a multigrid system can be done in two ways: 1) communication is done only at the interface between domains (Kurihara et al., 1979), in which case there is no need to compute currents in the overlapped area and the feedback from the child domain is considered as an internal boundary condition; 2)

communication is done at the interface and the feedback, in the overlapped area between domains. However, as the first technique forces the method to be coupled online and creates two boundary conditions – leading to implementation complications – the methodology selected for MOHID model will follow the second technique (Fox and Maskell, 1995; Oey and Chen, 1992).

When a Two-way nesting methodology is used, another boundary issue arises, caused by the parent domain update of physical variables from the child domain which are, in turn, dependent on the parent solution (Debreu and Blayo, 2008). In literature, and due to this Two-way communication, the term interface has been divided in two terms regarding domain areas, one for the traditional one-way information exchange – dynamic interface – and another for the update operation – feedback interface. In one-way nesting, the dynamic interface typically occupies the first two numerical cells of the parent domain to allow 2nd order interpolations from the parent to the child domain. On the other hand, if noise is produced in the child domain, it is expected to be heightened near the boundary with its parent domain. This can lead to the propagation of a disturbance from the child domain into the parent domain. In order to avoid such issues, several authors (Debreu et al., 2012), (Urrego-Blanco and Sheng, 2014), (Marchesiello et al., 2011), (Sannino et al., 2009), (Barth et al., 2005) separated these two interfaces. This interface separation, although acting as a restraint on the feedback of noise into the parent domain, may prevent a smooth transition between grids. For that reason authors have suggested the use of sponge cells with artificially high viscosity on the child domain near the boundary in order to remove spurious flow oscillations (Urrego-Blanco et al., 2016), (Debreu et al., 2012), (Barth et al., 2007). Acosta et al. (2015) did not separate these interfaces, but used a flow relaxation scheme to account for the noise between domains, also with good results.

3.2 Upscaling Algorithm

The algorithm described here and implemented in the MOHID model system is based on the work of Oey and Chen (Oey and Chen, 1992) and Fox and Maskell (Fox and Maskell, 1995) where feedback from CD occurs in the overlapped area. The variables included in the feedback procedure are velocity (horizontal), temperature, salinity and any biogeochemical property required by the user. Surface elevation and vertical velocities are left to evolve freely but the user can activate them at any time with specific keywords.

The proposed timescale for the interaction between the interpolation from the parent domain to the child domain is described in Figure 23.

It is considered, as in one-way nesting, that the CD time step is a multiple of its parent domain and, as such, an iteration starts with the integration of the PD for one time-step. After a full time-step, the parent domain provides open boundary conditions for the CD, which runs the same integration period. Feedback takes place next, with the CD updating the PD variables over an overlapped area.

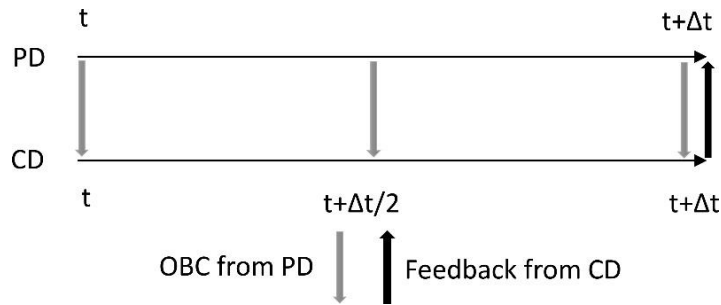


Figure 23: Two-way time scale for one parent domain iteration, with a time refinement factor of 2.

The proposed upscaling algorithm considers a relaxation of the PD to a CD solution over an overlapped area, which can be the entire CD area, if there is no separation between dynamic and feedback interface, or a smaller area if the separation of interfaces is desired. This separation is done by defining a number of CD cells which will not be considered in the feedback operation.

Two different upscaling options have been implemented into the MOHID code: 1) a volume weighted average operator, which considers the volume-based weight of a given CD cell inside a PD cell. To this end, the model uses routines that were already in place in MOHID, which create a matrix connection between PD and CD, and a new one was developed for the vertical structure – which means that the vertical discretization of the PD can be different from that of the CD as is the case in the transition to coastal areas. This option has the advantage of faster calculations and easier code implementation; 2) Inverse weighted distance method (IWD) which will give more importance to the CD cells closest to the PD property cell centre. This option is in line with Debreu et al. (2012), who proposed the use of a full-weighting operator, which gives more importance to CD cells closest to its respective PD cell. As their work suggests, without this option a sponge layer near the boundary will be needed to properly damp sub grid scale features. However, the IWD method has not been extensively tested in this thesis, the main reason being the higher error expected from this solution, because it tends to give too much importance to the centre cell of the CD which is solving scales not solved by its PD. These issues will need more research and more methods are bound to be implemented in

MOHID with future PhD students currently starting their journey into ocean modelling at Maretec, the recently created AIR centre and +Atlantic collaborative laboratory.

In a Two-way methodology, MOHID equations for the PD will now become:

$$\frac{\partial u_i^*}{\partial t} + \frac{\partial(u_i^* u_j)}{\partial x_j} = f u_j - \frac{1}{\rho} \frac{\partial p_{atm}}{\partial x_i} - g \frac{\partial \eta}{\partial x_i} - \frac{g}{\rho} \int_z^\eta \frac{\partial \rho}{\partial x_i} dz + \frac{\partial}{\partial x_j} \left(v \frac{\partial u_i^*}{\partial x_j} \right) \quad (22)$$

$$u_i = u_i^* + \left(\frac{u_i^{CD} - u_i^*}{Td} \right) \Delta t \quad (23)$$

$$\frac{\partial P^*}{\partial t} + \frac{\partial(P^* u_i)}{\partial x_i} = \frac{\partial}{\partial x_i} \left(v \frac{\partial P^*}{\partial x_i} \right) + S_P \quad (24)$$

$$P = P^* + \left(\frac{P^{CD} - P^*}{Td} \right) \Delta t \quad (25)$$

where u_i^{CD} and P^{CD} stand for the volume weighted average of the i velocity component and tracer property of the CD cells. Td stands for the relaxation period in seconds.

A considerable difference between the approach followed in this work and many of those mentioned in this article is the Td value, which will be set to a time frame of hours instead of a close multiple of the PD time step. This option will avoid the accumulation of mass conservation errors to dangerous levels and thus create erroneous circulation patterns or even produce numerical errors. As this is a critical step for the development and validation of the offline upscaling algorithm, a validation of the two-way coupling is performed in this thesis and includes four different schematic cases as well as a real case simulation of the 2013 extreme precipitation event in the Tagus ROFI area.

Validating the algorithm with schematic cases has the advantage of an easier analysis of the errors produced by the coupling as well as to find potential bugs in the program. However, many times these cases are too specific and demand for boundary conditions and formulations that are not suited for real case scenarios, such as the case of cyclic boundaries. As such, these new developments should be tested in real case scenarios with multiple hydrodynamic processes and highly variable bathymetries to test the robustness of the algorithm. During this thesis, the schematic tests were a valuable source of error identification and essential for sensibility testing, not only for the two-way coupling but also (and possibly more important) for studying the backend programming of the Navier-Stokes equations, the open boundary conditions (for single grids and for nested grids), the advection and diffusion processes, and many more. They allowed for the correction of many bugs in the model which would be difficult to find in bigger and more demanding real case simulations. Even then, many errors were

produced in the code which were only identified in the real case study of the Tagus ROFI, especially bugs related to a variable bathymetry and nearshore areas where the existence of covered cells (bottom) next to uncovered cells (water column) – which can easily be different from PD to CD – require more details in the algorithm.

3.2.1 Code implementation

The upscaling algorithm code in MOHID follows the modular approach standard to MOHID. This section briefly describes the online two-way implementation of the upscaling algorithm, while the offline upscaling is described in chapter 4.

In an online coupling simulation where both CD and PD run at the same time, an interface between the modules, although not necessary, greatly improves the scalability of the code, as it allows for an easier integration of new upscaling methods and routines without major changes to the remaining MOHID modules. As such, the Two-way module was created with responsibilities at the level of variable allocation, computation matrixes associated with the upscaling method, definition of mask matrixes, computation of auxiliary matrixes, and invocation of the upscaling functions. As this module is invoked by the “Hydrodynamic” and “WaterProperties” modules, it cannot invoke them (communication between modules is one-way), which means that every model domain must have its own instance of the Two-way module. This also facilitates the code management as it becomes more structured. All the main keywords associated with upscaling are defined in the CD domain – because in the MOHID structure the PD does not know who its CDs are – hydrodynamic and waterproperties files. Additionally, all the connection matrixes between CD cells and PD cells are already built for online downscaling, which means that part of the code needed for the upscaling process was already in place. However, a new routine was added to create a connection matrix for the vertical discretization, as PD and CD can have different numbers of vertical layers and thicknesses.

In both the “Hydrodynamic” module and the “Waterproperties” module, the upscaling routines are called at the end of CD iteration. Hydrodynamic and waterproperties objects (which take in all the variables, matrixes and keywords) are created for each modelling grid domain, and include the next grid domain (whether nested or not) in the list of domains to include in a simulation. This means that at any point of the code it is possible to know if there is a following domain that will need to be iterated. The activation takes advantage of this structure, by performing a verification of whether a next domain exists or not, and is performed because

there can be multiple levels of nested domains, each upscaling their information to their correspondent PD. To ensure that the upscaling is done at the proper time instance (when CD and PD are synchronized), the upscaling can only be initiated at the last grid domain available. For example, if a simulation includes 3 cascading domains, with time steps of 40, 20 and 10 s respectively, it is important for upscaling to be triggered by the last domain – the one running iterations with a frequency of 10 s – only when it completes 20 s, which is when it is synchronized with its PD. After this first upscaling, the next level domain (running at 20 s) will check if it is synchronized with its PD (running at 40 s), and will only perform the upscaling if it is synchronized. When it is time to update the PD fields, the hydrodynamic module sends the CD and PD field matrixes the Two-way module which will then update the PD fields with the CD fields, considering the upscaling method the user defined. This also means that, as in one-way simulations, the CDs time step must be a multiple of their PDs.

Examples of implementations files for Hydrodynamics and WaterProperties are presented in tables Table 7 and Table 8.

Table 7: Upscaling keywords needed in the hydrodynamic.dat implementation file of the nested Domains. Default values are included in parenthesis. These keywords are added outside any existing property block (which look like <begin....> <end....>).

Keyword	Value	Comment
SUBMODEL	: 1 (0)	Checks if the domain has a PD. 1=true;0=false
TWO_WAY	: 1 (0)	1=true;0=false
UPSCALING_TIME_DECAY	: 120 s (3600 s)	Time decay used in the nudging routines. Real type value
UPSCALING_COLD_PERIOD	: 0 s (0 s)	Amount of time before activating the upscaling. Real type value
UPSCALING_METHOD	: 1(1)	1: volume-weighted average 2: IWD
UPSCALING_IGNORE_CELLS	: 9 (0)	Number of CD cells to exclude, perpendicular to the open boundary. Integer type
UPSCALING_WATERLEVEL	: 0 (0)	1: upscale water level, 0 otherwise
UPSCALING_VELOCITY_W	: 0 (0)	1: upscale vertical velocity, 0 otherwise

Table 8: Upscaling keywords needed in the WaterProperties.dat implementation file of the nested Domains. Default values are included in parenthesis. These keywords are added inside existing property block which the user wants to upscale (which look like <begin....> <end....>).

Keyword	Value	Comment
TWO_WAY	: 1 (0)	1=true;0=false

SUBMODEL	:	1 (0)	Checks if the domain has a PD. 1=true;0=false
TWO_WAY_WAIT_PERIOD	:	0 s (0 s)	Amount of time before activating the upscaling. Real type value
TWO_WAY_COEF	:	120 s (3600 s)	Time decay used in the nudging routines. Real type value

The number of CD cells to be left out of the computation is only specified in the hydrodynamics file in order to force the model to use the same number in field velocities, water level, and any water property, ensuring consistency. When a nested model is detected and the “TWO_WAY” keyword is active in the hydrodynamic implementation file, then the hydrodynamic module will set these values into the Two-way module. Another advantage of having this module separate from the main modules is that it leaves space for usage by the MOHIDLand modules which are just as capable of calling the same routines, but with different matrixes and keywords, and is one possible solution for future couplings between ocean and watershed models.

Once the domains are synchronised, the hydrodynamic and waterproperties modules send the required field matrixes to the Two-way module, which, after identifying the upscaling method, computes the sum of all CD cell volumes inside each PD cell and sends these data into the respective upscaling routines. These are separated between 2D matrixes (water level) and 3D matrixes (all other variables, such as even 2D fields, are allocated as 3D arrays), and inside the 3D classes, scalar and vector fields are also separated. This separation of the 3D routines was made so as to increase the computational efficiency as, in contrast with velocity fields, scalar fields do not require a verification of whether the 2 adjacent cells are covered with water. Regardless of the routine, the equation is always the same and only the “do” cycles and the “if” statements change. The updated parent field matrix is updated with equations (26 and (27.

$$P_{PD}^* = V_{CD}^\omega \times P_{CD}^\omega \quad (26)$$

$$P_{PD} = P_{PD} + \left(\frac{P_{PD}^*}{V_{CD}^\omega} - P_{PD} \right) \times \frac{\Delta t}{Td} \times \frac{V_{CD}^\omega}{V_{PD}} \quad (27)$$

where P_{PD}^* is an auxiliary matrix that holds the total amount of a property (P_{CD}^ω) times the total volume of CD cells (V_{CD}^ω) inside each PD cell (ω), P_{PD} represents a PD property matrix, Δt the time step of the PD, Td the time decay for nudging the CD solution into the PD, and V_{PD} the volume of the PD cell.

In the following section three schematic cases will be analysed as regards the vector and scalar properties, by comparing a PD with and without upscaling against a reference domain with the

same size as the PD but with the grid step of the CD nested in the PD. The algorithm is then tested in a real case simulation of the Tagus ROFI area using the same domains and implementations as those presented in Chapter 2.

3.2.2 Schematic case: wave through a 1D channel

This test was largely based on tests performed in (Leitão, 2002) and consists of the analyses of the propagation of a wave with 10 cm of amplitude and a 2500 s period. To test the two-way algorithm implemented in MOHID, three domains were implemented. A parent domain (Level1) with a 900 x 900 m grid resolution and a length of 900 km, a nested domain (Level2) with a grid resolution of 300 x 900 m starting 39 km from the origin of Level1, and with a length of 90 km, and a reference domain with a grid resolution of 300 x 900 m with the same length of Level1. The latter is considered as a reference because a higher grid resolution domain inherently produces better hydrodynamic results.

All the domains use the same time step to minimize the sources of differences between domains to the grid resolution, and advection and diffusion processes are included. The domain depth is 10 m for all domains with a single sigma layer, and the grid viscosity was set to $90 \text{ m}^2\text{s}^{-1}$, $30 \text{ m}^2\text{s}^{-1}$ and $30 \text{ m}^2\text{s}^{-1}$, respectively for Level1, Level2 and Reference domains.

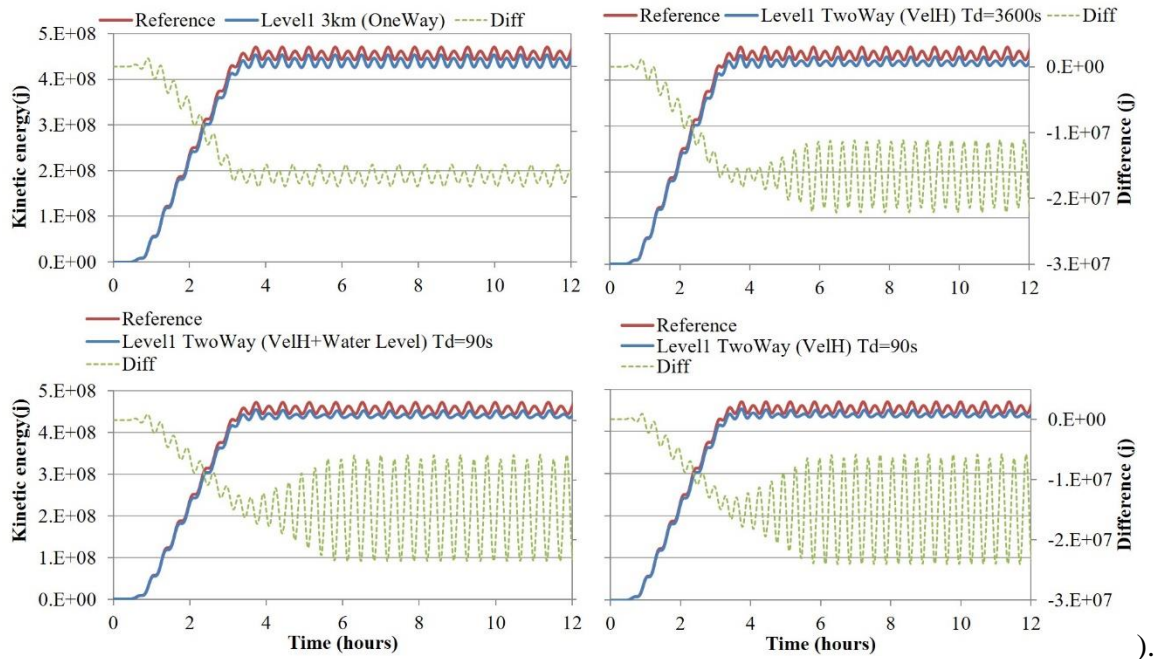
Regarding the open boundary conditions, both Level1 and the Reference domains use a Flather radiation scheme (Flather, 1976) for water level without a local solution, and a Flather radiation scheme with the PD as a local solution was implemented in Level2.

A domain depth of 10 m makes the wave propagate as a gravity wave which can be calculated as \sqrt{gh} giving a velocity of 9.8 ms^{-1} . At this velocity the wave will reach the end of Level1 and reference domains after 25.5 h. However, in order to lower the computational time, only 12 h were simulated. Considering the length of Level2, the wave will reach its eastern boundary approximately 3 h after the beginning of the simulation, which means that 12 h after the start thereof any perturbations to the water level and energy fields will be noticeable from radiation errors at the open boundary with its PD – Level1.

As in the remaining schematic cases, a sensibility analysis of the most impactful parameters of the upscaling algorithm was carried out, including the time decay, the number of CD to be ignored from the open boundary, the upscaling of vertical velocities and water level.

In this case, the major source of discrepancy between Level1 domain and the Reference domain is the grid resolution in the XX axis, by adding more numerical diffusion in the lower grid

resolution domain. The introduction of Level2 reduces the diffusion in the overlapped area between Level1 and Level2, which in a two-way simulation approaches Level1 towards the reference solution, as shown in Figure 24. Diffusion is also responsible for lower horizontal velocities, which then lowers the total amount of kinetic energy over the overlapped area between the nested domains (see Figure 25).



Regarding the upscaling parametrization, the following tests were performed:

- Upscaling of horizontal velocities + Td of 90 s
- Upscaling of horizontal velocities + vertical velocity + Td of 90 s
- Upscaling of horizontal velocities + water level + Td of 90 s
- Upscaling of horizontal velocities + water level + vertical velocity + Td of 90 s.
- Upscaling of horizontal velocities + Td of 3600 s
- 0, 6 and 9 CD cells from the open boundary excluded from the upscaling routines.

From Figure 24 it is clear that a lower time decay will produce a better match between Level1 and the Reference solution and that the upscaling of horizontal velocities plus the water level produce a slightly better result than the simulation where upscaling is only performed for the horizontal velocities. While the maximum difference between the Reference solution and Level1 is around 4 %, the same Level1 but with upscaling from Level2 reduces the maximum difference to 3 % with upscaling of horizontal velocities and a Td of 3600 s, 2.5 % with

upscaling of horizontal velocities and a Td of 90 s and 2 % with upscaling of horizontal velocities and water level and with a Td of 90 s.

Results for water level also indicate a shift in the difference curve towards the peaks of the waves. While in a one-way simulation the maximum differences occur after the peak amplitudes, in a two-way simulation, because the wave length approximates that of the reference solution, the maximum difference occurs at the peak amplitudes.

Upscaling of vertical velocities produced negligible changes to the results when compared to upscaling of only horizontal velocities, and for that reason the results are not presented here. Furthermore, a change in the number of CD cells ignored from the upscaling routines produced very small changes, which lead to a conservative approach of excluding the first 9 CD cells from the open boundaries.

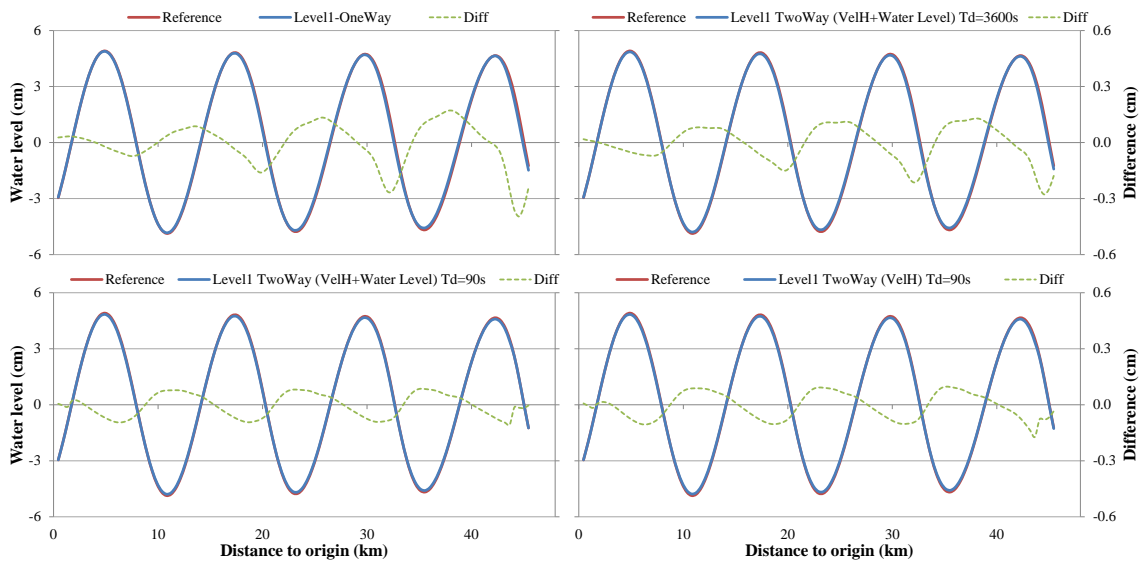


Figure 24: Water level produced by the parent (level1 in one-way and two-way) and the reference domains along the extent of the CD domain after a period of 6 h of simulation. Difference between domains is presented in green.

Changing the velocities and water level of the solution has a stronger impact on the kinetic energy of the system, as it is a function of the square of the velocities. Figure 25 shows how much an impact these formulations have on the solution. As expected, Level1 presents a lower amount of kinetic energy, and with a varying difference over time due to the impact of diffusion in the wave length and amplitude of the waves. Upscaling increases this variability two fold for the case of a Td of 3600 s where only horizontal velocities are upscaled, and three-fold in the remaining parametrizations. The maximum difference observed for the one-way implementation is around 4 % of the total kinetic energy, while simulations with upscaling

produced maximum differences of 5.1 % for horizontal velocities with a Td of 90 s, 5 % for horizontal velocities plus water level and a Td of 90 s, and 4.7 % for horizontal velocities with a Td of 3600 s.

Over time, all simulations reached equilibrium and if there is an impact from the open boundaries of Level2, this impact is not noticeable even after 12 h, when any perturbation produced at the eastern boundary had time to propagate to the western boundary and back again twice.

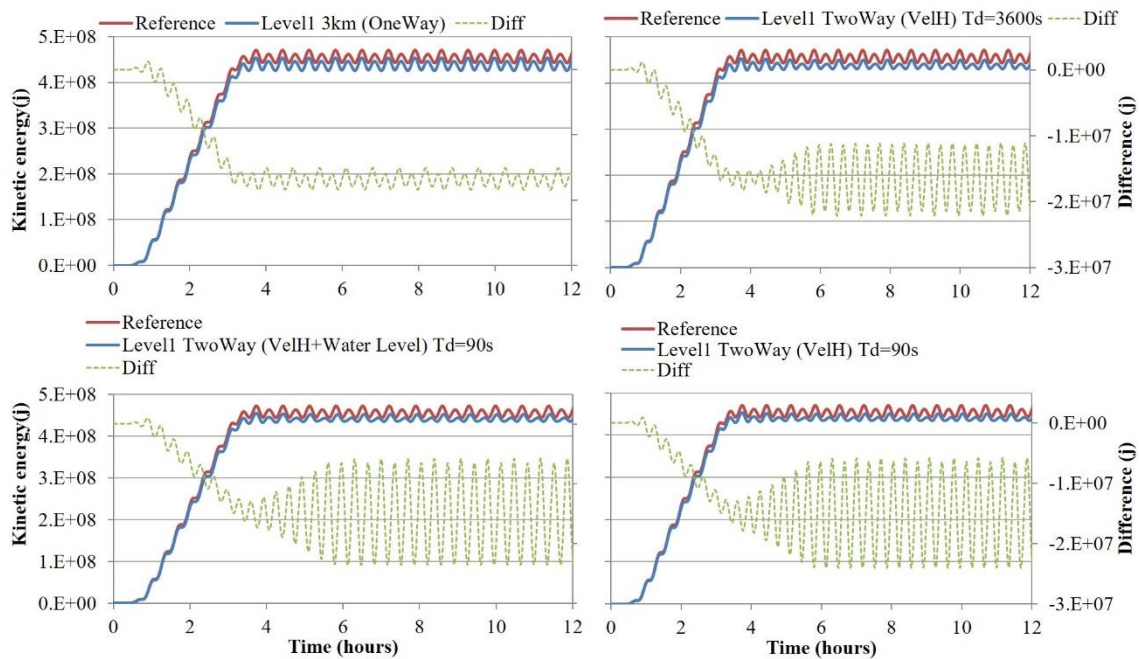


Figure 25: Kinetic energy variation obtained by the parent (level1 in one-way and two-way) and reference domains over 12 hours of simulation. Difference between domains is presented in green.

This test case shows that the use of upscaling from a CD with a higher grid resolution has a positive impact on the overall solution, although with a slight increase in the kinetic energy, which represents an increase in energy amplitude from 20 % (VelH + Td=3600 s) to 30 % (VelH + WL + Td = 90s) when compared to the one-way solution. The improvement of results can be sustainable and at a small cost in the total energy of the system.

Further tests not presented here also demonstrated that using the same viscosity in Level1 and Level2 still produced significant differences between Level1 and Level2, meaning that the numerical diffusion is the most important factor in the divergence between Level1 and the Reference solution.

3.2.3 Schematic case: stratified 3D domain under constant north wind

This schematic case focuses on the upwelling phenomena caused by a 3 ms^{-1} north wind blowing on a 3D domain with a slope bathymetry mimicking that of a coastal area, and whose water column is stratified.

Following the same strategy of the 1D channel, three grid domains were created: a Level1 with $540 \text{ km} \times 180 \text{ km}$ and a 9 km grid resolution; a nested Level2 domain with 3-km grid resolution; and a reference domain with a grid resolution of 3 km and of the same size as Level1. The bathymetries (Figure 26) were all computed from the same source of bathymetric points (evenly spaced at 1 km) in order to reproduce a more realistic scenario. The domains have open boundaries north, south and west, and a land boundary to the east, which in the northern hemisphere will generate upwelling from the deeper part of the domain (200 m) to the shallow coast (10 m) when north winds are applied.

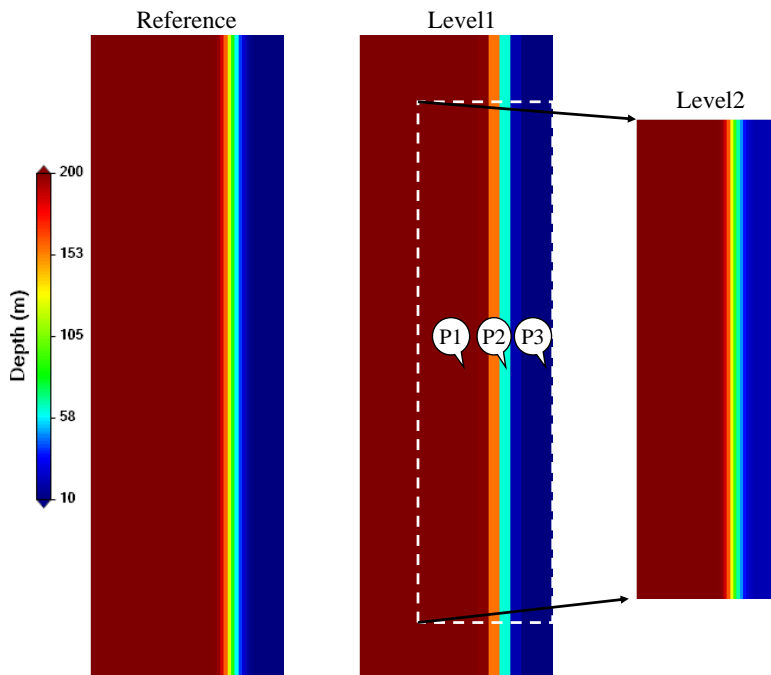


Figure 26: Bathymetries of the three domains simulated and locations of the vertical profiles used for the analysis of the stratification of the water column.

The vertical discretization of all domains is made of 12 Cartesian layers with the following thicknesses (from bottom to surface): 63, 50, 30, 20, 12, 9, 7, 6, 5, 4, 3, and 2. All domains are baroclinic, the salinity field was set constant to 36 and temperature was initiated as a profile, with values (from the bottom to the surface) of: 8.0, 9.8, 10.8, 11.6, 12.2, 12.5, 13.0, 14.0, 15.5, 17.0 and 18.0. Regarding the viscosity, the values chosen were $300 \text{ m}^2\text{s}^{-1}$ for Level1 and $100 \text{ m}^2\text{s}^{-1}$ for Level2 and the Reference domain.

As reported in (Leitão, 2002), the solution which remains stable longest is the one with a cyclic boundary condition. For that reason, open boundary conditions for both Level1 and the Reference domains were set as a cyclic boundary and a baroclinic radiation of velocities. A north wind forcing is also applied to all domains with an intensity of 3 ms^{-1} , and the Coriolis force was added as well as advection and diffusion terms. Level open boundary conditions include a Flather (Flather, 1976) radiation scheme for the barotropic velocities combined with a FRS applied to the first 10 numerical cells from the open boundaries. Due to the stratification of the water column, and to obtain a smooth transition to equilibrium, a slow start of five days of the baroclinic force was implemented, where the baroclinic force increases linearly during those five days. The total simulation period was 6 days in order to reduce the computational cost of the simulations.

The use of Cartesian coordinates has the disadvantage of producing more numerical vertical diffusion – created because internal waves cannot change the vertical layer's thickness as a function of vertical velocities – making any vertical movements transport temperature to the adjacent layers. However, the use of lagrangian layers (which change their thickness according to the vertical velocity) would prove difficult to implement in nested domains, due to different vertical structure near the open boundary of the domains and different time steps. As such, a degree of vertical mixing is expected due to this production of internal baroclinic waves. To reduce this issue, radiation of the baroclinic velocities was added, using a celerity value based on the 1st baroclinic mode: $\sqrt{\frac{\Delta\rho}{\rho_0}gh}$. For this purpose, the interface between the two layers was set at the 20 m bathymetric level, where the highest density gradient was found, and the celerity was computed using the average density of the surface and bottom layers, producing a value of 0.34 ms^{-1} .

A simple sensitivity analysis of the main upscaling parameters was performed and included the time decay and the upscaling of vertical velocities and water level. Results from the previous schematic case suggested that a conservative approach would be advised, which led to the exclusion of the first 9 cells of the CD from the upscaling routines, while different time decays were studied. The selected implementations include:

- Upscaling of horizontal velocities + Td of 90 s
- Upscaling of horizontal velocities + vertical velocity + Td of 90 s
- Upscaling of horizontal velocities + water level + Td of 90 s

- Upscaling of horizontal velocities + water level + vertical velocity + Td of 90 s.
- Upscaling of horizontal velocities + Td of 3600 s
- 9 CD cells from the open boundary excluded from the upscaling algorithm.

In all these parametrizations, temperature is also upscaled with the same Td of the velocities and water level.

3.2.3.1 Surface temperature fields

Surface temperature fields are presented in Figure 27 where a clear upwelling of deeper and colder waters is transported towards the surface due to the Coriolis force created with the north wind drag. Due to higher diffusivity (including numerical) of the Level1 domain, higher temperatures are observed in the one-way simulation, whereas in the reference solution temperatures reach a minimum value that is almost one degree lower in the eastern shallow area.

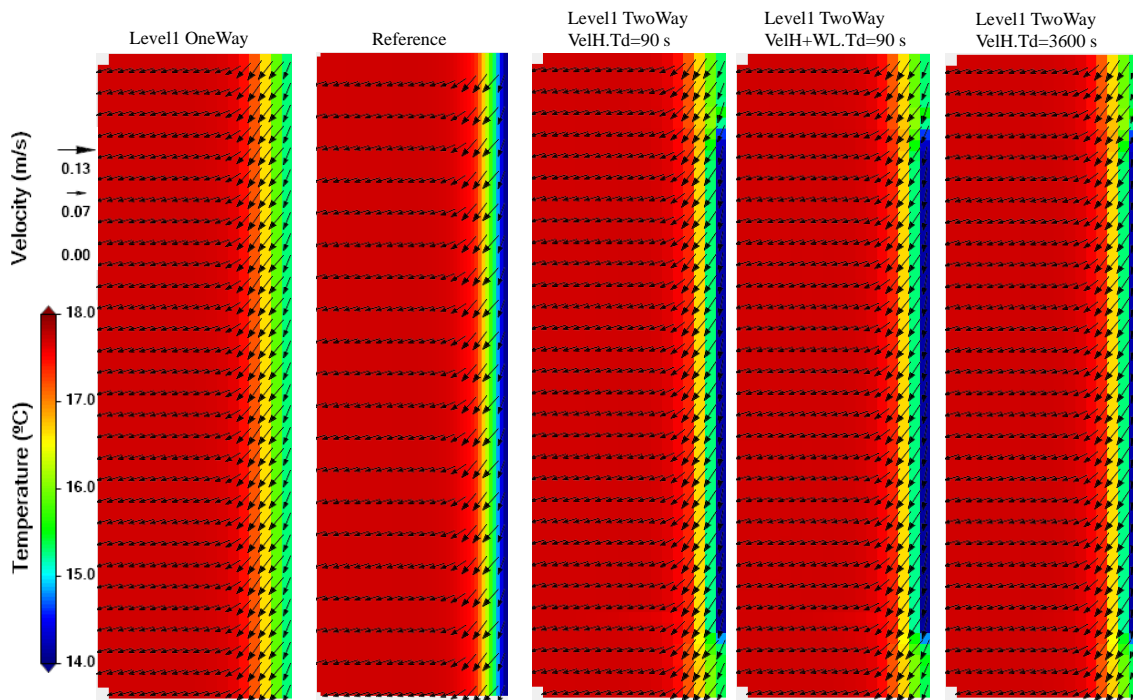


Figure 27: Surface temperature and velocity fields obtained by the Reference domain, Level1 in one-way and Level1 in two-way with three different parametrizations.

Surface results presented in Figure 28 show the most relevant parametrizations tested (many others were tested but with negligible impact on overall results), and suggest that the most coherent solution is that where only horizontal velocities are upscaled and a Td of 3600 s is used. Nevertheless, all two-way implementations are able to reduce the numerical diffusion of Level1 and are successful in approximating its solution to the Reference.

Visually, Figure 27 shows no perceptible difference between solutions, but it is nonetheless presented here because it shows that changes in the upscaling parametrizations produce small changes in surface patterns, and the velocity field overlaying the temperature makes it that much more difficult to analyse the image. However, in Figure 28 an inconsistency can be found at the transition between PD and CD, due to the absence of upscaling from the 9th cell of the CD and towards the open boundary with Level1. The figure also shows that using a higher Td greatly reduces this issue while still improving the overall solution. The parametrization that considers the upscaling of the vertical velocities has been removed because the results are almost identical to those produced by the implementation upscaling only the horizontal velocities.

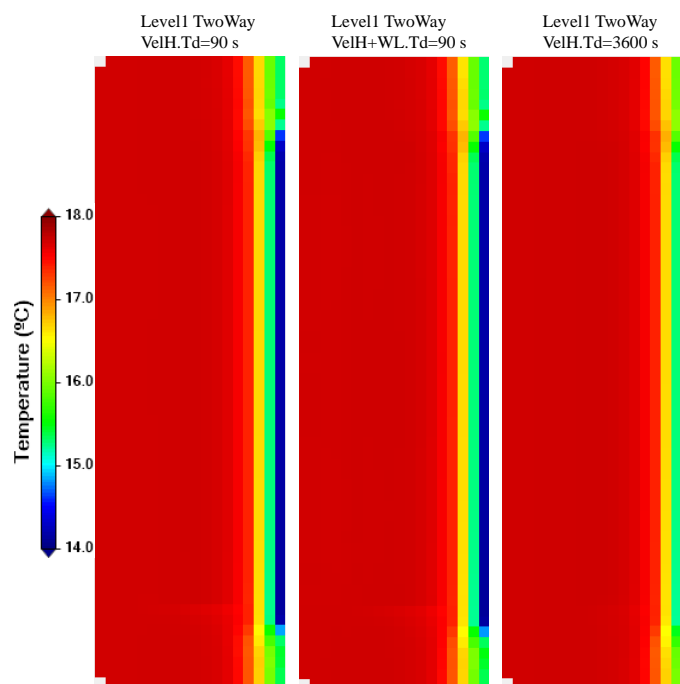


Figure 28: Surface temperature fields obtained by the Level1 in two-way, with three most impactful parametrizations.

3.2.3.2 Vertical stratification

Vertical profiles were extracted from the results at 3 different locations: one at the 200 m depth area (P1), one at slope area with depths around 60 m (P2) and another in the shallow area with depths of 10 m (P3) (see Figure 26) after six days of simulation. The objective is to analyse the upscaling impacts on the Level1 solution and compare them with the higher grid resolution Reference domain. Results shown in Figure 29 suggest higher temperatures are obtained in the lower depths by the Reference solution and Level1 with upscaling, in contrast with Figure 27 and Figure 28. However, this is because the vertical profile was extracted from the second PD

cell from the coast line, which due to the higher diffusion of Level1 without upscaling leads to a smoother spread of ocean temperature.

The vertical profiles also show the effect of the internal waves generated inside the domain, more noticeable in the first 20 m of depth. Over time, this numerical mixing will transfer much of the potential energy to kinetic energy and eventually destroy the vertical stratification.

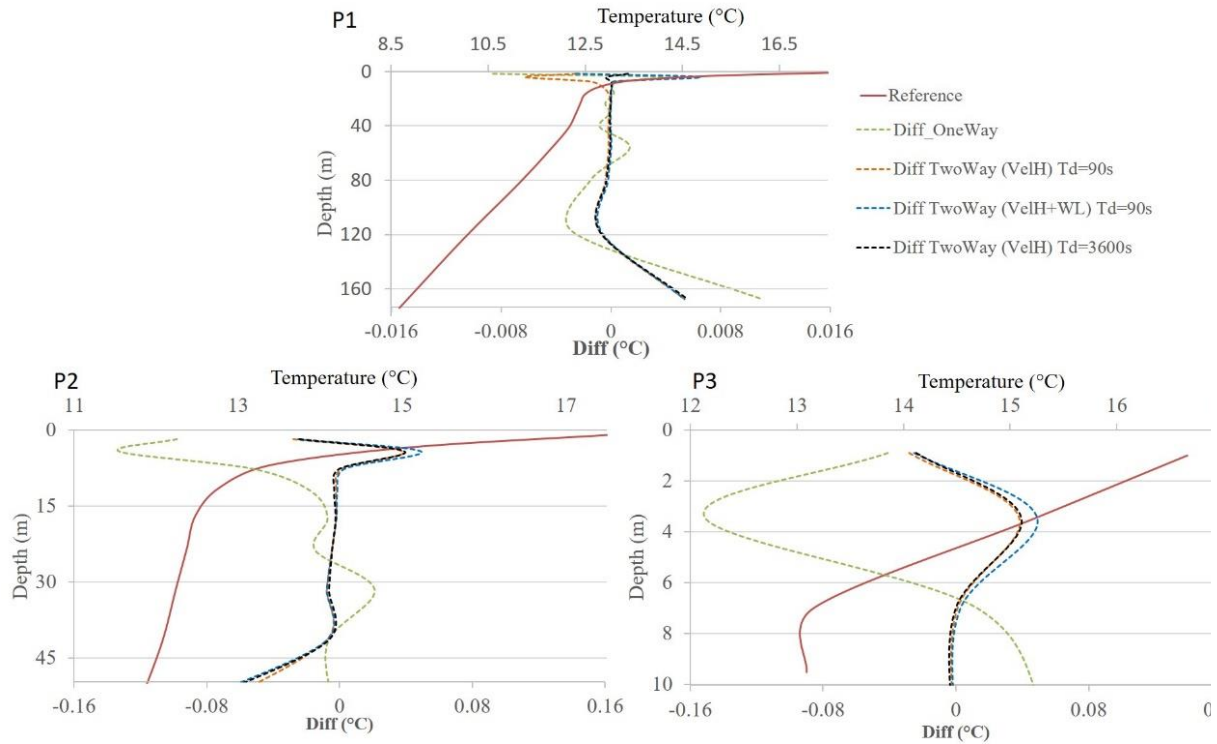


Figure 29: Vertical profiles of temperature at three different locations: in the deep area, at the slope and at the shallow area. Please note that the difference axis changes from P1 to P2 and P3, by a factor of 10.

Regarding the difference towards the Reference domain, upscaling with a higher time decay – 3600 s – presents a better solution in all the profiles, and according to Figure 30, this parametrization is also the one that causes the least impact on the total mass of the system and, consequently, on the average water level. In terms of temperature difference, Level1 run in one-way generates temperatures that are lower (maximum of 0.15 °C in P3) at the surface up to a depth of 20 m. At the deeper areas, from 120 m downwards, it produces temperatures (0.01 °C) higher than those produced by the Reference domain, and in the middle of the slope some variability is found, with higher temperatures in the 30-40 m depth zone and lower temperatures at the surface. Although the use of upscaling reduces the difference in almost every situation, it does seem to overcompensate in some depths, especially near the surface where an inversion of the tendency is observed for the difference towards the Reference domain. This is largely due to the difference in internal waves produced by Level1 and Level2, combined with the reduction of numerical diffusion provided by Level2 when upscaling is on. As in the reference

domain, Level2 will improve the vertical transport of temperature, leading to a higher transport in Level1 when upscaling is on, which is confirmed by lower differences in greater depths (Figure 29) when the algorithm is used.

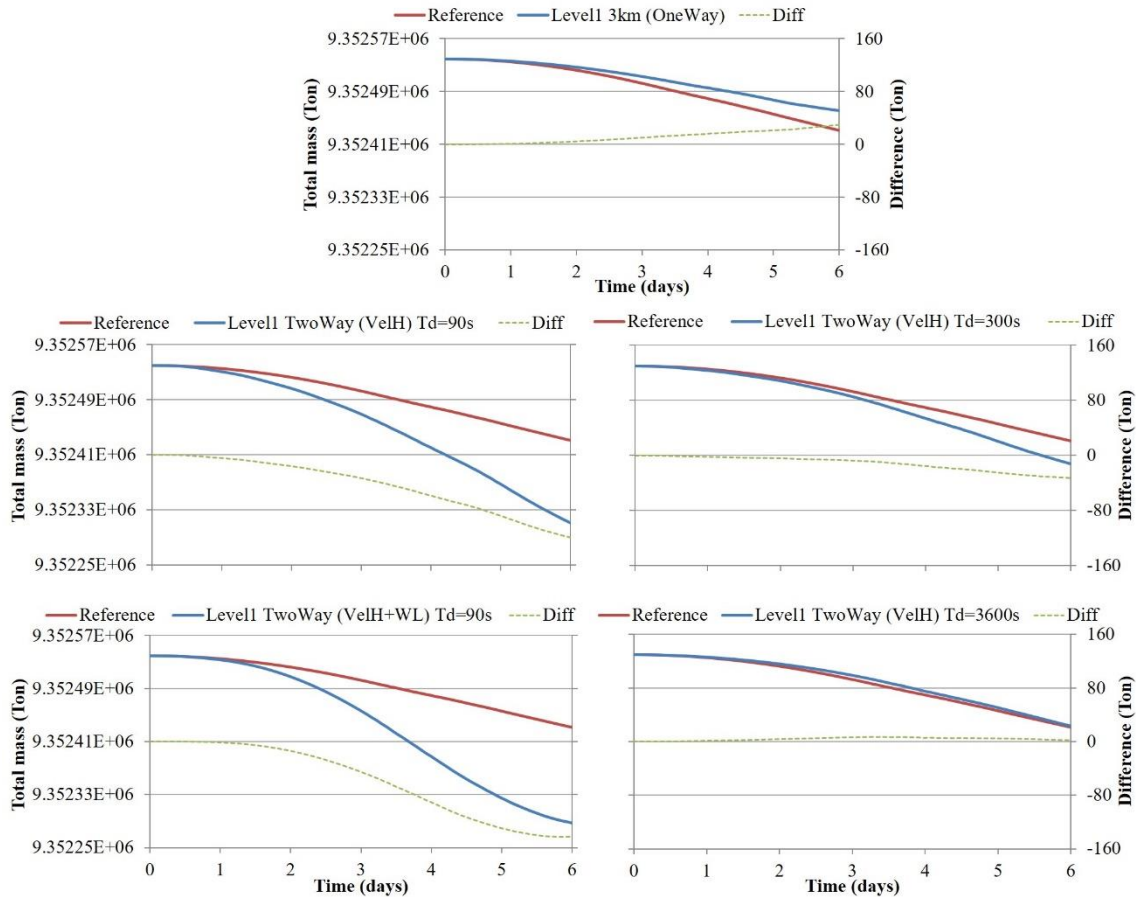


Figure 30: Total mass variation of the Reference and Level1 domains over the 6 days of simulation period.

Total mass loss over time is expected due to the type of open boundary conditions, and model results show that this loss is higher in the Reference domain, although after 6 days only about 0.0005 % was lost, due the open boundary conditions. The introduction of upscaling, especially when water level is also upscaled, leads to an increase in mass loss, to 0.0016 %, which triples the loss produced under a one-way simulation. Increasing the time decay to 300 s leads to an increase of mass loss of around 0.00009 %, and even less for a 3600 s decay time. However, in comparison with the one-way solution, the solution with upscaling always loses mass, as it tries to approximate to the Reference solution, which loses mass at a higher rate over time than the Level1 solution.

Upscaling the vertical velocities did not produce any significant change over the parametrization where only horizontal velocities were upscaled, and for that reason the results are not added here.

3.2.4 Schematic case: 3D Coastal domain with lateral discharge

The objective of this test is to assess the impact of the several upscaling parametrizations on the dispersion of a freshwater discharge in a lateral closed boundary, roughly imitating a river discharge in a coastal area. Until now, all the modelling domains were provided with the same exact forces and processes, although the different grid resolutions generated different results. In this test, the same methodology is applied, but a separate test is performed, where a new process (discharge) is added only in the Reference and Level2 domains, and upscaled from Level2 to Level1.

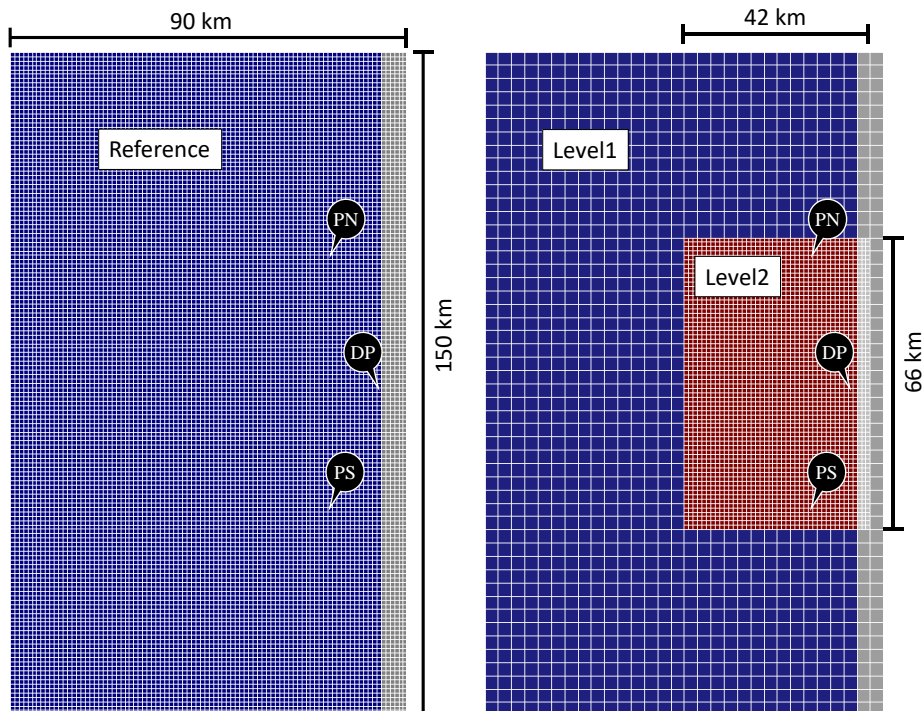


Figure 31: Reference, Level1 and Level2 domains with the locations of the time series PN (north point) and PS (south Point) used in the analyses of the fresh water plume discharge (DP).

The Reference domain consists of a 90x150 km domain with a 1-km grid resolution, Level1 domain is of the same size, but with a grid resolution of 3 km, and Level2 (nested in Level1) is 42 km wide and 66 km long, with a 1-km grid resolution (Figure 31), maintaining the ratio of 1:3 used in the previous schematic cases.

All domains have a constant depth of 5 m and compute advection and diffusion in 3D, as the vertical coordinate is made up of 3 sigma layers with thicknesses of 34 %, 33 % and 33% from

the bottom to the surface. Coriolis force is also active in order for the lateral momentum discharge to turn right (the average latitude of the domains is 38°N). Horizontal viscosity of the reference, Level1 and Level domains was set to $100 \text{ m}^2\text{s}^{-1}$, $300 \text{ m}^2\text{s}^{-1}$ and $100 \text{ m}^2\text{s}^{-1}$ respectively, but other values were tested, especially for Level1, to see if reducing the difference between viscosities would improve comparison. However, even with the use of the same viscosity in all domains a significant different was observed between Level1 in one-way and the Reference domain. As the grid viscosity is proportional to the grid step, the initial implementation was maintained, which is the one that is most similar to the rationale used in real case studies. Vertical viscosity was set to $0.0004 \text{ m}^2\text{s}^{-1}$ for all domains.

Regarding the discharge, its flow and velocities were set to $3000 \text{ m}^3\text{s}^{-1}$ and -1.5 ms^{-1} and 0 ms^{-1} (east-west and north-south direction) respectively and for all domains, except in the test where Level1 does not have a discharge. The discharge was set in the middle section of the domains and in the first cell adjacent to land at the surface layer.

Equal time steps (80 s) were chosen for all domains, in order to reduce the amount of differences between solutions produced by different grid resolutions. At the open boundaries of the Reference and Level1, a Flather radiation condition was applied with no local solution, and a null gradient for temperature and salinity was considered. For the Level2 open boundary, Flather radiation scheme was used with the Level1 as a local solution, temperature and salinity at the boundary were imposed by Level1, and a FRS was also applied for the first 9 cells of Level2.

Regarding the upscaling parametrizations, the following were tested:

- Upscaling of horizontal velocities + Td of 240 s
- Upscaling of horizontal velocities + vertical velocity + Td of 240 s
- Upscaling of horizontal velocities + water level + Td of 240 s
- Upscaling of horizontal velocities + water level + vertical velocity + Td of 240 s.
- Upscaling of horizontal velocities + Td of 3600 s
- 0 CD cells from the open boundary excluded from the upscaling routines.

In all these parametrizations, salinity is also upscaled with the same Td of the velocities and water level. The use of a negative velocity in the east-west direction will cause the discharge to carry momentum westward, which will then turn right due to the effect of the Coriolis force. As the discharge is a constant value, water level variations are not produced and if some are

created at the open boundaries, they will be too small to impact the solution and radiative boundaries will not produce significant changes.

3.2.4.1 Discharge in all domains

In this section an analysis is made to the impact of having two-way coupling between Level1 and Level2, in which a lateral discharge is added to both domains. These results are then compared to those obtained by the Reference domain (which also includes the lateral discharge). Figure 32 also shows the heightened diffusivity of Level1 without upscaling in comparison with the Reference domain in the far field. On Level2, which is relaxing its solution towards Level1, a salinity frame is formed over the west boundary as a result of the higher diffusivity identified in Level1. This effect is easier to identify in these schematic cases (thus their importance), due to the absence of other more intense forces such as tide which tends to mask some of this difference in salinity fields. When upscaling is added, the surface area covered by the plume in Level1 is reduced and a much smoother transition between modelling grids is observed.

In the interior of the domain, Figure 32 shows that in the domains with higher grid resolution (Reference and Level2), an eddy near the discharge is clearly visible with lower salinity values, but not in Level1 – under a one-way coupling – due to its higher diffusion of salinity. However, when upscaling is performed from Level2 to Level1, the salinity field of Level1 approaches the Reference domain solution and shows the eddy present near the discharge location. This improvement is verified for all parametrizations of the upscaling algorithm tested, although with a few minor differences between them – seen at the north boundary – where upscaling only the horizontal velocities with a Td of 3600 s or upscaling the horizontal velocities plus the water level with a td of 240 s produced a more flattened plume, with lower salinities near the coast line when compared to upscaling horizontal velocities at a Td of 240 s. These results are more consistent with those obtained by the reference solution, and, as a conservative approach would suggest using the highest Td possible to reduce the transfer of possible systematic errors, the best upscaling parametrization for this schematic case is the one that upscales only the horizontal velocities and with a Td of 3600 s (45 times the Δt of the simulation).

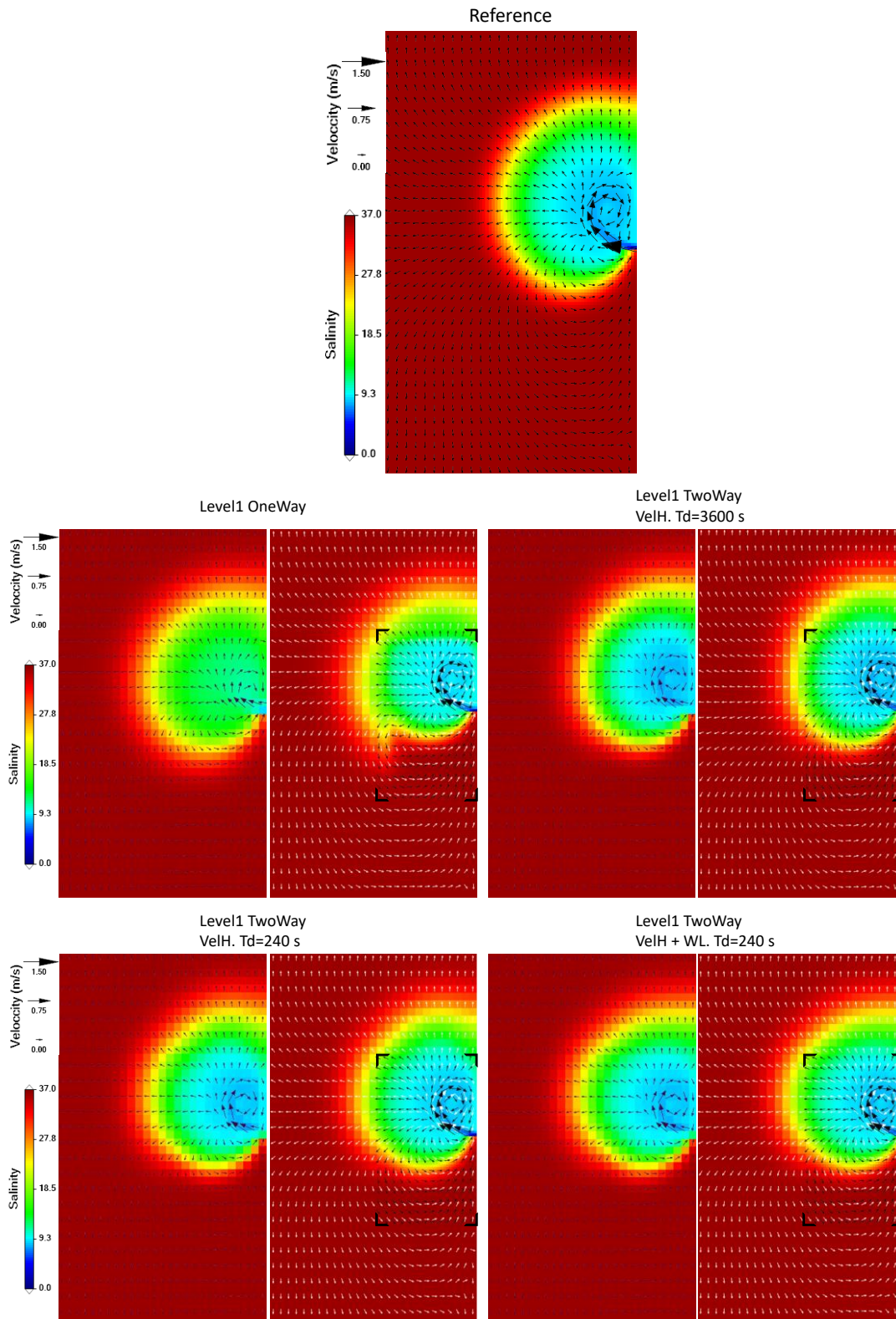


Figure 32: Surface salinity field overlapped by the velocity vectors, obtained by the Reference, Level1 and Level2 domains under the several upscaling parametrizations. Level1 alone is represented on the left, while an overlapping of Level2 on Level1 is represented on the right with a frame (in black) over the open boundary of Level2).

A more focused comparison between model solutions can be obtained by looking at the salinity variability of time at specific locations. In this case 2 locations were chosen: 1 in the north

boundary of Level2 (PN) (Figure 33) and another at its south boundary (PS) (Figure 34). Due to the Coriolis force, the fresh water plume will be transported northwards, and for that reason this border will see the majority of the salinity variability, while the south border will detect salinity variations caused by the higher diffusivity of the 3-km grid of Level1.

At the north boundary, Level1 simulation considering only one-way transfer of information produces a difference of around 4 salinity units at PN after 31 days of simulation. This difference shortens over time, although at ever lower rates but at the expense of more diffusion in the far field of the plume.

When upscaling is introduced and only horizontal velocities are upscaled, the Level1 solution difference towards the Reference solution is reduced to around 0.15 salinity units after 31 days of simulation, although with a slight upward trend. The same is observed when horizontal velocities and water level are upscaled and after 31 days the difference towards the Reference solution is the same as when only the horizontal velocities are upscaled. However, the difference towards the Reference solution does seem to increase at a higher rate.

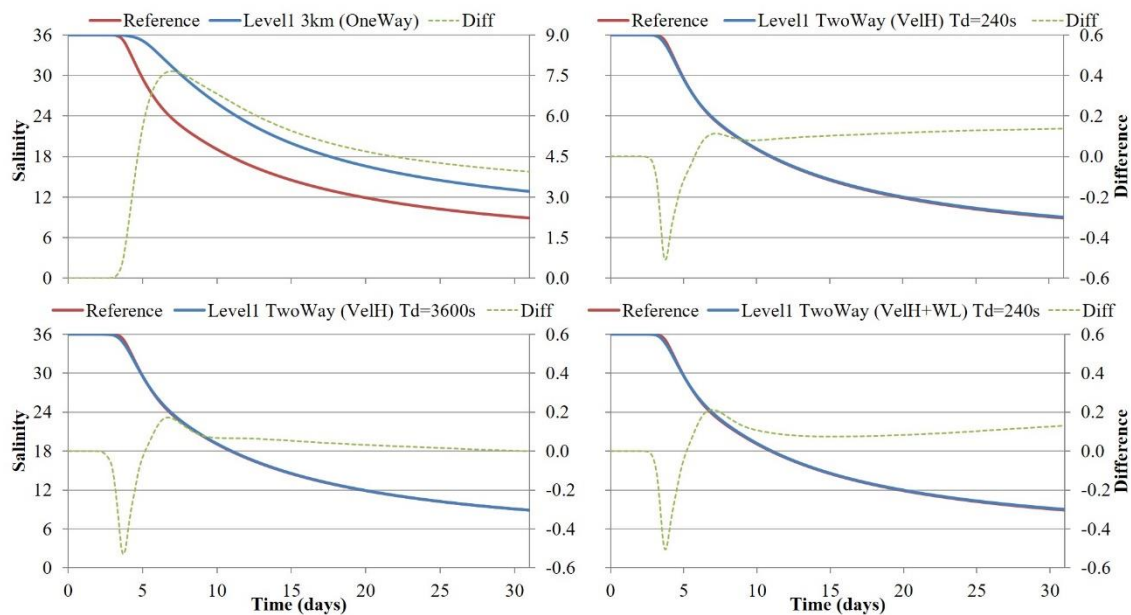


Figure 33: Salinity time series obtained at the north boundary (PN) of Level 2 by the Reference domain and Level1 domain under one-way and two-way modes (with three different parametrizations of upscaling).

Upscaling horizontal velocities from Level2 to Level1 at a Td of 3600 s produced even better results, reaching a 0 difference towards the Reference solution after 31 days and with a difference curve presenting a lower steepness.

Other implementations were also tested and included the upscaling of vertical velocities and excluded 9 numerical cells from Level2 in the upscaling operations, but these differences were negligible when compared to the ones presented here.

At the south border (PS - Figure 34), as observed in Figure 32, salinity values obtained by the Reference domain remain constant at 36 throughout the entire simulation period, as a result of the Coriolis force acting on the westward momentum generated by the lateral discharge. Once again, due to its higher numerical diffusion, Level1 domain running in one-way mode shows a decrease in salinity near PS of 0.25 units after 31 days of simulation, but at an increasing rate. This diffusion has been eliminated through the use of upscaling and all parametrizations have achieved the same result.

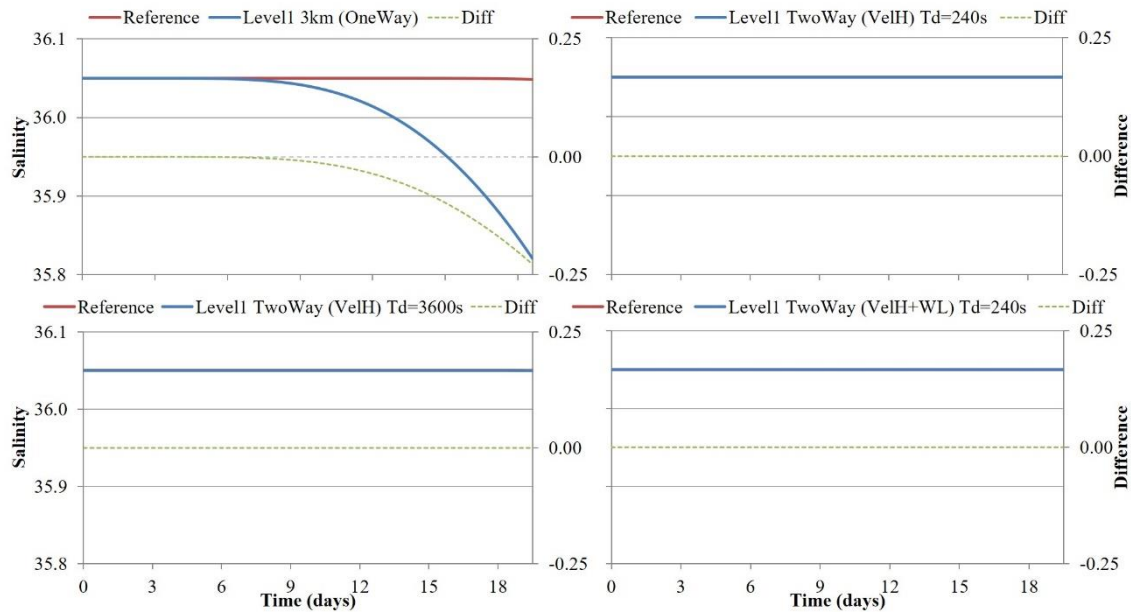


Figure 34: Salinity time series obtained at the south boundary (PS) of Level 2 by the Reference domain and Level1 domain under one-way and two-way modes (with three different parametrizations of upscaling).

3.2.4.2 Discharge only in the higher resolution domains

An important test to the upscaling algorithm is to include a process that only exists in the CD, which is particularly important in coastal areas with important freshwater discharges. In part, this test can be considered a preview of the next section where a real case implementation to the Tagus ROFI area is tested. The major differences include tide, bathymetric variability and wind forces which will produce completely different dynamics than those represented in this current test.

In order to maintain consistency with the previous test – where a discharge was implemented in both PD and CD – the same flow values and velocities were used, as well as the same open boundary conditions for all the domains. This means that Level2 is nudging its solution to Level1 (which does not have an active lateral discharge). Results show a very different picture

than when a discharge is present in both domains. When only the horizontal velocities are upscaled, and because the PD solution is completely stopped at the beginning of the simulation, the difference between water levels at the open boundary do not allow the plume originated in Level2 to leave easily through the north boundary, pushing it westward and destroying the entire solution. This generates a completely different plume, distorted at the open boundary of Level2, which moves north-westward (Figure 35 – “Level1 TwoWay VelH.Td=240 s”). However, when the water level is also upscaled with a Td of 240 s, the solution becomes almost identical to the results obtained when a discharge is also implemented in Level1 (Figure 32). In this case, increasing the time decay to 3600 s, although presenting a better solution when compared to when only horizontal velocities are upscaled, generates a distorted plume, with the same tendency as the one observed when water level is not upscaled. As such, in this particular schematic case when the PD does not include a lateral discharge, the most successful way to transfer information from the CD to the PD is through the upscaling of horizontal velocities and water level at a smaller time decay. However, it should be noted that this is a simplified domain where the bathymetries are identical between modelling domains and no other force is present aside from the lateral discharge, which produce a very small change in water level (average of 3 mm and maximum of 1 cm near the discharge) when compared to changes due to tides or winds.

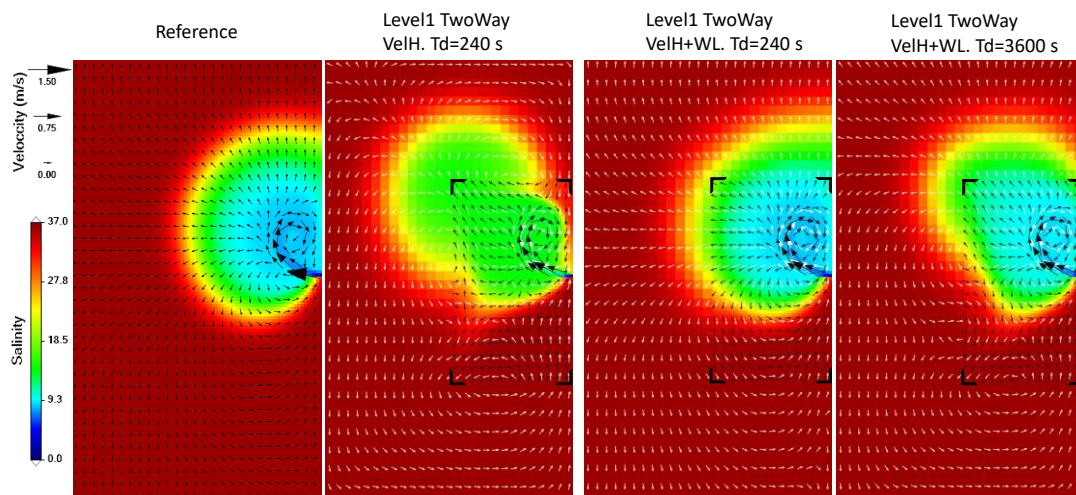


Figure 35: Surface salinity field overlapped by the velocity vectors, obtained by the Reference, Level1 and Level2 domains under three upscaling parametrizations. The Reference domain is represented on the left, while the remaining maps show the overlapping of Level2 on Level1 with a frame (in black) over the open boundary of Level2.

These results are corroborated in Figure 36, where a comparison between salinity values over time extracted from PN shows the higher divergence between Level1 and the Reference solution when upscaling only considers the horizontal velocities, while upscaling both the

horizontal velocity and the water level produces a much similar result to that of the Reference solution.

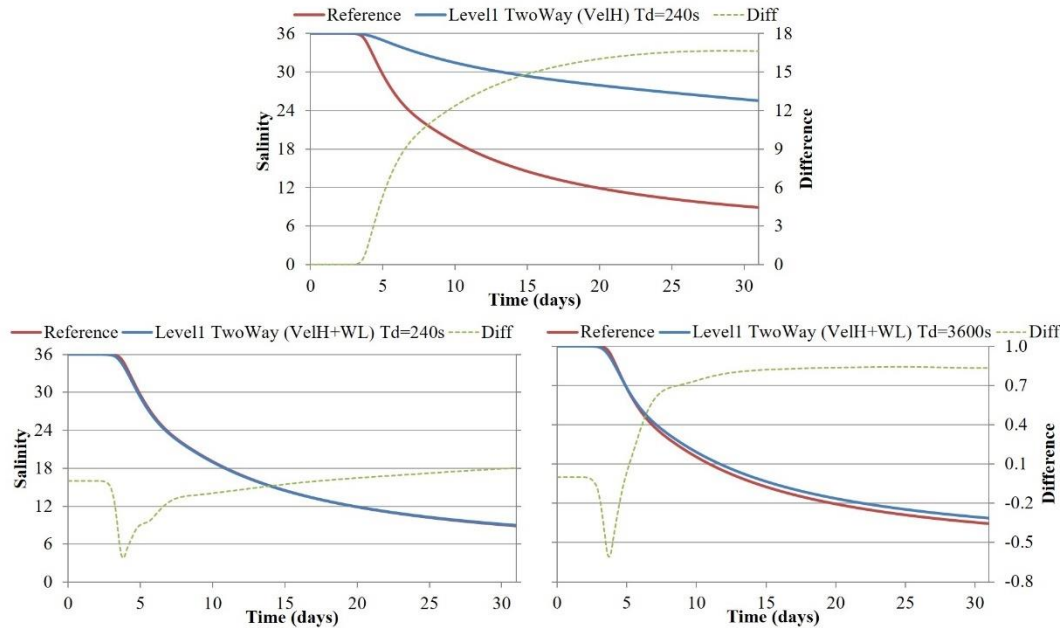


Figure 36: Salinity time series obtained at the north boundary (PN) of Level 2 by the Reference domain and Level1 domain under two-way mode (with three different parametrizations of upscaling). Schematic case: Geostrophic equilibrium

In this test, the upscaling algorithm is applied to a simple test case of a geostrophic equilibrium – which has an analytical solution – in order to assess not only the impact of the nested domain on its parent solution, but also to quantify any mass conservation issues derived from transferring information from child to parent domain. To this end, a validation was made by comparison between surface elevation and surface velocity obtained by PD and CD model domains – under one-way and two-way formulations – and the analytical solution. Also, temperature and volume results obtained by the PC and the CD model domains were compared to a reference solution. Part of these results were published in (Sobrinho et al., 2021b).

When two water masses of different density come into contact at the same depth a density front is created. This process creates a perpendicular (to the density front) transport that would only stop when the heaviest water mass lost its lateral contact with the lighter water mass. When the Coriolis force is present, this process ends when the pressure gradient at the front and the Coriolis force are in equilibrium.

This process has an analytical solution when the reduced gravity equations are used, combined with a null density gradient along the density front, infinite depth and a constant Coriolis frequency over the study domain. With these assumptions, the primitive equations are as follows:

$$\frac{\partial v}{\partial t} + v \frac{\partial v}{\partial y} + fu = -g' \frac{\partial h}{\partial y} \quad (28)$$

$$\frac{\partial u}{\partial t} + v \frac{\partial u}{\partial y} - fv = 0 \quad (29)$$

$$\frac{\partial h}{\partial t} + \frac{\partial}{\partial y}(hv) = 0 \quad (30)$$

where h stands for the layer thickness. Even though there is no solution for the transient regime, there is for the final solution when an equilibrium is met between Coriolis and pressure forces.

$$fu = g' \frac{\partial h}{\partial y} \quad (31)$$

The final equations can be consulted in (Cushman-Roisin, 1994) chapter 13.2 or in (Mellor, 1996) chapter 7.4 and are as follows:

$$h = H \left[1 - e^{\left(\frac{x-Ri}{Ri}\right)} \right] \quad (32)$$

$$u = \sqrt{g'H} \left[1 - e^{\left(\frac{x-Ri}{Ri}\right)} \right] \quad (33)$$

$$Ri = \frac{\sqrt{g'H}}{f} \quad (34)$$

where Ri is the Rossby deformation radius and corresponds to the distance along the front from which the Coriolis force equals the pressure force.

Physically, this process creates a surface elevation gradient towards the front that is eliminated due to the density gradient. Surface elevation (η_0) associated with the first baroclinic mode can be deduced by the oscillation of the interface (η_1):

$$\eta_0 = \left(\frac{\Delta\rho}{\rho_0}\right) \eta_1 \left(1 - \frac{\Delta\rho}{\rho_0}\right)^{-1} \quad (35)$$

From equations (32) and (33) one can determine the kinetic and potential energies variation, which are given by:

$$\Delta PE = -\frac{1}{4} g' H^2 R \quad (36)$$

$$\Delta KE = +\frac{1}{12} g' H^2 R \quad (37)$$

meaning that only a third of the potential energy is converted to kinetic energy. The rest will be transported out (perpendicularly to the front) by internal waves along the interface.

3.2.4.3 Model setup

For this case, three domains were created with a constant depth of 1000 m. The first two domains make a nested system with a parent domain (150 x 150 km and 3-km grid step) and its

nested domain at its centre (80 x 80 km and 1-km grid step). A separate domain (reference solution, with 150 x 150 km and 1-km grid step) overlaps the entire parent domain and was created to compare results obtained with one-way downscaling against the Two-way methodology presented here. Details of these implementations are presented in Table 9. For the analytical setup a 150 x 150 km domain with 1000 m depth and H equal to 100 m was considered.

On both modelling and analytical setups, a density gradient was created with a constant salinity of 36 for the two masses, but 18 °C ($\rho_1 = 1026.070 \text{ kg m}^{-3}$) for the lighter water mass and 15 °C ($1026.725 \text{ kg m}^{-3}$) for the heavier water mass. Assuming a latitude of 38°, the Coriolis frequency is $9 \times 10^{-5} \text{ s}^{-1}$ which leads to a Rossby deformation radius (Ri) of 9 km, and using the equations (32), (33) and (34), the thickness of the lighter water mass and velocity above the interface can be computed.

Table 9: Description of the model domain implementations for the geostrophic equilibrium schematic case.

Implementation	3-km grid domain (150 x 150 km)	Nested 1-km grid domain (80 x 80 km)	1-km grid domain (150 x 150 km)
Vertical discretization	12 cartesian layers – thickness(m) from surface: 10, 15, 20, 25, 30, 50, 50, 50, 50, 200, 200, 300		
Forces	Barotropic, Baroclinic, Coriolis and Diffusion		
Lateral Open Boundary Conditions	Flather radiation Baroclinic radiation* Null gradient for temperature and salinity	Flather radiation to PD FRS** with 9 cells and a Time decay of 600 s Baroclinic Radiation	Flather radiation Baroclinic radiation* Null gradient for temperature and salinity
Horizontal; Vertical Viscosity ($\text{m}^2 \text{s}^{-1}$)	30 ; 1e^{-4}	10 ; 1e^{-4}	10 ; 1e^{-4}
Biharmonic coefficient ($\text{m}^4 \text{s}^{-1}$)	6e^8	2.5e^7	2.5e^7
RAMP*** (days)	5	5	5
Time step (s)	45	15	15
Feedback	X	Volume-weighted average	X

*Baroclinic radiation developed by Leitão (Leitão, 2002) and based on the work of Marchesiello (Marchesiello et al., 2001).

**FRS: Flow relaxation scheme (Martinsen and Engedahl, 1987).

***RAMP: Period during which the baroclinic force is increased slowly through a factor of 0 to 1.

In order to create the two different water masses, temperature 3D field was initialized with a box method. This box covered the southern half of the domains and the first 4 vertical layers (until 100 m) and a temperature of 18 °C was set inside it. The remaining domain cells were

initialized at 15 °C. Since it is necessary to run the model 5 days until the baroclinic force is fully active, the simulation period used for this test ran for 11 days.

Regarding the upscaling parametrizations, the following were tested:

- Upscaling of horizontal velocities (VelH) + Td of 120 s
- Upscaling of horizontal velocities + vertical velocity + Td of 120 s
- Upscaling of horizontal velocities + water level (VelH+WL) + Td of 120 s
- Upscaling of horizontal velocities + water level + vertical velocity + Td of 120 s.
- Upscaling of horizontal velocities (VelH) + Td of 3600 s
- 9 CD cells from the open boundary excluded from the upscaling algorithm.

In all these parametrizations, temperature is also upscaled with the same Td of the velocities and water level. The results obtained with some of these configurations, such as the upwelling of vertical velocities, produced almost identical results as upscaling only horizontal velocities. For that reason, results associated with upscaling parametrizations where the vertical velocities are upscaled are not included here.

3.2.4.4 Results

Internal waves produced during the geostrophic equilibrium associated with Cartesian vertical coordinates produce numerical vertical diffusion and therefore contribute to a reduction of the density gradient on the first 100 m depth mark, drawing part of the available kinetic energy from up the 100 m layer. In the end, a smaller surface velocity is expected when compared to the analytical solution. Furthermore, horizontal numerical diffusion will lead to mixing near the interface. These factors are responsible for velocity diffusion near the interface, where a less steep curve on the perpendicular direction of the front is expected when compared to the theoretical velocity. In order to reduce the problem of horizontal diffusion, higher grid resolutions can be used – and its effect on nested domains is demonstrated in this section.

After 11 days of simulation under a one-way configuration, a clear front is visible in the 3-km grid domain (Figure 37). Velocities near the interface of the two water masses (Figure 38, right) reach their maximum of 0.36 m s^{-1} , generated by a surface elevation (pressure) gradient (Figure 38, left). The x velocity component as the flow moves towards the front increases rapidly near the interface, but instead of decreasing rapidly to zero, as shown by the analytical solution, it exhibits a concave curve. With a 1-km grid domain a better representation of the surface

elevation curve is obtained and less diffusion through the interface between water masses – an effect which is noticed in the 11th day – and the front's width becomes narrower (Figure 37). This steeper surface elevation gradient produces an equally steep velocity gradient (Figures Figure 37 and Figure 38).

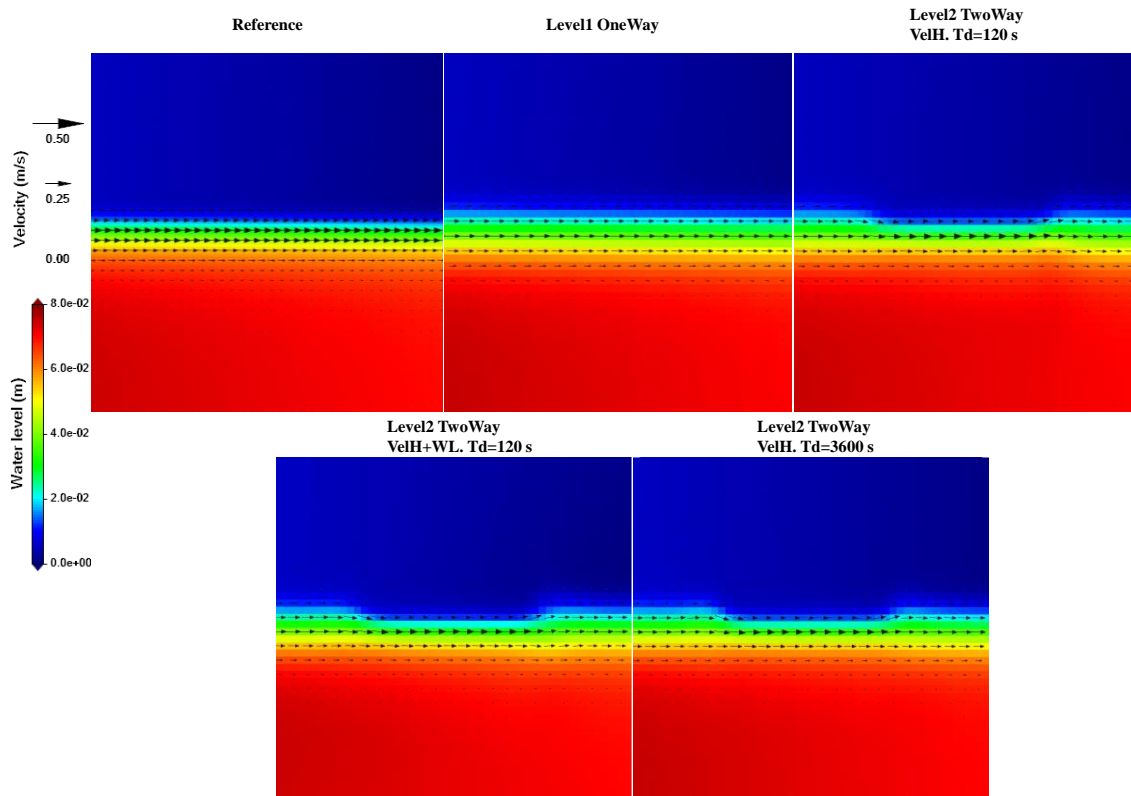


Figure 37: Surface elevation maps overlapped by the velocity fields, obtained for the geostrophic equilibrium by the Reference domain, Level1 domain in one-way mode and in two-way mode for three different upscaling parametrizations: Upscale of horizontal velocities with a Td of 120 s, upscale of horizontal velocities plus water level with a Td of 120 s, and upscale of horizontal velocities with a Td of 3600 s.

In order to get a better representation of the geostrophic equilibrium in the 3-km grid, an online coupling with the 1-km grid domain was made, and the upscaling step was added, following the implementation described in Table 9. Adding the contribution from its nested 1-km domain through upscaling brought its results closer to the ones obtained by the single 1-km grid solution, in the overlapped area between the 3-km and its 1-km nested domains (Figure 37 and Figure 38). Visually (in Figure 37), this effect was observed in all parametrizations of the upscaling algorithm. Results also show that this narrowing of the water level occurred only in the overlapped area, and the solution adjusted well after crossing the interface between the domains, both in water level and velocity (Figure 37). This effect can also be observed on a specific transect perpendicular to the front at the surface (and in the middle of the domain). Since both the reference and the 3-km grid solutions diverge over time due to their resolution,

the displacement observed in the x component of the velocity over this transect increases over time. An equal displacement value (1-km) obtained with and without feedback confirms this hypothesis.

Since the water level maps produced by the several upscaling parametrizations look almost identical, a more detailed analysis of their ability to represent the geostrophic equilibrium is needed as well as an analysis of the total mass and average temperature of the different implementations. These are presented in Figure 38 and Figure 39.

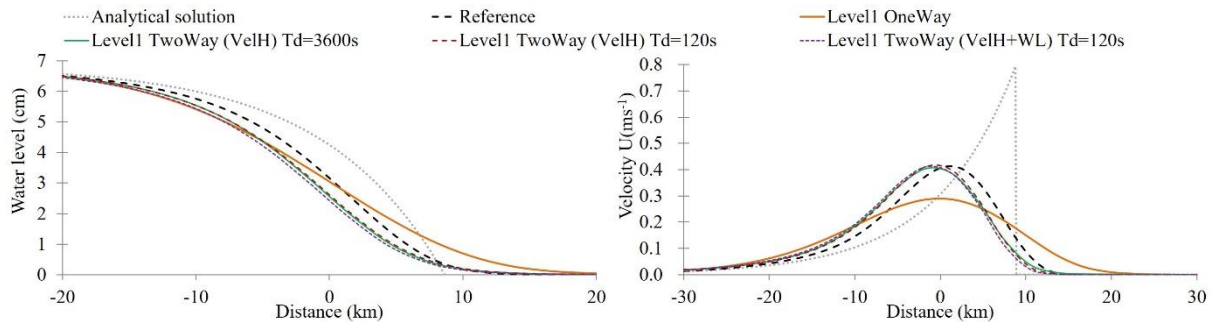


Figure 38: Water level (left) and normal velocity (right), perpendicular to the density front, obtained by the Reference, Level1 in one-way and two-way modes with different parametrizations, and by the analytical solution.

None of the two-way implementations were able to produce a solution equal to that of the Reference domain or the analytical solution. However, the most important comparison is with the Reference domain, because this domain will always be the one that produces a better solution – due to its higher grid resolution. That being said, when compared to the Reference solution, the upscaling parametrization that produced the best results included the upscaling of only the horizontal velocities with a Td of 120 s (although by a small margin to the parametrization which considers horizontal velocities and a Td of 3600 s).

As regards mass conservation, both volume and temperature were affected – although to a small degree – by the feedback operation. Results show an increase in divergence between the Level1 3-km grid and the Reference solution (Figure 39-left and Figure 39: Average temperature over the simulation period obtained by the Reference, Level1 in one-way and Level1 in two-way with the three different parametrizations).

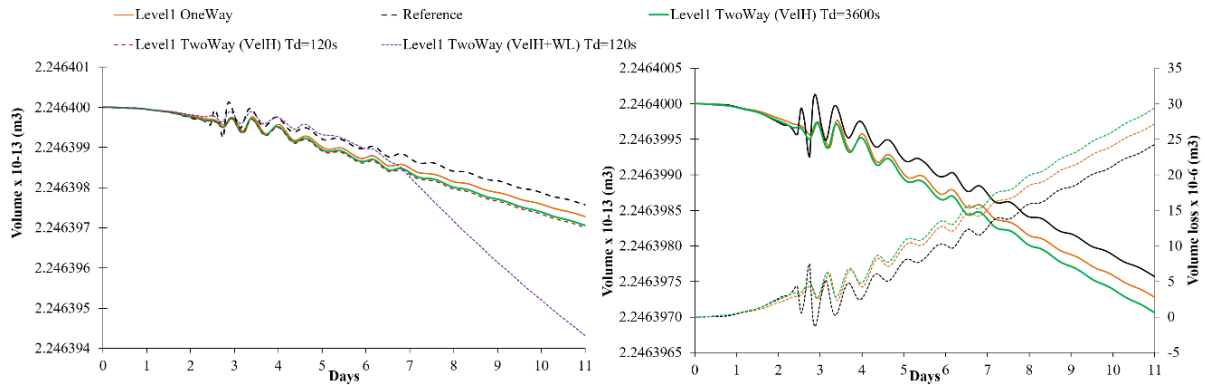


Figure 40-left) as a result of different grid step and diffusion. When horizontal velocities and temperature fields are updated using the CD solution, some divergence is expected, caused mainly by the inherent open boundary error from a low resolution domain to a higher resolution domain. The question is whether this error is significant enough to produce a future instability on the PD, which in this particular case rises over time at a rate of $2.5 \times 10^{-5}\%$ (with a Td of 120 s and $2 \times 10^{-5}\%$ for a Td of 3600 s at the end of the 11 days of simulation) in comparison with the Reference solution. However, the divergence between the 3-km grid domain without feedback and the Reference solution tends to stabilize near the end (Sobrinho et al., 2021b). As a result, the divergence between the 3-km grid domain with feedback decreases its rate of increase near the end of the simulation. When water level is also upscaled, the volume and temperature loss increases rapidly after the 6th day when the baroclinic force is computed at 100 %. Given these results, the best parametrization for upscaling in this schematic case was the one where only horizontal velocities and temperature were upscaled at a Td of 3600 s, as the Level1 solution with upscaling 1) generated a better solution than without upscaling; 2) the difference towards the upscaling with a Td of 120 s was negligible; and 3) the volume and temperature losses were lower in absolute value and in tendency over time.

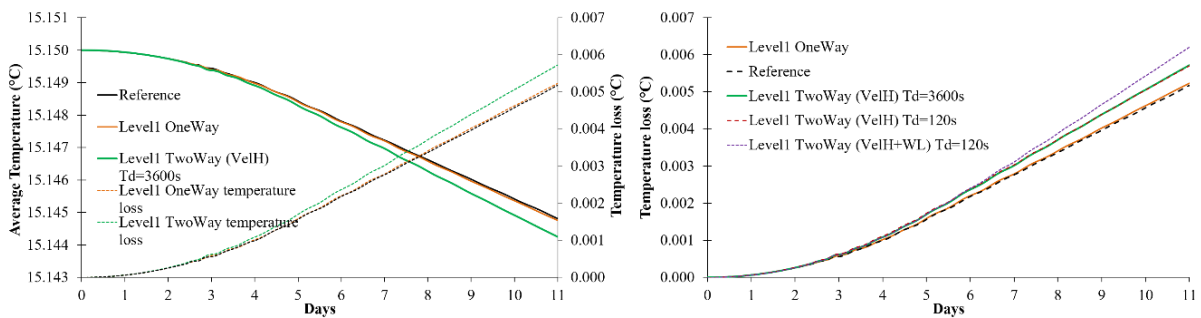


Figure 39: Average temperature over the simulation period obtained by the Reference, Level1 in one-way and Level1 in two-way with the three different parametrizations.

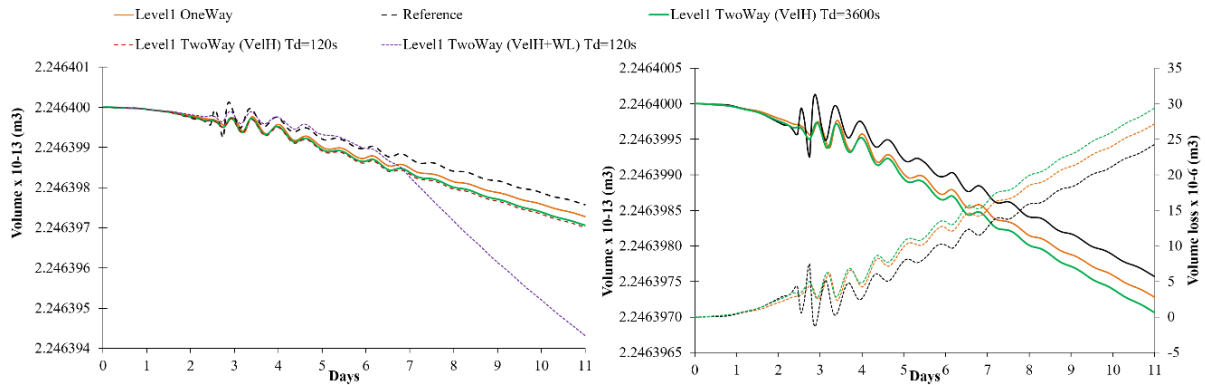


Figure 40: Total water volume variation (represented in both graphs) over the simulation period obtained by the Reference, Level1 in one-way and Level1 in two-way with the three different parametrizations. Volume loss referenced to the initial volume is represented on the right.

Although with a linear growth, the solution's volume and temperature mass divergence is small enough to be an acceptable cost to achieve a better overall solution. Note that the upscaling time decay used was purposely set low, to study a strong coupling. In real application downscaling systems, this nudging time decay from PD to CD is in the order of one day to a week (Franz et al., 2016), (Mateus et al., 2012b), (Pham et al., 2016), (de Pablo et al., 2019). As such, this divergence is expected to become smaller in real applications, while still improving the overall solution.

3.2.5 Two-way nesting in Tagus ROFI

In this real case, a three-month simulation period for the Tagus ROFI area (Portugal) was selected. It is a perfect replica of the implementation used in Chapter 2 for the Tagus ROFI, but this time upscaling is added to the system – making it a two-way simulation because both domains are running in online mode. In this mode the models run at the same time in the same machine and in the same computer process. The PD – Portuguese Coast Operational Modelling System (PCOMS) – runs one iteration and then waits until the CD (Tagus ROFI) runs the number of iterations needed to synchronise with the PD.

3.2.5.1 Setup

The nested system is comprised of three domains (Figure 7):

- 1) 2D barotropic regional domain with 5.7 km constant grid resolution for the Portuguese Coast (Level1) (33.5° N - 49.9° N, 1.0° W - 13.5° W) running only with tidal forcing from FES2004 (Lyard et al., 2006)-(Lefèvre et al., 2002);

2) 3D full baroclinic regional domain for the Portuguese Coast (Level2) (34.4° N–45.0° N and 12.6° W–5.5° W) with a grid resolution of 5.7 km and 50 vertical layers (7 sigma at the surface and 43 Cartesian below);

3) 3D full baroclinic domain for the TagusROFI (level3) and adjacent coastal area with a variable grid from 2 km to 200 m (38.15°N – 39.2°N, 10°W – 8.9°W), and 50 vertical layers (7 sigma at the surface and 43 Cartesian below). Results from this solution are then compared to the one-way methodology for the same nesting system (Chapter 2), and validated against surface elevation and salinity data available for the period of January to April 2013.

This two-way modelling methodology can be advantageous to any coastal area where strong gradients can occur over extensive areas. These areas include estuaries, rivers and their adjacent waters and cover not only salinity but also any water parameter with a strong gradient from fresh to salt water.

A full description of the first two domains running in one-way operationally in MARETEC is available in (Mateus et al., 2012b), and a description of the TagusROFI domain (one-way) is described in Campuzano et al. (Campuzano et al., 2012).

Initial conditions were not necessary as the system started from results of the operational systems. The period from January to April 2013 was simulated, corresponding to a period of high precipitation in Portugal, which lead to an extreme event (de Pablo et al., 2019) in the flow rate of the Tagus River.

As a full description of the modelling system would duplicate the description already made in Chapter 2, only the summary of the implementation is added here (Table 10), with the added parametrization of the upscaling algorithm.

Table 10. Model setup configuration for the Tagus ROFI area in two-way mode.

Settings	Level1 – West Iberia	Level2 – PCOMS	Level3 – Tagus ROFI
Model characteristics	2D - Barotropic	3D – Baroclinic	3D - Baroclinic
Grid corners	33.50° N - 49.90° N 1.00° W - 13.50° W	34.38° N – 45.00° N 12.60° W – 5.50° W	38.16° N – 39.21° N 10.02° W – 8.90° W
Grid dimension	208 x 156	177 x 125	121 x 146
Bathymetry	EMODnet Bathymetry portal	EMODnet Bathymetry portal	IH Data and GEBCO
Horizontal Grid	Regular: (≈ 5.7 km)	Regular: (≈ 5.7 km)	Irregular: 200 m to 2 km
Vertical Grid	1 layer	7 Sigma Layer (0 - 8.68 m)	7 Sigma Layer (0 - 8.68 m)

		43 Cartesian layers	43 Cartesian layers
Δt	60 seconds	60 seconds	6 seconds
Tides	FES2004	From Level1	From Level2
OBC Water	...	From MercatorOcéan PSY2V4 (Releases 1- 4)	From Level2
Nudging	...	Flow relaxation scheme of 10 cells with a time decay of 1 week at the open boundary and 1 year inside the domain	Flow relaxation scheme of 10 cells with a time decay of 900 s at the open boundary and 1 year inside the domain
OBC Atmosphere	-	MM5 (12 km and 9 km)	WRF (3 km)
Discharges	No	No	Tagus (hourly), Sorraia, Trancão (monthly)
Turbulence	...	GOTM*	GOTM*
Bottom	Rugosity of $0.0025 \text{ m}^2 \text{ s}^{-1}$	Rugosity of $0.0025 \text{ m}^2 \text{ s}^{-1}$	Rugosity of $0.0025 \text{ m}^2 \text{ s}^{-1}$
Upscaling Td (s)	X	X	3600
Variables upscaled	-	X	Horizontal velocities + Temperature + Salinity
Number of CD cells ignored	X	X	6

*General Ocean Turbulence Model (Burchard et al., 1999) coupled to MOHID (Ruiz Villarreal et al., 2005).

Due to the fact that the Tagus ROFI model grid is variable (with grid steps from 300 m to 2 km), and because previous tests obtained good results with 0 and with 9 CD cells ignored, only 6 cells were ignored in this test – a compromise that has not been fully tested as the impact of the number CD cells ignored was not studied in this test. Taking into consideration the remaining tests performed, only horizontal velocities, temperature and salinity were upscaled, as the upscaling of water level in combination with velocities leaves too few degrees of freedom for the PD to adapt to its CD. However, as the lateral discharge schematic test suggested, upscaling the water level could be important when a process is only present in one of the domains (which is the case with the Tagus ROFI). Future research in this field should include an analysis of the importance of upscaling water level in these conditions.

3.2.5.2 one-way vs two-way

In order to assess the impact of upscaling in this system, a comparison is made between results obtained in Chapter 2 (one-way grid coupling) and the recently implemented upscaling algorithm. This comparison is applied to the surface salinity fields, vertical profiles of temperature and salinity, water level (with comparison with the Cascais tide gauge) and in-situ salinity (provided by a CTD), all during the period of 1 January to 10 April. The location of the vertical profiles, CTD and the Cascais tide gauge are presented in Figure 41.

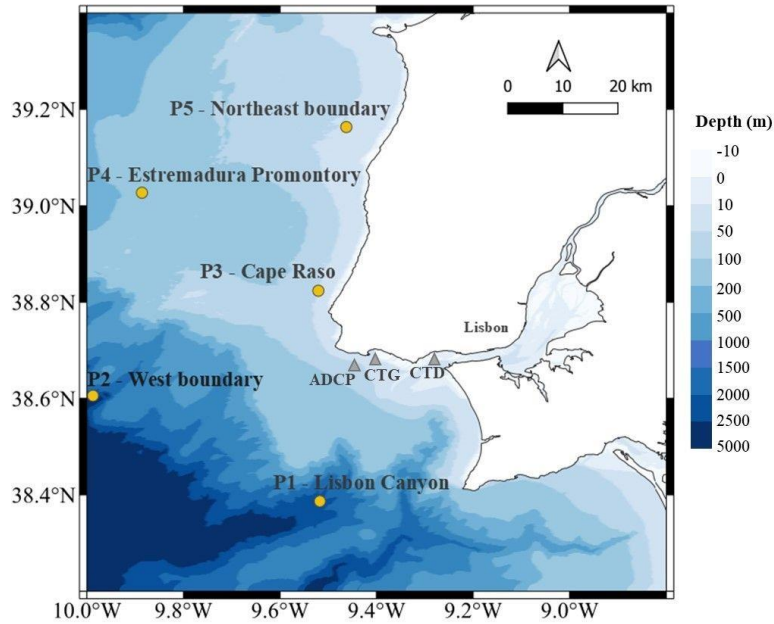


Figure 41: Map of the Tagus ROFI area showing the location of the in-situ stations used in the validation process, as well as the vertical profiles used for comparing modelling grids. CTG–Cascais Tide Gauge; CTD–Conductivity, Temperature, and Depth probe; P1–5 – vertical profiles.

3.2.5.2.1 Water level

Water level obtained by the four model implementations was validated against the Cascais tide gauge during the period between 11 January and 13 March, 2013 (Figure 42). Results obtained by either type of implementation (one-way and Two-way) for Levels 2 and 3 have correlations above 0.99, demonstrating the model capacity to represent water level variability. Mean bias values vary between 1.7 mm on Level 2 and 4.1 mm on Level 3, both with a Two-way implementation. Median values are more representative when extreme values occur, and in this particular case, for Level 2 it is double the height of the mean bias value, but one third for Level 3, indicating more extreme (overestimation) bias values in Level 2 and the opposite for Level 3. A higher decrease from mean to median is observed for Level 3 in Two-way, becoming smaller than that of a one-way implementation. The contrary was verified on the bias of Level 2, where some extreme values were corrected, at the cost of a slight rise in median bias. It is important to note, however, that these values are extremely small, as well as the differences between model implementations applied onto the same grid domain. In regards to correlation between model data and tide gauge data, all implementations provided results with a Pearson value higher than 0.99, indicating a good agreement with the tide gauge. RMSE values showed a higher variability between one-way and Two-way implementations for Level 2, indicating a

slight improvement of the results. These results are in agreement with those obtained by de Pablo et al. (de Pablo et al., 2019) and demonstrate both the ability of the MOHID model to reproduce water level in a highly dynamic region, and the small effect produced by the upscaling procedure presented in model performance.

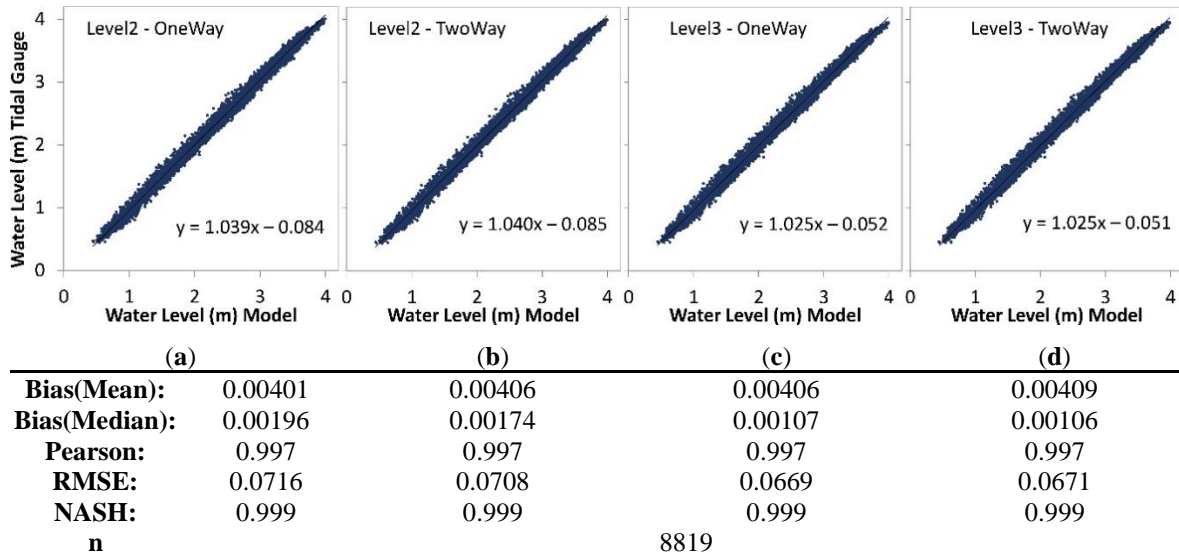
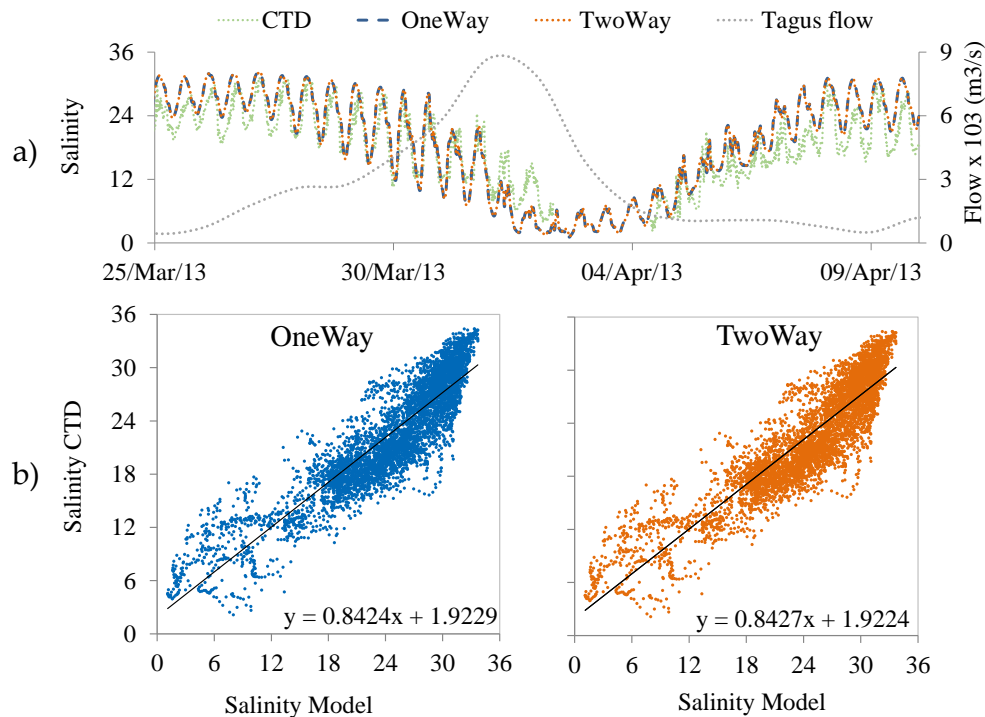


Figure 42: Correlation and performance results for the period of 11th of January to the 10th of April 2013, between the Cascais tide gauge and the different model implementations: a) Level2 in one-way, b) Level2 in two-way, c) Level3 in one-way and d) Level3 in two-way.

3.2.5.2.2 Salinity at the CTD location

Modelled surface salinity was validated against CTD data obtained between March and April 2013 (Figure 43) in a moored station located near Algés. Comparisons between data and both one-way and two-way implementations shows that the model was able to properly reproduce salinity variation during this period of extreme flow rate. Additionally, the model has the ability to fill the missing data gap in the first days of April – caused by a submergence of the buoy during the peak flow – which in this case points to a very low salinity of 1 at the mouth of the estuary. Modelled mean and median bias for one-way (2.04 and 1.98) and two-way (2.05 and 1.99) (Figure 43) implementations confirm an overestimation of the surface salinity throughout the simulated period.



Bias(Mean):	1.92	1.91
Bias(Median):	1.82	1.82
Pearson:	0.90	0.90
RMSE:	3.55	3.54
NASH:	0.693	0.695
n	5468	

Figure 43: Performance of model results (Level3 domain) against field data (obtained with a CTD). a) Comparison between salinity field data for the period between 25 March and 10 April, b) one-way (blue) and two-way (orange) correlations between model and CTD data for the period between 1 March and 10 April.

In regards to correlation and model performance, Pearson (0.89) and the NASH (0.68) values indicate a good agreement with field data, without any visible effect of the two-way over the one-way implementation, on all statistical indicators. These results demonstrate the importance of extreme flow rates from the Tagus river flow at the mouth of the estuary, which could explain the similarity between one-way and two-way formulations. For that reason, satellite data and inter model comparisons were made to assess the impact of these formulation over the entire domain and in more detail near the lateral open boundary of Levels 2 and 3.

3.2.5.2.3 *Salinity at the open boundary*

Although metrics for a point time series show the same performance for both implementations, it is at the open lateral boundary that a difference in the salinity results can be observed. As Figure 44 shows, the estuary plume reached the north and its influence was registered over 25 km north of the boundary – although in the figure only the first 15 km are shown – with differences in salinity in the order of 2.5. In contrast, under a one-way downscaling the estuary

plume abruptly stops at the boundary with Level2 (seen at 0 h of 5 April), which led to a more rapid shift towards the southwest during the following hours, as well as smaller salinity plume. This impact not only changes the solution but actively removes salinity from the entire nesting system. Although compensated later on by the flow relaxation scheme applied to boundary of Level2 (by the Mercator daily solution), this impact can be seen for over 4 days (Figure 45) after the minimum value is reached in both domains near their shared boundary. As such, during this shift, lower surface salinity – produced under a two-way nesting – entered through the northern boundary, improving the overall solution provided by the modelling system.

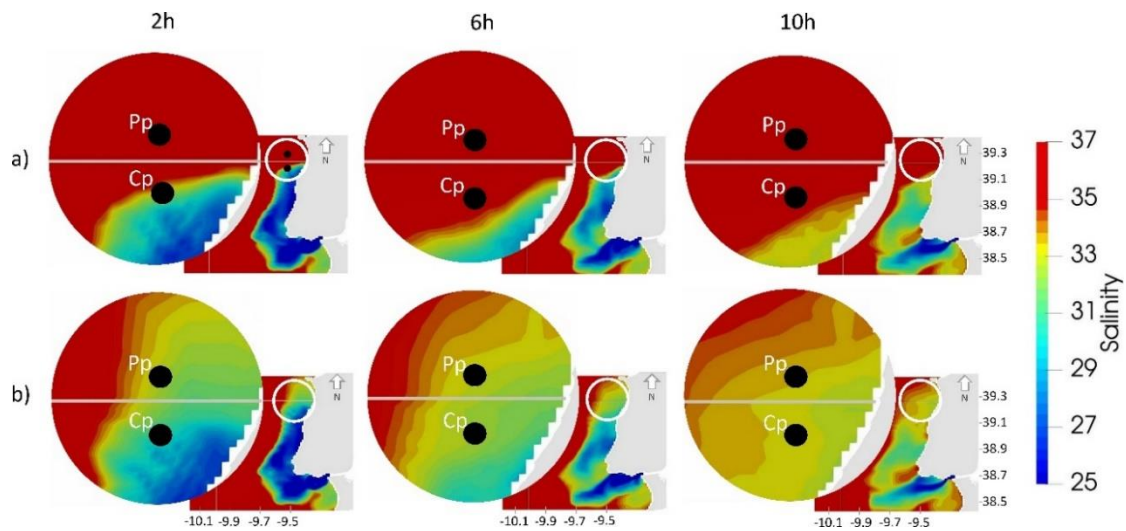


Figure 44. Impact of the feedback operation on the salinity field transition between Level2 and Level3 model grids during the Tagus plume evolution at its peak flow, from 0h to 10h of 5 April, under a) one-way and b) two-way methodologies.

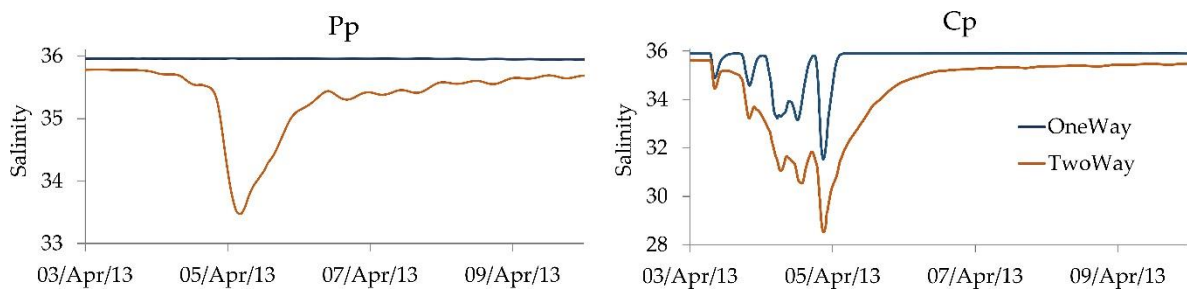


Figure 45. Time series of Salinity at Pp (computed by Level2) and Pc (computed by Level3) locations obtained through one-way and two-way methodologies.

A comparison between time series produced by Level2 and Level3 at Pp and Cp, respectively, shows that the Tagus plume's impact near the ocean model boundary was felt for over 7 days. Furthermore, this transport of salinity from Level3 to Level2 by feedback, considerably reduced the curve steepness from 5 April to 10 April on Cp, as its boundary condition for salinity – given by Level2 – had been corrected. Although less visible, one can also see the feedback impact on the evolution of the salinity peaks in Cp, which are smaller than those produced under

a one-way methodology. This is a result of salinity transport into Level2 which is then transported back into Level3 – when the currents shifted – at a lower (corrected by feedback) value. Therefore, the area between the two curves can be seen as the amount of salinity lost due to the one-way approach during this extreme event. These results show the advantage that this two-way nudging method can have in a nested modelling system subject to intense fresh water inputs without impacting the system's performance, including the capacity to properly simulate the surface buoyant plume commonly observed along the Portuguese Coast (Campuzano, 2018; Peliz et al., 2005; Teles-Machado et al., 2016).

3.2.5.2.4 Vertical profiles

As in Chapter 2, temperature and salinity profiles were extracted from 5 strategic locations: Lisbon Canyon, western boundary of Level3, Estremadura promontory, near-shore past Cape Raso, and the northeast boundary near the coastline (Figure 41).

Time series extracted from the surface at CTD location and at the northeast open boundary of Level3 already showed the improvement of the overall solution when the upscaling algorithm is applied. However, it is also important to study this impact in the rest of the overlapped area between domains not only at the surface but also in depth. Figure 46 shows the comparison between average temperature profiles obtained for the period of 11 January to 10 April and from 25 March to 10 April, which corresponds to the entire period of simulation and peak flow periods, respectively. In order to use comparable results, Level3 fields were previously interpolated (via simple average) into the Level2 grid, which means that some caution is advised when looking at the comparisons as the average partially distorts the results. Because Level3 grid step is variable, a weighted average would have produced more accurate comparisons, but due to time and programming constraints, a simple average was computed. In the results shown in Figure 46, the influence of the upscaling algorithm can be detected up to 100 m depth in the Lisbon canyon and at the west open boundary of Level3. At the remaining locations this influence is evident over the entire water column, even at the Estremadura promontory which is in one of the furthest points from the mouth of the estuary. In all locations Level2 temperature is nudged to that of Level3, rising about 0.1 °C at the surface and along the water column, which was the desired effect, as Level3 in one-way suggested the temperatures should be higher, due to the presence of the estuary, whose temperature near the end of March is higher than the ocean. The vertical structure of the water column is also corrected in Level2, with the curves approaching those produced by Level3, but the most notable effect is detected in Level3. When

run in two-way mode, Level3 results (particularly at the open boundaries) increase when compared to the Level3 solution run in one-way. This is because the open boundary condition of Level3 is no longer restricted by the lower temperatures provided by Level2. As such, upscaling the Level3 fields into Level2 produces improvements not only in Level2, but also in Level3, which will be more significant over time, as the open boundary of Level3 improves.

Salinity profiles (Figure 47) are easier to analyse due to the higher gradient between Level2 and Level3. Also, this variable is much more useful to identify the real impact of the estuary as it is the only source of salinity strong enough to produce the changes seen in the various profiles. These profiles show that the impact of the estuary is not limited to the west coast, but to the entire domain, with differences of around 0.6 salinity units at the surface in the west open boundary of Level3 and in the Lisbon Canyon. At the west coast, past the Cape Raso, the salinity profile of Level2 in one-way mode is constant at around 35.9, but due to the effect of the estuary during this extreme event salinity drop to 34.6 and 35 in the Cape Raso and northeast boundary profiles, respectively. As in temperature, these last profiles clearly show an improvement of the Level3 solution, which produces lower salinities at the boundaries when the constraint of Level2 is eliminated (in the “west boundary” this difference in Level3 is around 0.3).

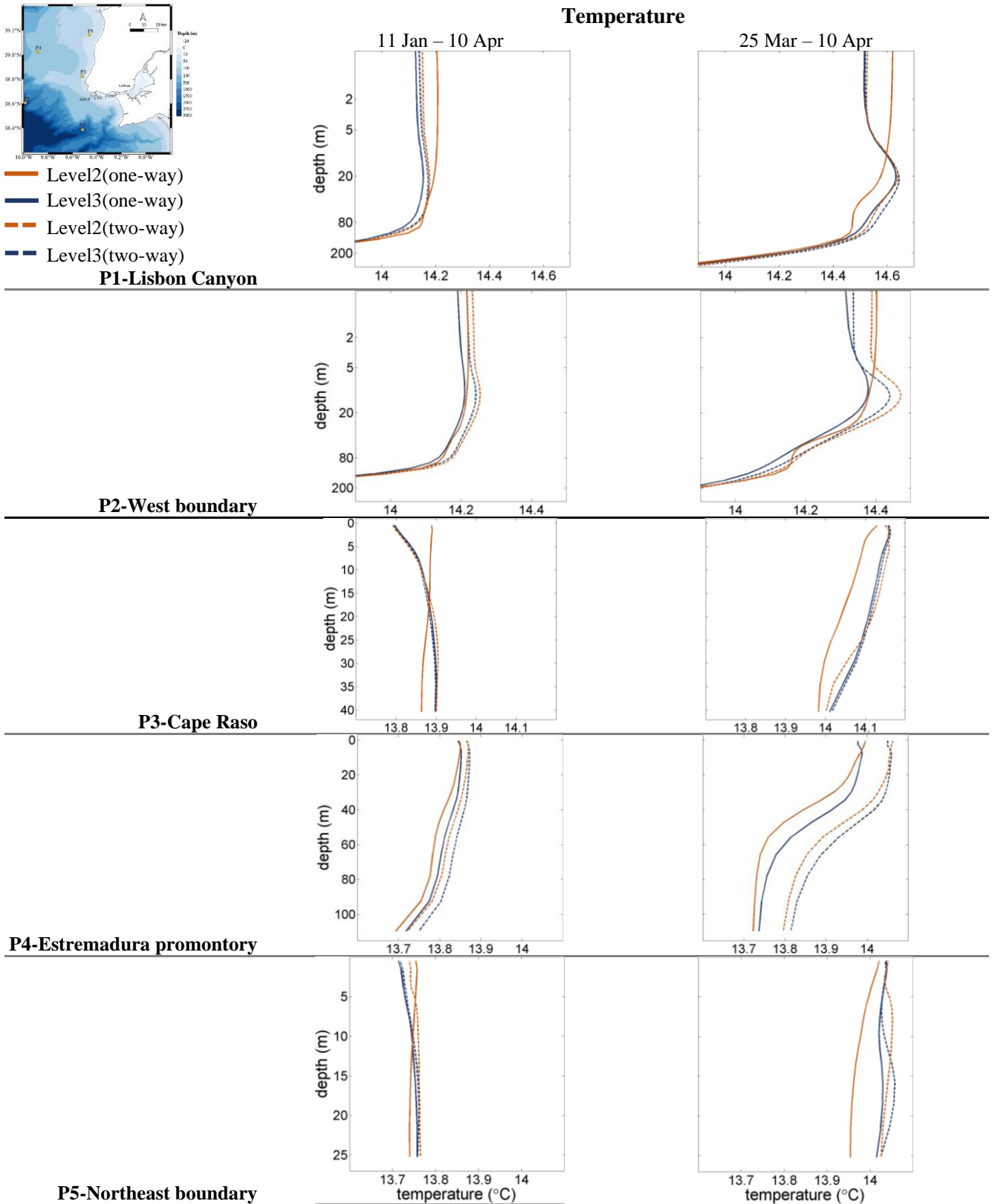
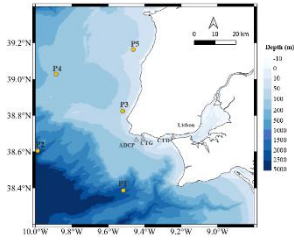


Figure 46: Comparison between vertical profiles of temperature obtained by Level2 and Level3 domains at the five defined locations for the three analysed periods, under one-way and two-way modes

Salinity

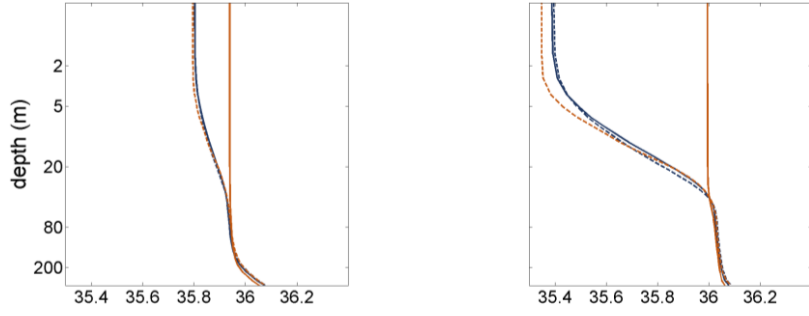
11 Jan – 10 Apr

25 Mar – 10 Apr

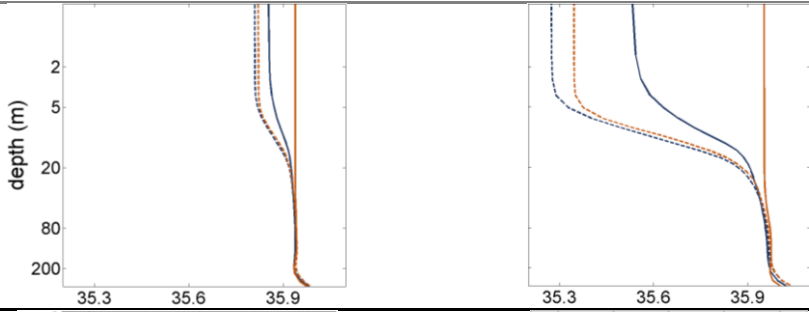


- Level2(one-way)
- Level3(one-way)
- - - Level2(two-way)
- - - Level3(two-way)

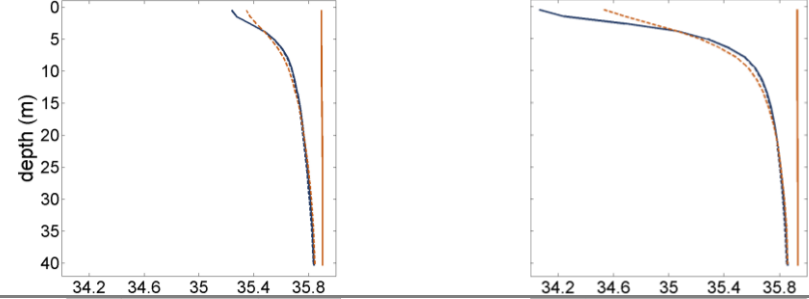
P1-Lisbon Canyon



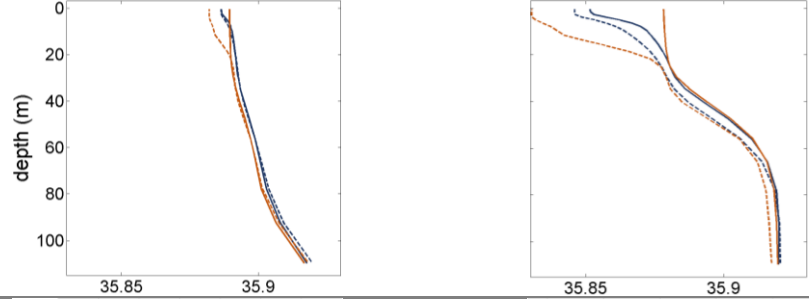
P2-West boundary



P3-Cape Raso



P4-Estremadura promontory



P5-Northeast boundary

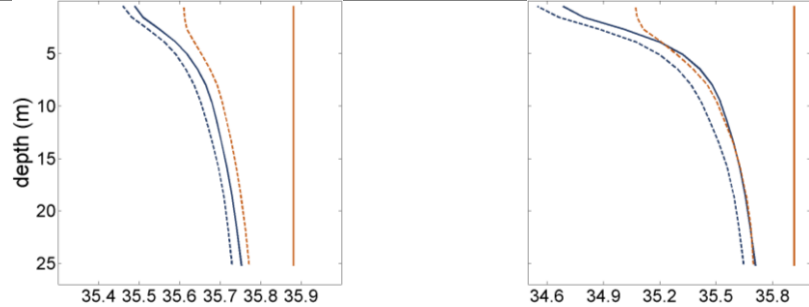


Figure 47: Comparison between vertical profiles of temperature obtained by Level2 and Level3 domains at the five defined locations for the three analysed periods, under one-way and two-way modes.

3.2.5.2.5 *Summary of the comparative analysis*

The comparative analysis made in this section (0) aimed to improve the knowledge on the importance of upscaling the solution of local domains (smaller domains with higher grid resolution that solve smaller scale processes, in comparison with larger domains simulation large scale processes with higher grid steps). This comparison included the following:

- Water level validation of Level2 (PCOMS) and Level3(Tagus ROFI) domains with the Cascais tide gauge and comparison with the traditional one-way approach.
- Surface salinity validation of the Level3 against a CTD located near the mouth of the estuary, and a comparison with the traditional one-way approach
- Surface salinity comparison between Levels 2 and 3 produced under one-way and two-way modes at the northeast open boundary of Level3.
- Comparison of temperature and salinity profiles obtained by the different domains in one-way and two-way modes.

The aim of all these comparisons was to assess the impact of the upscaling algorithm in an online nesting system where the local domain simulates a process not represented in a regional model (Level2).

Water level and salinity validations demonstrated the increased accuracy of the modelling system as a whole when upscaling is introduced, as both levels' statistical indicators improved (although more in Level2, due to the addition of the estuarine plume dynamic). Surface salinity at the open boundary was analysed with the aim of studying the impact of the upscaling in the transition of the estuarine plume across the open boundary between domains and to assess its importance to the Level3 solution over time. It showed that the use of upscaling produced a smoother transition between modelling grids and was responsible for lower salinities produced by Level3, because the domain was no longer restricted by the high salinities produced (and imposed at the open boundary) by Level2 when in one-way mode.

The temperature and salinity vertical profiles were important for a more comprehensive analysis of the vertical structure of the model domains and the upscaling impact thereon. They show that upscaling information from Level3 to Level2 approximates the Level2 vertical stratification to that of Level2 and allows the Level3 domain to improve its results due to a less restrictive open boundary on salinity and temperature. This influence was observed until around 80 m. Below these depths, the differences in bathymetry of Level2 and Level3 are too small to produce

significant differences in the flow field, and the hydrodynamics at these depths are much more stable over time (verified by the vertical profiles of Figure 18 and Figure 20) due to less influence from wind and tides.

3.3 Partial conclusions

This chapter describes the development, validation and application of an upscaling algorithm responsible for the transfer of information from a local modelling domain to a regional modelling domain. The development of such an algorithm has been long due in the MOHID modelling system, being first mentioned in (Leitão, 2002), who saw it as a natural evolution of the model. In the ocean modelling field, the transition to two-way nesting has followed the same slow tendency, with only small developments being made over the 2000s and fewer modelling applications in which two-way was used. However, in more recent years there has been an increase in the application of these nested systems, partially due to the existence of the AGRIF (Adaptive Grid Refinement in Fortran) coupling software which is available for models such as ROMS or NEMO. This software includes all the necessary routines for the upscaling and needs only an initial investment on the coupling between the software and the numerical model (Debreu et al., 2008; Herzfeld and Rizwi, 2019).

The use of upscaling has also grown due to the increase in grid resolution required in coastal areas or in regions whose hydrodynamic processes require lower grid steps (such as the Gibraltar strait for example – (Sannino et al., 2009)). This problem is particularly important in structured grids such as the ones used in MOHID, where a decrease in grid step leads to domains that are very demanding in terms of computational power. Such a demand is acceptable in some hindcast simulations where time is not a determinant factor, but is not acceptable in forecast services and operational modelling which must provide a days' worth of results every 2 or 3 h maximum.

The basic principle behind upscaling of information from a CD to a PD is the inherent higher accuracy of the CD in solving local processes, which depend not only on highly variable bathymetries, but also on local forces (such as wind and waves stresses) and local processes – such as mixing by estuaries. One important reason for the CD to produce a better solution is the lower numerical diffusion associated with lower grid steps, a fact that was observed in all the schematic tests performed in this chapter. It is, therefore, another drive for upscaling local domains into regional domains. In this thesis, one-way and two-way couplings are divided in two categories: the first considers online coupling, where both domains run in a single computer

process in the same computer and where transfer of information occurs at every PD time step; the second considers the offline downscaling (Campuzano et al., 2012) in which the modelling domains are run separately – in the same computer or otherwise – and where information is transferred at a specified time frequency using daily results which are saved with higher frequencies (typically 900 s when compared to a PD time step of 60 s). In this regard, this chapter treats the upscaling as a two-way coupling mode, and the CD and PD are run simultaneously.

Although the objective of the thesis is to produce an offline upscaling algorithm, this chapter is extremely important to account for any important source of error in the algorithm and to detect potential symptomatic errors (which will increase in time due to the feedback between the CD and PD) in the overall modelling application. In this regard, three schematic cases were analysed, focusing on the comparison between one-way and two-way solutions from the PD's perspective. Several parametrizations for the upscaling algorithm were tested, including the variables to be upscaled, the number of CD numerical cells to be excluded from the algorithm, and the time decay. Regarding the upscaled variables, tests included the combinations of the following:

- Horizontal velocities
- Vertical velocities
- Water level
- Temperature and salinity

In all baroclinic tests, temperature and salinity were always included, while in the 1D channel forced by a wave upscaled only the velocities and water level were tested.

From the results obtained with the several schematic tests, the following conclusions were drawn (considering that horizontal velocities are always upscaled):

- Upscaling vertical velocities does not produce significant changes either in the solution or in the total mass of the PD when compared to the simulations that upscale only the vertical velocities or the PD running in one-way mode. As such, and in order to provide as many degrees of freedom as possible for the PD solution – which will avoid overfitting issues and reduce conservation problems – it is recommended that only horizontal velocities be upscaled.

- When the water level is upscaled, an increased mass or volume of water of the PD is lost (although this comparison was not made in the lateral discharge). As regards the accuracy of the solution (which is compared to a reference solution or an analytical one in the case of the geostrophic equilibrium), upscaling the water level does not improve any of the schematic cases tested, except one. In all schematic cases, both the PD and the CD simulate the same processes, but in the lateral discharge test a separate simulation was performed in order to test the upscaling when a single process exists and only in the CD. In this case, upscaling water level was critical for the success of the simulation, achieving a very good result when compared to the reference simulation (performed by a domain with the size of the PD but the grid step of the CD and with the same lateral discharge). This proved that for modelling simulations where the PD is a static domain without any barotropic or baroclinic gradients except those produced by the upscaling, then upscaling water level may be necessary.
- The time decay used in the upscaling algorithm plays an important role in the solution as well as in mass conservation. In summary, lower time decays can produce slightly better solutions but at a higher cost of mass loss. For example, using 90 s or 3600 s produces very similar solutions, but with stronger losses in mass when 90 s is used. As these times are dependent not only on the time step of the PD and the processes that are at play, it is recommended that the user uses the largest time decay possible while still producing good results.
- The number of CD cells ignored from the upscaling procedure did not produce significant changes in these solutions, but in some simulations not reproduced herein some visual differences at the open boundary can be observed. Considering the advice of many authors mentioned in this chapter, it is recommended that at least the equivalent of 2 PD cells be ignored from the upscaling procedure.

In short, upscaling will always have a potential for positive impact on the overall solution but at the cost of mass conservation – below 0.005% in all schematic tests performed, although only shown for the 2 more dynamic tests (stratified 3D with north wind, and geostrophic equilibrium). The origin of this problem is related to the downscaling operations and open boundary conditions (because the PD cannot solve the lower scales of the CD) and so far cannot be avoided, but can be minimised through the selection of the proper variables to be upscaled, as well as the use of the most cost beneficial time decay.

A real case simulation of the Tagus ROFI modelling system was also performed, during a period of extreme precipitation and subsequent extreme flows from the Tagus River. In this test, only the vertical velocities were tested in combination with the horizontal velocities, as conclusions from the previous schematic testes suggested these would provide better solutions. Vertical velocities still produce very limited changes, although results not shown demonstrated that its impact is more visible than for the schematic tests, as a result of the higher bathymetric variability and more intense hydrodynamics of this ROFI region.

Overall results clearly show an improvement of the PD and CD solutions, not only in regards to the validation procedure, which included tide gauge and in-situ salinity from a CTD, but also in the entire overlapped area of the domains. Surface salinity at the open boundary of Level3 (Tagus ROFI domain) becomes smoother and with lower values, suggesting a more accurate representation of the estuarine plume, because Level2 (PCOMS domain) when upscaling from Level3 reduces its salinity at the boundary with Level3, therefore imposing lower values and allowing for the estuarine plume to pass through the Level3 open boundary without restriction. Vertical profiles were also important to detect the reach of the estuarine plume and its impact on the PD and CD. Even in the more distant locations such as the west boundary of Level3 and in the Estremadura promontory, a difference of 0.6 salinity unit in the average salinities was observed, and the impact can be seen until about 80 m depth, suggesting an impact not only due to the surface plume but also to the vertical mixing processes related to the bathymetric differences of the domains.

CHAPTER IV

This chapter originated the article:

Sobrinho, J., de Pablo, H., Pinto, L., and Neves, R. (2021). Upscaling local domains in regional domains: an offline approach. *Environ. Model. Softw.* (Submitted)

Chapter 4 Offline upscaling – Tagus ROFI

This chapter describes and validates an offline upscaling algorithm developed in the MOHID modelling system with the objective of performing time efficient upscaling simulations in operational forecasting services, as well as to take advantage of modelling solutions produced by different local entities and generated by different modelling systems. The new upscaling approach is applied to the Portuguese Coast Modelling System (PCOMS) and its nested domain, the Tagus estuary model application. As in the previous two chapters, the models were run for the period between Jan 11 to April 10, which included a period characterized by an extreme precipitation event and subsequent extreme flow rate of the Tagus River. Results demonstrate the potential for the use of this methodology in operational modelling systems, especially in regional model domains which can, through offline upscaling, improve their solutions near coastal areas covered by higher resolution model solutions and/or with additional physical or biological processes. These solutions can be derived from the same institution where the regional domain is running but also from any other institution and modelling software (as long as the results are in the same format such as HDF or NetCDF). This can lead to an increased collaboration between higher level institutions running regional and global ocean model domains and smaller, local institutions specialised in their area of coverage and running local high resolution model applications.

4.1 Rationale

In the last chapter, an upscaling algorithm was added to the MOHID modelling system for online simulations of nested domains. The algorithm was shown to produce good results with minimum error production. However, this methodology demands that both parent (PD) and child (CD) domains be run simultaneously, which is one of the biggest drawbacks of multi-level simulations, because the total simulation time is the sum of each modelling domain simulation time. In downscaling, this drawback was solved by the creation of window results, which cover only the overlapped area between PD and CD (plus 2 PC numerical cells necessary for the higher order advection schemes), but at a higher temporal frequency, typically of 900 s. This means that in operational modelling – where the PD is always one day ahead – the simulation time is dependent on the slowest modelling domain. Another advantage of the offline downscaling is the possibility

of using the same PD results to run multiple nested domains separate from the PD, which increases the efficiency of the entire operational system.

To build an operational modelling system consisting of nested domains running in two-way mode all domains must run on the same machine and with the same instance of the modelling software executable, increasing linearly the amount of time required for the entire procedure as a function of the number and size of the CDs nested in the PD. This thesis follows the same strategy as in the offline downscaling approach, where results from both PD and CD are saved at a higher temporal frequency in order to be used for the downscaling (applied to the CD) and upscaling (applied to the PD). The upscaling will use the same equations already described in Chapter 3.

Aside from the increased efficiency of upscaling in operational systems, the offline upscaling approach enables the coupling between different model implementations run at different institutions (Caldeira et al., 2016) which can be using different model software and simulating different physical or biogeochemical processes. For example, a regional model domain such as the Portuguese Coast Operational Modelling System (PCOMS) which covers the entire Portuguese coast and part of the Spanish coast would be able to benefit from local modelling systems implemented for estuaries, rivers, or the rias de Galicia. All this without the need to model these estuaries as a nested coupling system. These domains do not need to be classified as two-way systems, because a local model can get its open boundary conditions from a CMEMS product, while the PCOMS regional domain can upscale the local domain solution. Practically speaking this type of implementation is straightforward. However further investigations will be necessary to identify potential issues with regarding the compatibility of the modelling applications, at the level of hydrodynamics and biogeochemical data. In this chapter, downscaling and upscaling is performed on the same 2 domains, which classifies it as an offline two-way modelling system. Nevertheless, it does serve as a validation of the methodology and the upscaling algorithm as a useful tool for operational modelling, through the improvement of the regional and global modelling solutions such as those provided by CMEMS.

This line of ocean modelling development is not unique to this thesis, although there has not been any real development in the field. The upscaling of local models into regional models was presented during the course of this thesis, in (Vandenbulcke and Barth, 2019). These authors evaluated (with success) an assimilation-based technique to overcome the issues already mentioned regarding the

need to run both PD and CD at the same time – an issue also raised by (Mason et al., 2010). (Vandenbulcke and Barth, 2019) perform an offline upscaling of the CD into the PD via data assimilation processes, by considering, as in this thesis, that the solution provided by the CD is inherently better than the PD solution. The major difference between their method and the one presented here is the algorithm used. In the present work, data assimilation is replaced by nudging – much like in the traditional two-way nesting. However, there has been very few other developments in this field and no other methodologies or applications were found at the time of the writing of this chapter. Holt et.al, (2017) also mentioned offline upscaling in their work, but stated that online two-way nesting would provide better couplings (which is clear from a coupling point of view due to the higher frequency of information transfer) but with a higher need for boundary-produced noise control. This Chapters aims to answer part of the issues afore mentioned and provide a ready to use solution for operational forecasting. Nevertheless, a balance of pros and cons should always be made before implementing either online or offline upscaling. This balance should target the real need for upscaling, as many downscaling systems are perfectly capable of providing a good solution at an optimal cost (computational and accuracy-wise).

4.2 Code implementation

The overlaying concept behind the offline upscaling algorithm is the nudging of the PD solution towards CD solution, which is provided externally via the HDF results produced by the CD. These results must be volume-averaged into the PD model grid, and this is performed via the main routines developed for the two-way online coupling. In this sense, part of the programming code is the same as in online upscaling. The biggest difference is in the data collection necessary for the upscaling routines.

4.2.1 Modules and implementation files

To make use of some of the data collection, space and time interpolation routines already available in the MOHID code, the definition of the variables and HDF files names and location must now be defined in the “Assimilation.dat” implementation file of MOHID. All variables in this module are defined by characteristic blocks (one for each property), which would not allow for multiple CDs to be upscaled (due to repeated property names). As such, two new keywords have been added to the module, where the first states that the property is to be included in the upscaling procedure

(UPSCALING : 1) and the second sets an ID to each CD (UPSCALING_ID : X). The main calls to the upscaling procedures in “TwoWay” module are now a mixture between the Hydrodynamic, WaterProperties and the Assimilation modules (which makes use of the FillMatrix and Field4D modules). In the hydrodynamic implementation file, only the activation and choice of upscaling method is made, while in the WaterProperties, only the enabling of upscaling is necessary. All other parametrizations are set in the assimilation implementation file, which include the time decay and the number of CD cells to be excluded from calculations. Another important difference towards an online two-way simulation is the main driver of the upscaling algorithm. In an online two-way simulation, it is the CD that calls all the upscaling routines when it is synchronized with its PD. In an offline upscaling simulation, it is the PD domain which is responsible for the handling of operations. Like the online two-way nesting, when the CD covers an inland area not represented by the PD and which produces a tidal prism, a discharge is recommended in the PD to avoid issues in the numerical cells near the inlet location. This discharge will be computed by the upscaling algorithm assuming a null gradient of field velocities in the discharge cell. Without these discharges, artificially high water levels would be created during flood and artificially low during ebb, because the lateral face of the PD does not compute the normal velocity (adjacent cell is a land cell). This means that when water is entering an inlet (flood) of the CD from west to east, a positive u velocity is produced in the PD cell face opposite to the face in contact with a land cell. But because the face in contact with a land cell sets the u velocity to 0, then the conservation equation will force the water level to rise in compensation. This artificial increase of water level was found to induce a strong unrealistic water level gradient near the discharge location, damaging the solution, in tests not shown in this document. The opposite would happen during ebb. Although this issue is localised (nudging of the RD towards the LD on the rest of the overlapped area will remove this gradient), the solution is still degraded near the discharge and should be corrected by the aforementioned operation.

WaterProperties.dat – salinity	Discharges.dat
<code><beginproperty></code>	<code><begindischarge></code>
NAME : salinity	NAME : TagusEstuary
UNITS : psu	DESCRIPTION : Profile from CD
DESCRIPTION : Salinity	I_CELL : 72
IS_COEF : 1	J_CELL : 56
PARTICULATE : 0	K_CELL : 50
	DEFAULT_FLOW_VALUE : 1.9
	UPSCALING : 1
INITIALIZATION_METHOD : CONSTANT	UPSCALING_METHOD : 1
DEFAULTVALUE : 36.	VERTICAL_DISCHARGE : 6
DEFAULTBOUNDARY : 36.	<code><<beginproperty>></code>
BOUNDARY_INITIALIZATION : INTERIOR	NAME : salinity
BOUNDARY_CONDITION : 4	UNITS : psu
	DESCRIPTION : salinity from CD
OLD : 1	DEFAULTVALUE : 0.01
	<code><<endproperty>></code>
DISCHARGES : 1	
SUBMODEL : 0	<code><<beginproperty>></code>
DATA_ASSIMILATION : 1	NAME : temperature
SURFACE_FLUXES : 0	UNITS : celcius
	DESCRIPTION : temperature from CD
ADVECTION_DIFFUSION : 1	DEFAULTVALUE : 19.7
<code><endproperty></code>	<code><<endproperty>></code>
	<code><enddischarge></code>

Figure 49: Implementation files and respective parametrizations required for offline upscaling. Discharges are only required when the CD covers an inland area not represented by the PD and which produces and tidal prism

In Figure 49, another keyword is present, which refers to the upscaling method in the discharge implementation file. This keyword must be defined in accordance with the type of data and domains of the simulation. The first method considers the upscaling from an HDF whose domain size covers more than just the first numerical cell of the PD at the inlet of an inland water body (such as the one represented in Figure 48) and where the user only wants to perform a null gradient on the flux entering and exiting the inlet. However, as will be presented in the next chapter, the user may only want to upscale a discharge from a specific HDF where the CD only covers 2 or 3 numerical PD cells. In this case, better results will be obtained by simply adding a momentum discharge to the PD cell adjacent to land (light blue in Figure 48). The merits and disadvantages of this type of methodology will be discussed in the next chapter.

Coming back to the code structure, the upscaling of a CD into a PD from HDFs indicated in the assimilation implementation file is accomplished in a similar fashion to that of the offline downscaling, where every field is interpolated to the PD grid before use, except that in downscaling an interpolation is performed from a coarser grid to a finer grid and in upscaling the reverse occurs. Again, as in downscaling, nudging is performed in the hydrodynamic module via an acceleration force added to the momentum equation (for velocities) and sink/source (for water level), and in the WaterProperties module as a sink/source term (for properties such as temperature and salinity). As opposed to the offline downscaling, the acceleration and sink/source of every water property is

now computed in the two-way module. This module is invoked by the field4D module which, in turn, is invoked by the FillMatrix module which, in turn, is invoked by the Assimilation module. This code path is defined by two important keywords, the “UPSCALING” and the “FIELD4D” defined in the assimilation implementation file. Both keywords are used in the FillMatrix and Field4D modules to define the necessary routines that must be invoked. While the first keyword will be necessary for the invocation of the TwoWay module and its upscaling routines, the “FIELD4D” will be used in FillMatrix to invoke the Field4D module. The major difference between these two modules is that the field4D method can collect all grid variables needed for the upscaling (volumes, areas, distances), identify which cells are covered and which are not, and perform space and time interpolations, while the FillMatrix module can only perform the time and space interpolations, while the rest of the information must be provided before-hand. This is the only reason why upscaling code is present in both these modules.

4.2.2 Handling of multiple upscaling domains

As mentioned before, the Assimilation module is responsible for the handling of all upscaling property fields that need to be upscaled from a local, finer grid solution (or a solution with an additional physical or biogeochemical process). To distinguish multiple fields with the same property names, the keyword “UPSCALING_ID” was added. In the assimilation routines, when a new property with a repeated name is discovered in the assimilation implementation file (new block <begin_property> <end_property> was found) and the keyword “UPSCALING” is active for that property, the module searches for the “UPSCALING_DOMAIN_ID” keyword. If the ID already exists, then the routine will use all the auxiliary matrixes (distances, areas, volumes, covered/non-covered cells, etc) and pointers already created and stored for that domain ID, avoiding the allocation of duplicated matrixes. Information regarding all these matrixes and pointers are transferred to the FillMatrix module, which is responsible for filling the property matrix that the user wants to upscale with the values provided by the upscaling routines. However, since this module does not have the capability of using the information provided, it transfers the information to the Field4D module (enabled by the “FIELD4D” keyword). Furthermore, it is in this module that the two-way module responsible for the offline upscaling is invoked, which is determined by the presence of the “UPSCALING” keyword. In run-time, these routines are launched by the Hydrodynamic and WaterProperties modules when the “UPSCALING” keyword is active in their

respective implementation files, as well as the “DATA_ASSIMILATION” keyword. With it, these modules get the necessary upscaling property fields from the Assimilation module (through their specific property ID), which will get the updated matrixes from the FillMatrix and subsequently from the Field4D and two-way modules.

4.2.3 Time interpolation and grid communication

Since the frequency of results provided in the input file (HDF or NetCDF) is normally not synchronized with the model time step, time interpolation is required. In this case a linear time interpolation is used in the two matrixes produced by the volume-weighted average operation (applied to two instances of time present in the HDF or NetCDF file).

The amount of data per output file produced by the modelling systems is typically 1 day. In each of these files, any frequency of outputs is allowed, but usually frequency (>3600 s) is several times higher than the model time step (<120 s) that produced the results. This means more time interpolations and subsequent less accuracy, but the real difference is in the communication between nested model grids. In online two-way couplings, communication (Figure 50-left) is made at each time step (of the LD in downscaling procedure and of the RD in upscaling procedure), but in offline simulations the communication is done at a frequency equal to that of the time period covered by the input file provided. Take, for example, an offline upscaling simulation in operational mode (with forecasts of 2 days) in which the LD produces an output file for every day of simulation, containing one output every 900 s (Figure 50-right). This would lead to a 3-day simulation – today, tomorrow and the day of tomorrow – if the simulation started today. In this case, because the LD results are typically behind in time, a first one-day (day-0) simulation of the RD without upscaling is performed, followed by the LDs use the RD newly created results as open boundary conditions to run the same day. When the RD is finished, it can produce results for the following day (tomorrow – day1) and the next (day after tomorrow – day2) always without upscaling, followed by the rest of the LD simulations which begin as soon as the RD finishes each day. This would end the simulations for today. The following day – tomorrow – the computers will start the 3-day simulations beginning on day1 and ending on day 3. However, as there are now LD results available in files, the RD can run days 1 and 2 with upscaling (the LD has not yet run day 3 so upscaling cannot be performed for this last day). At the same time, the LD now has updated

boundary conditions from the RD (which improved its solution with upscaling). Moving forward to the end of the simulations starting the day after tomorrow, the system will have simulated day 2 3 times for each domain, once without upscaling and twice with upscaling and updated boundary conditions. Therefore, for systems running a forecast if 7 days, the transfer of information will be maximised, but at nearly no additional computation or time costs, as each day is simulated 8 times (today + 7 days) due to updates in atmospheric and open boundary conditions, regardless of using upscaling or not. In this work, one and two procedures are tested, which allow the analysis of the need for stronger couplings.

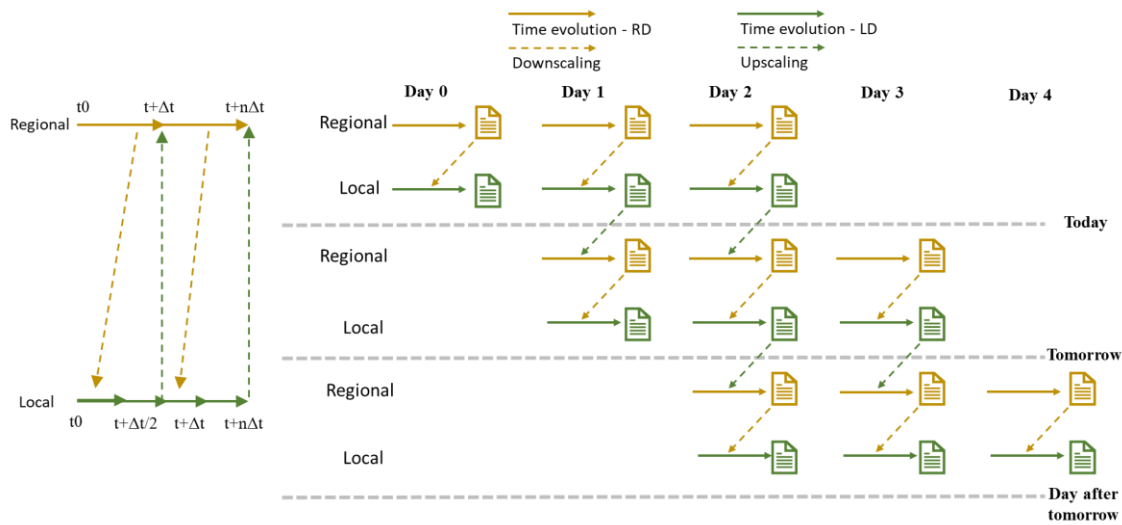


Figure 50: Time integration schemes for a simulation with a PD and a CD. On top: a representation of downscaling plus upscaling operations (in this scheme it is considered offline two-way). On the bottom: a representation of the online two-way simulation.

Another way of improving the communication between domains would be to reduce the integration size (in time) of each domain simulation, therefore increasing the communication between domains. Only the first option was tested in this thesis, as it was the easiest way to accomplish the offline upscaling, considering the operational tools available at Maretec (which are not prepared for less than one day of simulation per run). In this chapter, the offline system of downscaling plus upscaling is tested with 2 and 3 runs per domain, which means 1 and 2 iterations of upscaling for the PD (respectively) and 2 and 3 downscaling operations for the CD (respectively) for each day of simulation. The most important disadvantage of this approach is related with the time required for the simulation. In hindcast simulations the models are required to run each day twice or more, leading to highly demanding computational times. However, in operational modelling this proves

to be an advantage, because in operational forecasting, each day is always computed at least 3 times. This is due to the need to forecast at least 3 days into the future, plus at least one day of hindcast to feed the solution with the latest available meteorological and OBC from regional and global ocean model domains. As such, shifting from an operational forecasting system from an offline downscaling approach to an offline two-way approach is computationally free of charge. From a Regional modelling system perspective, upscaling from local domains (offline upscaling) will also be, for the same reasons, free of computational costs, allowing for the upscaling of multiple solutions provided by different entities, models or model implementations, which would greatly increase the solutions provided by these regional modelling solutions.

4.2.4 Parallelization

At the moment a good part of the upscaling code is only prepared to be run in serial or OpenMP modes. The main reason is related to shortage of time as well as some technical difficulties in preparing a code for MPI that requires many communication procedures between two nested grids and where different CD cells may need information from different MPI processors. However, these problems can be overcome and will have to in order to provide faster simulations. In this regard, some code optimizations were performed during this thesis which provided improvements in the order of 11-30% depending on the amount of WaterProperties being simulated and size of the domain (the model efficiency decreases less with grid size in comparison with previous MOHID versions. These improvements impact all modes – serial, openMP and MPI – which means that at this time even if openMP is necessary, and up to 6-8 processors, the model can run faster than in previous versions of the code. Nevertheless, MPI parallelization implementation in the two-way module will be critical for the model usefulness and is therefore included in the future work.

4.3 Real case test – PCOMS - Tagus ROFI modelling system

In this chapter, the offline upscaling approach is applied to the Tagus ROFI modelling system to maintain a coherent analysis of the upscaling algorithm. This way, one-way and two-way methodologies are tested in online and offline coupling of the modelling system and provide a more general overview of the upscaling. To that effect, all simulations run in this chapter use the same parametrizations as those used in the previous chapters. The only differences lie in the implementation files, code paths followed in the MOHID software, and in the downscaling and

upscaling frequencies – which are now dependent on the results output frequency of the separate domains, in this case of 900 s.

This real case test simulates the extreme precipitation event which occurred in March-April 2013 and led to a Tagus flow rate of around $7500 \text{ m}^3\text{s}^{-1}$ in comparison to its average flow rate of $258 \text{ m}^3\text{s}^{-1}$. In order to obtain comparable results, aside from the offline downscaling plus upscaling simulations, a one-way simulation of the modelling system using the offline downscaling approach is also made. The reason for this simulation is that online downscaling produces different results than offline downscaling – due to differences in the open boundary conditions produced by the lower frequency transfer of information from PD to CD.

As previously discussed, the lower frequency of transfer of information from CD to PD and vice-versa will make the overall solution take more time to reach an equilibrium. In this test, the transfer of information is made in a daily basis – which is the standard already in use for offline downscaling in Maretec. Two different simulations with upscaling are considered, one following the communication scheme presented in Figure 50-top where the PD is updated once per day of simulation, and another where each domain is run three times – thus including two PD runs with upscaling – which is a duplication of the procedure presented in Figure 50-top. These tests demonstrated the need for more than one run per day of simulation, by producing better solutions when the PD runs three times each day and upscaling from the CD is done twice.

4.3.1 Setup

4.3.1.1 Grid communication management

Offline simulations differ from online simulations only in the need for pre-processing and post-processing operations, while the parameterizations and open boundary conditions are quite similar. Some of these operations are already included in operational forecast modelling, which require the constant change in the simulation period (modified in a specific implementation file of MOHID called `model.dat`), as well as all the file management system. This system includes copy and renaming of input and output files required and produced (respectively) by MOHID from the work folders used by the model to the storage systems specified by a user – which in Maretec includes cataloguing all output files by date, with each file saved in its own folder named after the simulation period it refers to. Also, open boundary condition files as well as atmospheric and fresh water

discharges files must be transferred before any simulation takes place, as these files usually only contain one day of data per file. All of these data transfers are managed by a separate tool from MOHID, which has been updated during the course of this thesis to be able to run the offline upscaling simulations.

A new problem arrives when the same model domain needs to run the same day twice before moving towards a new simulation day (from day 0 to day 1). As the results from each domain are saved in a folder system where each folder with the denomination “Yi-Mi-Di_Yf-Mf-Df” contains the output files with standard constant names such as Hydrodynamic.hdf5 or WaterProperties.hdf5, after the first PD run – no upscaling – the PD will try and repeat that same day, but now with upscaling enabled. However, as the CD takes a certain amount of time to run its own simulation, when the PD searches for the upscaling file, it will not yet exist in the specified folder of the CD solution. To solve that problem a trigger system has been adapted from the operational modelling systems already in place at Maretec. The trigger system consists of simple text files containing the simulation period to which they refer, and a keyword that states the current status of the simulation (running or finished). With this system in place, the PD domain wanting to run the first day for the second time will have to wait for the “finished” status of the trigger file produced by the CD for that same day. The main adaptation made in this trigger system is that in the first PD run of each day (when upscaling must not occur), the trigger file is ignored, leaving the PD free to run that simulation. For the CD, this system is always in place because it always needs the most recent output from the PD. This lead to another problem, the first PD run of a given day must not try and perform upscaling, because it is ahead in time – on the first run of any given day the CD needs to have the OBC from the PD. A workaround to this problem was introduced directly in the MOHID code, in order to facilitate the management of the implementation files. If not, in the first run of a given day, the “Assimilation.dat” implementation file would have to exclude all the upscaling fields, the “Hydrodynamic.dat” would need to deactivate the “UPSCALING” keyword as well as all discharges related to the upscaling procedure. Therefore, a code solution was implemented, which performs the search for all upscaling fields (marked by the “UPSCALING” and “UPSCALING_DOMAIN_ID” keywords in the “Assimilation.dat” implementation file) and if the files are not present in the location the user specified, then the upscaling of those fields is disabled. This solution also solves the issue of failures in the local domains being upscaled by a regional domain. When a failure happens and an output file is not produced by a local domain, the regional

domain will still work – it will simply ignore the upscaling of that domain, and upscale any other existing domains.

4.3.1.2 Implementation setup

The modelling system is comprised of three domains (Figure 7) : 1) 2D barotropic regional domain with 5.7 km constant grid resolution for the Portuguese Coast (Level1) (33.5° N - 49.9° N, 1.0° W - 13.5° W) running only with tidal forcing from FES2004 (Lyard et al., 2006)-(Lefèvre et al., 2002); 2) 3D full baroclinic regional domain for the Portuguese Coast (Level2) (34.4° N–45.0° N and 12.6° W–5.5° W) with a grid resolution of 5.7 km and 50 vertical layers (7 sigma at the surface and 43 cartesian below); 3) 3D full baroclinic domain for the TagusROFI (Level3) and adjacent coastal area with a variable grid from 2 km to 200 m (38.15°N – 39.2°N, 10°W – 8.9°W), and 50 vertical layers (7 sigma at the surface and 43 cartesian below). As the rest of the system has already been described in Chapter2, only a summary is presented in Table 10, which describes the main parametrizations used in all systems.

Table 11. Model setup configuration for the Tagus ROFI area in two-way mode.

Settings	Level1 – West Iberia	Level2 – PCOMS	Level3 – Tagus ROFI
Model characteristics	2D - Barotropic	3D – Baroclinic	3D - Baroclinic
Grid corners	33.50° N - 49.90° N 1.00° W - 13.50° W	34.38° N – 45.00° N 12.60° W – 5.50° W	38.16° N – 39.21° N 10.02° W – 8.90° W
Cells dimension	208 x 156	177 x 125	121 x 146
Bathymetry	EMODnet Bathymetry portal	EMODnet Bathymetry portal	IH Data and GEBCO
Horizontal Grid	Regular: (\approx 5.7 km)	Regular: (\approx 5.7 km)	Irregular: 200 m to 2 km
Vertical Grid	1 layer	7 Sigma Layer (0 - 8.68 m) 43 Cartesian layers	7 Sigma Layer (0 - 8.68 m) 43 Cartesian layers
Δt	60 seconds	60 seconds	6 seconds
Tides	FES2004	From WestIberia	From PCOMS
OBC Water	...	From MercatorOcéan PSY2V4 (Releases 1- 4)	From PCOMS
Nudging	...	Flow relaxation scheme of 10 cells with a time decay of 1 year inside the domain	Flow relaxation scheme of 10 cells with a time decay of 900 days at the open boundary and 1 year inside the domain
OBC Atmosphere	-	MM5 (12 km and 9 km)	WRF (3 km)

Discharges	No	No	Tagus (hourly), Sorraia, Trancão (monthly)
Turbulence	...	GOTM*	GOTM*
Bottom	Rugosity of $0.0025 \text{ m}^2 \text{ s}^{-1}$	Rugosity of $0.0025 \text{ m}^2 \text{ s}^{-1}$	Rugosity of $0.0025 \text{ m}^2 \text{ s}^{-1}$
Upscaling Td (s)	X	X	900
Variables upscaled	-	X	Horizontal velocities + Temperature + Salinity
Number of CD cells ignored	X	X	6

*General Ocean Turbulence Model (Burchard et al., 1999) coupled to MOHID (Ruiz Villarreal et al., 2005).

Following the same approach as in Chapters 2 and 3, the validation of the model applications is performed by comparison against the Cascais tide gauge (PCOMS and Tagus ROFI), and against salinity data obtained by a CTD located at the mouth of the Tagus estuary (Tagus ROFI only). Other comparisons include surface salinity at the northeastern boundary of Tagus ROFI, and vertical profiles extracted from 3 different locations inside the overlapped area of the gridded domains. These comparisons refer to the entire period of simulation (January 15 to April 10) and a focus on the peak flow period (25 March to 10 April). The location of the vertical profiles: P1 – Lisbon Canyon (38.37°N , 9.51°W), P2 – western boundary of Tagus ROFI (38.61°N , 9.99°W) and P3- northeast boundary of Tagus ROFI (39.14°N , 9.45°W), and of the CTD (38.69°N , 9.23°W) and the Cascais tide gauge (CTG - 38.69°N , 9.42°W) are presented in Figure 50.

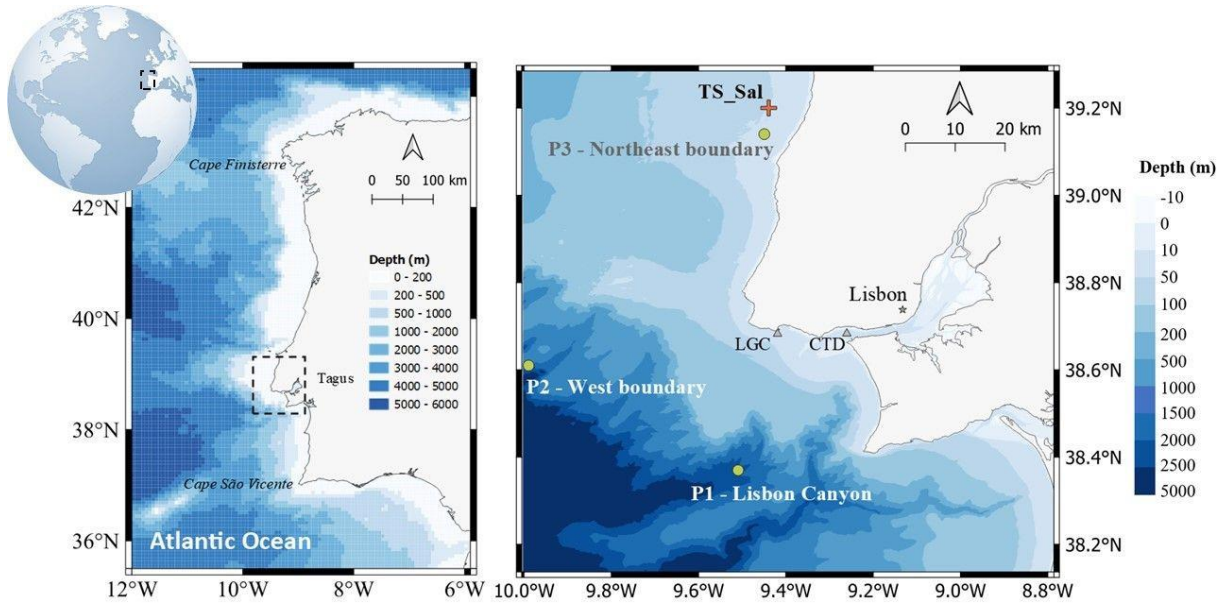


Figure 51: Model domains of PCOMS (left) and TagusROFI (right). The WestIberia bathymetry is the same as PCOMS, although with 2 more numerical cells in each direction. The location of the in-situ stations (CTG–Cascais Tide Gauge - 38.69°N, 9.42°W; CTD–Conductivity, Temperature, and Depth probe - 38.69°N, 9.23°W) used in the validation process, the vertical profiles (P1 – Lisbon Canyon (38.37°N, 9.51°W), P2 – western boundary of Tagus ROFI (38.61°N, 9.99°W) and P3- northeast boundary of Tagus ROFI (39.14°N, 9.45°W) used for comparing modelling grids and the time series extracted from near the open boundary of Tagus ROFI (39.19°N, 9.44°W) are presented on the right.

4.3.2 Results

In these next sections, a comparison between the 3 offline implementations is shown, and includes the traditional approach offline downscaling, the new downscaling + upscaling with one offline upscaling run, and one where two runs of the same day are performed with offline upscaling. The objective is to understand and quantify the effect offline upscaling in the regional PCOMS model application, and the importance of running more times the same day (to increase grid communication).

4.3.2.1 Water level validation

Water level obtained by the six model implementations (PCOMS and Tagus ROFI under the three different parametrizations) was validated against the Cascais tide gauge during the period between 11 January and 13 March, 2013 (PCOMS - Figure 52, Tagus ROFI - Figure 53). These figures show a direct comparison between the water level obtained by the three implementations and field data, a comparison between the bias of the three implementations, and the correlation between model and field data. As these figures show, including the Tagus estuary through upscaling does not bring any visible changes to Tagus ROFI or PCOMS model applications. This lack of change in the water level is not unexpected, as a very large flow rate from the Tagus would be necessary to produce significant changes in water level in Cascais (20 km away). This may have happened in during the peak flow, but at the time of the analysis there was no data available from the tide gauge for the period between 13 January to 10 April. However, results do show a good agreement with the tide gauge, which mean that at least in this coastal area and very near the mouth of the estuary where the bathymetry and the estuary play an important role, the model is able to properly represent the tidal variability. Also, a statistical analysis including bias, RMSE and Pearson correlation coefficient (Table 12) suggest, overall that the solutions are very similar, although globally with a slight increase of bias and RSME. In PCOMS, a small increase of the mean bias in PCOMS is verified when one day of upscaling is performed (from 4.02 mm to 4.09 mm) although with a reduction in the median bias (from 2.21 mm to 1.84 mm). RMSE values diminish when upscaling is made, whether running the same day once with upscaling (from 0.0739 to 0.0710). As for the correlation values, all implementations show the same good agreement with the tide gauge. However, when instead of running only one day with upscaling, two days are used, some metrics are reverted. Median bias, for example, increases from 1.84 mm to 2.24 mm again (the implementation with only downscaling produced a value of 2.21 mm), whereas RMSE values, although smaller than when using only downscaling, increase from 0.071 to 0.0724 (using one or two days of upscaling, respectively). Once again, correlation and NASH values remain equal in all implementation. Regarding the Tagus ROFI, the same analysis can be made about the mean and median bias values. However, RMSE values obtained by the offline two-way system, whether running the same day once or twice with upscaling are higher (from 0.068 obtained by the offline one-way system to 0.069 and 0.071, respectively). The same Pearson correlation coefficient and NASH parameters were obtained by the all implementations.

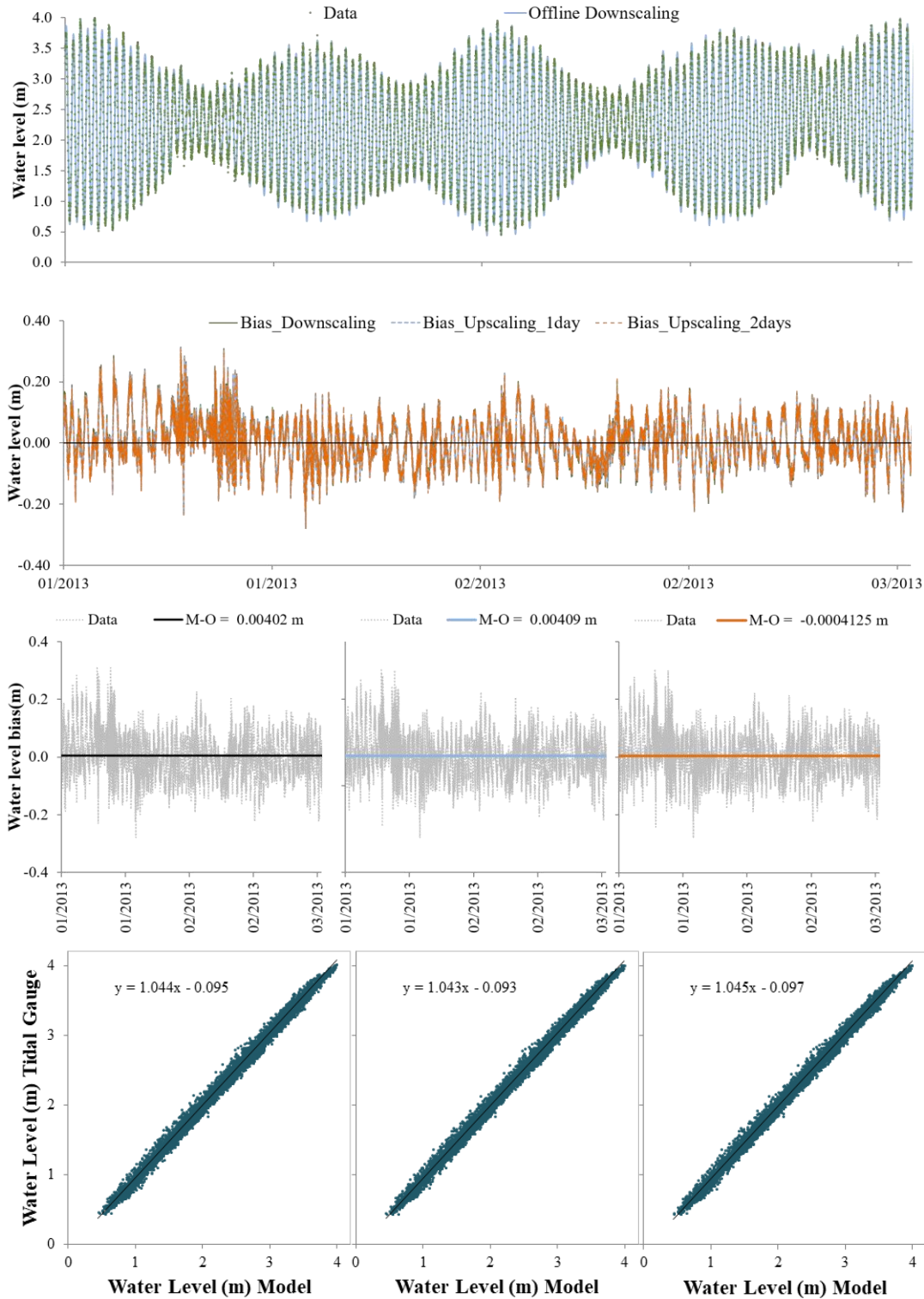


Figure 52: Comparison between water level obtained by the different PCOMS model implementations. From the top: water level over the simulation period obtained by the tide gauge and the one-way offline downscaling implementation; Overlapped bias of the different implementations towards the tide gauge; Bias of the different model implementations and their average bias towards the tide gauge; correlation between each implementation and the tide gauge.

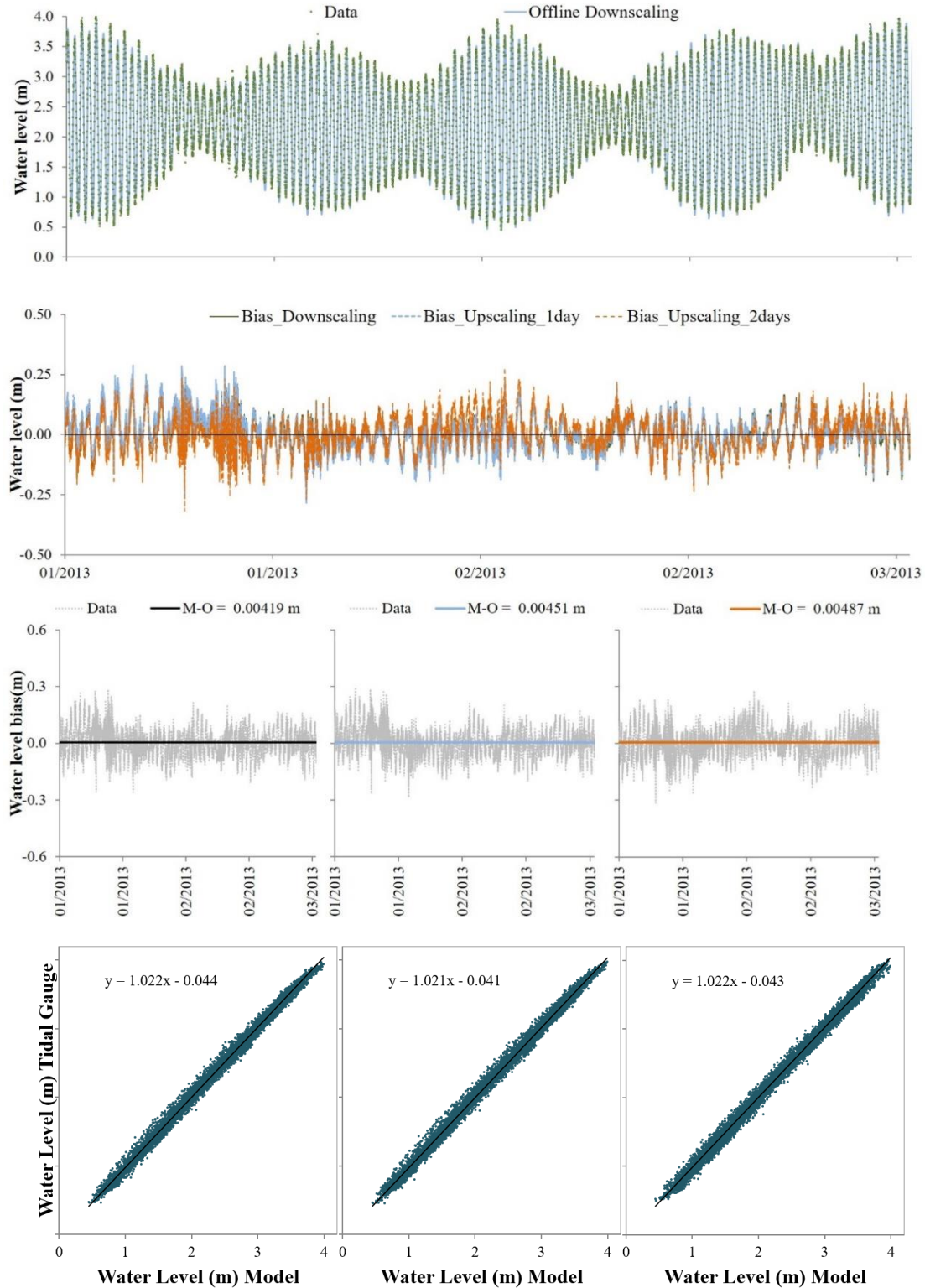


Figure 53: Comparison between water level obtained by the different Tagus model implementations. From the top: water level over the simulation period obtained by the tide gauge and the one-way offline downscaling implementation; Overlapped bias of the different implementations towards the tide gauge; Bias of the different model implementations and their average bias towards the tide gauge; correlation between each implementation and the tide gauge

Table 12: Statistical parameters of the three implementations: offline downscaling, offline downscaling plus upscaling with one and two runs of the same day with upscaling enabled, for the water level at the Cascais tide gauge.

Parameter	PCOMS			Tagus ROFI		
	Downscaling	Upscaling 1 day	Upscaling 2 days	Downscaling	Upscaling 1 day	Upscaling 2 days
Bias(Mean):	0.00402	0.00409	0.00413	0.00419	0.00451	0.00487
Bias(Median):	0.00221	0.00184	0.00224	0.0021	0.00158	0.00387
Pearson:	0.997	0.997	0.997	0.997	0.997	0.997
RMSE:	0.0739	0.0710	0.0724	0.068	0.069	0.071
NASH:	0.999	0.999	0.999	0.999	0.999	0.999
n	8819					

This analysis shows that all model applications performed quite well when compared with the tidal gauge, with very small differences between themselves, which means that there is no significant degradation of any of the solutions during this period. However, the most impact of these implementations is not expected to occur neither in water level nor in the vicinity of the mouth of Tagus ROFI, but in the interior of the domain and especially near the open boundaries of Tagus ROFI.

4.3.2.2 Surface salinity validation

Surface salinity obtained by Tagus ROFI under the three implementations was compared against field data from the moored buoy located near the mouth of the Tagus estuary and for the period of 11 Jan to 10 April (Figure 54). Results demonstrate the ability of the model application to reproduce the salinity variability over time, especially during the peak flow event at the end of March, beginning of April. This peak flow is represented in grey in Figure 54 and shows the extreme flow rate registered at the time (which eventually submerged the buoy, stopping the data acquisition of salinity during part of the event). There are no significant differences between salinity obtained by the different implementations, much due to the location of the buoy, which is in a location dominated by the estuary's salinity plume and as such will have little impact from the changes occurring at the open boundary of Tagus ROFI. That being said, and as observed with water level, there is a slight increase in model error when models are run three times each day (the last two using upscaling), although with a small advantage of the one day of upscaling implementation over the downscaling. However, and like in the water level comparisons, the statistical parameters (Table 13) suggest that the model accuracy obtained by all implementations is hardly affected by the use of upscaling near the estuary mouth.

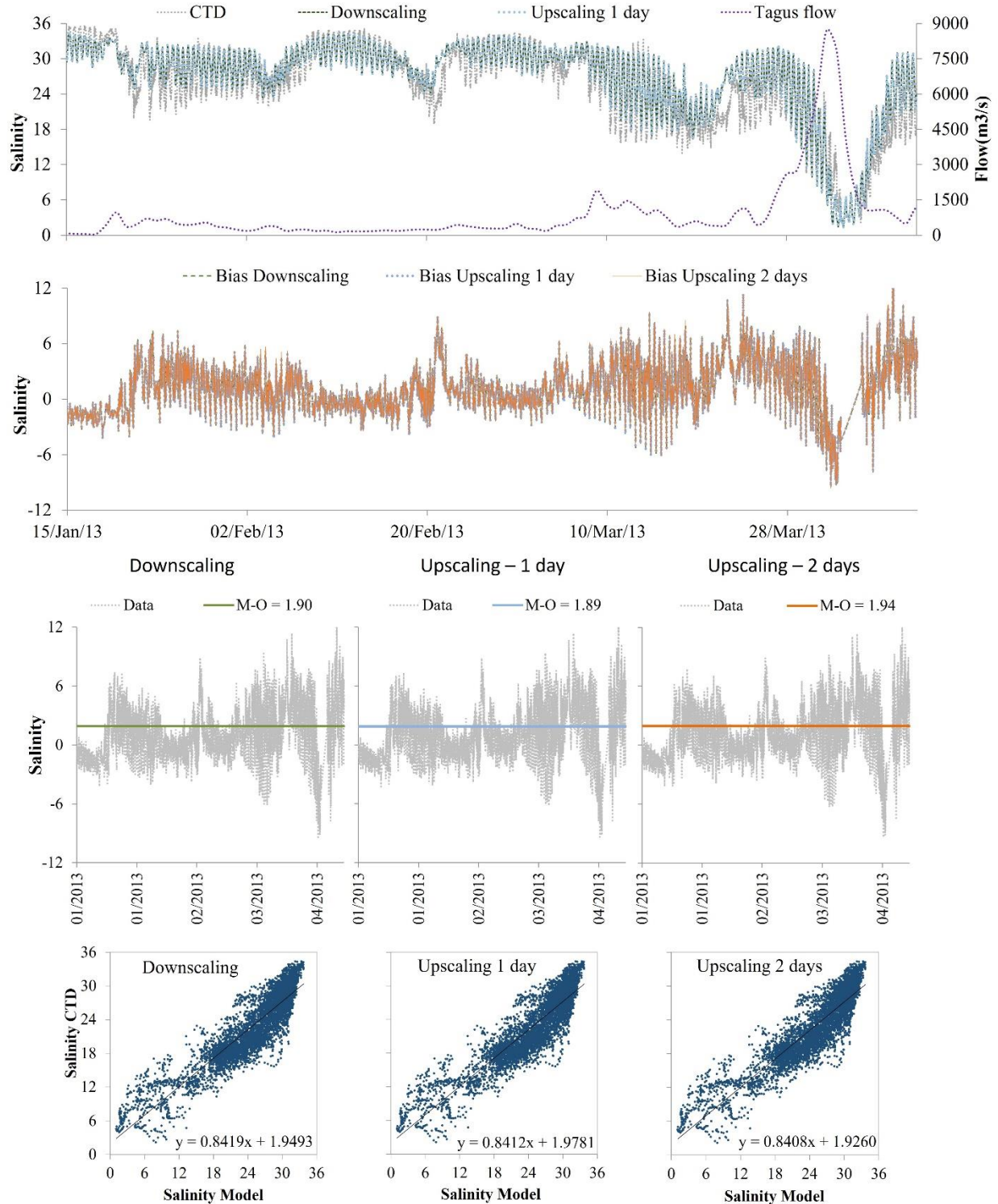


Figure 54: Comparison between surface salinity obtained by the different model implementations of Tagus ROFI. From the top: surface salinity time series over the simulation period obtained by the CTD, the one-way offline downscaling implementation, and the offline two-way implementation with one 1 day of upscaling; Overlapped bias of the different implementations towards the CTD; Bias of the different model implementations and their average bias towards the CTD; correlation between each implementation and the CTD.

Table 13: Statistical parameters obtained for the comparison against surface salinity at Algés, of the three implementations: offline downscaling, offline downscaling plus upscaling with one and two runs of the same day with upscaling enabled.

Parameter	Tagus ROFI		
	Downscaling	Upscaling -1 day	Upscaling-2 days
Bias(Mean):	1.90	1.89	1.96
Bias(Median):	1.81	1.81	1.90
Pearson:	0.900	0.900	0.900
RMSE:	3.55	3.54	3.58
NASH:	0.69	0.69	0.69
n		5468	

4.3.2.3 Salinity transition at the open boundary

As previously mentioned, the major changes expected in surface salinity will occur not near the estuary mouth but further offshore, and especially near the open boundaries of Tagus ROFI where the gradient between Tagus ROFI running in one-way offline mode and Level running in two-way offline mode will be highest. Therefore, time series of surface salinity extracted from both PCOMS and Tagus ROFI results were compared between themselves. Figure 55 shows this comparison for the majority of the simulation period (between Jan 25 and April 10). In Tagus ROFI (top graph of Figure 55) implementations in which upscaling was applied, the minimum salinity values in April 2 are lower (from 32 to 29) in the, and decrease with the addition of another day of upscaling (from 29 to 28). However, the most noticeable change is the lower variability of the salinity as the grid communication increases. The amplitudes obtained by the one-way offline methodology decrease significantly when one day of upscaling is performed, and even more so when two runs of the same days are run with upscaling. The reason for this is related to the improvement of the open boundary condition for salinity, as observed in the bottom graph of Figure 55. As the salinity of PCOMS is not affected by a land discharge in the one-way offline methodology, it provided Tagus ROFI with a constantly higher salinity value than that computed by PCOMS. As such, when the flow direction changes from northward to southward, the salinity of Tagus ROFI will decrease much rapidly and the opposite when the flow changes from southward to northward. However, in the two-way offline methodology, when the flow direction changes from northwards to southwards, the salinity values provided by PCOMS – which upscales salinity from Tagus ROFI – is lower and more compatible with the salinity values computed by Tagus ROFI at its open boundary. As such, the variability of salinity will decrease, and more so as grid communication increases (from 1 day of upscaling to 2 days of upscaling). Figure 56 shows the salinity field difference between downscaling and 1 day

of upscaling implementations obtained for the period between 25 March and 10 April 2013, when the flow is mostly northwards. The results shows that major differences occur near the open boundaries, with higher salinity values obtained when using downscaling methodology, and in front of Tagus mouth, with lower values obtained when using downscaling methodology. The reason for this is that when the downscaling methodology was used, the Tagus plume was not able to reach the open boundaries (due to the imposed Level 2 boundary conditions), and was deviated further to south, whereas with upscaling methodology the plume is able to go easily to the north. With a second day of upscaling these differences are accentuated, confirming that the smoother open boundaries allow for a less restricted estuarine plume.

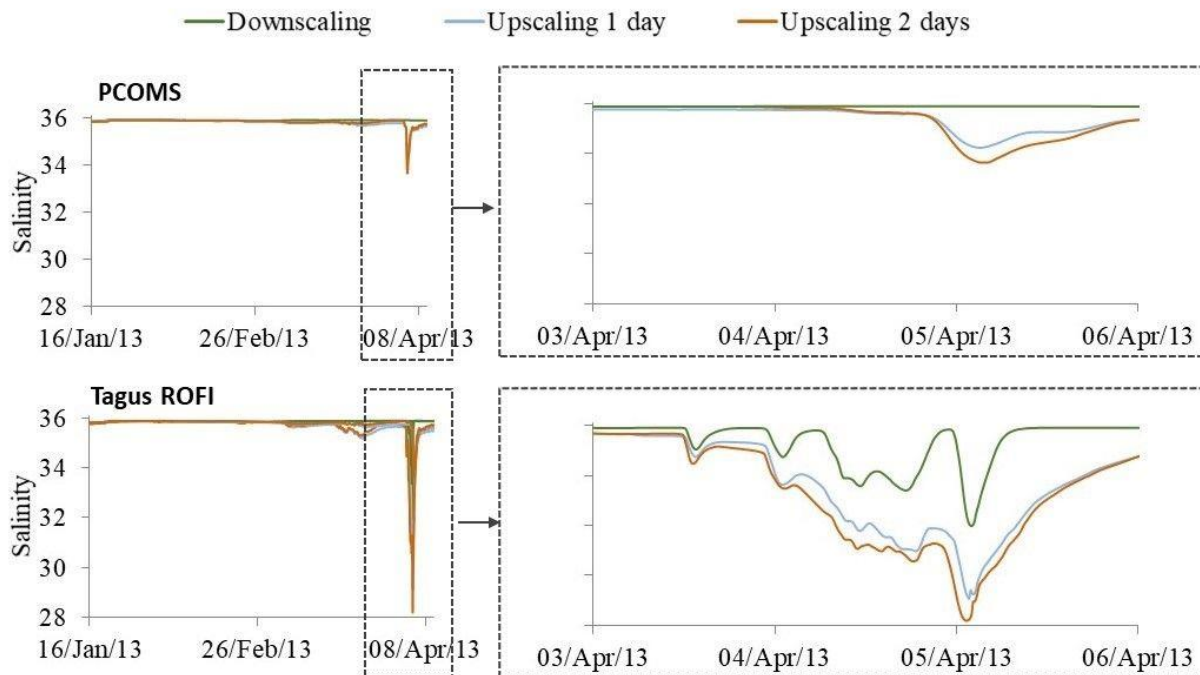


Figure 55: Time series of surface salinity at the northeastern open boundary of Tagus ROFI, obtained by PCOMS and Tagus ROFI, showing the impact of upscaling in the transition between model grids and the feedback it generates into Tagus ROFI when the upscaling procedure is executed 2 times per day.

This improvement is quite important for a regional model application covering the Iberian Peninsula, as the lower salinities observed so far from the mouth of the Tagus estuary will be transported northwards during winter and spring, and its plume, together with that of the Sado estuary can merge and produce a large enough plume that joins with the West Iberian Buoyant Plume (WIBP), as observed in Campuzano (2018).

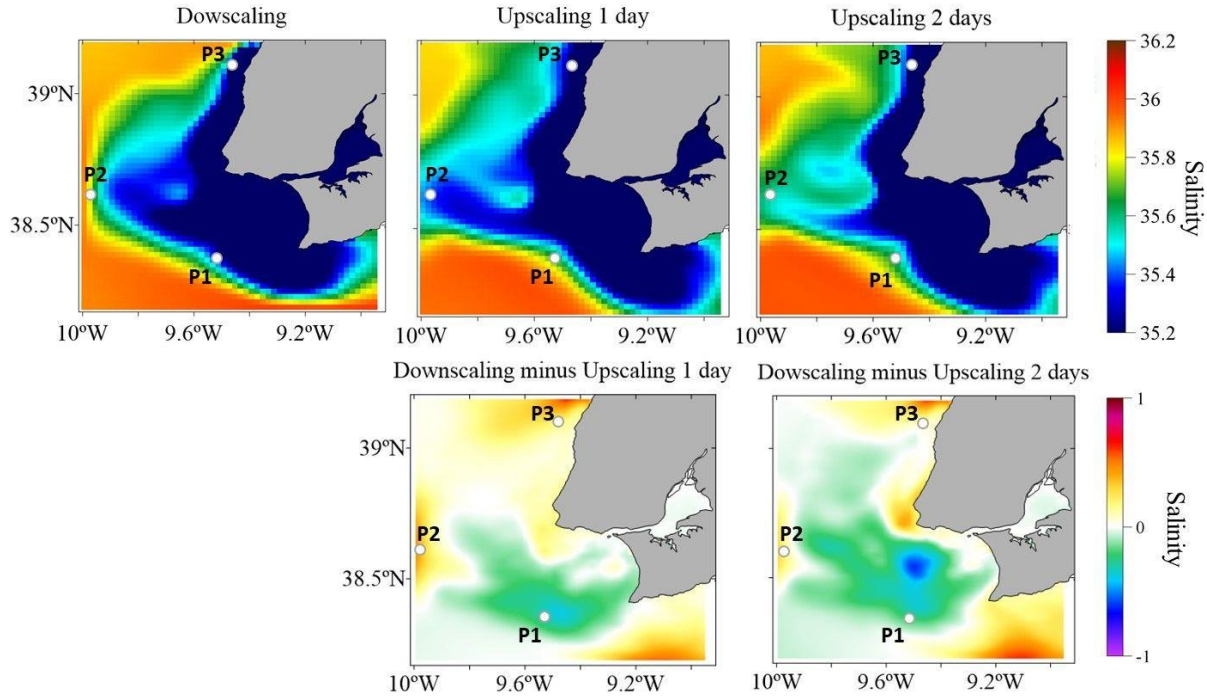


Figure 56. Salinity fields obtained by the three implementations. At the top: offline downscaling (left), 1 day of offline upscaling (middle) and two days of offline upscaling (right); at the bottom: difference between the downscaling simulation and the 1 day upscaling simulation (left), and the difference between the downscaling simulation and the 2 days upscaling simulation (right), for the period between 25 Mar and 10 April 2013.

4.3.2.4 Vertical profiles

As in Chapters 2 and 3, temperature and salinity profiles were extracted from 3 strategic locations: Lisbon Canyon (P1), western boundary of Tagus ROFI (P2), and the northeast boundary of Tagus ROFI near the coastline (P3) (see location in Figure 51). Time series of salinity extracted from PCOMS and Tagus ROFI at the surface near the open boundary of Tagus ROFI already showed the improvement of the solution when upscaling is applied. In this section, the impact of the method on temperature and salinity in depth will be analysed. Figure 57 shows the comparison between time-averaged temperature profiles obtained for the period of 25 March to 10 April, which corresponds to the peak flow period. This period was chosen so as this chapter is in accordance with the previous chapters, and because it helps identify the impact of the peak flow in the entire area of study. In order to use comparable results, Tagus ROFI fields were previously interpolated (via simple average) into the PCOMS grid, which means that some caution is advised when looking at the comparisons as the average partially distorts the results in areas where the grid resolution of PCOMS is highest, and near the coast, as some PCOMS cells are only partially covered by Tagus

ROFI. These results show an influence of the upscaling algorithm that can be detected up to 100 m depth in the Lisbon canyon and at the west open boundary of Tagus ROFI, which is similar to what was already verified in the previous chapters 2 and 3. Near the coast, where the depth is lower, this influence is evident over the entire water column. Furthermore, there is a tendency towards the approximation of the temperature and salinity vertical structures of the model domains, which was the objective of the method. Regarding the number of runs per day of simulation where upscaling is performed, the temperature fields produced by PCOMS and Tagus ROFI became more similar in all three locations but with a slight increase in temperature from the one-way to the two-way implementation running once per day with upscaling in P1 and P2 (0.15 °C for both locations) and negligible changes in P3, followed by a increase from the latter to the two-way implementation running twice per day with upscaling (0.15 °C, 0.5 °C and 0.2 °C respectively for P1, P2 and P3). This is a result of both the changes in local currents verified in Figure 56 and Figure 58, promoted by the Tagus ROFI solution increased influence in the PCOMS currents and subsequent boundary values provided to the Tagus ROFI, and the higher river discharge temperature in comparison to the ocean temperature. In particular, because of the Tagus estuary domain effect on the coastal currents, which increase the water level near the shore and drive the currents northward due to the Coriolis force, the warmer waters from the south are now dragged northwards (Figure 58). Salinity profiles (Figure 57) demonstrate the increased nudging between PCOMS and Tagus ROFI domains when more runs per day with upscaling are performed. Another effect that was already visible in comparisons made at the surface near the open boundary of Tagus ROFI is the lower salinity limit at the locations where the estuary plume exerts more influence (such as the Lisbon canyon or the northeastern open boundary). Nevertheless, the range of salinity values produced by the two-way simulations using 1 or 2 runs per day with upscaling is always below 0.4 salinity units. Although these results are averages in time, and include days with higher salinity differences, this means that using an extra day of simulation does not bring many changes to the overall solution.

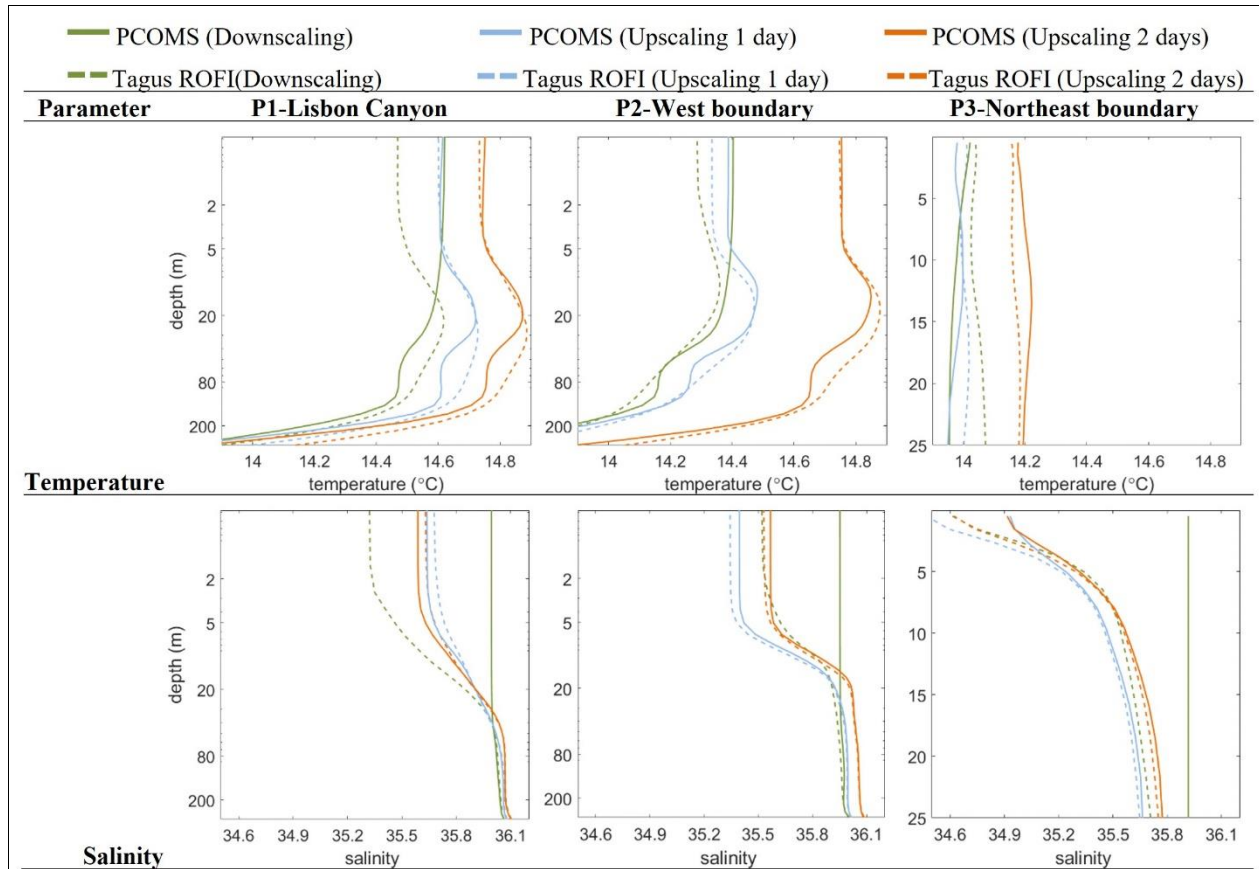


Figure 57: Comparison between vertical profiles of temperature obtained by PCOMS and Tagus ROFI domains at the five defined locations for the two analysed periods, under one-way and two-way modes.

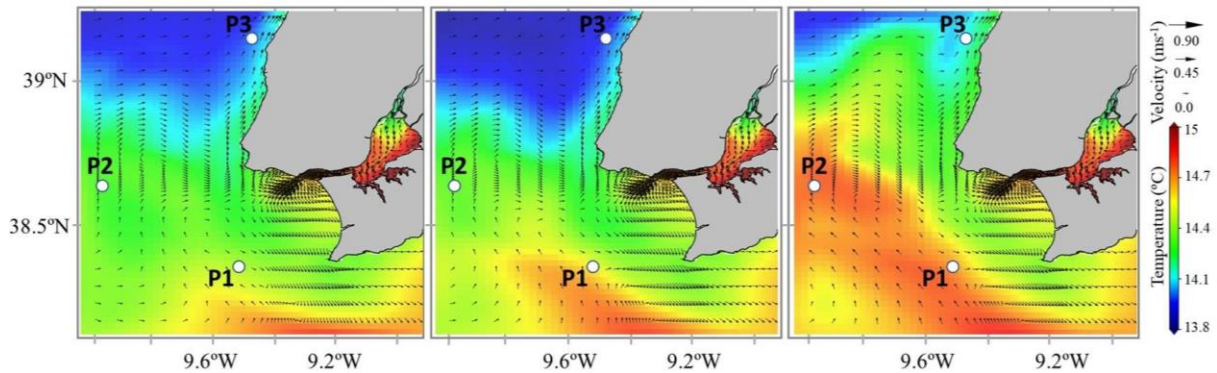


Figure 58: Surface temperature and velocity fields produced by the offline one-way (only downscaling) and offline two-way (with one and two incremental offline upscaling days) implementations.

In the end, and for operational modelling forecast purposes, there is no inconvenient to running more times each day to increase grid communication – at least to what computational time is concerned. In this thesis only simulations using one and two runs per day with upscaling were tested, but there is a need to test these limits using up to 7 days, which is the reference for operational forecasting.

4.4 Partial conclusions

In this chapter, a new upscaling algorithm was developed and integrated in MOHID. This algorithm is now a part of the offline upscaling methodology proposed in this thesis, and which enables a regional model to upscale multiple higher grid resolution domains (or local domains) without neither the need for them to be nested in the regional domain nor the need for online coupling such as the one presented in Chapter 3. As such, this new algorithm can be used in operational forecast systems which can upscale domains from any other institution that has an implementation running. For example, the PCOMS regional model application would now be able to upscale from a Tagus estuary model application developed and maintained by any other institution than Maretec (which has an operational implementation running), and whose results are freely available. This can surely be exported to any other location, including the Madeira and Azores Islands which have their own local models running and which could provide better solutions for upscaling into an ocean scale model such as the Lusitania domain running at Maretec and which covers the entire Portuguese ZEE. One future source of information may be the CMEMS repository which does not yet hold results from such local domains, but could in the future. As such, and following the same structure as in Chapters 2 and 3, a model implementation including PCOMS and the Tagus estuary model application (Tagus ROFI) was run for the same period (15 January to 10 April) and validated using the same available in-situ data, including the Cascais tide gauge and the surface salinity provided by the Algés CTD. This validation was successful in demonstrating the accuracy of the model as well as the new algorithm. As the offline upscaling algorithm has a lower grid communication factor – communication is done after one full day of simulation instead of for each time step – two implementations were tested. The first considered two model runs per day of simulation, which include a first run without upscaling in PCOMS (as it is ahead of Tagus ROFI) and a second run, but now with the upscaling of Tagus ROFI (which performs a run after PCOMS finished its first run), and followed by the second run of Tagus ROFI which now receives its open boundary condition from the updated version of PCOMS. The second considers an additional run of the same day in each model domain, therefore performing two runs with upscaling on and increasing the grid communication and similarity of the results produced by both domains. All comparisons against in-situ data included these two implementations, and an additional comparison between model implementations was performed, focusing on the northeast open boundary of Tagus ROFI

– where the most impact was expected due to the northward transport of the estuarine plume – and in the vertical impact over the water column by means of vertical profiles extracted from PCOMS and Tagus ROFI domains. These comparisons highlighted the importance of upscaling the Tagus estuary into the PCOMS domain, as well as the improvement obtained when an additional run per day using the offline upscaling algorithm is applied. Applying the upscaling promoted a better representation of the circulation due to the salinity fields provided by PCOMS and therefore improved the open boundary conditions of Tagus ROFI whose salinity variability was reduced significantly. This improvement is also important in the bigger context of the Tagus ROFI domain, which by covering a much larger area will produce a better solution outside the overlapped area with PCOMS, for example in the representation of the Western Iberian Buoyant Plume (WIBP) further North, which will be analysed in the next chapter. However, it must be considered that the original PCOMS solution does include freshwater discharges, which made it easier for the upscaling to provide a better solution. As such, in the near future new tests must be performed considering a PCOMS solution that includes the Tagus river flow discharge (even if without the mixture provided by the estuary). This comparison would shed more light in the issue of diffusion in regional models, which is expected to be reduced when a local domain covering a large portion of a Region Of Freshwater Influence (ROFI) is upscaled into the regional model domain, when compared to an implementation of the latter taking a single discharge imposed at the mouth of an estuary/river. Another important aspect of the offline upscaling is its independence regarding simulation time of the local domains when operational forecast solutions are concerned. In operational forecasting, each day is run several times, but usually between 3 and 7, which means that the offline upscaling can be performed between 2 and 6 times per day without changing the overall simulation time. This is an important improvement to the upscaling algorithm developed in Chapter 2 and will facilitate the integration of the method into operational modelling. In the next chapter, a new approach to the upscaling is presented, with a focus on the tidal fluxes produced by local domains and excluding the rest of their domain from the upscaling procedure. A new approach is also presented, and concerns the use of schematic approximations of rivers and estuaries that run much faster and are easier to include in a regional model application, improving the entire operational system from several perspectives.

CHAPTER V

This chapter originated the article:

Sobrinho, J., de Pablo, H., Campuzano, F., Neves, R., 2021. Coupling Rivers and Estuaries with an Ocean Model: An Improved Methodology. *Water* 13, 2284. <https://doi.org/10.3390/w13162284>

Chapter 5 Coupling rivers and estuaries with an ocean model: an improved methodology

In this chapter, a novel methodology is presented as a solution for coupling rivers and estuaries with regional ocean model applications, with immense potential for use in operational modelling. It considers a combination of a new approach to the representation of estuaries and rivers – which greatly reduces the simulation time of an estuary and, more importantly, the mixing process between fresh and ocean water – and a new methodology for upscaling these estuaries and rivers into a regional model application. The methodology is applied to the Iberian Peninsula, with a focus on its western coast and the south of Portugal, through the coupling between a regional ocean model application and the major Portuguese rivers (Minho, Douro, Mondego, Tagus, Sado and Guadiana) plus the Guadalquivir River in the southwest of Spain. A global analysis of the performance of the new methodology is done through the comparison with a version of the regional ocean model without freshwater inputs as well as with the methodology developed by Campuzano et al. (2018). Results of these three versions are then validated against field and satellite data and the two methodologies which consider freshwater inputs show a good model fit in the ROFI areas of the rivers included in the simulations. What sets apart the novel methodology from that developed in Campuzano et al. (2018) is both the reduction of human error and size of the model implementation, through the optimization of the offline upscaling procedure, which was integrated in the MOHID code. This chapter concludes the objectives of this thesis related to the development of a new methodology which contributes to the advances of operational ocean modelling by improving the coupling between ocean, estuaries and rivers. This methodology is also of extreme value for the ongoing effort of a stronger coupling between ocean and watershed modelling, contributing as a stepping stone to the next students and/or researchers with interest in this coupling. The majority of this chapter is a part of the published article by Sobrinho et al. (2021a)

5.1 Rationale

Coastal areas have been in the centre of human development due to the availability of water, fertile grounds, and abundance of food – marine and terrestrial. This is especially true for the Iberian coast, with its many rivers and estuaries serving as natural marine life maternities, and the seasonal upwelling phenomena in the western coast, which is responsible for the replenishment of nutrients

and subsequent high marine biodiversity (Santos et al., 2007, 2004) and abundance of fish for local populations, whose socioeconomic development greatly depended on it (Canuel et al., 2012). There are also essential areas for carbon storage with an important role in the fight against climate change, where an increase in human population will undoubtedly require a significant effort towards a sustainable management of coastal ecosystems resources (Ward et al., 2020). In this context, coastal areas such as the Iberian Peninsula (IP) have been extensively studied through monitoring and modelling, but often separating between watershed and coastal area. This separation is done mainly at the level of the rivers that feed watersheds. One of the reasons is the difficulty of coupling watershed models with coastal models, which require not only specific programming and software to couple them, but also multidisciplinary teams (or research projects) with members specialised in both systems. The study of this whole system, from watershed to coastal area – also known as “watershed-coast continuum” (Salomons, 2005) – is especially important in areas with strong variabilities of the fluxes between the two systems (Chen et al., 2019; Malara et al., 2020), which is the case of the Western Iberia Peninsula, with its tides, seasonal variations of river flows, and its coastal morphology.

Due to their importance as a source of energy, drinking water, for irrigation, and of nutrients and sediments to the estuaries and beaches, rivers were intensively monitored throughout the 20th century and the first decade of the 21st century, which generated a sizeable database on rivers’ flow and properties. However, economic constraints from the 2010s resulted in a reduction of maintenance operations of the hydrological stations, which led to a decline in the number of operational stations, following a global tendency of reduction in hydrometric networks (Mishra and Coulibaly, 2009). This decline in the number of stations in Portugal has been steadily offset by the improvement of watershed modelling solutions, an example of which is the work of (Brito et al., 2015). In their work, a watershed model application was implemented for the IP, whose results are extremely important as they provide flow and water properties of all the major river systems in the IP to the operational ocean modelling systems (and in forecast mode), with a more natural variability than the more standard method of climatology.

A move towards integrated modelling solutions considering both the watershed and ocean mediums can provide a better representation of the coastal processes, due to its better representation of flood and draught events and their variability in time and space, which affect water mixing processes in density driven currents such as in Region Of Freshwater Influence (ROFI) areas

(Campuzano et al., 2016; Sotillo et al., 2021a). In fact, performance of modelling forecasts of salinity in these areas has room to improve, as (Aznar et al., 2016) concluded in their analysis of the Iberia-Biscay-Ireland (IBI) system, who linked it with uncertainties in the river flow data, especially during storm events (Ruiz-Parrado et al., 2020; Sotillo et al., 2021b).

An accurate representation of river and estuarine fluxes into the coastal area is paramount for modelling of biogeochemical and ecological processes in coastal areas, due to the amount of nutrients discharged through them. This is especially important when increased loads of land-based nutrients are increasing eutrophication problems (Andersen et al., 2017; Le Moal et al., 2019), which can become worse when combined with fish farming activities (Du et al., 2018; Smith and Schindler, 2009). As such, correctly estimating the nutrient loads into coastal areas will 1) improve the knowledge available for decision and policy makers at national and transnational levels (Desmit et al., 2018) as currents will transport nutrients and organic matter across maritime borders, and 2) allow scientists to improve their quantifications of nutrient budgets, paths, and influence of river load variability on fish recruitment (Santos et al., 2004).

Regarding the implementation of a river discharge into an ocean model, (Herzfeld, 2015) makes a good review of the different approaches, where the most common is a point-source volume discharge in the coastline with zero salinity. A more accurate approach is to also include the velocity through an artificial channel added to the coastline (Lacroix et al., 2004) as it provides momentum to the discharges, and an initial mixing between fresh and salt waters. Naturally, the most accurate solution would be to properly represent the mixing area, by including, for example, an estuary in the regional model. This would reproduce the mixing processes and hydrodynamics through proper bathymetric features and total volume of an estuary, as shown in MacCready et al. (MacCready et al., 2009) and Liu et al. (Liu et al., 2009), who applied the method to the Colombia River. This is not evident in areas such as the Mediterranean Sea, whose very low tides are not the main driver for mixing between fresh and salt water, and where a simple discharge of volume without prior mixing can be implemented with reasonable accuracy (Estournel et al., 1997). Vertically, discharges can be either uniform along the water column or implemented in specific layers, the most common of which is a surface discharge, due to the lower density of fresh water. However, Herzfeld (2015) proposed a dynamic adjustment to obtain more realistic inputs in the coastal area, which tries to better estimate the depth of the model cell where the discharge is implemented and modify the flow profile and tracer properties accordingly.

Recently, the European component of the Global Ocean Observing System of the Intergovernmental Oceanographic Commission of UNESCO (EUROGOOS) group analysed the different methodologies for including river discharges into regional models, and made a recommendation (Capet et al., 2020) towards a more integrated watershed-ocean approach, as its improved temporal variability of river inputs led to better regional ocean modelling results. Campuzano et al. (Campuzano et al., 2016), who compared the use of river climatology with modelled data from a watershed modelling solution, also concluded that using watershed models improved the overall solution of the Portuguese Coast Operational Modelling System (PCOMS).

As typical grid resolutions of regional ocean models are greater than 1 km, a proper representation of all major rivers and estuaries in the Iberian Peninsula (or elsewhere) would prove to be very complicated. Another issue is the collection of local bathymetric data for initial setup as well as their update over the years due to sediment dynamics. This chapter of the thesis aims to overcome this barrier by improving land-ocean interactions through the input of river flows into schematic rivers and estuaries. The solution is based on the use of schematic rivers and estuaries, which are run separately from the regional model following an offline downscaling approach (Campuzano et al., 2012; Mateus et al., 2012b) followed by an offline upscaling that considers only a momentum discharge in the regional model (hereby defined as an offline two-way system). In the case of the IP, the Portuguese Coast Operational Modelling System (PCOMS) version does not yet include freshwater discharges, which compromises the results of the model in the nearshore. A first approach to include these discharges was developed in (Campuzano, 2018) which intakes estuarine discharges from the operational estuarine model applications. However, this approach proved difficult to maintain due to the amount of time required to simulate the bigger estuaries – increased total time of a day's simulation – and has not been reactivated since. The methodology presented in this chapter provides a solution to this problem, by using schematic representations of the main freshwater sources in the Western Iberian Peninsula – Minho, Douro, Mondego, Tagus, Sado, Guadiana and Guadalquivir – which mix fresh and salt water before being discharged into PCOMS – with very little increase in computational time. With this methodology, the PCOMS system can now receive land boundary conditions from a watershed modelling system covering the entire Western Iberian Peninsula, as well as from in-situ and climatological data, and generate an initial mixing with saltwater, therefore improving the representation of the haline fronts characteristic of this region. This work can have a strong impact in long term studies and more so in operational

fore-cast modelling systems, due to the lower computational time, robustness, and ease of land sources implementation in regional model domains, which are important scientific issues faced by the modelling community in coastal areas.

5.2 Offline upscaling by discharge

Offline upscaling is characterized, in this thesis, by the upscaling of a local model application into regional model application, but where the two applications are run separately, like the offline downscaling (Campuzano et al., 2012), often applied in ocean modelling.

In MOHID, the online upscaling has been developed in Chapter 3, and published in Sobrinho et al. (2021b), following a similar methodology as in (Oey and Chen, 1992; Spall and Holland, 1991). However, the online upscaling algorithm was made to upscale the entire overlapped area between two nested model domains, which means that for a regional domain (RD) to benefit from local domains (LD) simulating rivers or estuaries, it would need to upscale directly from full scale bathymetric implementations of these coastal features. LDs would also need to cover a large enough area of the RD to improve the transfer of information and avoid issues at the open boundaries (for a more extensive review of the issues in online two-way couplings and upscaling, the readers are referred to (Debreu et al., 2012; Debreu and Blayo, 2008)). The problem is that online upscaling from large LDs increases the total simulation time of the RD, which is unsustainable for the time sensitive operational forecast modelling. This chapter aims to provide a proof-of-concept that can solve this issue. To accomplish it, upscaling only considers the information of the few numerical cells of a schematic version of the LD that simulates the exchange of water in tidal inlets such as in estuaries. To further improve this methodology, an offline upscaling approach is proposed, in which horizontal velocities and tracer properties computed by the schematic LDs are used to produce a lateral momentum discharge in a numerical cell of the RD. This methodology is compared to that developed in (Campuzano, 2018) (hereafter Detached methodology) which can also be defined as an offline upscaling, designed for discharge intake into a regional domain.

The difference between these two offline upscaling methodologies is procedural only. In both of them, flow rate, velocity, and tracer properties are computed from the output of the schematic rivers and estuaries by computing the normal velocity of the flow (Figure 59), which can be a single value

or an average weighted value (if more than one model cell of the schematic river or estuary is in contact with a PCOMS discharge cell). However, while in the detached methodology the discharge properties are obtained through an external tool, where the user must define the location of the cross section, and one discharge file (time series containing flow, velocity and tracer properties) is produced for each vertical layer of the estuary model application, in the integrated methodology the discharge properties are obtained directly in run-time by the MOHID model, where the user only needs to provide the HDF (or netCDF) outputs of the schematic rivers and estuaries along with the coordinates of the PCOMS model cell where the discharge is to be made. In this case, MOHID will automatically detect the schematic river or estuary model cells that are required for the computation of the flow, velocity, and tracer properties and apply them to the user-specified PCOMS model cell(s). Computation also takes into account the vertical structure by making a correspondence between vertical layers of both model applications. This means that different vertical discretizations can be used in the regional and local model applications, as the model will identify to which PD vertical layer each CD vertical layer belongs to. The flow is computed using the equation:

$$F = \sum_{CD} (u_i^* \cdot A_k^h)_{i=1,2}$$

Which is a simple summation of all local domain fluxes (ex: u_{CD}^* multiplied by the vertical area of its correspondent cell face – in the right-most green dashed line square of Figure 59) crossing the cell faces of the regional domain cell identified by the user, in this case it is imposed in the blue filled PD cell of Figure 59. F is computed for every vertical layer of the PD, creating one discharge point per vertical layer. In this equation, u_i^* represents the normal velocity of the cross section (in Figure 59 the dashed green line where u_{CD}^* is computed). A_k^h stands for the vertical area of the CD cell associated to u_{CD}^* , where k is the vertical layer and h de depth of the cell at the face. As these fluxes are obtained by output files of the CD, a linear temporal interpolation is performed using the nearest two time instants of the output file, to be imposed in the current time instant of the PD.

By automating this entire procedure, the implementation of several schematic rivers and estuaries becomes easier for the user and reduces the chance of human error in the implementation of multiple land discharges in a regional model application such as the PCOMS.

5.3 Code implementation

The overlaying concept behind the new offline upscaling algorithm is the ability of a regional ocean model application (henceforth regional domain) to extract flow, velocity and tracer properties from an HDF or NetCDF file output produced by a local ocean model (local domain) application of an estuary or bay not included in the regional domain. The main difference between this algorithm and the one presented in Chapter 4 is its applicability. This algorithm was designed specifically to detect the numerical cells of the local domain that are needed to compute a flow, velocity and tracer properties which will then be discharged into the regional domain (in the numerical cell or cells provided by the user). That means it will not perform any type of nudging, neither in the regional domain discharge cell neither in the overlapped area between model domains. Therefore, new routines had to be developed in order for the MOHID model to be able to detect which local domain cells should be included in the calculations, as well as to perform the necessary computations. The algorithm is always executed by the regional domain (because the simulation is done offline) and can be described in 5 steps:

1. Reading of the user implementation files concerning the discharge locations and local domains output files location and numbering – which must be consistent with the numbering of the discharge files. For example, if three local domains are to be upscaled, then six model outputs (MOHID writes one output with velocities and one with tracer properties) each with a domain number set by the user, for example 1,2 and 3 must be added in the “Assimilation” implementation file. Then, three discharges must be implemented in the “Discharges” implementation file with the same IDs and the same order – 1, 2 and 3. The model verifies this information in order for all computations to be correctly done.
2. Identification of the local domain cells that belong to the first regional domain land cell whose adjacent cell is a water cell. This is necessary to know which local domain cells need to be included in the velocity and tracer averaging and flow computation. This identification is done for each vertical layer and a connection matrix is created (generated in the first iteration and remains constant for the entire simulation).
3. Verification of whether a local domain cell has been identified – stop if not.
4. Computation of the volume-average velocity and tracer properties and subsequent flow rate, and storage of the results in the respective matrixes in the “TwoWay” module to be used by the responsible modules such as the “Hydrodynamics” and WaterProperties modules.
5. Retrieval of the flow, velocity and tracer properties by the “Hydrodynamics” and “WaterProperties” modules to be applied as momentum discharges.

These steps are exactly the same as the ones executed in the offline upscaling algorithm developed in chapter 4 but without the nudging (nudging and discharges were separated in the code) so as to accept one without the other. The only difference is in the computational method used, which in this case does not consider the null gradient of velocity in the regional domain cell face in contact with a land cell, but considers the computation of the actual flow, velocity and tracer property discharged into or from the regional domain.

An illustration of a grid nesting with a 1:3 ratio showing the velocity points used in the upscaling applied to a PD cell adjacent to land is shown in Figure 59. The two most eastern cells of the local domain (in green) are used to compute the flow, velocity and tracer properties to be added in the regional domain – flow and tracer properties in the blue cell, and the velocity in the western cell face of the easternmost velocity cell (right red cell). In this example a simple channel is present in the local domain in the grey cell of the regional domain. However, if more local domain cells are present (in the north-south direction) then a volume-average computation is made.

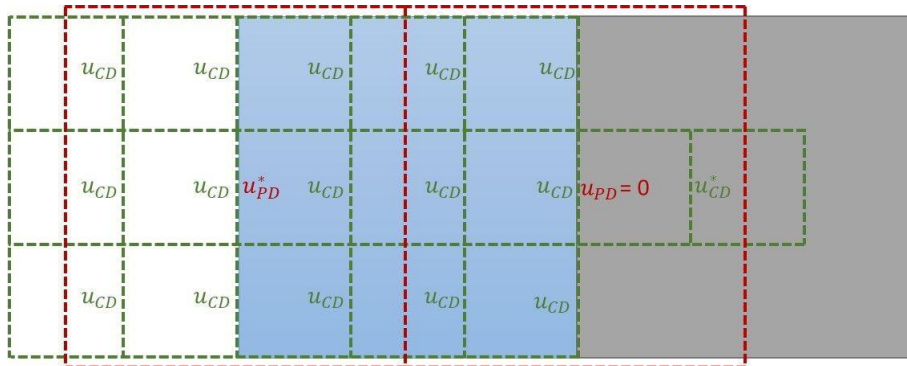


Figure 59: Illustration of an example where the CD has numerical cells in an area where the PD cell is land. Grid ration is 1:3. In red: the CD cells that will be used to compute the volume-weighted average for the upscaling into the PD u velocity. In green the grid of the CD. In light blue: a PD cell adjacent to land (velocity is computed at the faces -as these are Arakawa-C type grids). In Gray: PD land cell

5.3.1 Implementation files

To make use of some of the data collection, space and time interpolation routines already available in the MOHID code, the definition of the variables and HDF names where they are located must now be defined in the “Assimilation.dat” implementation file of MOHID. All variables in this module are defined by characteristic blocks (one for each property), which would not allow for multiple CDs to be upscaled (due to repeated property names). In Chapter 4 three new keywords have been added to the module, where the first states that the property is to be included in the upscaling procedure (UPSCALING : 1), the second sets an ID to each CD (UPSCALING_ID : X)

and the third sets the upscaling method (UPSCALING_METHOD : 1). However, when a particular HDF or Netcdf file is to be used only to add a momentum discharge the upscaling method changes to 3 (UPSCALING_METHOD : 3). This information alone is not enough, and the user must define the “UPSCALING : 1” keyword in the Hydrodynamic implementation file, and to define the discharges in the discharges implementation file where the keyword UPSCALING_METHOD : 3 must be added.

An example of the implementation files for the regional domain is presented in Figure 60.

<p style="text-align: center;">Assimilation.dat</p> <pre> <beginproperty> NAME : velocity U UNITS : m/s DIMENSION : 3D OUTPUT_HDF : 0 <<begin_field>> INITIALIZATION_METHOD : HDF FILE_IN_TIME : HDF FILENAME : ../../Hydrodynamic.hdf5 DEFAULTVALUE : 0 TYPE_ZUV : z FIELD4D : 1 UPSCALING : 1 UPSCALING_DOMAIN_ID : 1 UPSCALING_METHOD : 3 <<end_field>> <<begin_coef>> DEFAULTVALUE : 900 TYPE_ZUV : u FILE_IN_TIME : NONE REMAIN_CONSTANT : 1 INITIALIZATION_METHOD : CONSTANT <<end_coef>> <endproperty> </pre>	<p style="text-align: center;">Hydrodynamic.dat</p> <pre> UPSCALING : 1 UPSCALING_METHOD : 3 CONTINUOUS : 1 BIHARMONIC : 1 BIHARMONIC_COEF : 5.5e9 BAROCLINIC : 1 TIDE : 0 TIDEPOTENTIAL : 1 CORIOLIS : 1 WIND : 1 RADIATION : 2 LOCAL_SOLUTION : 7 SUBMODEL : 1 MISSING_NULL : 1 DATA_ASSIMILATION : 1 BRFORCE : 1 WATER_DISCHARGES : 1 MOMENTUM_DISCHARGE : 1 OUTPUT TIME : 0 10800 </pre>
<p style="text-align: center;">WaterProperties.dat – salinity</p> <pre> <beginproperty> NAME : salinity UNITS : psu DESCRIPTION : Salinity IS_COEF : 1 PARTICULATE : 0 INITIALIZATION_METHOD : CONSTANT DEFAULTVALUE : 36. DEFAULTBOUNDARY : 36. BOUNDARY_INITIALIZATION : INTERIOR BOUNDARY_CONDITION : 4 OLD : 1 DISCHARGES : 1 SUBMODEL : 0 DATA_ASSIMILATION : 1 SURFACE_FLUXES : 0 ADVECTION_DIFFUSION : 1 <endproperty> </pre>	<p style="text-align: center;">Discharges.dat</p> <pre> <begindischarge> NAME : Douro Estuary DESCRIPTION : Douro Estuarine Proxy I_CELL : 113 J_CELL : 66 K_CELL : 50 DEFAULT_FLOW_VALUE : 1.9 UPSCALING : 1 UPSCALING_METHOD : 3 VERTICAL_DISCHARGE : 6 !Upscaling type discharge (one flux per K cell) <<beginproperty>> NAME : salinity UNITS : psu DESCRIPTION : salinity in ETAR GUia DEFAULTVALUE : 0.01 <<endproperty>> <<beginproperty>> NAME : temperature UNITS : celcius DESCRIPTION : temperature in ETAR GUia DEFAULTVALUE : 19.7 <<endproperty>> <enddischarge> </pre>

Figure 60: Implementation files and respective parametrizations required for a discharge via offline upscaling of a local domain.

The handling of multiple upscaling domains, time integration and grid communication are performed in the same way, with the exception of the discharges, as mentioned in this section. However a time integration scheme is presented in Figure 61 to improve readability of the chapter. In short, each day of simulation is run at least twice by each domain. A first run is made by the regional domain which runs without the input from the local domain, which will run the same day using the now available output from the regional domain. Finally, the regional domain runs again the same day, now with the input from the local domain.

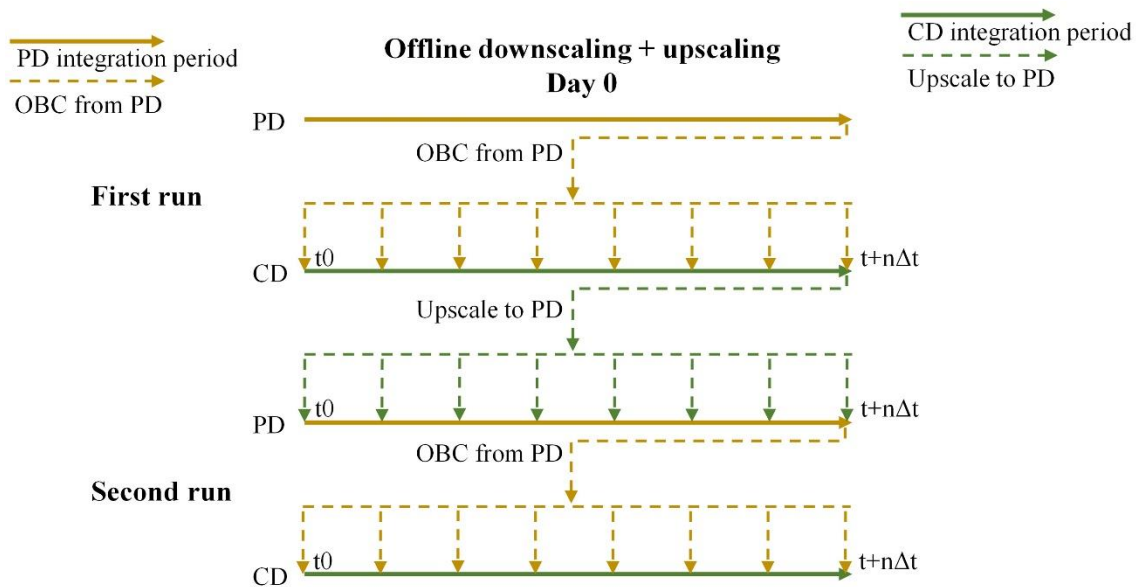


Figure 61: Time integration schemes for a simulation with a regional and a local domain. On top: a representation of downscaling plus upscaling operations (in this scheme it is considered offline two-way). On the bottom: a representation of the online two-way simulation.

5.4 Application to the Iberian Peninsula

In this section, the schematic representation of rivers and estuaries is applied to the PCOMS domain (Figure 62), through the use of two different upscaling approaches, which are tested and compared against the current version of PCOMS – which does not have freshwater inputs (hereafter No Rivers) – in-situ and satellite data. The first upscaling approach follows the Detached methodology and the second follows the Integrated methodology. Schematic rivers and estuaries have the advantage of a very simple representation of the river channels and estuaries – easy to update over time – but the new upscaling methodology allows for a simpler implementation of the freshwater discharges into the regional model, which only needs to receive an HDF or NetCDF from each

separate estuary. The main objective of the comparison against the Detached methodology was to validate the integrated methodology. A good correlation between them would suggest that the integration into the MOHID code is viable as an improvement to the detached methodology.

To validate the schematic rivers and estuaries methodology and the two methods of offline upscaling, a comparison was made against in-situ sea surface temperature (SST) and salinity data on the period between Jan 1-May 1 and March 18-April 1 of 2018. Satellite SST data regarding the period between Jan 1-May 1 of 2018 was used to validate SST fields produced by the integrated methodology and the No Rivers implementation of PCOMS. A separate salinity comparison was also made between the two offline upscaling methods (detached and integrated) against the No Rivers version of PCOMS in order to assess the advantages of including the freshwater inputs and to compare results from the two offline upscaling methods.

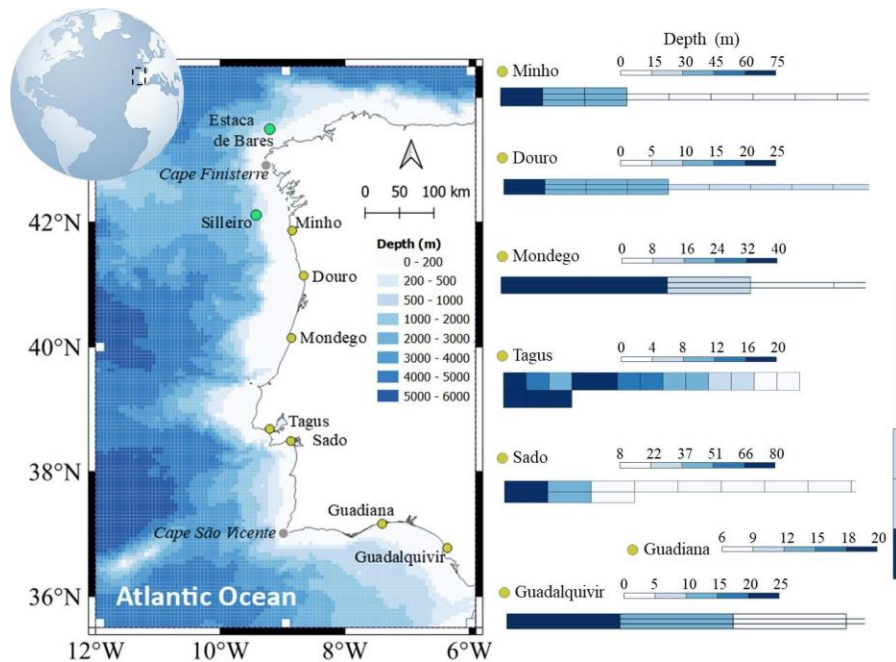


Figure 62: Representation of the study area as well as the most important bathymetric features and location of the time series used in the validation of the results. The area corresponds to the PCOMS grid domain and its bathymetry (on the map) and that of each schematic river and estuary (on the right) is also shown (in this case the dimensions are shortened in order to fit in the image. The real dimensions of these domains are presented in Table 15).

Regarding in-situ data, the comparison was made against the moored buoys of Sillero and Estaca de Bares located near the Galician rias and Cape Finisterre, respectively (see Figure 62) and for the period of January 1 to May 1 of 2018. Statistical parameters of bias, Pearson correlation and Root Mean Square Error (RMSE) were computed and are shown in the results section. Satellite images were retrieved from the ODISSEY product, a 2 km gridded RS data product

(<http://marine.copernicus.eu/>) (Autret et al., 2017), and compared to the PCOMS solution under integrated and the No Rivers methodologies. In order to obtain a better comparison between methodologies, validation focused on the peak flow period (March 18-April 1 of 2018), using the global average of this period (by averaging satellite and model data over the selected period). Like in the comparison against in-situ data, the bias, Pearson correlation coefficient and the RMSE statistical parameters were calculated.

5.4.1 Automatic running tool

In order to run all model applications (PCOMS and schematic rivers and estuaries), the automatic running tool (ART) (G Franz et al., 2014; Kenov et al., 2014) developed in MARETEC was improved. The tool is responsible for all file transfers (including meteorological model input files and open boundary conditions), invocation of external tools and the MOHID model itself, as well as for storing all results. In the case of the detached methodology, the ART is responsible for calling a specific tool designed to extract the flow, velocity and tracer properties from an HDF file produced by a schematic channel. This tool takes as user inputs an HDF file, a cross section that the user must identify, and outputs n time series containing date, flow, velocity and tracer properties, where n is the number of vertical layers in the HDF. This is not necessary in the new integrated methodology proposed herein, as all these computations are done directly by MOHID, but the ART tool, in this case, is responsible for copying the HDF files produced by the schematic rivers and estuaries into the designated input folders of PCOMS implementation. The main improvement made to the ART tool refers to the launch of multiple runs per simulation (each day must be run more than once) combined with a trigger system which forces the model domains to wait for their parent (PCOMS) or son (schematic rivers or estuaries) domain (Figure 61) results.

5.4.2 Model setup

The PCOMS system was run for the period between October 1 to May 1, with three different implementations, two offline upscaling methodologies and one version without rivers. The PCOMS system is a nested grid configuration comprised of two domains: i) 2D barotropic regional domain with 5.7 km constant grid resolution for the Portuguese Coast (WestIberia-Level1) (33.5° N - 49.9° N, 1.0° W - 13.5° W) running only with tidal forcing from FES2004 (Lyard et al., 2006)-

(Lefèvre et al., 2002); ii) 3D full baroclinic regional domain for the Portuguese Coast (hereafter PCOMS) (34.4° N–45.0° N and 12.6° W–5.5° W) with a grid resolution of 5.7 km and 50 vertical layers (7 sigma at the surface and 43 Cartesian below). A full description of the PCOMS is available in (Campuzano, 2018; Mateus et al., 2012b).

A new initialization was performed with a spin-up period of 3 months for both the PCOMS and the schematic rivers and estuaries. PCOMS domain receives its lateral open boundary conditions from the 2D barotropic domain and the [Mercator Ocean Psy2V4](#), linearly superimposed to the Level barotropic velocities, as proposed in Leitão et al. (Leitão et al., 2005). Regarding PCOMS, a Flather radiation scheme (Flather, 1976) was applied at the open boundary to radiate water level, followed by a Flow Relaxation Scheme (FRS) applied to the baroclinic velocities and tracer properties as proposed by Martinsen and Engedahl (Martinsen and Engedahl, 1987) provided by the Mercator solution as described in Leitão et al. (Leitão et al., 2005). The flow relaxation scheme applied decreases exponentially a relaxation coefficient from 10^5 s in the outmost open boundary cell to 10^9 s in the 10^{th} outmost cell (perpendicular to the open boundary). The rest of the domain was nudged to the Mercator solution with a coefficient of 10^9 s. Additionally, a biharmonic filter of $5.5 \times 10^9 \text{ m}^4 \text{ s}^{-1}$ was applied to reduce high frequency noise inside the domain. As for the schematic rivers and estuaries, they receive their open boundary conditions from PCOMS HDF outputs holding 3D data every 900 s. The same radiation and relaxation schemes are applied but, due to the small number of numerical cells located inside the first water point of PCOMS, only 3 or 4 cells are used the FRS (depending on the channel). Their bathymetries were created taking into consideration the bathymetric values of the PCOMS domain near the discharge location so as the have the same values in the overlapped area of water points as well as in the work of Campuzano et al. (Campuzano et al., 2018). At the atmospheric boundary, both PCOMS and the schematic rivers and estuaries were forced by the meteorological model MM5 (Grell et al., 1994; Trancoso, 2012), with 9 km resolution for the Portuguese coast. Time steps used in the 2 levels of the PCOMS system were 120 s and 60 s respectively and the time step of the several channels was 30 s. A summary of the implementation is presented in Table 14 and Table 15.

Table 14: Model setup configuration for the TagusROFI area.

Settings	Level 1 – WestIberia	Level2 – PCOMS	Schematic rivers and estuaries
Model characterization	2D - Barotropic	3D – Baroclinic	3D - Baroclinic
Grid corners	33.50° N - 49.90° N 1.00° W - 13.50° W	34.38° N – 45.00° N 12.60° W – 5.50° W	38.16° N – 39.21° N 10.02° W – 8.90° W
Cells dimension	208 x 156	177 x 125	^a
Bathymetry	EMODnet ^b Hydrography portal	EMODnet ^b Hydrography portal	(Campuzano et al., 2018)
Horizontal Grid	Regular: (\approx 5.7 km)	Regular: (\approx 5.7 km)	^a
Vertical Grid	1 layer	7 Sigma Layer (0 - 8.68 m) 43 Cartesian layers	7 Sigma Layer (0 - 8.68 m) 43 Cartesian layers
Δt	60 s	60 s	30 s
Tides	FES2004	From Level1	From PCOMS
OBC Water	...	From MercatorOcéan PSY2V4 (Releases 1- 4)	From PCOMS
Assimilation	...	Flow relaxation scheme of 10 cells with a time decay of 1 week at the open boundary and 10 ⁹ s inside the domain	Flow relaxation scheme of 3 or 4 cells with a time decay of 900 s at the open boundary and 10 ⁹ s inside the domain
OBC Atmosphere		MM5 (9 km)	
Discharges	No	From schematic rivers and estuaries	Minho, Douro, Mondego, Tagus, Sado, Guadiana, Guadalquivir
Turbulence	...	GOTM ^c	GOTM ^c
Bottom	Rugosity: 0.0025 m ² s ⁻¹	Rugosity: 0. 0025 m ² s ⁻¹	Rugosity: 0. 0025 m ² s ⁻¹

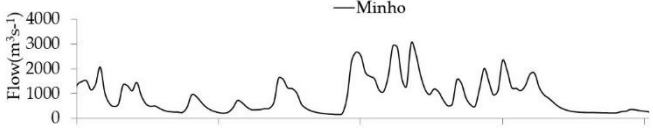
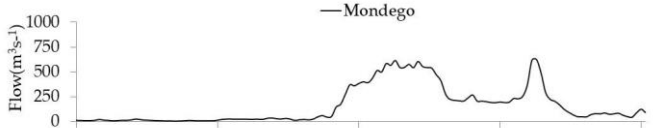
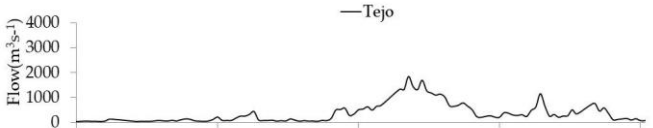
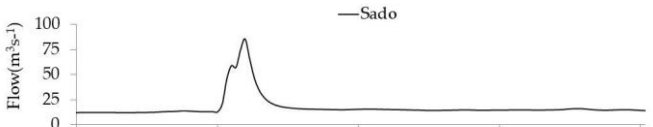
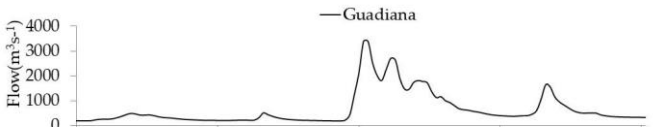
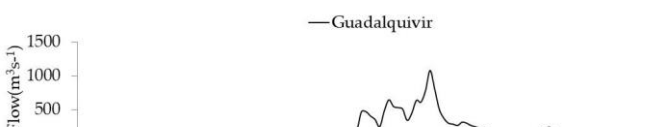
^a dimensions are presented in Table 15. ^b <https://www.emodnet-bathymetry.eu/>. ^c (Ruiz Villarreal et al., 2005)

Table 15: Dimensions of the schematic river and estuary domains.

Model domain	Dimensions	Horizontal grid
Minho	14 x 3	3.4 km x 630 m
Douro	15 x 3	1.9 km x 300 m
Mondego	14 x 3	3.8 km x 170 m
Tagus	14 x 3	4.3 km x 5.3 km
Sado	14 x 3	6.8 km x 2.2 km
Guadiana	3 x 14	300 m x 3.9 km
Guadalquivir	14 x 3	9.4 km x 520 m

Discharge flow, temperature and salinity were obtained from different sources according the river in question, which are described in Table 16. Sources include in-situ data, climatological data and watershed model, which was implemented and validated in Campuzano et al. (Campuzano et al., 2016). A main event can be observed in March (Table 16), which is visible in all rivers with the exception of Sado, whose watershed was not fed during this event. Most of these rivers are highly artificialized, which combined with the absence of dams in the watershed models can lead to unrealistic flow values. However, this is not the scope of this thesis.

Table 16: River flow and respective source of data used to feed the schematic channels.

Flow time series	Source
	Watershed model
	In-situ (Crestuma dam) (https://snirh.apambiente.pt/)
	In-situ (Pte Coimbra) (https://snirh.apambiente.pt/)
	In-situ (Almourol) (https://snirh.apambiente.pt/)
	Watershed model
	Watershed model
	In-situ (Alcala) (https://www.emodnet-physics.eu/map/platinfo/piroosplot.aspx?platformid=974539)

5.4.2.1 Grid communication

Both methodologies tested in this chapter can be considered as offline two-way. However, in the detached methodology, the LDs never receive the updated open boundary condition from the RD, while in the new integrated methodology they do. In fact, in the detached methodology, a simulation of the entire period is done by the RD, followed by the simulation of the same period by the LDs using the newly created RD results. Then, a second simulation (also of the entire period) is performed by the RD, but now with upscaling of the just made available LD results. This means

that the grid coupling in the detached methodology is very limited (there is now daily update of open boundary conditions from the RD or tidal fluxes from the LD). In the integrated methodology, results produced by the regional domain (RD) are downscaled into the local domains (LD) in an offline manner and for the entire simulation period. However, and in contrast with the detached methodology, the flux of information between model grids is performed at a daily basis. Therefore, after a one-day simulation of the RD without upscaling (because the LD results are typically behind in time), the LDs are forced with the RD results as open boundary conditions to run the same day. After the LD simulation is finished, the RD runs the same day, a second time but now upscaling the LD results. After this second RD run, the updated RD results are again downscaled into the LDs (Figure 61).

In both cases, the information is transferred on a daily basis, where each model simulates one day at a time and then transfers the information. This procedure can be repeated any number of times, increasing the grid communication of the coupling. In this work however, only one repetition is performed, which means upscaling is only performed one time.

5.4.3 Results

5.4.3.1 Estuaries tidal prism

Tidal prism is an important metric for estimating the mixing capacity of an estuary, as it indicates the amount of salt water available for mixing with freshwater. This is more important when compared to the river flow, which can be used to determine the dominance of the river flow over ocean water. As such, when the tidal prism is much greater than the river flow, the importance for density currents – particularly from the regional ocean domain perspective – will be small, when compared to a case where the river flow represents a greater part of the tidal prism. However, this type of analysis cannot be static in time, because the river flow varies in time. An example of this argument is the Tagus estuary, whose Tagus flow rate is immensely inferior to the tidal prism during most of the time, except during high precipitation events. During the extreme precipitation event of April 2013, the flow rate of the Tagus reached an astonishing 9800 m³/s and a value superior to 7500 m³/s for three consecutive days (the average flow rate is around 250 m³/s). When compared to the tidal prism (640 x 10⁶ m³), the average flow rate of the Tagus river represents

around 0.8%, while in the extreme event this value increased to 25%, dominating the circulation of the estuary and its adjacent coastal area (de Pablo et al., 2019)

In this chapter, the schematic rivers and estuaries attempt to represent the more real (currently in use in the operational modeling systems of Maretec) version of them – herein denominated real rivers and estuaries. This means that some differences in total volume of the estuary, as well as their natural dynamics will be different, especially because the domains only have a 2D channel representing the estuaries. Although the objective of the chapter does not include the optimization of these domains, a short analysis is performed in order to help explain differences in the results obtained later on. Figure x shows the simulated tidal prism – by real and schematic domains – in which the flow rate is considered positive in flood and negative in ebb tides. The general tendency is of an underestimation of the tidal prism, with the most noticeable difference in the Douro and Mondego estuaries. In the Douro case, the ebb becomes dominant from the beginning of the major peak flows. Up until that time there is a slight overestimation of the ebb, which suggests that the overall mixing process is not well represented – confirmed when a high flow rate greatly increases the differences between real and schematic estuary. The opposite seems to occur in the Guadiana estuary, where the real Guadiana estuary shows a greater impact from the river flow rate than the schematic version. In this case however, there are other variables to explain these differences. In the real estuary, the Guadiana river flow was obtained from a hydrometric station, whereas in the schematic version the flow was computed by the watershed model (which does not include any of the many dams in the Portuguese and Spanish sides). In the end, the advantages of using this methodology far outweigh this disadvantage, as it provides the necessary mixing prior to discharge into the PCOMS domain.

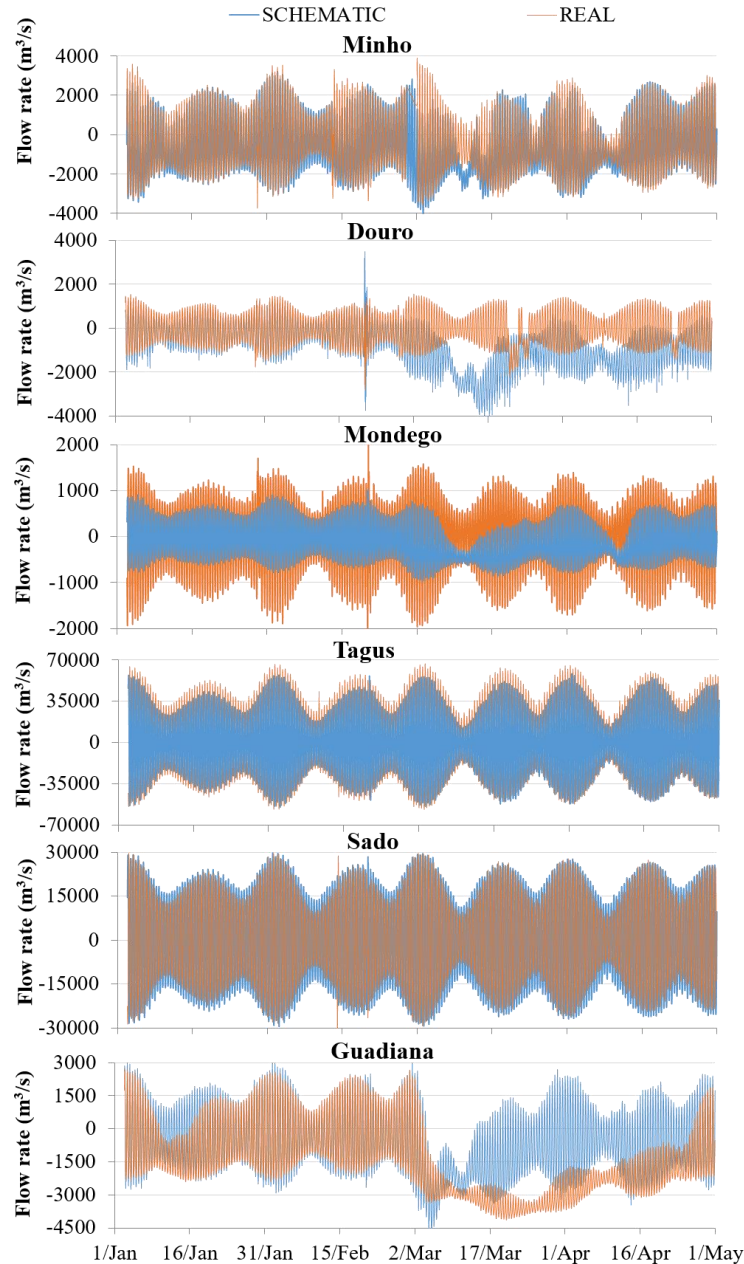


Figure 63: Tidal prism flow rate obtained by the schematic and real representations of the Douro, Minho, Mondego, Tagus and Guadiana rivers and estuaries. A positive flow rate is observed in the flood tide and a negative one in the ebb tide. Guadalquivir was not included because a real representation of this estuary was not being simulated in Maretec.

5.4.3.2 Comparison with in-situ data

Temperature and salinity obtained by the three PCOMS implementations (without rivers, detached and integrated offline upscaling) were validated against the Silleiro and Estaca de Bares moored stations during the period between Jan 1 and May 1 of 2018 (Figure 64 and Figure 65). As the

moored station of Silleiro is closest to the last Portuguese river included in PCOMS (Minho), the riverine plume signal is easier to detect. Figure 64 shows the signal of the rivers, especially during the period between March 18 and April 1, due to the higher flow rates of the Northern rivers (from Mondego upwards - Table 16). Furthermore, the separation between waters is best seen in salinity as the gradient between ocean waters (≈ 36) and freshwater (≈ 0) is much higher than the temperature gradient (usually less than $10\text{ }^{\circ}\text{C}$). Regarding salinity validation, PCOMS without river inputs failed to reproduce the variability verified during the event, which is clearly dominated by land discharges as it correlates well with results shown in Table 16. The PCOMS solution was improved when rivers were introduced in the detached methodology, which is sufficient to produce a signal similar to that observed by the in-situ data. However, although the variability and timing of the events are well represented, the model produced an excess of salinity in the first event (March 18-April 1) and underestimated it in the second event (April 23-May 1). The solution improves again with the integrated methodology, which produces lower salinities during the first event and higher during the second, following the in-situ data. This improvement is mainly because in the new methodology the schematic rivers and estuaries run a second time, with the updated PCOMS solution, a step that was not present in the detached methodology. As such, the new integrated methodology can produce lower salinities, simply because its open boundary condition values of salinity decrease with the river flow rates. During the second event, and due to the stronger influence of the northern river plumes during the entire simulation period (the schematic rivers and estuaries received feedback from the updated PCOMS model lowering the open boundary salinity values) led to a more intense combined plume obtained by the integrated methodology, which remains closer to shore in the particular latitude of the moored buoy. With the exception of the No Rivers PCOMS methodology, which fails to represent the variability measured by moored buoy, temperature results are more consistent between methodologies. In the two previously identified events, a shift in temperature can be observed when both offline upscaling methodologies are compared with field data and the No Rivers PCOMS methodology. While in the first the freshwater inputs are responsible for a decrease in temperature, in the second – due to the increase of freshwater temperature during the spring – the river inputs contributed to the increase of temperature in the coastal area.

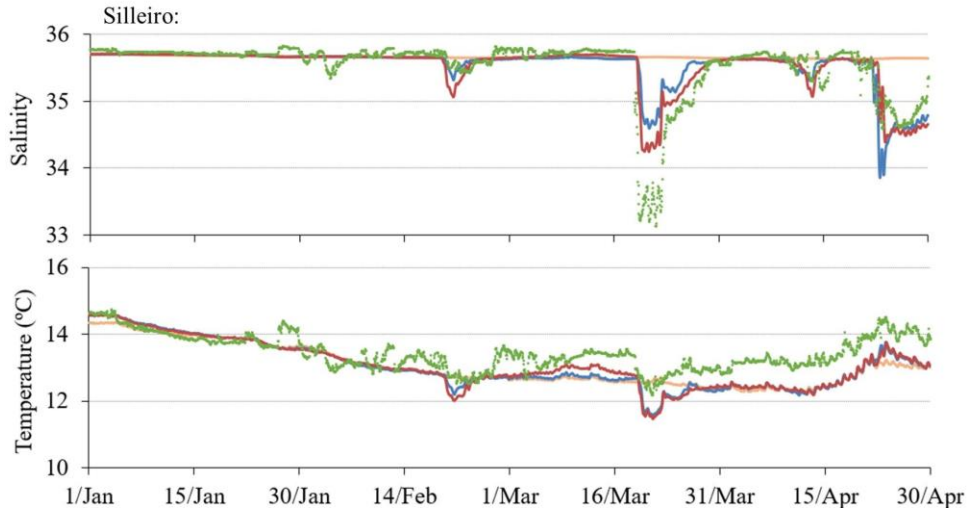


Figure 64: Salinity and temperature time series produced by the three PCOMS implementations and the Silleiro in-situ moored buoy during the period between Jan 1 and May 1 of 2018.

Table 17: Statistical parameters obtained for the validation of the three methodologies against field data (Silleiro moored buoy).

Comparison	Parameter	Jan 1 – May 1 (n = 2876)				Mar 18 – May 1 (n = 1053)			
		r	r ²	RMSD	BIAS	r	r ²	RMSD	BIAS
Data-Detached	Sal	0.752	0.565	0.982	0.013	0.863	0.745	0.454	-0.522
	Temp	0.837	0.701	0.671	0.415	0.842	0.709	0.392	0.647
Data-Integrated	Sal	0.865	0.748	0.963	0.031	0.920	0.847	0.333	-0.357
	Temp	0.845	0.714	0.653	0.394	0.856	0.733	0.404	0.660
Data-No rivers	Sal	0.227	0.052	1.047	-0.111	-0.712	0.507	0.693	-0.833
	Temp	0.753	0.567	0.684	0.420	-0.178	0.032	0.296	0.392

The statistical analyses (Table 17 and Table 18) focused on the global simulation period (Jan 1 and May 1 of 2018) and in the main peak flow period (March 18-April 1 of 2018). Results produced by the new integrated methodology show smaller average bias than the detached methodology for temperature regarding the entire simulation period and salinity. RMSD values improved in the integrated methodology for all periods and parameters, with the exception of temperature during the peak flow. Nevertheless, differences between bias and RMSD values obtained by these two methodologies are quite small and indicate a similar accuracy. However, the correlation coefficients obtained for the different periods and parameters improved substantially with the use of the integrated methodology (r^2 always above 0.7). As expected, the No Rivers PCOMS methodology provided the lowest accuracies and correlations with the exception of the temperature bias and RMSD for the peak flow period, which is associated with low variability of the time series, combined with the casual similarity of temperature during this particular time period.

Further north, near Cape Finisterre, the freshwater influence from the most northern Portuguese rivers is hardly felt (Figure 65), not only due to the distance (which leads to a higher diffusion of the freshwater plumes) but also to the absence of the northern Spanish river inputs which were not included in this work. However, the influence of these freshwater discharges is noticed in the in-situ data which shows a salinity drop at the same time as temperature increases sharply. As such, for an accurate representation of density currents near the north-western coast of the IP the main rivers outflowing in the Spanish coast are required. An effort is already being made towards solving this issue with the recently finished Lambda project, where a data basis on river flow inputs has been compiled using watershed models to cope with the lack of hydrographic stations (Lambda Project, 2020).

The statistical analysis of the results obtained by the different methodologies on the two selected periods confirms what was observed in Figure 65, where the absence of the Spanish rivers reduces the reach of the freshwater plume along the north-western coast of the IP.

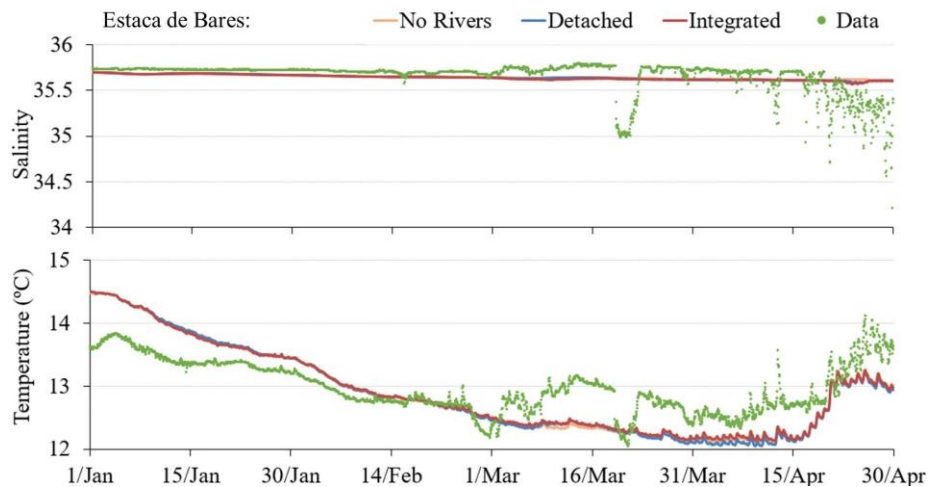


Figure 65: Salinity and temperature time series produced by the three PCOMS implementations and the Estaca de Bares in-situ moored buoy during the period between Jan 1 and May 1 of 2018.

Table 18: Statistical parameters obtained for the validation of the three methodologies against field data (Estaca de Bares moored buoy).

Methodologies compared	Parameter	Jan 1 – May 1 (n = 2876)				Mar 18 – May 1 (n = 1053)			
		r	r ²	RMSD	BIAS	r	r ²	RMSD	BIAS
Data-Detached	Sal	0.487	0.237	0.162	0.025	-0.267	0.071	0.267	-0.015
	Temp	0.826	0.683	0.440	0.085	0.159	0.025	0.499	0.432
Data-Integrated	Sal	0.449	0.202	0.164	0.025	-0.143	0.021	0.265	-0.014
	Temp	0.827	0.684	0.417	0.066	0.192	0.037	0.464	0.393
Data-No rivers	Sal	0.371	0.138	0.166	0.020	-0.454	0.206	0.268	-0.023
	Temp	0.828	0.686	0.433	0.081	0.182	0.033	0.494	0.428

5.4.3.3 *Surface salinity maps*

A comparison between salinity maps (Figure 66) produced by the three methodologies is important for a broader analysis of their impact on the evolution of river plumes in the western coast of the IP. As such, time-average surface maps of salinity were computed from the model outputs for the period of March 18 to April 1, which corresponds to the strongest precipitation event as observed in Table 16. Results show the obvious impact of adding river inputs in the PCOMS system, which were responsible for the formation of a buoyant plume (WIBP) produced by the three Portuguese rivers North of the Tagus mouth (Mondego, Douro and Minho).

Very small differences were observed between results obtained by the two offline upscaling methodologies (detached and integrated - Figure 67). The first is in the vicinity of the Tagus estuary where the new methodology produced higher salinity values (1 to 1.5) instead of the expected lower values (due to the higher level of grid communication). The explanation for this difference is more complex and is related to the schematic volume available combined with the difference in the methodology. Because in the detached methodology the rivers and estuaries open boundary conditions were always fed by the No Rivers PCOMS version, their open boundary values of salinity are constantly high (above 35). When combined with the lower volume of the channel when compared with the current operational version of the Tagus estuary model domain (described and validated in de Pablo et al. (2019), lower salinity values will be produced near the estuary mouth (from where the fluxes are retrieved and added to PCOMS). As such, there will be less vertical mixing between ocean and river water, which leads to a higher surface gradient of salinity when high river flow rates are present. Another important factor is visible on the tidal prism fluxes (Figure 63), which shows an overestimation during the ebb tide. A strong contribution for this issue could also come from the fact that the schematic estuary gets its open boundary condition from a PCOMS version without rivers. As such, not only currents but also the water level will be different from the integrated methodology (fed by a version of PCOMS with freshwater inputs). However, and due to the different grid communication between the detached and the integrated methodologies, this issue was not further pursued. Instead, and as future work, an implementation should be done considering the same grid communication on both methodologies, where the schematic rivers and estuaries run the second day of simulation using open boundary condition values from a PCOMS version with freshwater inputs. In the northern rivers this effect does not take place, most likely due to a better volume correlation between the schematic rivers and estuaries

and their real version, and due to their higher flow rate in comparison to their tidal prism. Therefore, in the northwest coast of the IP, the integrated methodology produced slightly lower values (around 0.5) of surface salinity – as expected when the schematic rivers and estuaries receive updated boundary conditions from PCOMS. In the adjacent area of the Guadiana and Guadalquivir mouths (Figure 66 and Figure 67), the impact of the two offline upscaling methodologies is quite similar which can be caused by the local hydrodynamics – through higher mixing in the area – which can increase diffusion and therefore reduce the differences between methodologies.

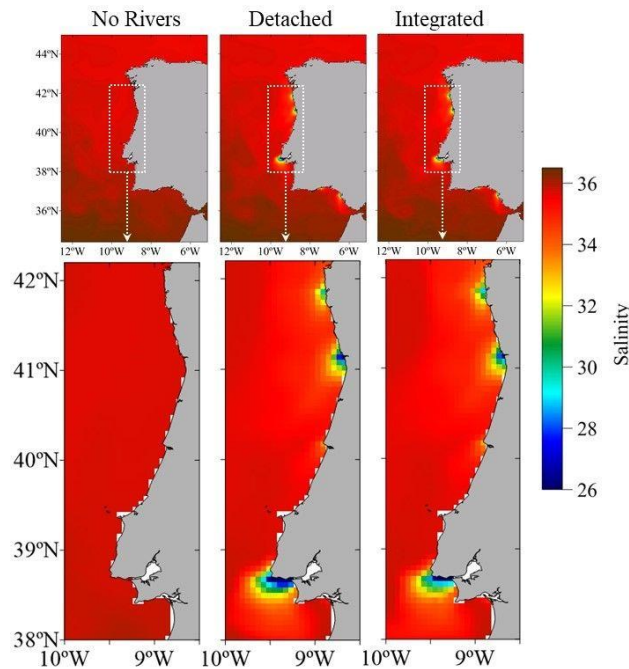


Figure 66: Average surface salinity maps for the entire domain (top) and a zoom over the area of interest in the west coast of the IP (bottom) produced by the three implementations: No Rivers (Left), De-tached (middle) and Integrated (right) methodologies over the peak flow period (Mar 18 to Apr 1 of 2018).

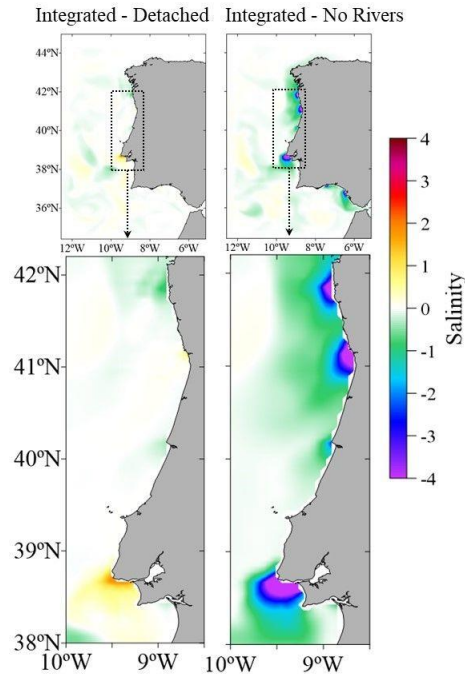


Figure 67: Difference between average surface salinity maps for the entire domain (top) and a zoom over the area of interest in the west coast of the IP (bottom) produced by: Integrated minus Detached (Left) and Integrated minus No Rivers (right) over the peak flow period (Mar 18 to Apr 1 of 2018).

5.4.3.4 Satellite SST analysis

An analysis of surface temperature maps against satellite data during the peak river flow (March 18- April 1) was made aiming for the validation of the schematic rivers and estuaries methodology and the integrated offline upscaling, but also to obtain a broader view of the surface temperature patterns over the coastal area of the western coast of the IP when river inputs are considered. The comparison (Figure 68) was made only for the No Rivers and the integrated methodology for the period of peak flow (March 18- April 1) due to the high similarity between the latter and the detached methodology.

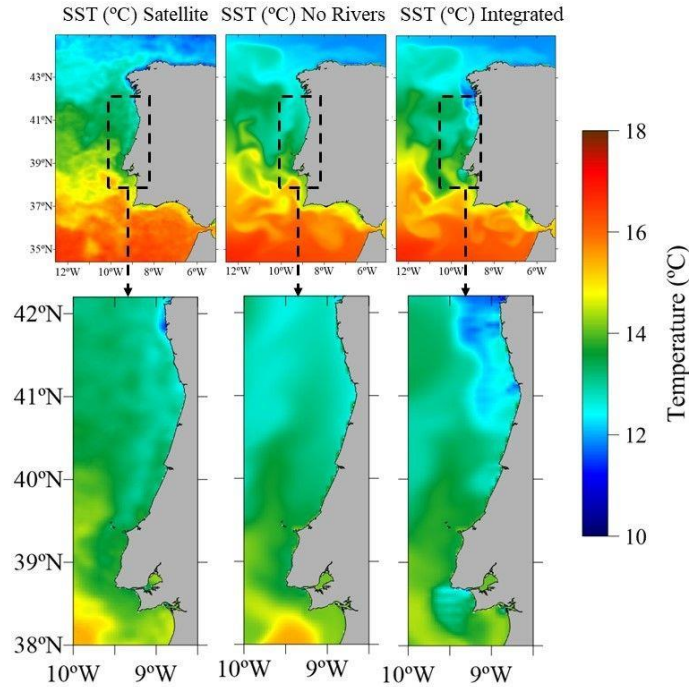


Figure 68: Average surface temperature maps for the entire domain (top) and a zoom over the area of interest in the west coast of the IP (bottom) produced by the two implementations: Satellite SST (left), No Rivers (middle) and Integrated (right) methodologies and at the peak flow (Mar 20 of 2018).

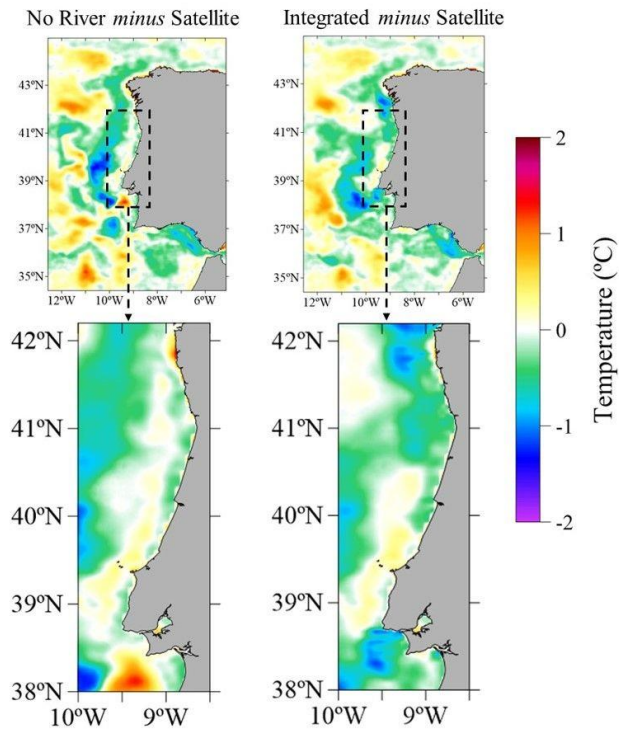


Figure 69: Difference between surface temperature maps for the entire domain (top) and a zoom over the area of interest in the west coast of the IP (bottom) produced by: No Rivers minus Satellite (Left) and Integrated minus Satellite (right) at the peak flow period (Mar 20 of 2018).

At a first glance, results (Figure 68) show the typical northern hemisphere North-South temperature gradient with increasing temperatures towards the equator in both methodologies. However, major differences were obtained in the coastal area of the IP and near its ROFI areas (Figure 69), where the influence of the freshwater inputs (present only in the PCOMS version where the integrated offline upscaling methodology) was applied. River inputs played a key role in surface temperature near the coast and up to 80 km off-shore, in the latitude of the Douro and Minho Rivers mouth, which have the highest flow rates (Table 16). However, a more detailed analysis of the SST pattern (Figure 8 and Figure 9) near coastal areas suggest that the No Rivers methodology compared better against satellite than the Integrated methodology, and suggests an overestimation of SST by the satellite, as confirmed by the comparison against the Silleiro moored buoy (Figure 64). In this location, the in-situ data shows a value of around 12.2 °C, while the satellite suggests a value above 13 °C. Although this difference is small, Figure 64 shows a decrease in temperature of 1.3 °C associated with the plumes around Mar 18, whereas the satellite observed a constant temperature of during these days for that location. In these coastal areas a possible issue is related to the accuracy of satellite SST near the coastal area, which is described by Brewin et al., (2017) as having a bias in the order of 0.45 - 0.51°C with satellite SST values. This issue was also addressed in (Mateus et al., 2012b). Another possible reason for the discrepancy between SST and model is the solar radiation effect on surface temperature. When a discharge of fresh water takes place and its temperature is lower than the ocean, the solar radiation will warm mainly the first millimetres and during the day. Therefore, the temperature signal from the discharges will disappear rapidly and can easily be missed by the satellite (but not by in-situ stations measuring below this dept). Moreover, satellite images are taken only once per day, and for that reason punctual river signals can be lost from one day to the other.

On a broader analysis of the entire domain, differences can be explained by the fact that satellite SST measures the temperature at the “skin” of the ocean, which represents approximately the top 0.01 mm, while the model SST is the average temperature in the top cell of the model domain, 0.95 m plus tidal range. This is also a possible explanation for the detection, by the satellite, of the Douro and Minho plumes traveling along the coastline to the Galician rias in the north, while the model results suggest this influence is felt further away from the coast.

5.5 Partial conclusions

A good model representation of the coastal hydrodynamic processes in the IP, namely those associated with freshwater discharges, such as the WIBP and the WICP requires the input of all major river sources. These processes are important to subsequent ecological and morphodynamic processes which will then affect all human coastal activities and respective coastal management policies, especially relevant for climate change studies focusing on the impact of extreme precipitation event, sea level rise and storm surge. However, to properly add freshwater discharges in regional ocean models, horizontal and vertical mixing between freshwater and ocean water due to tidal prism is necessary so as to correctly compute the haline fronts. In the case of the western IP, the Portuguese coast operational modelling system (PCOMS) – a regional mode application – has been running since 2009 without freshwater sources (No Rivers methodology), which has partially compromised its results with regard to surface temperature and salinity near the coast. A first approach to solve this issue was presented in Campuzano et al. (2018), who added freshwater discharges through the coupling of the ocean model with real case estuaries and rivers (Detached methodology). However, this improvement of the regional model came at a great cost in computational time, as results produced by PCOMS now needed to wait for the slower estuarine model application. Another complication was related to the implementation of the several discharges files (one per river per vertical layer) by the user, as well as the need to run an external tool also implemented by a user. All these steps increase the chance for human error, making the entire system more demanding in terms of maintenance. A new solution is proposed in this thesis, whereby the heavier, real river and estuary applications are replaced by simpler and less time consuming schematic versions of these applications. As such, the total amount of time required for the PCOMS version with freshwater inputs to simulate one day increased only around two minutes, making this methodology much more attractive for operational modelling purposes. Results obtained by the three aforementioned methodologies were compared against in-situ sea surface salinity and temperature data, and against satellite observations of sea surface temperature. They showed an improvement from the No Rivers methodology to the Detached and Integrated methodologies, particularly in the coastal area of the IP. It was also found that satellite observations have some difficulties in detecting freshwater sources via surface temperature, as confirmed by the detection of these sources by the Silleiro moored buoy off the coast of Galicia. This reinforces the

need for accurate land-discharges implemented in coastal modelling applications, which have the ability to fill in the gaps of satellite data. The idea behind the application of these methodologies was mainly to validate the integration of the upscaling discharge approach into the MOHID code, since the advantages of human error reduction as well the ease to add new river inputs were considered as a given. The results obtained showed a great similarity between temperature computed by the two methodologies where river inputs were added to PCOMS, particularly over the coastal area of the IP. As such, the new integrated methodology is confirmed as an optimal methodology to be used in the operational modelling of coastal areas where freshwater sources play an important role. In the near future this offline upscaling methodology combined with the use of schematic rivers and estuaries which get their flow from watershed models, hydrometric stations or climatological data will take advantage of the newly created databases for river flow rates developed in the Lambda project (Lambda Project, 2020), providing the regional operational modelling with the necessary tools for an increased performance near coastal areas. This performance is not only related to surface temperature and haline fronts but also to the local currents that generate them. Finally, the main objective of adding the offline upscaling via a discharge with momentum was to provide a stepping stone for a better integration with watershed models. By validating the methodology, new students can now pick up where this thesis left and begin the full integration with a watershed model where not only river runoff but also ground water fluxes can be explored, allowing for a better representation of nutrient exchange or even saline intrusion processes.

CHAPTER VI

Chapter 6 Conclusions and future work

This chapter summarises the conclusions drawn from this thesis and provides an answer to the major objectives the thesis set out to accomplish.

6.1 Conclusions

Increasing demand for high resolution model applications by government agencies, aquaculture and energy companies is driving private and public entities to develop updated grid domains for coastal areas. Higher resolution nested grids lead to better numerical skills of the model and allow the use of more refined bathymetric and atmospheric data, improving the overall hydrodynamic solution and reducing the errors of the downstream transport models. This higher level of detail allows a direct comparison between very local field data (e.g. currents) and model results, increasing the modelling system's confidence. Downscaling from regional to a local domain is still the most common option to simulate the effect of large-scale features on local processes (Campuzano, 2018; Campuzano et al., 2015; Dabrowski et al., 2014; Desmit et al., 2018; Fossati and Piedra-Cueva, 2013; Gallego et al., 2017; Janeiro et al., 2017; Katavouta and Thompson, 2016; Nagy et al., 2017; Yin et al., 2019).

6.1.1 Downscaling overview

Chapter 2 provides an overview of the advantages and disadvantages of the downscaling approach. To create a basis for comparison against the online and offline two-way methodologies developed in Chapters 3 and 4, a model application composed of the PCOMS model domain (Level2) and the Tagus estuary model domain (Level3) was used to simulate an extreme precipitation event which took place in March/April 2013. The Tagus ROFI area is one of the most studied estuaries in Portugal by Maretec and many other research groups, which contributed to a well-established consensus of the circulation patterns as well as the main features determining the circulation inside the estuary and in its adjacent coastal area. During the simulated period, flow rates of the Tagus River were higher than 7500 m³s⁻¹ for over 72 h, when average flow rate is 258 m³s⁻¹, which was useful to produce a strong freshwater plume which would reach the open boundaries of the model domain. A comparison between surface salinity obtained by the Tagus domain and PCOMS showed a strong difference in the interior of the Tagus domain – particularly near the coast past

Cape Raso – due to the influence of this plume. Other comparisons included salinity time series extracted from both domains at the northern open boundary of the Tagus domain, which demonstrated the extent of the estuaries' plume during this event. In this open boundary, salinity produced by the Tagus domain dropped from 36 to 31.5, observed during the peak flow, contrasting with the PCOMS salinity of 36 during the entire domain. As such, a high variability of the salinity at this location was observed, as very low values are observed when the plume moves northwards, and very high otherwise (due to the constantly high values being provided by PCOMS). Several vertical profiles complemented this information, showing that the Tagus plume impact could be felt up to 50 m in depth (differences towards PCOMS were in the order of 0.1 salinity units below 20m) even near the western open boundary of the domain, where the influence is clearly observed until a depth of 10 m. A global analysis of the temperature profiles also suggested an increase in upwelled waters, whose influence can be from the simple effect of having the discharge, which can increase upwelling at a local level, but also due to higher bathymetric detail, especially near the continental slope and submarine canyons.

Offline downscaling, which is now a requirement in operational forecasting due to its ability to introduce several nested domains in a regional model application without increasing the total forecast time, was applied to the Moroccan coast, Canary Islands and Madeira Islands using multiple nested domains. The operational forecast system was able to reproduce the surface temperature patterns as well as the vertical distribution of temperature and salinity, providing good correlations (above 0.99 for water level, temperature and salinity) and low bias values against a tide gauge, vertical profiles from PLOCAN and Argo buoys, and a sea surface temperature from satellite imagery. The nesting of a higher grid resolution domain (2 km) for the Canary Islands and another nested within with 100 m covering the port of Las Palmas provided a better fit between model and field data. This methodology was essential for the success of the MARPOCS project, where an oil and HNS spill online platform used the results provided by the nested system to perform forecasts and backtracking of the spills in order to determine their origin and future trajectory, providing valuable information for decision-makers regarding coastal risks.

6.2 Upscaling local into regional ocean model domains

As verified in Chapter 2, a downscaling approach does not take advantage of the higher grid resolution of local domain results, which may include features not present in the regional domain, such as estuaries and rivers. Regional ocean models also suffer from higher diffusivity, which can be reduced by upscaling from local domains. This problem can be solved in two different ways: using unstructured grids or through the use of upscaling.

The initial idea for this thesis was, in fact, the development of an unstructured grid version of the MOHID hydrodynamic model, with the same aim as presented in this thesis: to obtain better model results in coastal areas where regional domains, due to their lower grid resolution and higher numerical diffusion, have difficulties representing bathymetric driven currents as well as freshwater plumes. This idea was set aside in favour of the development of an upscaling methodology which would cope with the issues mentioned above, without the need to develop and validate an entire hydrodynamic model. Another contribution for this decision was the increasing need to improve the coupling between ocean and watershed models, and to which the upscaling could potentially provide solutions at different levels, as the algorithms could one day be used to upscale from a watershed model output. As such, adding an upscaling capability to the MOHID model became the subject of this thesis, with benefits not only for the coupling between nested (or not) regional and local models, but also as a stepping stone towards the coupling of ocean and watershed model domains. An advantage of the multidisciplinary team present at Maretec is the parallel development of the MOHIDLand, a watershed model which shares a good part of the code with the MOHID ocean model (MOHIDWater), making it easier for a future coupling (whether online or offline).

As defined in this thesis, upscaling can take different shapes, each addressed in a different chapter:

1. Through online coupling of a regional and one or several local model domains – Chapter 3 – in which upscaling takes place in the overlapped area between domains, where information is transferred at each time step.
2. Through offline coupling of a regional and one or several local model domains – Chapter 4 – in which upscaling takes place in the overlapped area between domains, but in this case the domains transfer information at a lower rate.

3. Through offline coupling of a regional and one or several local model domains – Chapter 5 – in which only a few cells of the local domain are used to impose a momentum discharge in the regional domain.

6.2.1 Online upscaling coupling

The development of an upscaling capability in MOHID – which would enable two-way couplings – was long due and first mentioned in Leitão (Leitão, 2002). As model grid resolution requirements increase, so do their associated model applications simulation time. This is expected, but unsustainable when regional domains are extensive, as it forces the domains to increase their whole grid resolution due to parts of a coastal area such as a ROFI or in the case of a strait such as Gibraltar (Sannino et al., 2009). As defined in this thesis, an online two-way coupling is characterized by a simulation where a regional (or parent domain-PD) and a local (or child domain-CD) are run simultaneously, transferring information at each time step. When information is transferred from the CD to the PD, it is denominated upscaling, and in this thesis it is performed on the whole overlapped area between domains, with the exception of a few PD cells from the open boundary of the CD, which is known in the literature (and confirmed in implementations of the schematic tests not presented in this thesis) to reduce the noise produced near the open boundary of the CD.

Regarding the upscaled variables, the model can now perform it to:

- Horizontal velocities
- Vertical velocities
- Water level
- Temperature, salinity and any other tracer property included by the user.

Upscaling is performed through a volume-weighted average of all CD cells inside a PD's cell. To validate the algorithm, several schematic tests were performed, including:

- Imposed wave through a 1D channel
- Stratified 3D domain under constant north wind
- 3D Coastal domain with a lateral discharge
- Geostrophic equilibrium

These were extremely important to detect errors in the code and to perform tests regarding the number of CD cells from the open boundary to be ignored in the upscaling computations, the time decay used in the nudging equation, and the usefulness of upscaling water level and vertical velocities. The following conclusions could be drawn from these tests:

- Vertical velocities did not produce an improvement of the PD and CD solutions. As such, the default option in the MOHID code is not to upscale the vertical velocities (although the user can enable this option).
- Upscaling water level, in addition to not producing an improvement of the solutions, leads to a water mass and temperature loss on the PD, which was the basis to exclude this variable from the default parametrization of the upscaling method (once again the user can activate it with a keyword). However, in the lateral discharge test, upscaling water level was critical to obtain a good representation of the freshwater plume.
- In general, lower time decays used in the upscaling produce better solutions, although at a higher cost of mass conservation problems. As such, the choice of time decay should consider the lowest value that achieves the minimum result improvement accepted by the modeller. This choice also needs to consider the processes represented in the RD and in the LD, and the time decay value should be as low as possible when the LD's processes are dominant over the RD's processes.

Conservation errors were accounted for and represented, for all the tests, a value of the order of 0.005%. These errors are produced in the downscaling, making it more difficult to offset, but can be minimized with the correct upscaling parametrizations.

The upscaling algorithm was also applied to the same model domains as in Chapter 2, PCOMS and the Tagus estuary model domains, covering the same extreme precipitation event. In this case, and considering the conclusions drawn from the schematic tests, only the addition of the vertical velocities was tested – but did not produce noticeable changes. Results show an overall improvement of the PD and CD solutions when compared against field data (the Cascais tide gauge and surface salinity from the Algés buoy). These improvements were also visible in the entire Tagus estuary domain, whose estuary plume became smoother and with lower values, reaching 28.5 instead of the 32 in a one-way approach at the northern open boundary. There was also a stronger influence of the estuary plume in the vertical profiles (up to 80 m) produced by the two-way

implementation in comparison with the traditional one-way approach. For example, in the Estremadura promontory, a difference of 0.6 salinity units in the average salinities was observed. The main driver for these improvements is related to the open boundary values provided by the regional model PCOMS to the local Tagus estuary model domain. Due to the upscaling, PCOMS salinity values at the open boundaries of the Tagus estuary domain became lower and more compatible with those produced by the Tagus model domain (from 36 to 33.5). As such, the estuarine plume computed by the Tagus estuary domain under a two-way approach was able to more easily exit the domain without being diverted when colliding with a much higher salinity values of PCOMS. This also led to a lower variability of salinity at the open boundary of the Tagus estuary domain.

6.2.2 Offline upscaling

As for the downscaling approach, offline upscaling is a natural and necessary evolution for operational model forecast services, which are required to simulate each day as fast as possible. Although online upscaling provides a better coupling between model domains – much like the online downscaling – it requires that all domains are run simultaneously, which leads to a higher computational effort and increased simulation time. This would render the use of upscaling in operational modelling unsustainable. Nevertheless, in scenario or event studies a two-way coupling can still prove to be a good option as there are less time restrictions. In these studies, using the offline upscaling methodology would in fact increase the total simulation time – which was verified in Chapter 4 – because both domains would need to run each day, at least twice, as opposed to an online coupling. However, in operational forecast services, each model domain always runs at least 3 times, but the tendency is to run them 7 times a day because they forecast at least 3 days, plus a hindcast of 1 or 2 days if not more. As such, the same day must run many times, regardless of the methodology followed, which enables the application of the offline upscaling methodology at zero computational time cost. Another important advantage of the offline upscaling is the ability of a regional model application to improve its solution from model results produced by different entities and/or numerical model. Indeed, an ocean model covering the North Atlantic would now be able to upscale from regional and/or local model applications provided by different institutions from different European countries directly or from CMEMS, contributing to a higher level of cooperation between institutions.

The methodology was applied to the PCOMS and the Tagus model applications, as in Chapters 2 and 3. Two different setups were followed: in the first, only one day with upscaling was run – which means two runs per day per domain, where the first day does not include upscaling – and in the second, two days with upscaling were performed, increasing the transfer of information rate. Results showed the same level of improvement in the open boundaries as observed when online upscaling was performed, especially when two days of offline upscaling were performed. The variability of salinity at the open boundary was reduced from the traditional offline downscaling methodology to the offline two-way methodology, and decreased more when an additional day of upscaling was performed. This improvement is also important in the bigger context of the PCOMS regional domain, which, by covering a much larger area than the Tagus estuary ROFI, will produce a better solution outside the overlapped area, for example in the representation of the Western Iberian Buoyant Plume (WIBP) further North, as demonstrated in Campuzano (2018).

6.2.3 Upscaling via momentum discharge

The final objective of this thesis was to provide a pathway towards an improved coupling methodology between oceans and watersheds. To accomplish this objective, an adaptation to the upscaling algorithms implemented in MOHID was performed in Chapter 5, allowing for the offline upscaling from model results as in the offline upscaling developed in Chapter 4. The difference now is that the algorithm is designed to receive information regarding discharge locations in the regional model that are computed from local domains (Integrated methodology). This means that only discharges will be imposed on the regional model domain. The idea behind this implementation is the integration of the upscaling method with the use of schematic estuaries and rivers which can already be fed by watershed models (Campuzano et al., 2018). A connection between ocean, estuary and watershed model applications needs to be accurate but also fast, in order to be used in operational modelling. Including the intermediary between ocean and watershed is extremely important for the correct representation of haline fronts and density-driven currents through the tidal mixing that occurs inside them. This is why schematic estuaries were developed to replace the real estuary applications, and which are much more time consuming. The algorithm takes a standard model output format – HDF or NetCDF – and searches for the lateral discharges (with the help of user defined grid locations on the regional domain). When a possible discharge is found, the model will compute the section of the connecting cells between regional and local model

domains at the first land cell of the regional domain, as well as velocities, temperature, salinity and the total flow per vertical layer of the model. By automating this process directly in the MOHID code, many human errors can be spared, as well as the production of several discharge files containing the time series of flow, velocity and tracer properties, as was developed in Campuzano (2018). The new methodology was tested using the PCOMS regional model application and a schematic version of the main Portuguese rivers – Minho, Douro, Mondego, Tagus, Sado and Guadiana) plus Guadalquivir. These schematic versions take only around 2 min for simulating one day, which is negligible in comparison with real model domains for these rivers estuaries. In this case, however, only one day of upscaling was performed, as the intention of the tests was only to validate the use of schematic estuaries combined with upscaling. These results were compared with those obtained using the same implementations but following the methodology of (Campuzano et al., 2018) (Detached methodology), in which the discharges are computed with external tools, and with a version of PCOMS without freshwater inputs (No Rivers methodology). Validations were also performed against in-situ sea surface salinity and temperature data, and satellite observations of sea surface temperature, which showed an improvement from the No Rivers methodology to the Detached and Integrated methodologies, particularly in the coastal area of the IP. The results obtained showed a great similarity between the two methodologies where river inputs were added to PCOMS, particularly near the coast, which confirm the new Integrated methodology as a suitable methodology for operational modelling of coastal areas where freshwater sources play an important role. Finally, this methodology can improve regional models further when data from river flows, current in development in projects such as the Lambda project (Lambda Project, 2020) begin to be included in them through the use of fast running schematic representations of estuaries and rivers.

6.3 Future work

In this thesis, many new developments were introduced in MOHID and tested in schematic and real case applications. However, in the case of the upscaling algorithms, some more testing should be performed. The most important line of validation of the online and offline algorithms working by nudging of the PD towards the CD is the importance of upscaling the water level when a lateral discharge is present only in the CD. Because this schematic test was performed after running most of the real case applications, the upscaling of water level in the online and offline upscaling chapters was not considered. However, water level upscaling was determinant for a good solution in the

schematic test. As such, future work should include the testing of upscaling water level in nested systems such as the PCOMS and Tagus estuaries, which is similar to that of the schematic lateral discharge. In regard to the offline upscaling via discharges computed from model outputs, future work should include the optimization of the schematic estuaries, in order to better reproduce the tidal prisms and associated mixing processes. Furthermore, a new line of research should focus on the direct integration of ocean models with watershed models capitalizing on the offline upscaling via discharges, as an infinite number of these can be defined in MOHID, and which can be defined in the implementation files through polylines (thus covering entire coastlines). The ocean model could then compute surface and underwater discharges alike – whose fluxes are included in watershed models – and vice versa through development of the same upscaling methodology in the MOHIDLand watershed model. Finally, parallelization of the code only included openMP directives in the main upscaling routines, but MPI parallelization has shown to produce faster solutions. Therefore, an effort should be made to enable MPI capabilities in the developments. Nevertheless, there is enough interest from several institutions that the methodologies developed in this thesis be further tested and applied to current operational systems, which will fuel a fast development of the MPI capability.

References

- Abbott, M.B., Damsgaard, A., Rodenhuis, G.S., 1973. System 21, “Jupiter” (A design system for two-dimensional nearly-horizontal flows). *J. Hydraul. Res.* 11, 1–28.
<https://doi.org/10.1080/00221687309499788>
- Acosta, M., Anguita, M., Fernández-Baldomero, F.J., Ramón, C.L., Schladow, S.G., Rueda, F.J., 2015. Evaluation of a nested-grid implementation for 3D finite-difference semi-implicit hydrodynamic models. *Environ. Model. Softw.* 64, 241–262. <https://doi.org/10.1016/j.envsoft.2014.10.015>
- Ambar, I., Fiúza, A.F.G., 1994. Some features of the Portugal current system: a poleward slope undercurrent, an upwelling-related summer southward flow and an autumn-winter poleward coastal surface current. *Proc. Second Int. Conf. Air-Sea Interact. Meteorol. Oceanogr. Coast. Zo.* 286–287.
- Andersen, J.H., Carstensen, J., Conley, D.J., Dromph, K., Fleming-lehtinen, V., Gustafsson, B.G., Josefson, A.B., Norkko, A., Villn, A., 2017. Long-term temporal and spatial trends in eutrophication status of the Baltic Sea. *Biol. Rev.* 92, 135–149. <https://doi.org/10.1111/BRV.12221>
- Ascione, I., 2014. Development and application of a process-oriented model for benthic marine systems 214 pp.
- Autret, E., Paul, F., Tandéo, P., Hackett, B., 2017. For Level 3 and 4 ODYSSEA SST products over the global ocean and north western shelves—SST_GLO_SST_L3_NRT_OBSERVATIONS_010_010—SST_NWS_SST_L4_NRT_OBSERVATIONS_010_003, 2017.
- Aznar, R., Sotillo, M.G., Cailleau, S., Lorente, P., Levier, B., Amo-Baladrón, A., Reffray, G., Álvarez-Fanjul, E., 2016. Strengths and weaknesses of the CMEMS forecasted and reanalyzed solutions for the Iberia-Biscay-Ireland (IBI) waters. *J. Mar. Syst.* 159, 1–14.
<https://doi.org/10.1016/j.jmarsys.2016.02.007>
- Barth, A., Alvera-Azcárate, A., Beckers, J.M., Rixen, M., Vandenbulcke, L., 2007. Multigrid state vector for data assimilation in a two-way nested model of the Ligurian Sea. *J. Mar. Syst.* 65, 41–59.
<https://doi.org/10.1016/j.jmarsys.2005.07.006>
- Barth, A., Alvera-Azcárate, A., Rixen, M., Beckers, J.M., 2005. Two-way nested model of mesoscale circulation features in the Ligurian Sea. *Prog. Oceanogr.* 66, 171–189.
<https://doi.org/10.1016/j.pocean.2004.07.017>
- Berger, M.J., Colella, P., 1989. Local adaptive mesh refinement for shock hydrodynamics. *J. Comput. Phys.* 82, 64–84. [https://doi.org/10.1016/0021-9991\(89\)90035-1](https://doi.org/10.1016/0021-9991(89)90035-1)
- Bjerknes, V., 1999. The Problem of Weather Forecasting as a Problem in Mechanics and Physics. *Life Cycles Extratropical Cyclones* 1–4. https://doi.org/10.1007/978-1-935704-09-6_1
- Blumberg, A.F., Kantha, L.H., 1985. Open Boundary Condition for Circulation Models. *J. Hydraul. Eng.* 111, 237–255. [https://doi.org/10.1061/\(asce\)0733-9429\(1985\)111:2\(237\)](https://doi.org/10.1061/(asce)0733-9429(1985)111:2(237))
- Braunschweig, F., Leitao, P.C., Fernandes, L., Pina, P., Neves, R.J.J., 2004. The object-oriented design of the integrated water modelling system MOHID. *Dev. Water Sci.* 55, 1079–1090.
[https://doi.org/10.1016/S0167-5648\(04\)80126-6](https://doi.org/10.1016/S0167-5648(04)80126-6)
- Braunschweig, F., Martins, F., Chambel, P., Neves, R., 2003. A methodology to estimate renewal time scales in estuaries: The Tagus Estuary case. *Ocean Dyn.* 53, 137–145.
<https://doi.org/10.1007/s10236-003-0040-0>

- Brewin, R.J.W., de Mora, L., Billson, O., Jackson, T., Russell, P., Brewin, T.G., Shutler, J.D., Miller, P.I., Taylor, B.H., Smyth, T.J., Fishwick, J.R., 2017. Evaluating operational AVHRR sea surface temperature data at the coastline using surfers. *Estuar. Coast. Shelf Sci.* 196, 276–289. <https://doi.org/10.1016/j.ecss.2017.07.011>
- Brito, D., Campuzano, F.J., Sobrinho, J., Fernandes, R., Neves, R., 2015. Integrating operational watershed and coastal models for the Iberian Coast: Watershed model implementation - A first approach. *Estuar. Coast. Shelf Sci.* 167, 138–146. <https://doi.org/10.1016/j.ecss.2015.10.022>
- Burchard, H., Bolding, K., Villarreal, M.R., 1999. GOTM, a general ocean turbulence model. Theory, implementation and test cases, European Commission, Report EUR 18745 EN. Athens, Greece.
- Caldeira, R., Couvelard, X., Vieira, R., Lucas, C., Sala, I., Casanova, I.V., 2016. Challenges of building an operational ocean forecasting system for small island regions: Regional to local. *J. Oper. Oceanogr.* 9, 12. <https://doi.org/10.1080/1755876X.2016.1205304>
- Campuzano, F., 2018. Coupling watersheds, estuaries and regional seas through numerical modelling for Western Iberia. PhD. University of Lisbon, Portugal.
- Campuzano, F., Brito, D., Juliano, M., Fernandes, R., de Pablo, H., Neves, R., 2016. Coupling watersheds, estuaries and regional ocean through numerical modelling for Western Iberia: a novel methodology. *Ocean Dyn.* 66, 1745–1756. <https://doi.org/10.1007/s10236-016-1005-4>
- Campuzano, F.J., Fernandes, R., Leitão, P.C., Viegas, C., de Pablo, H., Neves, R., 2012. Implementing local operational models based on an offline downscaling technique: The Tagus estuary case. 2.as Jornadas Eng. Hidrográfica, 20-22 June 2012, Lisbon, Port. Ext. Abstr. 105–108.
- Campuzano, F.J., Gutiérrez, J., Mateus, M., Senabre, T., Belmonte, A., Perán, A., 2015. A Modelling Approach to Estimate the Environmental and Productive Carrying Capacity for a Mediterranean Coastal Marine Culture Park. *J. Aquac. Res. Dev.* 6. <https://doi.org/10.4172/2155-9546.1000373>
- Campuzano, F.J., Juliano, M., Sobrinho, J., Pablo, H. de, Brito, D., Fernandes, R., Neves, R., 2018. Coupling Watersheds, Estuaries and Regional Oceanography through Numerical Modelling in the Western Iberia: Thermohaline Flux Variability at the Ocean-Estuary Interface. *Estuary.* <https://doi.org/10.5772/intechopen.72162>
- Canas, Â., 2009. Modelling and Data Assimilation Techniques for Operational Hydrodynamic Forecast in Tagus Estuary. PhD thesis. Technical University of Lisbon, Portugal.
- Canas, A., Santos, A., Leitão, P., 2009. Effect of large scale atmospheric pressure changes on water level in the Tagus Estuary. *J. Coast. Res.* SI 56, 4–8.
- Canuel, E.A., Cammer, S.S., McIntosh, H.A., Pondell, C.R., 2012. Climate change impacts on the organic carbon cycle at the land-ocean interface. *Annu. Rev. Earth Planet. Sci.* 40, 685–711. <https://doi.org/10.1146/annurev-earth-042711-105511>
- Capet, A., Fernández, V., She, J., Dabrowski, T., Umgiesser, G., Staneva, J., Mészáros, L., Campuzano, F., Ursella, L., Nolan, G., El Serafy, G., 2020. Operational Modeling Capacity in European Seas—An EuroGOOS Perspective and Recommendations for Improvement. *Front. Mar. Sci.* 7, 1–19. <https://doi.org/10.3389/fmars.2020.00129>
- Carrere, L., Lyard, F., Cancet, M., Guillot, A., Roblou, L., 2013. FES 2012: A New Global Tidal Model Taking Advantage of Nearly 20 Years of Altimetry, in: Ouwehand, L. (Ed.), 20 Years of Progress in Radar Altimetry, ESA Special Publication. p. 13.
- Chen, Y., Cheng, W., Zhang, H., Qiao, J., Liu, J., Shi, Z., Gong, W., 2019. Evaluation of the total

- maximum allocated load of dissolved inorganic nitrogen using a watershed–coastal ocean coupled model. *Sci. Total Environ.* 673, 734–749. <https://doi.org/10.1016/j.scitotenv.2019.04.036>
- Coelho, H.S., Neves, R.R., Leitão, P.C., Martins, H., Santos, A.P., 1999. The slope current along the western European margin : A numerical investigation 15, 61–72.
- Cushman-Roisin, B., 1994. *Introduction to Geophysical Fluid Dynamics*. Upper Saddle River, N.J. : Prentice Hal.
- Dabrowski, T., Lyons, K., Berry, A., Cusack, C., Nolan, G.D., 2014. An operational biogeochemical model of the North-East Atlantic: Model description and skill assessment. *J. Mar. Syst.* 129, 350–367. <https://doi.org/10.1016/j.jmarsys.2013.08.001>
- Davies, H.C., 1976. A lateral boundary formulation for multi-level prediction models. *Q. J. R. Meteorol. Soc.* 102, 405–418. <https://doi.org/10.1002/qj.49710243210>
- de Pablo, H., Sobrinho, J., Garcia, M., Campuzano, F., Juliano, M., Neves, R., 2019. Validation of the 3D-MOHID Hydrodynamic Model for the Tagus Coastal Area. *Water* 11, 1713. <https://doi.org/10.3390/w11081713>
- Deacon, M., 2018. *Scientists and the Sea, 1650–1900: A Study of Marine Science*. <https://doi.org/10.4324/9781315243610>
- Debreu, L., Blayo, E., 2008. Two-way embedding algorithms: A review. *Ocean Dyn.* 58, 415–428. <https://doi.org/10.1007/s10236-008-0150-9>
- Debreu, L., Marchesiello, P., Penven, P., Cambon, G., 2012. Two-way nesting in split-explicit ocean models: Algorithms, implementation and validation. *Ocean Model.* 49–50, 1–21. <https://doi.org/10.1016/j.ocemod.2012.03.003>
- Debreu, L., Vouland, C., Blayo, E., 2008. AGRIF: Adaptive grid refinement in Fortran. *Comput. Geosci.* 34, 8–13. <https://doi.org/10.1016/j.cageo.2007.01.009>
- Delhez, É.J.M., Deleersnijder, É., 2007. Overshootings and spurious oscillations caused by biharmonic mixing. *Ocean Model.* 17, 183–198. <https://doi.org/10.1016/j.ocemod.2007.01.002>
- Delpy, M., 2013. Etude de la dispersion horizontale en zone littorale sous l ’ effet de la circulation tridimensionnelle forcée par les vagues - Application à la baie de Saint Jean de Luz - Ciboure et au littoral de Guéthary-Bidart To cite this version : HAL Id : tel-0081.
- Desmit, X., Thieu, V., Billen, G., Campuzano, F., Dulière, V., Garnier, J., Lassaletta, L., Ménesguen, A., Neves, R., Pinto, L., Silvestre, M., Sobrinho, J.L., Lacroix, G., 2018. Reducing marine eutrophication may require a paradigmatic change. *Sci. Total Environ.* 635. <https://doi.org/10.1016/j.scitotenv.2018.04.181>
- Dias, J.M., Valentim, J.M., Sousa, M.C., 2013. A numerical study of local variations in tidal regime of Tagus estuary, Portugal. *PLoS One* 8. <https://doi.org/10.1371/journal.pone.0080450>
- Dickinson, R.E., 1989. National Center for Atmospheric Research*, Boulder, CO 80307-3000, U.S.A. *Atmos. Res.* 383–384.
- Du, J., Shen, J., Park, K., Wang, Y.P., Yu, X., 2018. Worsened physical condition due to climate change contributes to the increasing hypoxia in Chesapeake Bay. *Sci. Total Environ.* 630, 707–717. <https://doi.org/10.1016/j.scitotenv.2018.02.265>
- EEC, 2001. 2001/720/EC: Commission Decision of 8 October 2001 granting Portugal a derogation regarding urban waste water treatment for the agglomeration of the Estoril coast (notified under

- document number C(2001) 2657). http://europa.eu.int/eur-lex/en/lif/reg/en_register_15102020.html.
- Estournel, C., Kondrachoff, V., Marsaleix, P., Vehil, R., 1997. The plume of the Rhone: Numerical simulation and remote sensing. *Cont. Shelf Res.* 17, 899–924. [https://doi.org/10.1016/S0278-4343\(96\)00064-7](https://doi.org/10.1016/S0278-4343(96)00064-7)
- Fernandes, R., 2018. Risk Management of Coastal Pollution from Oil Spills Supported by Operational Numerical Modelling.
- Fernández-Nóvoa, D., Gómez-Gesteira, M., Mendes, R., deCastro, M., Vaz, N., Dias, J.M., 2017. Influence of main forcing affecting the Tagus turbid plume under high river discharges using MODIS imagery. *PLoS One* 12, e0187036.
- Fiúza, A.F. de G., Macedo, M.E. de, Guerreiro, M.R., 1982. Climatological space and time variation of the Portuguese coastal upwelling Upwelling Portugal Coastal winds Sea surface temperature Sardine Upwelling Portugal Vents côtiers Temperature de surface de la mer Sardine ABSTRACT RÉSUMÉ. *Oceanol. Acta* 5, 31–40.
- Fiuza, A.F.G., 1983. Upwelling Patterns Off Portugal. *NATO Conf. Ser. 4 Mar. Sci.* 10 A, 85–98. https://doi.org/10.1007/978-1-4615-6651-9_5
- Flather, R.A., 1976. A tidal model of the northwest European continental shelf. *Mem. Soc. R. Sei. Liège* 10, 141–164.
- Fortunato, A.B., Oliveira, A., Baptista, A.M., 1999. On the effect of tidal flats on the hydrodynamics of the Tagus estuary. *Oceanol. Acta* 22, 31–44. [https://doi.org/10.1016/S0399-1784\(99\)80030-9](https://doi.org/10.1016/S0399-1784(99)80030-9)
- Fortunato, A.B., Pinto, L., Oliveira, A., Ferreira, J.S., 2002. Tidally generated shelf waves off the western Iberian coast. *Cont. Shelf Res.* 22, 1935–1950. [https://doi.org/10.1016/S0278-4343\(02\)00069-9](https://doi.org/10.1016/S0278-4343(02)00069-9)
- Fossati, M., Piedra-Cueva, I., 2013. A 3D hydrodynamic numerical model of the Ria de la Plata and Montevideo's coastal zone. *Appl. Math. Model.* 37, 1310–1332. <https://doi.org/10.1016/j.apm.2012.04.010>
- Fox, A.D., Maskell, S.J., 1995. Two-Way Interactive Nesting of Primitive Equation Ocean Models with Topography. *J. Phys. Oceanogr.* 25, 2977–2996. [https://doi.org/10.1175/1520-0485\(1995\)025<2977](https://doi.org/10.1175/1520-0485(1995)025<2977)
- Franz, G., 2017. Numerical modelling of hydrodynamics and sediment transport in coastal systems 2–3. <https://doi.org/10.13140/RG.2.2.12031.71849>
- Franz, G., Delpy, T.M., Brito, D., Neves, R., Leitão, P., Pinto, L., 2017. Modelling of sediment transport and morphological evolution under the combined action of waves and currents. *Ocean Sci.* 13, 673–690. <https://doi.org/10.5194/os-13-673-2017>
- Franz, G., Fernandes, R., de Pablo H., J., Viegas, C., Pinto, L., Campuzano, F., Ascione, I., Leitão, P., Neves, R., 2014. Tagus Estuary hydro-biogeochemical model: Inter-annual validation and operational model update. 3.as Jornadas Eng. Hidrogr.
- Franz, G., Pinto, L., Ascione, I., Mateus, M., Fernandes, R., Leitão, P., Neves, R., 2014. Modelling of cohesive sediment dynamics in tidal estuarine systems: Case study of Tagus estuary, Portugal. *Estuar. Coast. Shelf Sci.* <https://doi.org/10.1016/j.ecss.2014.09.017>
- Franz, G.A.S., Leitão, P., dos Santos, A., Juliano, M., Neves, R., 2016. From regional to local scale modelling on the south-eastern Brazilian shelf: Case study of Paranaguá estuarine system. *Brazilian J. Oceanogr.* 64, 277–294. <https://doi.org/10.1590/S1679-875920161195806403>
- Gallego, A., Side, J., Baston, S., Waldman, S., Bell, M., James, M., Davies, I., O'Hara Murray, R., Heath,

- M., Sabatino, A., McKee, D., McCaig, C., Karunarathna, H., Fairley, I., Chatzirodou, A., Venugopal, V., Nimalidinne, R., Yung, T.Z., Vögler, A., MacIver, R., Burrows, M., 2017. Large scale three-dimensional modelling for wave and tidal energy resource and environmental impact: Methodologies for quantifying acceptable thresholds for sustainable exploitation. *Ocean Coast. Manag.* 147, 67–77. <https://doi.org/10.1016/j.ocecoaman.2016.11.025>
- Garel, E., Ferreira, 2015. Multi-year high-frequency physical and environmental observations at the Guadiana Estuary. *Earth Syst. Sci. Data* 7, 299–309. <https://doi.org/10.5194/essd-7-299-2015>
- Garel, E., Nunes, S., Neto, J.M., Fernandes, R., Neves, R., Marques, J.C., Ferreira, Ó., 2009. The autonomous Simpatico system for real-time continuous water-quality and current velocity monitoring: Examples of application in three Portuguese estuaries. *Geo-Marine Lett.* 29, 331–341. <https://doi.org/10.1007/s00367-009-0147-5>
- Gómez-Letona, M., Ramos, A.G., Coca, J., Arístegui, J., 2017. Trends in primary production in the canary current upwelling system-A regional perspective comparing remote sensing models. *Front. Mar. Sci.* 4, 1–18. <https://doi.org/10.3389/fmars.2017.00370>
- Greatbatch, R.J., Sheng, J., Eden, C., Tang, L., Zhai, X., Zhao, J., 2004. The semi-prognostic method. *Cont. Shelf Res.* 24, 2149–2165. <https://doi.org/10.1016/j.csr.2004.07.009>
- Grell, G.A., Dudhia, J., Stauffer, S.R., 1994. A description of the Fifth-generation Penn State/NCAR Mesoscale Model (MM5). NCAR Tech. Note NCAR/TN-398+STR 121. <https://doi.org/10.5065/D60Z716B>
- Guerreiro, M., Fortunato, A.B., Freire, P., Rilo, A., Taborda, R., Freitas, M.C., Andrade, C., Silva, T., Rodrigues, M., Bertin, X., Azevedo, A., 2015. Evolution of the hydrodynamics of the Tagus estuary (Portugal) in the 21st century. *J. Integr. Coast. Zo. Manag.* 15, 65–80. <https://doi.org/10.5894/rgci515>
- Gutiérrez JM, C.F., Mateus MD, S.T., Belmonte A, P.A., 2015. A Modelling Approach to Estimate the Environmental and Productive Carrying Capacity for a Mediterranean Coastal Marine Culture Park. *J. Aquac. Res. Dev.* 6. <https://doi.org/10.4172/2155-9546.1000373>
- Haley, P.J., Lermusiaux, P.F.J., 2010. Multiscale two-way embedding schemes for free-surface primitive equations in the “multidisciplinary simulation, estimation and assimilation system,” *Ocean Dynamics*. <https://doi.org/10.1007/s10236-010-0349-4>
- Henrichs, S., Bond, N., Garvine, R., Kineke, G., Lohrenz, S., 2000. Coastal Ocean Processes (CoOP): Transport and Transformation Processes Over Continental Shelves with Substantial Freshwater Inflows, CoOP report. University of Maryland.
- Herzfeld, M., 2015. Methods for freshwater riverine input into regional ocean models. *Ocean Model.* 90, 1–15. <https://doi.org/10.1016/j.ocemod.2015.04.001>
- Herzfeld, M., Rizwi, F., 2019. A two-way nesting framework for ocean models. *Environ. Model. Softw.* 117, 200–213. <https://doi.org/10.1016/j.envsoft.2019.03.015>
- Hidromod, 1998. Estudo da dispersão da zona difusora do emissário da Guia.
- Hidromod, 1997. Novo terminal fluvial na Trafaria - Modelação matemática de hidrodinâmica.
- Hidromod, 1996. Terminal de Contentores de Pedroucos. Modelação matemática da agitação e da hidrodinâmica. Dezembro 1996.
- Hill, G., 1968. Grid Telescoping in Numerical Weather Prediction. *J. Appl. Meteorol.* 7, 29–38.

- [https://doi.org/https://doi.org/10.1175/1520-0450\(1968\)007<0029:GTINWP>2.0.CO;2](https://doi.org/https://doi.org/10.1175/1520-0450(1968)007<0029:GTINWP>2.0.CO;2)
- Holt, J., Hyder, P., Ashworth, M., Harle, J., Hewitt, H.T., Liu, H., New, A.L., Pickles, S., Porter, A., Popova, E., Icarus Allen, J., Siddorn, J., Wood, R., 2017. Prospects for improving the representation of coastal and shelf seas in global ocean models. *Geosci. Model Dev.* 10, 499–523. <https://doi.org/10.5194/gmd-10-499-2017>
- Huhn, F., von Kameke, A., Allen-Perkins, S., Montero, P., Venancio, A., Pérez-Muñuzuri, V., 2012. Horizontal Lagrangian transport in a tidal-driven estuary-Transport barriers attached to prominent coastal boundaries. *Cont. Shelf Res.* 39–40, 1–13. <https://doi.org/10.1016/j.csr.2012.03.005>
- IMAR, 2007. Modelação dos Meios Receptores da SIMTEJO.
- Janeiro, J., Neves, A., Martins, F., Relvas, P., 2017. Integrating technologies for oil spill response in the SW Iberian coast. *J. Mar. Syst.* 173, 31–42. <https://doi.org/10.1016/j.jmarsys.2017.04.005>
- Jouanneau, J.M., Garcia, C., Oliveira, A., Rodrigues, A., Dias, J.A., Weber, O., 1998. Dispersal and deposition of suspended sediment on the shelf off the Tagus and Sado estuaries, S.W. Portugal. *Prog. Oceanogr.* 42, 233–257. [https://doi.org/https://doi.org/10.1016/S0079-6611\(98\)00036-6](https://doi.org/https://doi.org/10.1016/S0079-6611(98)00036-6)
- Kantha, L.H., Clayson, C.A., 2000. Numerical Models of Oceans and Oceanic Processes. International Geophysics.
- Katavouta, A., Thompson, K.R., 2016. Downscaling ocean conditions with application to the Gulf of Maine, Scotian Shelf and adjacent deep ocean. *Ocean Model.* 104, 54–72. <https://doi.org/10.1016/j.ocemod.2016.05.007>
- Kelly, S.M., Lermusiaux, P.F.J., Duda, T.F., Haley, P.J., 2016. A Coupled-Mode Shallow-Water Model for Tidal Analysis: Internal Tide Reflection and Refraction by the Gulf Stream. *J. Phys. Oceanogr.* 46, 3661–3679. <https://doi.org/10.1175/JPO-D-16-0018.1>
- Kenov, I.A., Campuzano, F., Franz, G., 2014. Advances in Modeling of Water Quality in Estuaries Chapter 10 Advances in Modeling of Water Quality in Estuaries. <https://doi.org/10.1007/978-3-319-06326-3>
- Koch, S.E., Mcqueen, J.T., 1987. A survey of nested grid techniques and their potential for use within the MASS weather prediction model 1–26.
- Kurihara, Y., Tripoli, G., Bender, M., 1979. Design of a Movable Nested-Mesh Primitive Equation Model. *Mon Weath Rev* 239–249.
- Lacroix, G., Ruddick, K., Ozer, J., Lancelot, C., 2004. Modelling the impact of the Scheldt and Rhine/Meuse plumes on the salinity distribution in Belgian waters (southern North Sea). *J. Sea Res.* 52, 149–163. <https://doi.org/10.1016/j.seares.2004.01.003>
- Lambda Project, 2020. CMEMS Service Evolution Project.
- Le Moal, M., Gascuel-Oudou, C., Ménesguen, A., Souchon, Y., Étrillard, C., Levain, A., Moatar, F., Pannard, A., Souchu, P., Lefebvre, A., Pinay, G., 2019. Eutrophication: A new wine in an old bottle? *Sci. Total Environ.* 651, 1–11. <https://doi.org/10.1016/j.scitotenv.2018.09.139>
- Leendertse, J.J., 1967. Aspects of a Computational Model for Long Water Wave Propagation. Santa Monica, CA: RAND Corporation, 1967.https://www.rand.org/pubs/research_memoranda/RM5294.html.
- Lefevre, F., 2000. Modélisation des marées océaniques à l'échelle globale : assimilation de données in situ et altimétriques. DOCTEUR DE L'UNIVERSITE TOULOUSE III - PAUL SABATIER,.

- Lefèvre, F., Lyard, F.H., Le Provost, C., Schrama, E.J.O., 2002. FES99: A global tide finite element solution assimilating tide gauge and altimetric information. *J. Atmos. Ocean. Technol.* 19, 1345–1356. [https://doi.org/10.1175/1520-0426\(2002\)019<1345:FAGTFE>2.0.CO;2](https://doi.org/10.1175/1520-0426(2002)019<1345:FAGTFE>2.0.CO;2)
- Leitão, P., 2002. Integração de escalas e de processos na modelação do ambiente marinho. Universidade Técnica de Lisboa - Instituto Superior Técnico. http://www.mohid.com/PublicData/Products/Thesis/PhD_PauloLeit%C3%A3o.zip.
- Leitão, P., Coelho, H., Santos, A., Neves, R., 2005. Modelling the main features of the Algarve coastal circulation during July 2004: A downscaling approach. *J. Atmos. Ocean Sci.* 10, 421–462. <https://doi.org/10.1080/17417530601127704>
- Liu, Y., MacCready, P., Hickey, B.M., Dever, E.P., Kosro, P.M., Banas, N.S., 2009. Evaluation of a coastal ocean circulation model for the Columbia river plume in summer 2004. *J. Geophys. Res. Ocean.* 114, 1–23. <https://doi.org/10.1029/2008JC004929>
- Lyard, F., Lefevre, F., Letellier, T., Francis, O., 2006. Modelling the global ocean tides: modern insights from FES2004. *Ocean Dyn.* 56, 394–415. <https://doi.org/10.1007/s10236-006-0086-x>
- MacCready, P., Banas, N.S., Hickey, B.M., Dever, E.P., Liu, Y., 2009. A model study of tide- and wind-induced mixing in the Columbia River Estuary and plume. *Cont. Shelf Res.* 29, 278–291. <https://doi.org/10.1016/j.csr.2008.03.015>
- Malara, G., Zema, D.A., Arena, F., Bombino, G., Zimbone, S.M., 2020. Coupling watershed - coast systems to study evolutionary trends: A review. *Earth-Science Rev.* 201, 103040. <https://doi.org/10.1016/j.earscirev.2019.103040>
- Marchesiello, P., Capet, X., Menkes, C., Kennan, S.C., 2011. Submesoscale dynamics in tropical instability waves. *Ocean Model.* 39, 31–46. <https://doi.org/10.1016/j.ocemod.2011.04.011>
- Marchesiello, P., McWilliams, J.C., Shchepetkin, A.F., 2001. Open boundary conditions for long-term integration of regional oceanic models. *Ocean Model.* 1–20. <https://doi.org/10.1016/j.str.2017.03.004>
- Martins, F., 1999. Modelação matemática tridimensional de escoamentos costeiros e estuarinos usando uma abordagem de coordenada vertical genérica. PhD thesis. Technical University of Lisbon, Portugal.
- Martins, F., Leitão, P.C., Silva, A., Neves, R., 2001. 3D modelling in the Sado estuary using a new generic vertical discretization approach. *OCEANOLOGICA ACTA* 24, 51–62.
- Martins, F.A., Neves, R.J., Leitão, P.C., 1998. A three-dimensional hydrodynamic model with generic vertical coordinate. *Hydro-informatics* 98 1403–1410.
- Martinsen, A.E., Engedahl, H., 1987. Implementation and testing of a lateral boundary scheme as an open boundary condition in a barotropic ocean model. *Coast. Eng.* 11, 603–627. [https://doi.org/https://doi.org/10.1016/0378-3839\(87\)90028-7](https://doi.org/https://doi.org/10.1016/0378-3839(87)90028-7)
- Mason, E., Molemaker, J., Shchepetkin, A.F., Colas, F., McWilliams, J.C., Sangrà, P., 2010. Procedures for offline grid nesting in regional ocean models. *Ocean Model.* 35, 1–15. <https://doi.org/10.1016/j.ocemod.2010.05.007>
- Mateus, M., 2006. A process-oriented biogeochemical model for marine ecosystems: development, numerical study, and application. Universidade Técnica de Lisboa - Instituto Superior Técnico.
- Mateus, M., Leitão, P.C., de Pablo, H., Neves, R., 2012a. Is it relevant to explicitly parameterize chlorophyll synthesis in marine ecological models? *J. Mar. Syst.* 94, S23–S33.

- <https://doi.org/10.1016/j.jmarsys.2011.11.007>
- Mateus, M., Neves, R., 2013. Ocean modelling for coastal management. IST Press.
- Mateus, M., Neves, R., 2008. Evaluating light and nutrient limitation in the tagus estuary using a process-oriented ecological model. *Proc. Inst. Mar. Eng. Sci. Technol. Part A J. Mar. Eng. Technol.* 43–54. <https://doi.org/10.1080/20464177.2008.11020213>
- Mateus, M., Riflet, G., Chambel, P., Fernandes, L., Fernandes, R., Juliano, M., Campuzano, F., de Pablo, H., Neves, R., 2012b. An operational model for the West Iberian coast: products and services. *Ocean Sci.* 8, 713–732. <https://doi.org/10.5194/os-8-713-2012>
- McWilliams, J.C., 1996. Modeling the oceanic general circulation. *Annu. Rev. Fluid. Mech.* 28, 215–248.
- Mellor, G.L., 1996. *Introduction to Physical Oceanography*. AIP Press. New York.
- Mellor, G.L., Yamada, T., 1982. Development of a turbulence closure model for geophysical fluid problems. *Rev. Geophys.* 20, 851–875. <https://doi.org/https://doi.org/10.1029/RG020i004p00851>
- Mishra, A.K., Coulibaly, P., 2009. Developments in hydrometric network design: a review. *Rev. Geophys.* 1–24. <https://doi.org/10.1029/2007RG000243>
- Moita, M.T., Oliveira, P.B., Mendes, J.C., Palma, A.S., 2003. Distribution of chlorophyll a and *Gymnodinium catenatum* associated with coastal upwelling plumes off central Portugal. *Acta Oecologica* 24, 125–132.
- Nagy, H., Elgindy, A., Pinardi, N., Zavatarelli, M., Oddo, P., 2017. A nested pre-operational model for the Egyptian shelf zone: Model configuration and validation/calibration. *Dyn. Atmos. Ocean.* 80, 75–96. <https://doi.org/10.1016/j.dynatmoce.2017.10.003>
- Neves, R., 1998. Programa de monitorização do emissário submarino da guia: modelação matemática.
- Neves, R., Marecos do Monte, H., Santos, C., Quintino, V., Matos, J., Zenha, H., 2002. *Integrated Wastewater Management in Coastal Areas* : pp. 16–20.
- Neves, R.J.J., 1985. *Étude Expérimentale et Modélisation des Circulations Transitoire et Résiduelle dans l’Estuaire du Sado*. Univ. Liège.
- Oey, L.Y., Chen, P., 1992. A nested-grid ocean model: With application to the simulation of meanders and eddies in the Norwegian Coastal Current. *J. Geophys. Res.* 97, 20 063–20 086. <https://doi.org/https://doi.org/10.1029/92JC01991>
- Orlanski, I., 1976. A simple boundary condition for unbounded hyperbolic flows. *J. Comput. Phys.* 21, 251–269. [https://doi.org/10.1016/0021-9991\(76\)90023-1](https://doi.org/10.1016/0021-9991(76)90023-1)
- Palma, E.D., Matano, R.P., 2000. On the implementation of open boundary conditions for a general circulation model: The three-dimensional case. *J. Geophys. Res.* 105, 8605–8627.
- Palma, E.D., Matano, R.P., 1998. On the implementation of passive open boundary conditions for a general circulation model: The barotropic mode. *J. Geophys. Res. Ocean.* 103, 1319–1341. <https://doi.org/10.1029/97jc02721>
- Peliz, Á., Dubert, J., Santos, A.M.P., Oliveira, P.B., Le Cann, B., 2005. Winter upper ocean circulation in the Western Iberian Basin - Fronts, Eddies and Poleward Flows: An overview. *Deep. Res. Part I Oceanogr. Res. Pap.* 52, 621–646. <https://doi.org/10.1016/j.dsr.2004.11.005>
- Peliz, Á., Rosa, T.L., Santos, A.M.P., Pissarra, J.L., 2002. Fronts, jets, and counter-flows in the Western

- Iberian upwelling system. *J. Mar. Syst.* 35, 61–77. [https://doi.org/10.1016/S0924-7963\(02\)00076-3](https://doi.org/10.1016/S0924-7963(02)00076-3)
- Perkins, A.L., 1997. A new nested boundary condition for a primitive equation ocean model. *J. Geophys. Res. C Ocean.* 102, 3483–3500. <https://doi.org/10.1029/96JC03246>
- Pham, V.S., Hwang, J.H., Ku, H., 2016. Optimizing dynamic downscaling in one-way nesting using a regional ocean model. *Ocean Model.* 106, 104–120. <https://doi.org/10.1016/j.ocemod.2016.09.009>
- Pinardi, N., Cavaleri, L., Coppini, G., De Mey, P., Fratianni, C., Huthnance, J., Lermusiaux, P.F.J., Navarra, A., Preller, R., Tibaldi, S., 2017. From weather to ocean predictions: An historical viewpoint. *J. Mar. Res.* 75, 103–159. <https://doi.org/10.1357/002224017821836789>
- Portela, L., 1996. Modelação matemática de processos hidrodinâmicos e da qualidade da água no estuário do Tejo.
- Qi, J., Chen, C., Beardsley, R.C., 2018. FVCOM one-way and two-way nesting using ESMF: Development and validation. *Ocean Model.* 124, 94–110. <https://doi.org/10.1016/j.ocemod.2018.02.007>
- Quaresma, L.S., Pichon, A., 2013. Modelling the barotropic tide along the West-Iberian margin. *J. Mar. Syst.* 109–110, S3–S25. <https://doi.org/10.1016/j.jmarsys.2011.09.016>
- Rhomad, H., Khalil, K., Neves, R., Bougadir, B., Elkalay, K., 2021. Modeling investigation of the nutrients and phytoplankton dynamics in the Moroccan Atlantic coast: A case study of Agadir coast. *Ecol. Modell.* <https://doi.org/10.1016/j.ecolmodel.2021.109510>
- Richardson, L.F., 1922. *Weather Prediction by Numerical Process*. Cambridge University Press, Cambridge, England.
- Riflet, G., 2010. Downscaling large-scale ocean-basin solutions in coastal tri-dimensional hydrodynamic models. PhD thesis. Technical University of Lisbon, Portugal.
- Robinson, A.R., Carton, J.A., Mooers, C.N.K., Walstad, L.J., Carter, E.F., Rienecker, M.M., Smith, J.A., Leslie, W.G., 1984. A real-time dynamical forecast of ocean synoptic/mesoscale eddies. *Nature* 309, 781–783. <https://doi.org/10.1038/309781a0>
- Rodrigues, D.A., Teles, M., Leendertse, J.J., 1982. Numerical modeling of the Tejo Estuary for currents and water quality predictions. RAND Corporation PP - Santa Monica, CA.
- Roe, P.L., 2003. Characteristic-Based Schemes for the Euler Equations. *Annu. Rev. Fluid Mech.* <https://doi.org/10.1146/annurev.fl.18.010186.002005>
- Ruiz-Parrado, I., Genua-Olmedo, A., Reyes, E.; Murre, B., Rotllán, P.; Lorente, P., García-Sotillo, M., Tintoré, J., 2020. Coastal ocean variability related to the most extreme Ebro River discharge over the last 15 years. Section in Copernicus Marine Service Ocean State Report, Issue 4. *J. Oper. Ocean.* s160–s165.
- Ruiz-Villarreal, M., 2002. Hydrodynamic Model Study of the Ria de Pontevedra Under Estuarine Conditions. *Estuar. Coast. Shelf Sci.* 54, 101–113. <https://doi.org/10.1006/ecss.2001.0825>
- Ruiz Villarreal, M., Bolding, K., Burchard, H., Demirov, E., 2005. Coupling of the GOTM turbulence module to some three-dimensional ocean, in: H.Z. Baumert, J.H.S. & J.S. (Ed.), *Marine Turbulence: Theories, Observations, and Models - Results of the CARTUM Project*. Cambridge University Press., pp. 225–237.
- Salomons, W., 2005. Sediments in the catchment-coast continuum. *J. Soils Sediments* 5, 2–8. <https://doi.org/10.1065/jss2005.01.129>

- Sannino, G., Herrmann, M., Carillo, A., Rupolo, V., Ruggiero, V., Artale, V., Heimbach, P., 2009. An eddy-permitting model of the Mediterranean Sea with a two-way grid refinement at the Strait of Gibraltar. *Ocean Model.* 30, 56–72. <https://doi.org/10.1016/j.ocemod.2009.06.002>
- Santos, a, Martins, H., Coelho, H., Leitão, P., Neves, R., 2002. A circulation model for the European ocean margin. *Appl. Math. Model.* 26, 563–582. [https://doi.org/10.1016/S0307-904X\(01\)00069-5](https://doi.org/10.1016/S0307-904X(01)00069-5)
- Santos, A., 1995. Modelo hidrodinâmico tridimensional de circulação oceânica e estuarina. PhD thesis. Technical University of Lisbon, Portugal.
- Santos, A.M.P., Chícharo, A., Dos Santos, A., Moita, T., Oliveira, P.B., Peliz, Á., Ré, P., 2007. Physical-biological interactions in the life history of small pelagic fish in the Western Iberia Upwelling Ecosystem. *Prog. Oceanogr.* 74, 192–209. <https://doi.org/10.1016/j.pocean.2007.04.008>
- Santos, A.M.P., Peliz, A., Dubert, J., Oliveira, P.B., Angélico, M.M., Ré, P., 2004. Impact of a winter upwelling event on the distribution and transport of sardine (*Sardina pilchardus*) eggs and larvae off western Iberia: A retention mechanism. *Cont. Shelf Res.* 24, 149–165. <https://doi.org/10.1016/j.csr.2003.10.004>
- Saraiva, S., 2014. Modelling bivalves in estuaries and coastal areas. PhD thesis. University of Lisbon, Portugal.
- Smith, V.H., Schindler, D.W., 2009. Eutrophication science: where do we go from here? *Trends Ecol. Evol.* 24, 201–207. <https://doi.org/10.1016/j.tree.2008.11.009>
- Sobrinho, J., de Pablo, H., Campuzano, F., Neves, R., 2021a. Coupling Rivers and Estuaries with an Ocean Model: An Improved Methodology. *Water* 13, 2284. <https://doi.org/10.3390/w13162284>
- Sobrinho, J., de Pablo, H., Pinto, L., Neves, R., 2021b. Improving 3D-MOHID water model with an upscaling algorithm. *Environ. Model. Softw.* 135. <https://doi.org/10.1016/j.envsoft.2020.104920>
- Sotillo, M.G., Campuzano, F., Guihou, K., Lorente, P., Olmedo, E., Matulka, A., Santos, F., Amo-Baladrón, M.A., Novellino, A., 2021a. River freshwater contribution in operational ocean models along the european atlantic façade: Impact of a new river discharge forcing data on the cmems ibi regional model solution. *J. Mar. Sci. Eng.* 9. <https://doi.org/10.3390/jmse9040401>
- Sotillo, M.G., Mourre, B., Mestres, M., Lorente, P., Aznar, R., García-León, M., Liste, M., Santana, A., Espino, M., Álvarez, E., 2021b. Evaluation of the Operational CMEMS and Coastal Downstream Ocean Forecasting Services During the Storm Gloria (January 2020). *Front. Mar. Sci.* 8, 1–27. <https://doi.org/10.3389/fmars.2021.644525>
- Spall, M. a., Holland, W.R., 1991. A Nested Primitive Equation Model for Oceanic Applications. *J. Phys. Oceanogr.* 21, 205–220. [https://doi.org/10.1175/1520-0485\(1991\)021<0205:ANPEMF>2.0.CO;2](https://doi.org/10.1175/1520-0485(1991)021<0205:ANPEMF>2.0.CO;2)
- Spall, M.A., Robinson, A.R., 1989. A new open ocean, hybrid coordinate primitive equation model. *Math. Comput. Simul.* 31, 241–269. [https://doi.org/10.1016/0378-4754\(89\)90162-6](https://doi.org/10.1016/0378-4754(89)90162-6)
- Stark, J.D., Donlon, C.J., Martin, M.J., McCulloch, M.E., 2007. OSTIA: An operational, high resolution, real time, global sea surface temperature analysis system. *Ocean. 2007 - Eur.* <https://doi.org/10.1109/oceanse.2007.4302251>
- Teles-Machado, A., Peliz, Á., McWilliams, J.C., Couvelard, X., Ambar, I., 2016. Circulation on the Northwestern Iberian Margin: Vertical structure and seasonality of the alongshore flows. *Prog. Oceanogr.* 140. <https://doi.org/10.1016/j.pocean.2015.05.021>
- Trancoso, A.R., 2012. Operational Modelling as a Tool in Wind Power Forecasts and Meteorological

- Warnings. Instituto Superior Técnico - Universidade de Lisboa.
- Urrego-Blanco, J., Sheng, J., 2014. Study on subtidal circulation and variability in the Gulf of St. Lawrence, Scotian Shelf, and Gulf of Maine using a nested-grid shelf circulation model. *Ocean Dyn.* 64, 385–412. <https://doi.org/10.1007/s10236-013-0688-z>
- Urrego-Blanco, J., Sheng, J., Dupont, F., 2016. Performance of One-Way and Two-Way Nesting Techniques Using the Shelf Circulation Modelling System for the Eastern Canadian Shelf. *Atmos. - Ocean* 54, 75–92. <https://doi.org/10.1080/07055900.2015.1130122>
- Vallis, G.K., 2016. Geophysical fluid dynamics: Whence, whither and why? *Proc. R. Soc. A Math. Phys. Eng. Sci.* 472. <https://doi.org/10.1098/rspa.2016.0140>
- van Leer, B., 1979. Towards the ultimate conservative difference scheme. V. A second-order sequel to Godunov's method. *J. Comput. Phys.* 32, 101–136. [https://doi.org/10.1016/0021-9991\(79\)90145-1](https://doi.org/10.1016/0021-9991(79)90145-1)
- van Leer, B., 1974. Towards the ultimate conservative difference scheme. II. Monotonicity and conservation combined in a second-order scheme. *J. Comput. Phys.* 14, 361–370. [https://doi.org/10.1016/0021-9991\(74\)90019-9](https://doi.org/10.1016/0021-9991(74)90019-9)
- Vandenbulcke, L., Barth, A., 2019. Upscaling of a local model into a larger-scale model. *Ocean Sci.* 15, 291–305. <https://doi.org/10.5194/os-15-291-2019>
- Vaz, N., Mateus, M., Pinto, L., Neves, R., Dias, J.M., 2020. The tagus estuary as a numerical modeling test bed: A review. *Geosci.* <https://doi.org/10.3390/geosciences10010004>
- Vaz, N., Mateus, M., Plecha, S., Sousa, M.C., Leitão, P.C., Neves, R., Dias, J.M., 2015. Modeling SST and chlorophyll patterns in a coupled estuary-coastal system of Portugal: The Tagus case study. *J. Mar. Syst.* 147, 123–137. <https://doi.org/10.1016/j.jmarsys.2014.05.022>
- Verelst, N., 2008. Variability of water fluxes off Portugal derived from an operational model. MSc dissertation thesis. Instituto Superior Técnico, Technical University of Lisbon, Portugal; Université de Liège, Belgium.
- Viegas, C.N., Nunes, S., 2009. Streams contribution on bathing water quality after rainfall events in Costa do Estoril- a tool to implement an alert system for bathing water quality. *J. Coast. Res.* 2009.
- Ward, N.D., Megonigal, J.P., Bond-Lamberty, B., Bailey, V.L., Butman, D., Canuel, E.A., Diefenderfer, H., Ganju, N.K., Goñi, M.A., Graham, E.B., Hopkinson, C.S., Khangaonkar, T., Langley, J.A., McDowell, N.G., Myers-Pigg, A.N., Neumann, R.B., Osburn, C.L., Price, R.M., Rowland, J., Sengupta, A., Simard, M., Thornton, P.E., Tzortziou, M., Vargas, R., Weisenhorn, P.B., Windham-Myers, L., 2020. Representing the function and sensitivity of coastal interfaces in Earth system models. *Nat. Commun.* 11, 1–14. <https://doi.org/10.1038/s41467-020-16236-2>
- Williams, J.J., Esteves, L.S., 2017. Guidance on Setup, Calibration, and Validation of Hydrodynamic, Wave, and Sediment Models for Shelf Seas and Estuaries. *Adv. Civ. Eng.* 2017, 5251902. <https://doi.org/10.1155/2017/5251902>
- Williamson, D.L., Browning, G.L., 1974. Formulation of the Lateral Boundary Conditions for the Near Limited-Area Model. *J. Appl. Meteorol.* 13, 8–16. [https://doi.org/10.1175/1520-0450\(1974\)013<0008:FOTLBC>2.0.CO;2](https://doi.org/10.1175/1520-0450(1974)013<0008:FOTLBC>2.0.CO;2)
- Wunsch, C., Ferrari, R., 2018. 100 Years of the Ocean General Circulation. *Meteorol. Monogr.* 59, 7.1-7.32. <https://doi.org/10.1175/amsmonographs-d-18-0002.1>
- Yin, Y., Karunarathna, H., Reeve, D.E., 2019. Numerical modelling of hydrodynamic and

morphodynamic response of a meso-tidal estuary inlet to the impacts of global climate variabilities. *Mar. Geol.* 407, 229–247. <https://doi.org/10.1016/j.margeo.2018.11.005>

Annex

1 An operational system for the Canary Islands and Moroccan coast

The need for regional cooperation in the NE Atlantic to face marine pollution has been previously demonstrated by historic accidents in the Spanish, Moroccan, French and Portuguese coasts. The Lisbon Agreement, recently ratified (2014) by the mentioned countries and the EU, envisions the cooperation in the case of pollution incidents. Transnational strategies to face marine pollution with hazardous and noxious substances, (HNS) and especially with oil spills, have been under development in different regions in the context of international agreements and EU RTD projects. However, the sub-region in the Atlantic involving Morocco, Madeira and Canary Islands has not been similarly prepared in an integrated manner.

The MARPOCS Interreg MED project proposed to fill this gap. Its overarching goal was to take advantage of previously developed work at international and EU level in different aspects of accidental marine pollution with a view to developing and implementing an integrated operational framework for preparedness and response to oil and HNS spills in the Atlantic sub-region involving Morocco, Madeira and Canary Islands in the context of Lisbon Agreement, making it easily transferable and extendable to other areas.

The objectives were achieved through:

- Operational and tactical model-based DSSs supported by the 3D oil and HNS spill modelling system, using new and/or improved high resolution meteocean forecasting systems;
- Automatic early warning spill forecasting connected to existing maritime surveillance automatic services (EMSA's CLEANSEANET service: satellite-based oil spill detection);
- Training sessions, courses, drills and hands-on demonstrations, with special focus on emergency preparedness or response scenarios involving multiple nations;
- Characterisation of typical and dynamic shoreline holistic risk from spills in the area of interest (in order to identify "hot spots", to improve management of the distribution of response resources, and to allow real time risk shoreline monitoring).

One of the outcomes of the project was the Marpocs platform (<http://marpocs.eu/tools>), an interface to forecast spill behaviour and impacts, supporting tactical preparedness and response to oil and

HNS spill events. The platform gathers meteorological and ocean model forecasts, including wind, waves, currents, field data, AIS data, and coastal sensitivity indexes, and the tool runs in a dedicated server. As such, users can simulate oil and HNS spills directly in the platform, without having to run them with their own resources. Knowing the location, substance and amount spilled, the platform is able to simulate the spills' trajectory and potential impact on land – through the association with coastal sensitivity indexes.

The publication in the MARPOCS platform of the metocean model forecasts in the 3 areas of study are made available on a daily basis and the model results can be used in safety and marine pollution model-based decision support tools.

All of the MOHID hydrodynamic model domains were implemented in the course of drafting of this thesis and a description of the system as well as some of the validations performed are presented next. The hydrodynamic model results produced during this project were later used to study the biogeochemical cycle off the coast of Agadir, Morocco (Rhomad et al., 2021).

1.1 The operational modelling system

The implemented model domains (Figure 70) include:

- A 4 km resolution regional domain covering the Madeira and Canary Islands, and a part of the western coast of Morocco;
- A 2 km resolution local domain for the Canary Islands nested in the 4 km domain;
- A 500 m resolution local domain for the northeast part of Gran Canary;
- A 100 m high resolution local domain for the Las Palmas port;
- A 2 km resolution local domain for the Agadir region in Morocco;
- A 500 m resolution local domain for the Agadir port nested in the 2 km resolution domain for the Agadir region;

The size and reach of these domains are given in Table 19.

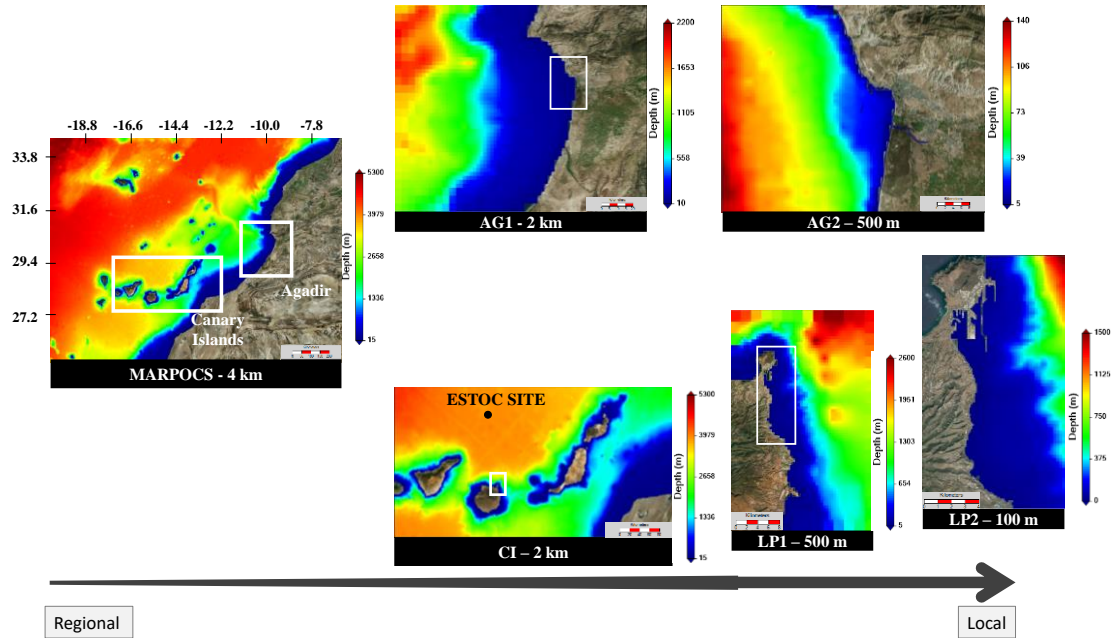


Figure 70: Model domains implemented for the MARPOCS project.

All bathymetries were obtained using a linear inverse weight distance method (IWD) for the interpolation of bathymetric points into the model grid. The bathymetric data used for the 4 km resolution domain included SRTM15 data with a resolution of approximately 200 m, as well as data provided by the University of Las Palmas de Gran Canaria. To generate the bathymetries of the local Canary Islands domains, a combination of the SRTM15 and data provided by the University of Las Palmas was used. The Agadir domains were created with a combination of SRTM15 data and data from the National Institute for Fisheries Research (INRH).

Table 19: Implemented domain grids.

Domain Name	Step	Cells	Min Depth	Max Depth	Min Lon	Max Lon	Min Lat	Max Lat
TIDE	4 km	248x369	15	5300	-20.98	-6.40	24.83	34.74
MARPOCS	4 km	238x359	15	5300	-20.79	-6.51	25.04	34.55
CI	2 km	118x250	15	4080	-17.27	-12.27	27.35	29.71
AG1	2 km	56x56	15	2133	-10.67	-9.63	29.74	30.86
AG2	500 m	24x21	5	133	-9.91	-9.61	30.23	30.55

The shapefile used to build the land mask was retrieved from NOAA and refined locally with Google Earth, data from the University of Las Palmas (Canary) and the INRH (Morocco). All the bathymetries were created with the same land mask.

Vertical grid

The vertical discretization of all modelling domains is identical from the water surface to the bottom, the difference being the total depth and, thus, the number of vertical layers. The TIDE domain has a 2D geometry consisting of one sigma layer. MARPOCS domain is nested in the TIDE domain. It is a regional baroclinic model with 7 sigma layers at the surface (up to 8.68 m) and 43 Cartesian layers below. Domains AG1 and AG2 have 40 and 24 layers respectively, 7 of which are sigma layers at the surface. Domains CI, LP1 and LP2 vertical discretization include 7 sigma layers at the top plus 44, 42 and 39 Cartesian layers respectively.

Tide

Tidal boundary conditions were obtained from the FES 2012 (Finite Element Solution) tide model (Carrere et al., 2013), based on a hydrodynamic model that assimilates tide gauges and altimeter data (Topex/ Poseidon, Jason-1, Jason-2, ERS-1, ERS-2 and ENVISAT). The FES 2012 model comprises global coverage of tidal components at a resolution of $1/16^\circ$. Water level at the open boundary of the TIDE domain was obtained from tidal components extracted from FES2012.

Open boundary conditions

Open boundary conditions were considered from Mercator-Ocean [GLOBAL ANALYSIS FORECAST PHY 001 024](#) for the North Atlantic region at a spatial resolution of 8x8 km. The vertical resolution of the database includes 50 vertical layers between 0-6000 m. The database contains the average daily distribution of temperature, salinity, velocity, and water level.

The open boundary conditions for MARPOCS were defined by interpolating the Mercator-Ocean solution over the MARPOCS grid. Domains CI and AG1 receive their boundary conditions from the MARPOCS domain, AG2 from AG1, LP1 from CI and LP2 from LP1.

All boundary conditions include the combination of barotropic Flather radiation scheme with the flux relaxation scheme, as well as a higher viscosity (sponge layer) with exponential increase from the 10th cell of the child domain up to the boundary cells. In order to remove high frequency oscillations a biharmonic filter was also added.

All the domains were run using the downscaling approach in an offline manner, where windows of results were generated from each model with a time frequency of 900s for the correspondent nested domains to use in the open boundary conditions.

Atmospheric forcing

Atmospheric data was provided by a WRF solution with hourly results implemented by project partner ActionModulers and covered the entire MARPOCS domain. This data included atmospheric pressure, wind velocity, solar radiation, air temperature, relative humidity, downward long wave radiation, PBL Height and Albedo, and was interpolated to the MAPROCS domain grid in HDF5 format.

Two other domains were nested into the 9 km domain WRF, both with a resolution of 3 km. The first covers the area for the Canary Islands and the second covers the Agadir region. This data was then interpolated to the ocean model domains. The WRF with 3 km resolution for Agadir, together with the 9 km solution were interpolated into the AG2 domain, as the higher resolution WRF model for Agadir did not cover the entire area of AG2.

A summary of the implementation characteristics applied to the different domains is presented in table x (Agadir domains) and y (Canary Islands domains).

Table 20: Model setup configuration for the various implemented domains.

Settings	MARPOCS	AG1	AG2	CI	LP1	LP2
Model characteristics	3D - Baroclinic					
Bathymetry	SRTM15 + U. Las Palmas	SRTM15 + INRH		SRTM15 + U. Las Palmas		
Horizontal Grid	Regular (4 km)	Regular (2 km)	Regular (500 m)	Regular (2 km)	Regular (500 m)	Regular (500 m)
Vertical Grid	7 Sigma (0 - 8.68 m)	7 Sigma (0 - 8.68 m)		7 Sigma (0 - 8.68 m)		
	43 Cartesian	40 Cartesian	24 Cartesian	44 Cartesian	42 Cartesian	39 Cartesian
Δt	60 s	30 s	15 s	30 s	10 s	5 s
Tides	FES2012	MARPOCS	AG1	MARPOCS	CI	LP1
OBC Water	Mercator-Ocean	MARPOCS	AG1	MARPOCS	CI	LP1
Nudging	...	Flow relaxation scheme of 10 cells with a time decay of 1 week.				
OBC Atmosphere	WRF (9 km)	WRF (9 km + 3 km)	WRF (3 km)	WRF (9 km)	WRF (3 km)	
Turbulence	GOTM					
Viscosity m^2s (OB/Interior)	50000 / 150	8000 / 100	1000 / 60	8000 / 100	2500 / 50	500 / 10
Bottom rugosity	0.0025 $m^2 s^{-1}$					

Automation and forecast implementation

All the domains run once per day when new results of meteorological data (WRF) are produced by action modulers in their servers. The data is transferred via an FTP protocol and saved in the Maretec storage server. Results from WRF are then copied automatically to a storage server when a new WRF file appears in the Maretec's FTP server. All simulations are initiated via the Windows task manager and upon the start of the simulation results from WRF are copied from the storage server into the server where simulations are run. The simulation period did not consider a hindcast period and ran only 2 days into the future due to the lack of meteorological forcing (WRF only runs forecasts and does not repeat the previous day). Once the MOHID results are generated, they are sent to the FTP server and sent to the ActionModulers servers to be fed into the MARPOCS platform.

1.2 Validation

The validation of the modelling system included data from a tide gauge located in the port of Las Palmas de Gran Canaria, temperature and salinity profiles provided by PLOCAN through the ESTOC site near the Canary islands (<http://www.fixo3.eu/observatory/estoc/>), Argo profiles, and remote sensing of SST.

1.2.1 Water level

Water level was validated against a tide gauge located near the port of Las Palmas – the data of which was obtained through the CMEMS website – for two periods of two weeks, one for April 2017 and the second for the period between 15 August and 1 September 2017. Only the second period is shown in this thesis as the LP2 domain (with 100 m) was only initiated at on 1 June 2017. Results are presented in Figure 71 and demonstrate the ability of the model configurations to represent the water level, with small differences between the CI and the LP2 domains. The MARPOCS and LP1 domains were not included because the first has a very low resolution and the latter is just a transition for LP2 (and results would be quite similar).

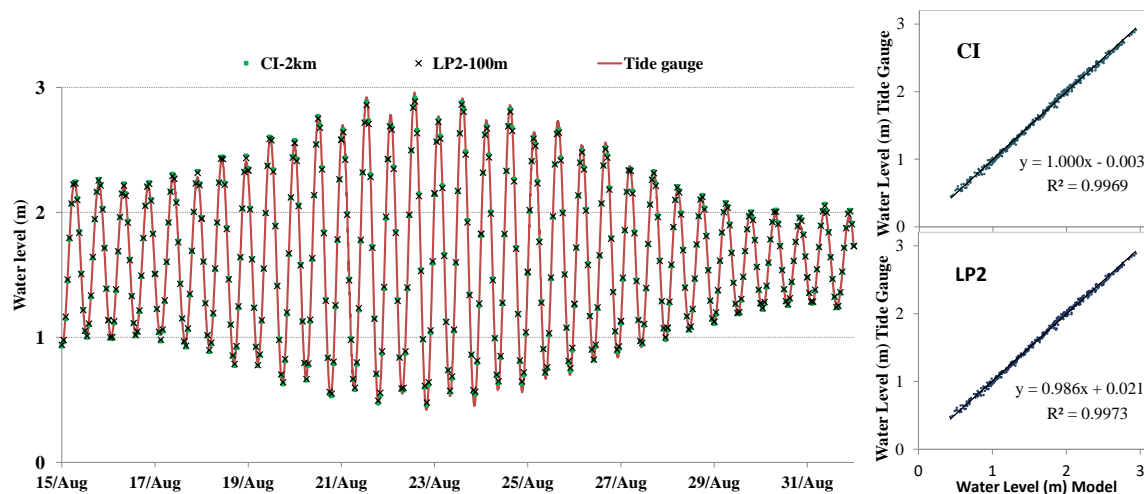


Figure 71: Water level obtained by LP1 and LP2 domains and by the tide gauge.

1.2.2 Vertical profiles

Vertical profiles from in situ measurements were provided by PLOCAN for two consecutive days and compared to the model results in Figure 72. For a broader validation, Argo buoys profiles were

compared to the MARPOCS and CI domain, the results of which are presented in Figure 73 and Figure 74.

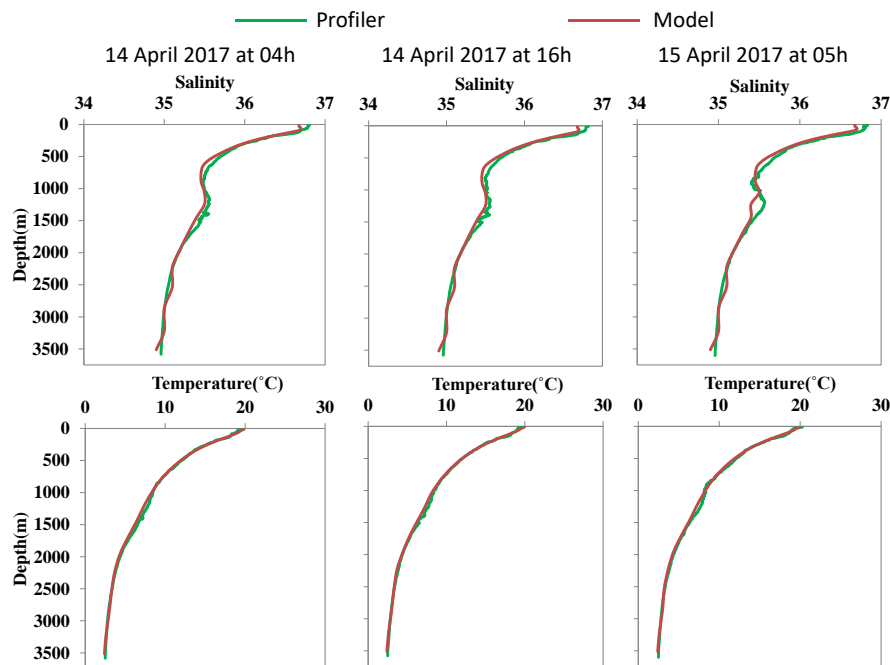


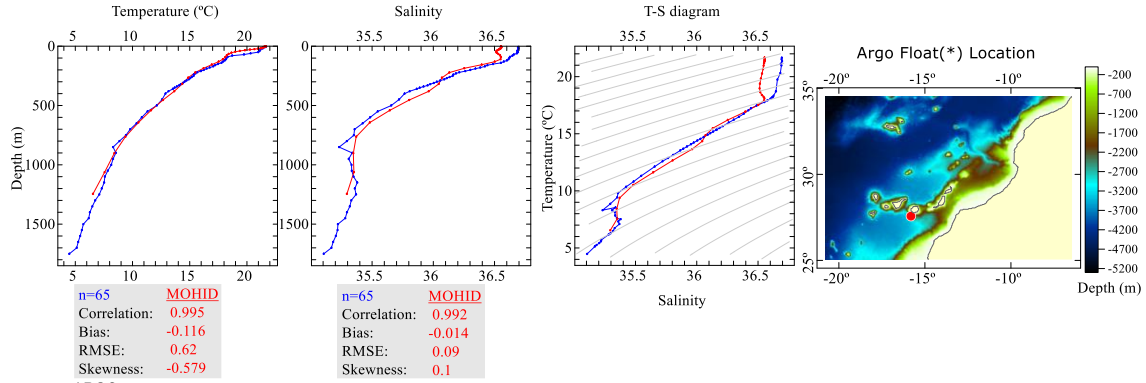
Figure 72: Vertical profiles from the PLOCAN field campaign and MARPOCS model domain for the three samplings made by PLOCAN.

All the profiles – be them from PLOCAN or from ARGO buoys – show that the model was able to accurately represent the vertical structure of the water column, as correlations obtained by the comparison of model results with ARGO floats are all above 0.994. Bias values for temperature and salinity did not drop below 0.142 °C and 0.028 respectively. On the 15th of May there is a small salinity and temperature difference (0.1 and 1°C respectively) between model results and ARGO at the surface layers – for salinity this difference extends to 450 m. However, this location is closer to land (Gran Canaria Island) which could affect model results due to its low grid resolution. A proof of the importance of the bathymetric resolution is the improved results provided by the 2 km CI domain. Its results show a stronger correlation – 0.998 and 0.995 for temperature and salinity respectively as opposed to 0.995 and 0.992 – than the results obtained by the MARPOCS domain. Although the BIAS increased, the RMSE values decreased which also shows an improvement of the overall results.

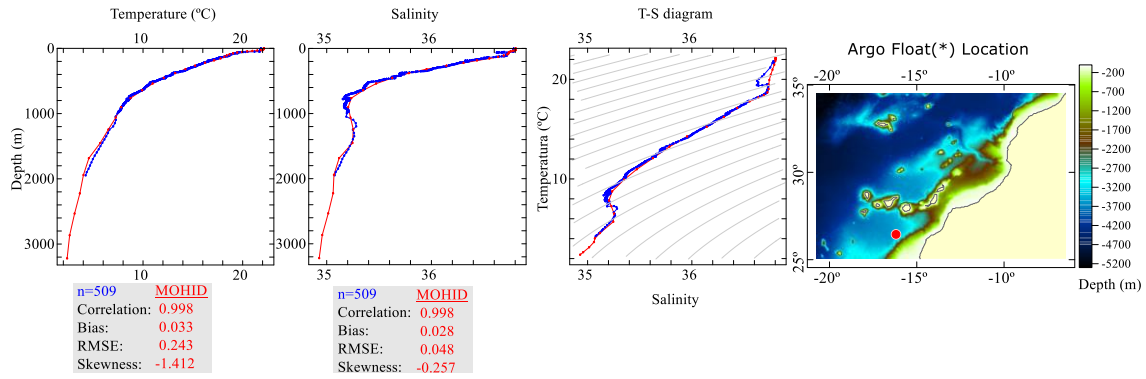
ANNEX

ARGO 
 MOHID 

Time: 15-May-2017 14:44
 Location: 27.57°N , 15.812°W
 Id: 6901240 Cycle No. 113(A)



Time: 19-May-2017 14:44
 Location: 26.448°N , 16.19°W
 Id: 6901165 Cycle No. 110(A)



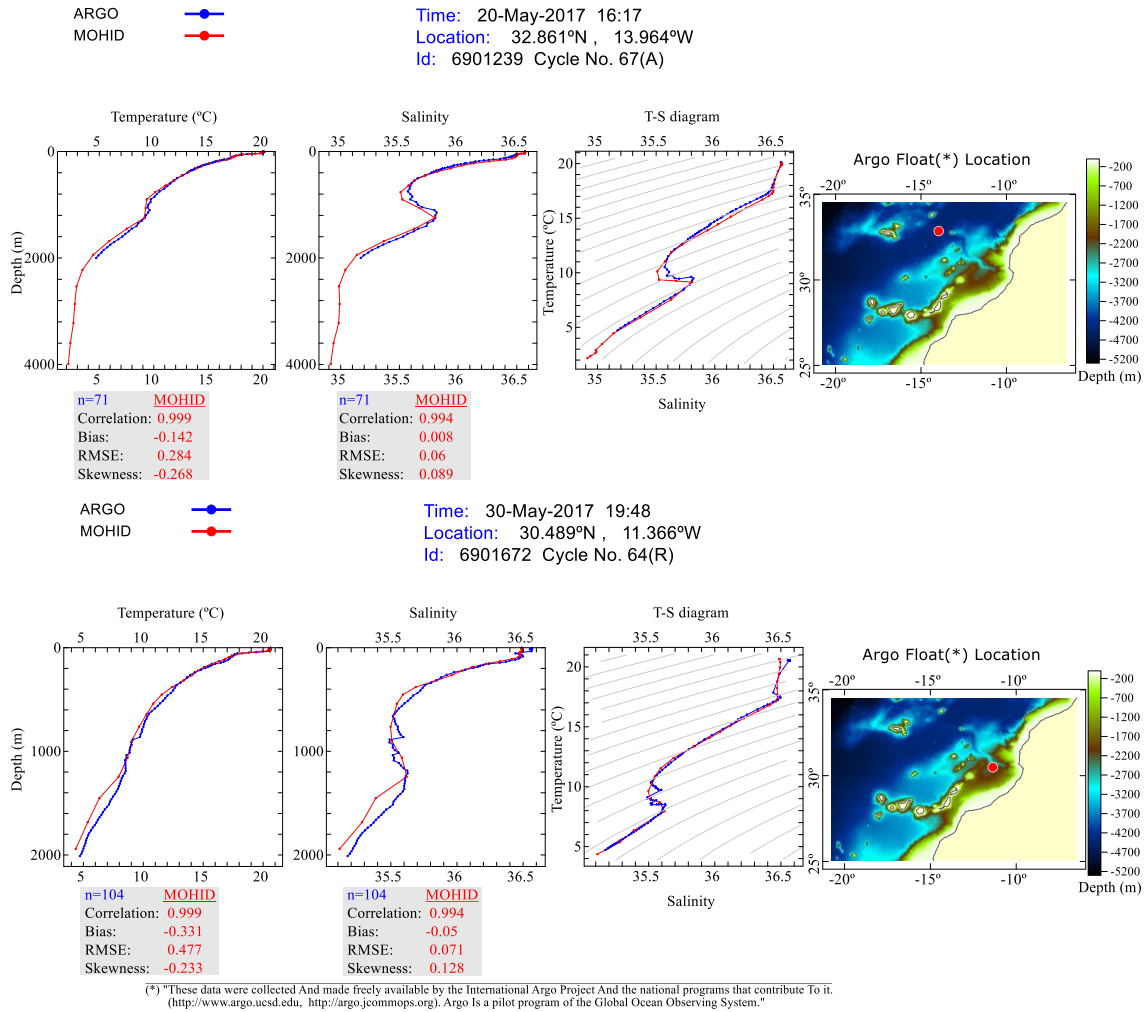


Figure 73: Comparison between profiles obtained with ARGO buoys and MARPOCS modelling domain.

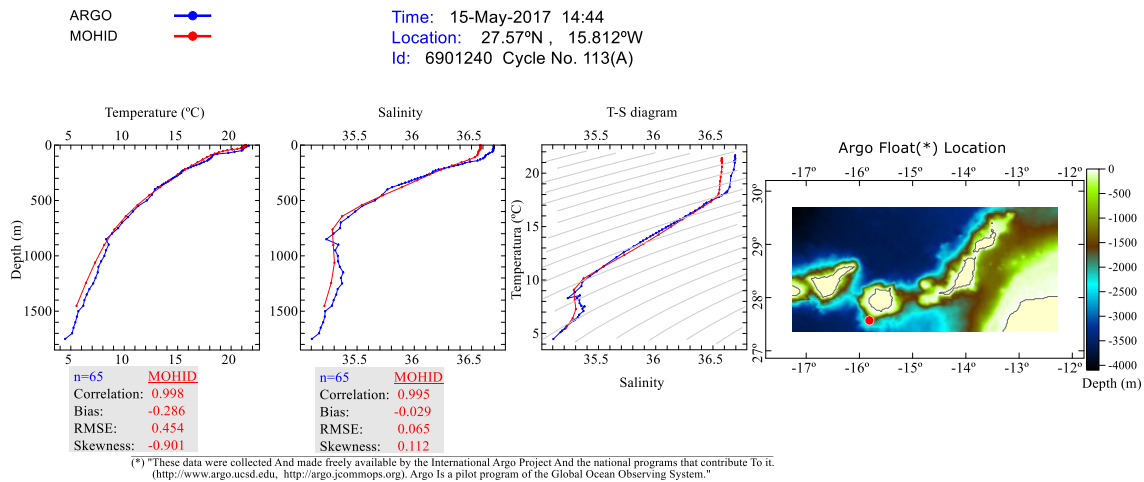


Figure 74: Comparison between profiles obtained with ARGO buoys and the CI modelling domain for 15 May 2017

1.2.3 Remote sensing

Remote sensing validation was performed for surface temperature using satellite data from the [FUSION](#) solution, which has a grid resolution of 9-10 km and produces daily images. One year of model results were used for the validation starting in March 2019 until March 2020. Other time periods were initially considered, but due to the loss of model data (disk corruption) older periods are not presented. This did not affect the profile validations because the original validation process was done in another disk along with its results. The analysed period was divided between seasons, and computation of BIAS, R^2 and RMSE were computed as averages as well as its evolution over time. Results are presented in Figure 76, ordered by season (spring, summer, autumn and winter) and demonstrate the ability of the model to represent the spatial-temporal variations in temperature, with correlations of 0.899, 0.718, 0.899 and 0.646, mean BIAS of 0.07, -0.092, -0.041 and -0.08, and mean RMSE of 0.345, 0.419, 0.445 and 0.435 respectively. For the Moroccan coast, results suggest a more or less constant upwelling, although with more intensity during the summer where the temperature gradient from coast to open ocean was around 3-4 °C. These results are in agreement with (Gómez-Letona et al., 2017), who include this region in a permanent (20 °N) and weak permanent (°N) upwelling area (Figure 75). The highest source of error is located near AGADIR and may be caused by the combination of coastal orography and bathymetric resolution.

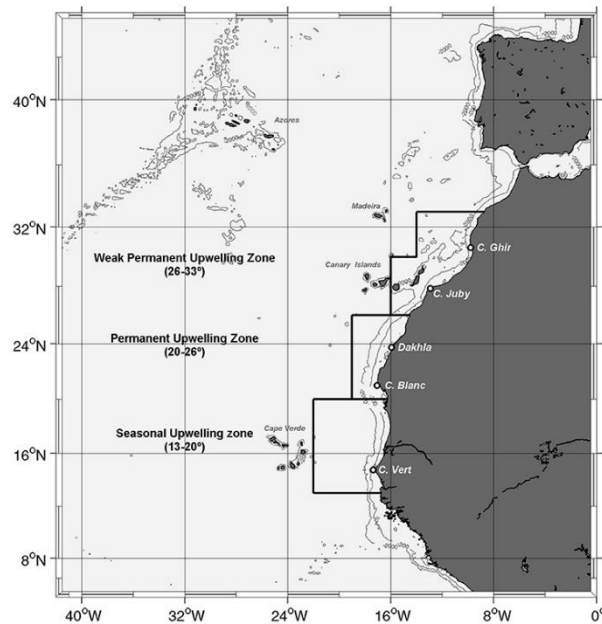
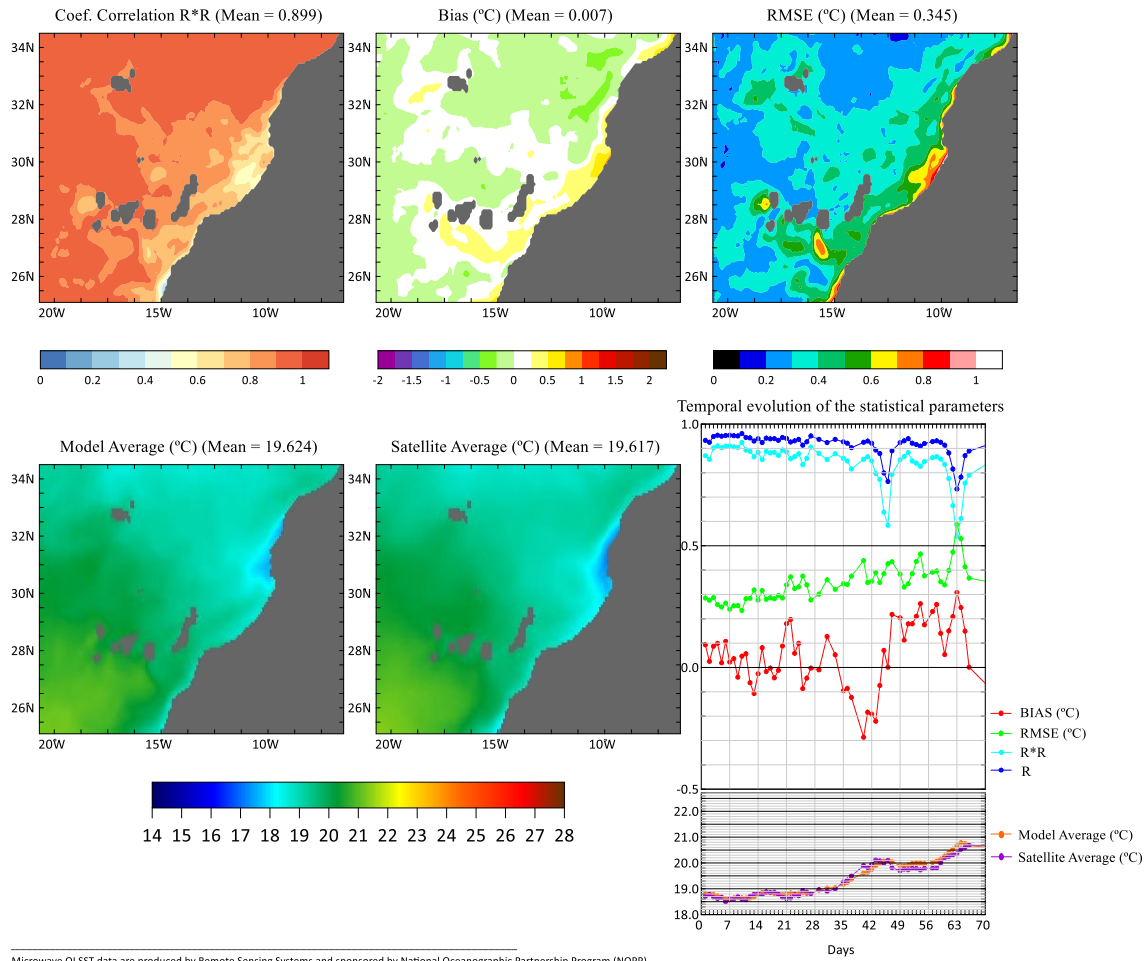


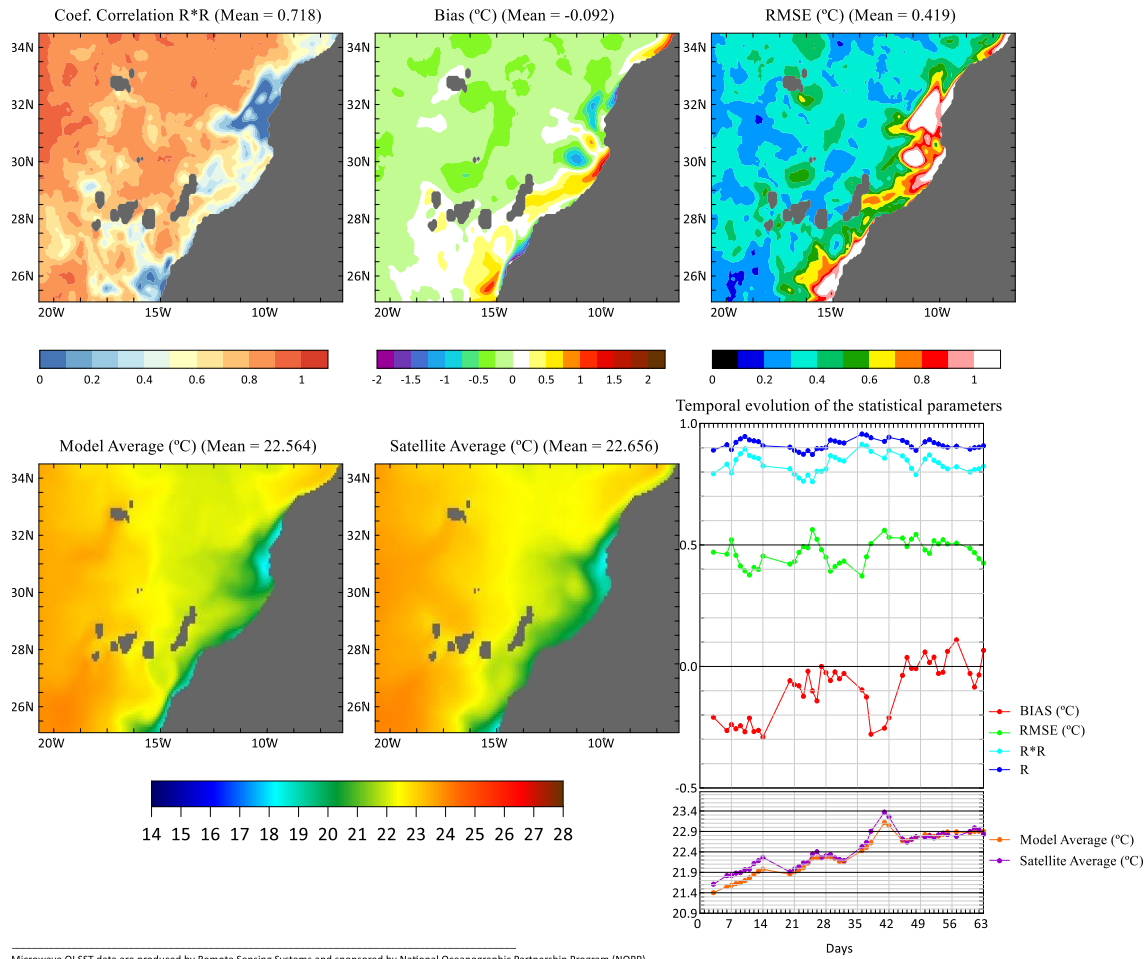
Figure 75: Seasonal, permanent and weak permanent upwelling zones in the west coast of Africa, where a good part of the MARPOCS domain is located. From: (Gómez-Letona et al., 2017).

MOHID SST vs Satellite SST (Microwave + Infra-red)(*)



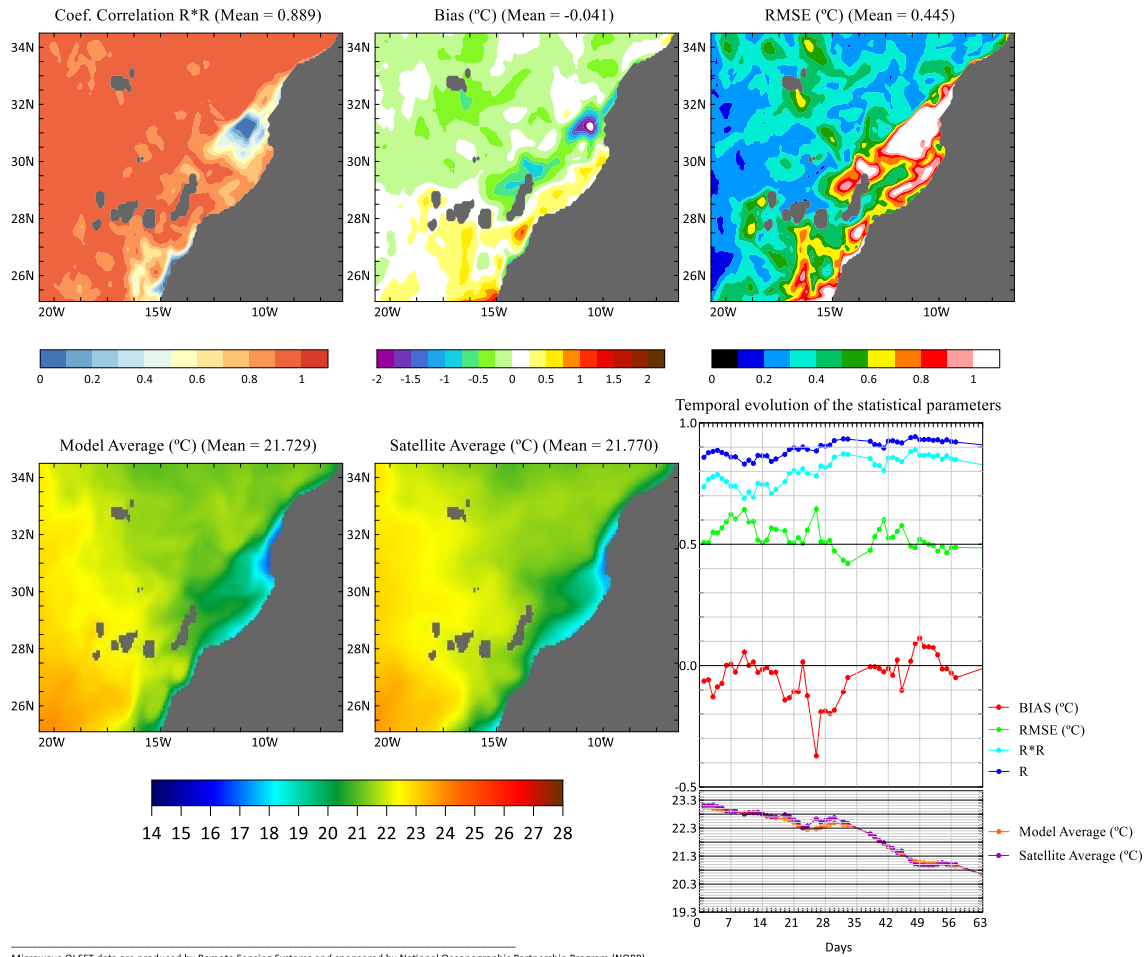
Microwave OI SST data are produced by Remote Sensing Systems and sponsored by National Oceanographic Partnership Program (NOPP) NASA Earth Science Physical Oceanography Program and the NASA REASoN DISCOVER Project.
 * are available at www.remss.com.

MOHID SST vs Satellite SST (Microwave + Infra-red)(*)



Microwave OI SST data are produced by Remote Sensing Systems and sponsored by National Oceanographic Partnership Program (NOPP) NASA Earth Science Physical Oceanography Program and the NASA REASoN DISCOVER Project. Data are available at www.remss.com.

MOHID SST vs Satellite SST (Microwave + Infra-red)(*)



Microwave OI SST data are produced by Remote Sensing Systems and sponsored by National Oceanographic Partnership Program (NOPP) NASA Earth Science Physical Oceanography Program and the NASA REASoN DISCOVER Project.
 * are available at www.remss.com.

MOHID SST vs Satellite SST (Microwave + Infra-red)(*)

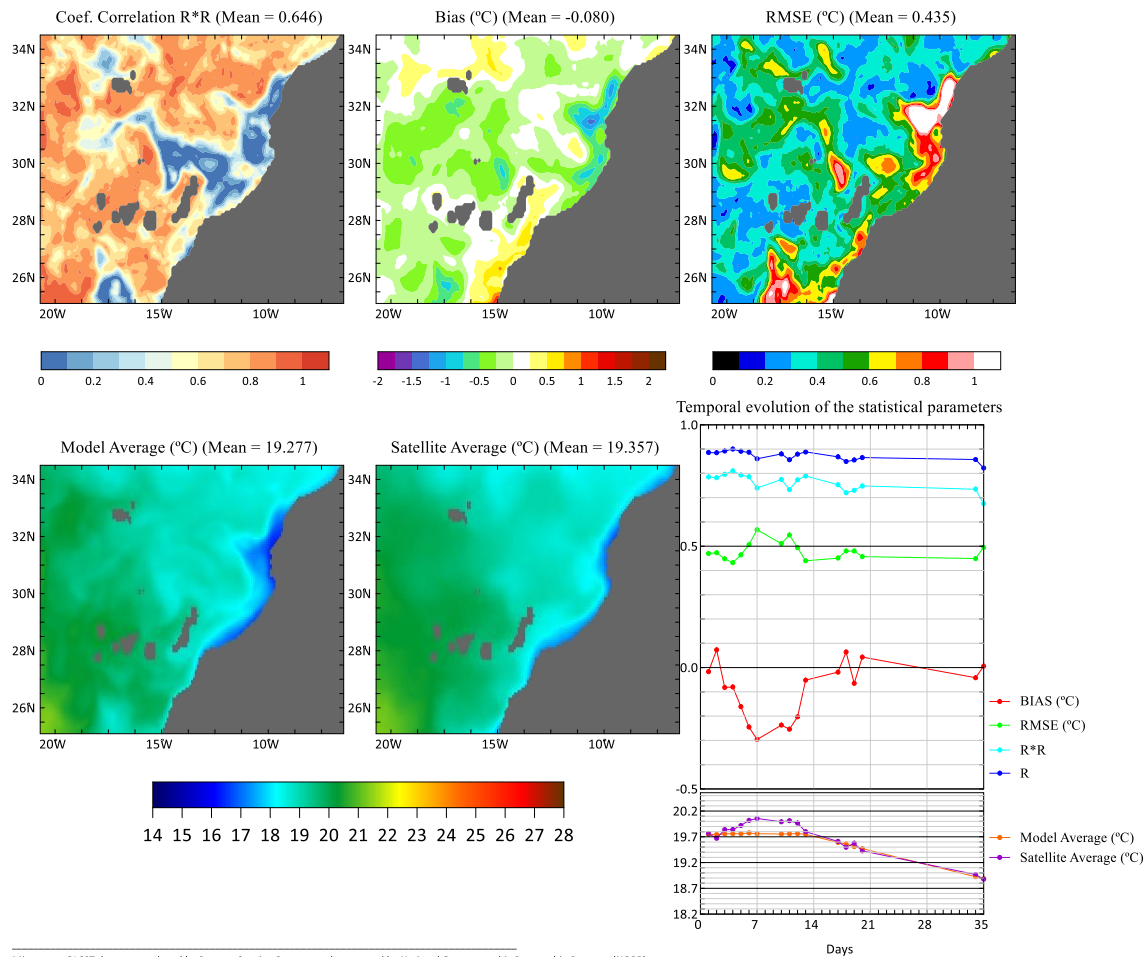


Figure 76: Comparison between surface temperature obtained by the MARPOCS model domain and Fusion satellite product over (from top to bottom): spring, summer, autumn and winter.

1.3 Residual circulation

Residual circulation of the entire area was produced with the 4 km grid MARPOCS domain in order to identify the major surface currents at play (Figure 77). The most important feature in the entire domain is the Canary Current near the west coast of Africa which funnels between the Fuerteventura Island and the Moroccan coast due to the lower depths of the ocean platform. This funnelling intensifies the currents to a velocity near 0.5 ms^{-1} and is an area with intense maritime traffic – an important reason for the implementation of the MARPOCS project.

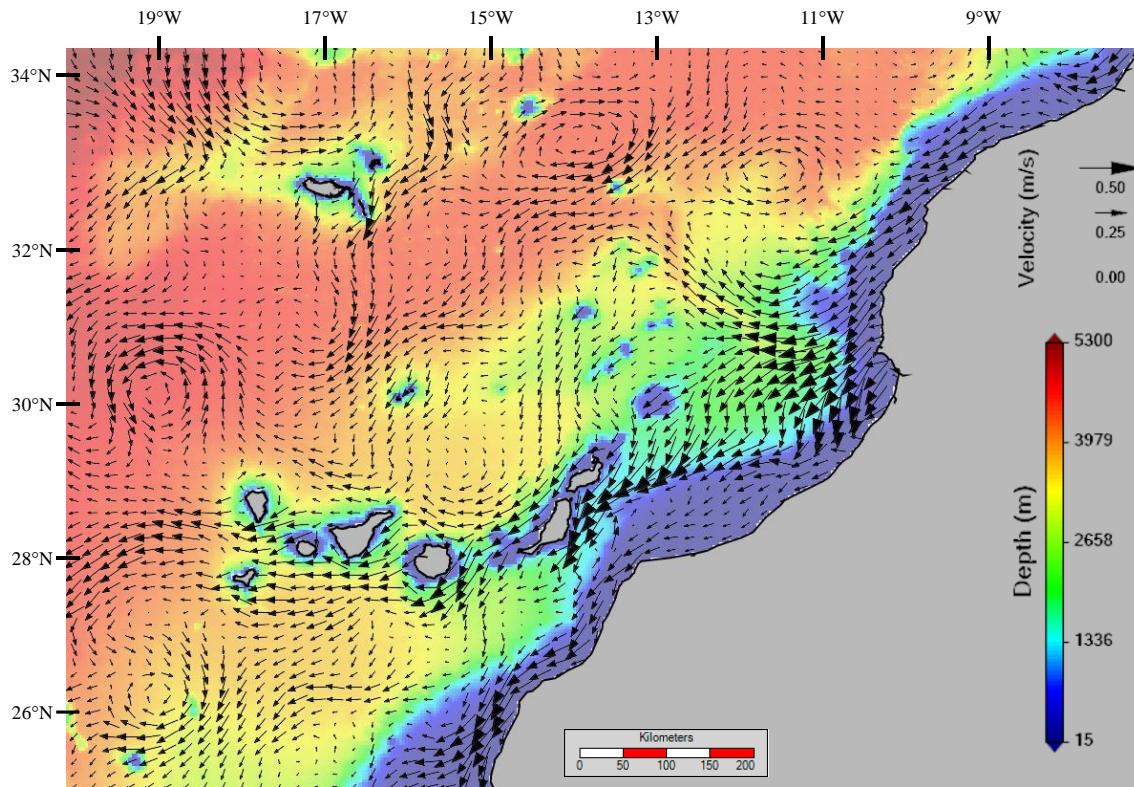


Figure 77: Residual circulation from Jun 2017 to March 2020. Velocities arrows overlay the bathymetry colour.

The MARPOCS modelling implementations were validated with some of the information available, including a tide gauge, sea surface temperature by remote sensing and vertical profiles from Argo buoys and PLOCAN. Most of the validation was performed for the 4 km domain which is critical for the success of its nested domains. However, water level obtained by the highest grid resolution model domain (LP2 – 100 m), temperature and salinity profiles obtained by the CI domain with 2 km, demonstrated improvement of the solutions with the offline downscaling approach. This modelling system has until March 2020 fed the MARPOCS platform, which uses these results to launch oil and HNS lagrangian simulations who are subsequently used to assess coastal risks.